FACULTY OF SCIENCES

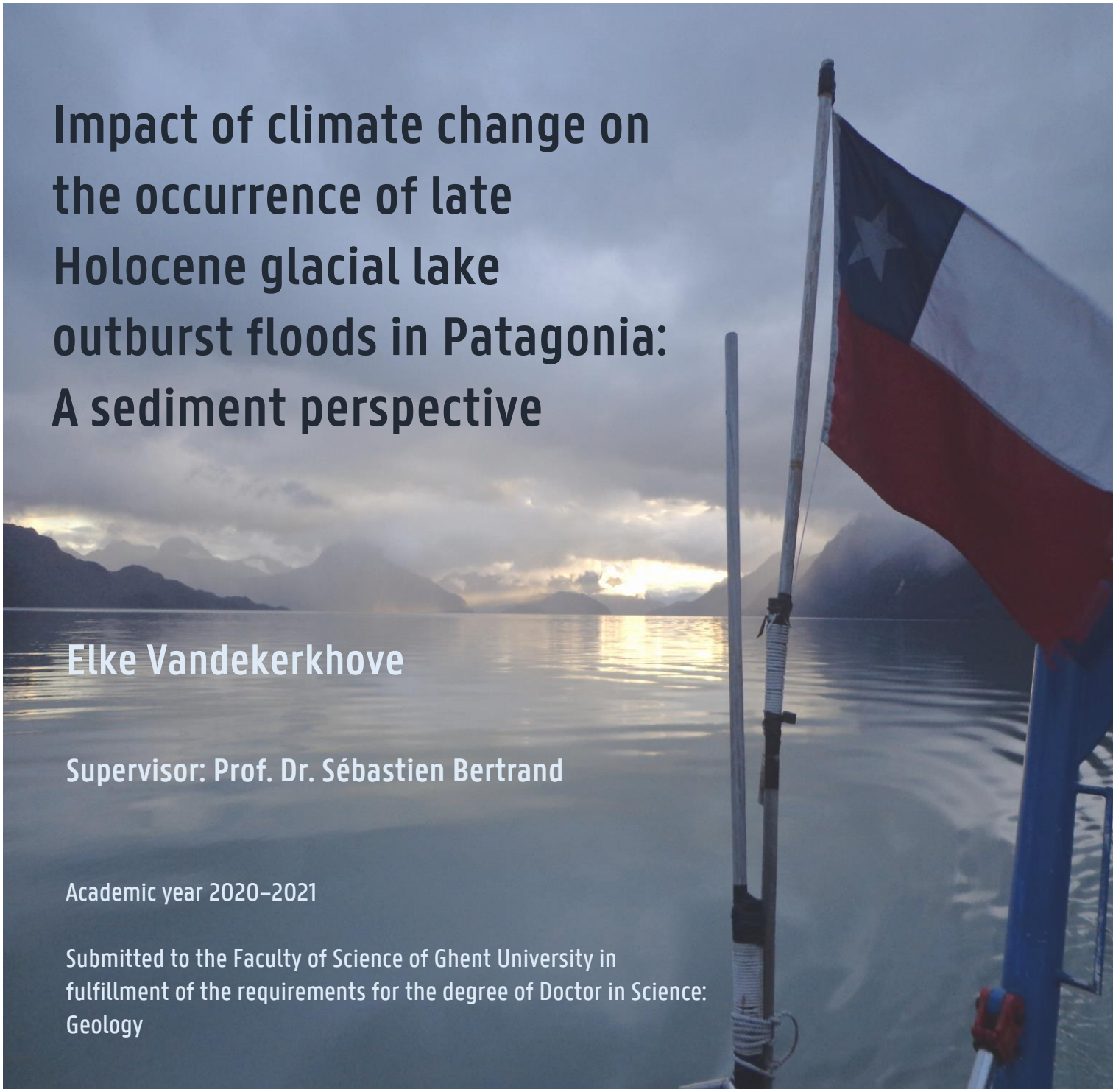

Impact of climate change on the occurrence of late Holocene glacial lake outburst floods in Patagonia: A sediment perspective

Elke Vandekerkhove

Supervisor: Prof. Dr. Sébastien Bertrand

Academic year 2020–2021

Submitted to the Faculty of Science of Ghent University in fulfillment of the requirements for the degree of Doctor in Science: Geology

GHENT UNIVERSITY

Members of the examination committee:

Prof. dr. S. Louwye (Ghent University, Belgium): chair
Prof. dr. M. De Batist (Ghent University, Belgium): secretary
Prof. dr. M. Van Daele (Ghent University, Belgium)
Dr. B. Amann (Ghent University, Belgium)
Dr. B. Reid (Centro de Investigación en Ecosistemas de la Patagonia, Chile)
Prof. dr. C. Lange (University of Concepción, Chile)
Prof. dr. G. Benito (National Museum of Natural Sciences, Spain)

This research was carried out by Elke Vandekerkhove with financial support of the Research Foundation Flanders (Paleo-GLOFs project: n°G0D7916N)

To refer to this thesis: Vandekerkhove, E. (2021) Impact of climate change on the occurrence of late Holocene Glacial Lake Outburst Floods in Patagonia: A sediment perspective. PhD thesis, Ghent University, Ghent, Belgium.

Table of Contents

Summary

Glacial Lake Outburst Floods (GLOFs) constitute one of the most notorious and destructive geohazards worldwide. They have occurred throughout recorded history and form a constant threat for local communities near glacierized regions. Although the recent deglaciation resulted in an increase in glacial lakes, both in size and number, worldwide, little is known about the possible relationship between climate variability and GLOF occurrence. Yet, it is generally assumed that GLOF frequency is currently increasing due to global glacier retreat. This is mainly due to a lack of continuous long-term flood records. Current records of GLOF occurrence, which are based on instrumental and historical data, are intrinsically limited to the last centuries. Consequently, the effect of climate change on GLOF occurrence and the likely evolution of GLOFs under future climate change scenarios remains unclear. However, a comprehensive understanding of the link between climate change, glacier variability, and GLOF occurrence is fundamental for future GLOF predictions and to improve flood hazard assessments.

As in many other glacierized regions, GLOFs are a well-known phenomenon in the Patagonian Andes. They are particularly pronounced in the Baker region of Chilean Patagonia (47–48 °S), where repeated GLOFs occurred from the abrupt drainage of ice-dammed Cachet 2 Lake between April 2008 and November 2020. During these events, water from Cachet 2 Lake spills into Colonia River, a tributary of Baker River, and increases both river discharge and sediment suspended concentrations. Colonia GLOFs are able to block the regular Baker River flow and result in the inundation of large areas upstream of the Colonia-Baker confluence, such as the Valle Grande floodplain. Downstream, the Baker River triples in discharge and large amounts of sediment are transported, and ultimately deposited, in fjords. The repeated Baker River GLOFs during the 21st century and the location of the Baker River, which drains most of the eastern side of the Northern Patagonian Icefield (NPI) and therefore integrates meltwater from several lake-river systems, makes the Baker region ideally suited to investigate GLOFs and to study the impact of climate change on GLOF occurrence.

To examine how GLOFs are recorded in fjord sediments, this study mapped the bathymetry of the head of Martínez Channel, i.e. the fjord in which the Baker River discharges, using multibeam echosounding. Results show that the subaquatic delta of Baker River is deeply incised by sinuous channels. The presence of sediment waves and coarser sediment within these channels suggest recent channel activity by turbidity currents. The latter is confirmed by sediment records collected at the head of the fjord, which reveal the presence of turbidites intercalated within silty background sediments, particularly on the delta plain in front of the main submarine channel. Although the turbidity currents are most likely generated by elevated river discharge and the associated relatively high suspended sediment loads, most turbidites are not related to GLOFs. Instead, they seem to represent other extreme discharge events, such as extreme precipitation or rain-on-snow events.

By comparing geochemical and sedimentological results obtained on the sediment cores to the recent GLOF history of Baker River, we show that the recent 21st century Cachet 2 GLOF deposits can be distinguished from background sediments by their finer grain size and lower organic carbon content, reflecting the increased input of glacial sediments during GLOFs. In addition, the results obtained on the fjord sediment cores demonstrate that the 21st century GLOFs from Cachet 2 Lake, which occurred less than one year apart, are not recorded as individual layers but as units richer in sediment of glacial origin. This suggests that it is not possible to reconstruct GLOF frequency nor magnitude solely based on fjord sediments. Although 21 GLOFs from Cachet 2 Lake occurred between 2008 and 2017, the deposits with

the clearest GLOF signature represent the initial events, implying that more glacial sediment was released during those first GLOFs, possibly due to lake-bed erosion. Consequently, it appears that sediment availability plays a more important role than flood magnitude in controlling GLOF deposit properties. Although GLOF frequency and magnitude cannot be accurately reconstructed using fjord sediments, high accumulation rates at the head of Martínez Channel highlight the potential of fjord sediment archives to establish pre-historical GLOF records at high temporal resolution.

In addition, the bathymetric imagery and the sediment records obtained at the head of Martínez Channel show that site selection and multi-coring are fundamental to reconstruct the Baker River GLOF history, as fjord heads are dynamic sedimentary environments with rapidly migrating channels. Ideal locations to reconstruct GLOFs are found on the delta slope, away from any submarine channel influence. GLOF deposits are best identified close to the river mouth, as background sediments become progressively finer and less organic, thus more similar to GLOF deposits, with increasing distance from the lip of the Baker River delta. Given the unique context of the Baker River system, where a significant portion of the watershed is vegetated and where the fine and organic-poor signature of GLOF deposits clearly contrasts with the slightly coarser and organic background sediments, our results may only be applicable to fjord sediments from temperate regions. Distinguishing GLOF deposits from background sediments would likely be more challenging in high latitude fjords.

Sediments deposited in floodplains constitute another faithful recorder of Baker River GLOFs. In the Valle Grande floodplain, which is located immediately upstream of the Colonia-Baker confluence, GLOFs are registered as organic-poor deposits intercalated within organic-rich background sediments. In contrast to marine archives, the sediments of the Valle Grande floodplain have lower accumulation rates, and can therefore be used to determine changes in GLOF occurrence on longer timescales (late Holocene). Based on four radiocarbon-dated sediment cores collected in the Valle Grande floodplain, our results show that high-magnitude GLOFs occurred intermittently in the upper Baker River watershed over the past 2.75 kyr. Two periods of increased flood activity occurred between approximately 2.57 and 2.17 cal kyr BP, and from 0.75 to 0 cal kyr BP. Comparison with independent proxy records of glacier variability reveals that these two periods of increased flood frequency match with Neoglacial advances. These advances seem to result from lower-than-average temperatures and wetter conditions.

Based on these results, we suggest that there is a strong, yet indirect, link between climate variability and GLOF occurrence. We hypothesize that, on multi-millennial timescales, high-magnitude GLOFs from eastern NPI glaciers are more frequent at times when glaciers are larger and thicker, as such glaciers most likely form larger and stronger ice dams, which in turn are able to retain larger lakes. Our results therefore suggest that the probability that high-magnitude GLOFs occur decreases as glaciers thin and retreat. Conversely, the frequency of lower magnitude GLOFs tends to increase during glacier recession because of the rapid growth of glacial lakes and formation of new lakes. Although isolated cases of new lakes formed behind large glaciers could still produce large GLOFs locally, the likelihood of large lake drainage and therefore high-magnitude GLOF occurrence decreases. This study supports the use of sediment-based GLOF records in other GLOF-prone regions for proper flood hazard assessment. A broader knowledge of the impact of climate change on GLOF occurrence can help to prevent further development in flood-prone regions and will reduce the vulnerability of communities to floods. Long-term paleoflood records can be of great importance for integrating spatial planning and planned infrastructure projects, such as hydroelectric dams, particularly since electricity demand is increasing with economic growth.

Samenvatting

Catastrofale overstromingen veroorzaakt door het abrupt leeglopen van gletsjermeren, een fenomeen ook wel gekend onder de naam *GLOF* (*Glacial Lake Outburst Flood*) of de van oorsprong Ijslandse term *jökulhlaup*, vormen één van de meest beruchte en destructieve geologische risico's wereldwijd. Ze kwamen voor doorheen de geschreven geschiedenis en vormen een constante dreiging voor de lokale bevolking nabij gletsjergebieden. Hoewel het recent smelten van gletsjers resulteerde in een toename van gletsjermeren, zowel in aantal als volume, is er weinig gekend over de mogelijke relatie tussen klimaatschommelingen en het voorkomen van GLOFs. Toch wordt er algemeen verondersteld dat de frequentie van GLOFs momenteel toeneemt door het recent smelten van gletsjers wereldwijd. Dit is voornamelijk door een gebrek aan ononderbroken overstromingsarchieven op lange termijn. De huidige GLOF archieven die gebaseerd op instrumentale en historische data zijn daardoor gelimiteerd tot de laatste eeuwen. Bijgevolg is het effect van klimaatschommelingen op het voorkomen van GLOFs en de vermoedelijke evolutie van GLOFs onder toekomstige klimaatsverandering scenario's onduidelijk. Nochtans is een uitgebreide kennis omtrent het verband tussen klimaatschommelingen, gletsjervariabiliteit, en het voorkomen van GLOFs fundamenteel voor GLOF voorspellingen en om overstromingsgevaar te evalueren.

Zoals in vele andere gletsjerregio's zijn GLOFs een gekend fenomeen in de Patagonische Andes. GLOFs zijn bijzonder uitgesproken in de Baker regio in Chileens Patagonië (47–48 °Z), waar GLOFs herhaaldelijk voorkwamen tussen april 2008 en november 2020 door het abrupt leeglopen van het door ijs afgedamd Cachet 2 meer. Tijdens deze gebeurtenissen stort het vrijgekomen water van het Cachet 2 meer uit in de Colonia rivier, een zijrivier van de Baker rivier, en stijgt het debiet en de concentratie van sediment in suspensie. De Colonia GLOFs zijn in staat om de stroming van de Baker rivier te blokkeren en daardoor grote gebieden stroomopwaarts, zoals de Valle Grande overstromingsvlakte, blank te zetten. Stroomafwaarts verdrievoudigt het debiet van de Baker rivier en worden grote hoeveelheden sediment getransporteerd en uiteindelijk afgezet in fjorden. Het herhaaldelijk voorkomen van GLOFs in de Baker rivier gedurende de 21ste eeuw en de locatie van de Baker rivier, die smeltwater afkomstig van verschillende meer- en riviersystemen aan de oostelijke kant van het noordelijk Patagonische ijsveld (NPI) afvoert, maken van de Baker regio het ideale studiegebied om GLOFs te bestuderen en om de impact van klimaatsverandering op het voorkomen van GLOFs te onderzoeken.

Om te bestuderen hoe GLOFs worden geregistreerd in fjord sedimenten werd de bathymetrie aan de ingang van het Martínez kanaal, het fjord waarin de Baker rivier uitmondt, in kaart gebracht via multibeam metingen. Onze resultaten tonen aan dat de delta aan de monding van de Baker rivier onder water diep is ingesneden door sinusoïdale kanalen. De aanwezigheid van sedimentgolven en grofkorreliger sediment in deze kanalen suggereert het recent voorkomen van turbidietstromen. Dit laatste werd bevestigd door de sedimentkernen die verzameld werden aan de ingang van het Martínez kanaal, waar turbidieten ingebed zijn in siltig sediment, vooral op de delta vlakte voor het voornaamste onderwater kanaal. Ondanks dat de turbidietstromen hoogstwaarschijnlijk ontstaan door een verhoogd debiet en de bijhorende relatief hoge lading aan sediment in suspensie, zijn de meeste turbidieten niet geassocieerd met GLOFs. In plaats daarvan lijken de turbidieten afkomstig te zijn van kortstondige debiet verhogingen ten gevolge van extreme precipitatie of regen op sneeuw.

Door de geochemische en sedimentologische resultaten die verworven werden uit de sedimentkernen te vergelijken met de recente GLOF geschiedenis van de Baker rivier, kan er aangetoond worden dat de

afzettingen afkomstig van de 21ste-eeuwse Cachet 2 GLOFs onderscheiden kunnen worden van de achtergrond sedimenten door hun fijnere korrelgrootte en lagere organische koolstofgehalte. Deze eigenschappen weerspiegelen de verhoogde toevoer aan glaciale sedimenten tijdens GLOFs. Bovendien tonen de resultaten die bekomen werden uit de sedimentkernen aan dat de 21ste-eeuwse Cachet 2 GLOFs, die minder dan één jaar uit elkaar plaatsvonden, niet geregistreerd worden als individuele lagen maar als eenheden rijk aan glaciaal sediment. Dit laatste wijst erop dat het niet mogelijk is om de frequentie noch de magnitude van GLOFs te reconstrueren uitsluitend op basis van fjord sedimenten. Hoewel er 21 GLOFs afkomstig van het Cachet 2 meer voorkwamen tussen 2008 en 2017, vertegenwoordigen de afzettingen met de duidelijkste GLOF kenmerken de initiële gebeurtenissen. Dit duidt erop dat er meer glaciale sedimenten vrijgegeven werden tijdens deze eerste GLOFs, mogelijks door erosie van de meerbedding. Bijgevolg lijkt het erop dat de beschikbaarheid aan sediment belangrijker is dan de overstromingsmagnitude voor het bepalen van de kenmerken van GLOF afzettingen. Ondanks dat de GLOF frequentie en magnitude niet nauwkeurig gereconstrueerd kunnen worden aan de hand van fjord sedimenten, wijzen de hoge accumulatiesnelheden aan de ingang van het Martínez kanaal op het potentieel van fjord sedimenten om pre-historische GLOF archieven te maken met een hoge temporele resolutie.

De bathymetrische beelden en de sedimentkernen die verzameld werden aan de ingang van het Martínez kanaal tonen ook aan dat de selectie van locaties en het verkrijgen van meerdere kernen fundamenteel zijn om de geschiedenis van Baker rivier GLOFs te reconstrueren vanwege het feit dat er een dynamisch sedimentair milieu heerst met kanalen die snel migreren. Ideale locaties om GLOFs te reconstrueren bevinden zich op de onderzeese deltavlakte, weg van de invloed van de onderwater kanalen. GLOF afzettingen worden het gemakkelijkst onderscheiden dicht bij de riviermonding omdat de achtergrond sedimenten geleidelijk aan fijnkorreliger en minder organisch, en dus eerder gelijkaardig aan GLOF afzettingen, worden naarmate ze verder van de Baker riviermonding verwijderd zijn. Vanwege de unieke context van het Baker rivier-systeem, waar een beduidend deel van het stroomgebied begroeid is en waar de fijnkorrelige en organisch-arme kenmerken van GLOF afzettingen duidelijk te onderscheiden zijn van de ietwat grovere en organische-rijkere achtergrond sedimenten, kunnen onze resultaten enkel toegepast worden op fjord sedimenten in gematigde klimaatgebieden. Het onderscheiden van GLOF afzettingen ingebed in achtergrond sedimenten zal vermoedelijk meer uitdagend zijn in fjorden op hogere breedtegraden.

Sedimenten afgezet in overstromingsvlakten vormen een ander betrouwbaar archief van Baker rivier GLOFs. In de Valle Grande overstromingsvlakte, die gelegen is nabij de samenvloeiing van de Colonia en Baker rivieren, zijn GLOFs geregistreerd als organisch-arme afzettingen ingebed in organisch-rijke achtergrond sedimenten. In tegenstelling tot mariene archieven hebben sedimenten in de Valle Grande overstromingsvlakte lagere accumulatiesnelheden, en kunnen ze bijgevolg gebruikt worden om veranderingen in het voorkomen van GLOFs te bepalen op langere tijdschalen (laat Holoceen). Op basis van de vier radiokoolstof-gedateerde sedimentkernen die verzameld werden in de Valle Grande overstromingsvlakte kan er aangetoond worden dat GLOFs van grote omvang periodiek voorkwamen in het hoger gelegen gedeelte van het Baker stroomgebied gedurende de laatste 2.75 ka. Twee periodes met verhoogde overstromingsactiviteit kwamen voor tussen ongeveer 2.57 en 2.17 cal ka BP, en 0.75 en 0 cal ka BP. De vergelijking met onafhankelijke archieven van gletsjervariabiliteit toont aan dat deze twee periodes overeenkomen met Neoglaciaties. Deze Neoglaciale voortschrijdingen lijken te resulteren van lager dan gemiddelde temperaturen en nattere klimaatcondities.

Deze resultaten doen ons vermoeden dat er een sterke, maar indirecte, link is tussen klimaatschommelingen en het voorkomen van GLOFs. Wij veronderstellen dat, op tijdschalen van meerdere millennia, GLOFs van grote magnitude, afkomstig van gletsjermeren ten oosten van het Noordelijk Patagonische ijsveld, frequenter voorkomen wanneer gletsjers omvangrijker zijn. Omvangrijkere gletsjers vormen vermoedelijk grotere en sterkere ijsdammen, die op hun beurt grotere meren in stand kunnen houden. Hierdoor doen onze resultaten vermoeden dat de kans op GLOFs van grote omvang daalt naarmate gletsjer terugtrekken. GLOFs met een lagere magnitude zullen daarentegen de neiging hebben meer voor te komen tijdens het smelten van gletsjers door de snelle groei van gletsjermeren en het vormen van nieuwe meren. Hoewel alleenstaande gevallen van nieuwe meren die gevormd worden bij omvangrijke gletsjers nog steeds lokaal GLOFs van hoge magnitude kunnen teweegbrengen, achten we dat de kans op grote meeruitbarstingen en dus het voorkomen van GLOFs van grote omvang daalt. Deze studie staaft het gebruik van GLOF archieven op basis van sediment afzettingen in andere GLOF-gevoelige regio's voor een adequate evaluatie van het overstromingsgevaar. Een bredere kennis omtrent de impact van klimaatsverandering op het voorkomen van GLOFs kan de verdere ontwikkeling in overstromingsgevoelige gebieden voorkomen en zal de kwetsbaarheid van gemeenschappen doen dalen. Langetermijn archieven van historische overstromingen kunnen uitermate belangrijk zijn om ruimtelijke ordening en geplande projecten, zoals hydro-elektrische dammen, te integreren, in het bijzonder vanwege de economische ontwikkeling die gepaard gaat met een stijgende stroombehoefte.

Acknowledgements

First of all, I would like to express my greatest gratitude to my promotor Sébastien Bertrand. Without him, this work would not have seen the light. Thank you, profe, thank you for your confidence in me, and for giving me the opportunity to work on this project. You were always (emphasize on always) there, offering me wise advice and giving me new insights. You have been a vital support during my PhD, both as a promotor but also as a person. Motivating someone to improve is one of the many amazing skills you possess and that I admire you for, and you taught me another level of scientific writing. In my opinion (and probably the opinion of all your students), you are the best promotor a PhD student could wish for and I can praise myself lucky. Therefore, mil gracias Seb!

I also want to thank everyone who helped out during the field expeditions in Chile. Thank you Koen De Rycker, Fernando Torrejón, Krystyna Saunders, Francois De Vleeschouwer, Loïc Piret, Eleonora Crescenzi Lanna, and Helena Pryer for your help in collecting all samples and for the memorable moments both on land and offshore. Special thanks also to captain Rodrigo Mansilla and Lucho of the R/V Sur Austral for their inestimable help, and their endless knowledge and experience. The kind host Valeria at Brisas del Sur in Caleta Tortel will be remembered for her great hospitality and amazing food, which always warmed our hearts after the long, sometimes cold, days on the field or fjords. I am also grateful to Silvio Pantoja, Romina San Martín, Brian Reid and his colleagues at CIEP, and Olaf Wuendrich for easing the organization of the field expeditions and all their help. I would like to acknowledge Elie Verleyen, Wim Vyverman, Alain De Wulf, Annelies Vandenbulcke, Emmanuel Blanchard, Alberto Araneda, Dirk Verschuren, and Anita Abarzua for lending us their equipment during the expeditions.

All my colleagues at RCMG are thanked for providing such a great work atmosphere at the S8 building. The fun conversations during lunch at the resto served as an excellent short break from science. Thank you Nore, Maarten, Inka, Thomas M., Evelien, Shan, Dawei, Loïc, Matthias, Benjamin, Thomas V., Carmen, Katleen, Tim, Stijn, Maikel, Marc, David V.R., Eleonora, Ann, Vasileios, Tine, David G.M., Stan, Romain, and Alice. I would also like to thank Wim, Marc, Marion, and Kurt for easing the administration and answering all my questions on any computer-related topic. Lab experts Veerle and Ann-Eline were much appreciated as they helped me out many times with their convenient tips and tricks.

Finally, this work would have been an impossible task without the endless support of my family. Arne, thank you for enduring me and always listening, willingly and unwillingly, to my frustrations. You provided the necessary distraction from work and gave me a constant motivation throughout this PhD. I cannot express how grateful I am to you for taking care of Lize and Linus as the combination between a PhD and raising children (associated with countless sleepless nights) was not always evident. Finally, I want to thank my parents deeply. They always had faith in me and consistently supported me in everything. Thank you mom and dad for your endless encouragement throughout my studies.

List of abbreviations

Abbreviation	Paraphrase
ACR	Antarctic Cold Reversal
CDI	Cordillera Darwin Icefield
CFCS	Constant Flux-Constant Sedimentation
CIC	Constant Initial Concentration
CLR	Centred-Log Ratio
CRS	Constant Rate of Supply
CT	Computed Tomography
CTD	Conductivity, Temperature, Depth
DGA	Dirección General de Aguas (Chilean Water Directorate)
DW	Dry Weight
EA	Elemental Analyzer
FC	Fjord Core
FP	Floodplain
GLOF	Glacial Lake Outburst Flood
GS	Grab Sample
LIA	Little Ice Age
LGM	Last Glacial Maximum
LOI	Loss-On-Ignition
MCMC	Markov Chain Monte Carlo
MS	Magnetic Susceptibility
MSCL	Multi-Sensor Core Logger
NPI	Northern Patagonian Icefield
PCA	Principal Component Analysis
PIS	Patagonian Ice Sheet
PF	Polar Front
SAF	Sub-Antarctic Front
SPI	Southern Patagonian Icefield
SSC	Suspended Sediment Concentration
SST	Sea Surface Temperature
STF	Subtropical Front
SWWB	Southern Westerly Wind Belt
TOC	Total Organic Carbon
XRF	X-ray Fluorescence

List of figures

List of tables

1. Introduction

Climate conditions have changed throughout the Earth's history. During the last centuries, the fast growth of human civilizations and the associated greenhouse gas emissions, together with other anthropogenic drivers, have transformed global climate at a drastic and unprecedented rate (IPCC, 2014; Zalasiewicz and Williams, 2016). As a result, the Earth's average surface temperature has increased approximately 1 °C above pre-industrial levels (IPCC, 2018), and ice sheets are losing hundreds of billion tons of ice per year (Velicogna et al., 2020), which increased global sea level by almost 20 cm over the past 100 years (Nerem et al., 2018; Oppenheimer et al., 2019).

Changing climate conditions, such as variations in precipitation and temperature, can greatly affect the occurrence of natural hazards like floods, landslides, tropical storms, avalanches, heat waves, droughts, and wildfires. Across the world, these events can severely impact communities as they can cause damage to infrastructure and result in the loss of human lives and crops and livestock resources. For instance, the occurrence of Glacial Lake Outburst Floods (GLOFs) is expected to be significantly influenced by climate change via its impact on glacier mass balance (e.g. Nadeem et al., 2012; Craigmile, 2018; Carrivick and Tweed, 2016; Harrison et al., 2018).

There are currently 700 million people living in close contact with the cryosphere, mostly in high mountains and the Arctic, which are increasingly exposed to these risks as climate changes (Abram et al., 2019). An appropriate understanding of the climate-flood relationships on short and longer timescales is required to generate accurate hazard assessments, predict the likelihood of future floods, and eventually protect communities against these threats.

1.1. Glacial Lake Outburst Floods

GLOFs, also known by the Icelandic term *jökulhlaups*, are catastrophic flooding events that occur when a lake dammed by a glacier or a moraine suddenly empties (e.g. Benn and Evans, 2010). They are particularly notorious and they form a constant threat to local communities in glacierized regions (Carrivick and Tweed, 2016). GLOFs are a worldwide phenomenon (Fig. 1.1). They have been described in the European Alps (e.g. Haeberli, 1983; Eisbacher and Clague, 1984), Scandinavia (e.g. Røthe et al., 2019), Iceland (e.g. Thorarinsson, 1939; Björnsson, 2002), North America (e.g. Mayo, 1989; Clague and Evans, 2000), Greenland (e.g. Russell, 1989), South America (e.g. Lliboutry, 1977; Hauser, 1993; Walder and Costa, 1996; Harrison et al., 2006; Dussaillant et al., 2010; Iribarren Anacona et al., 2015; Aniya, 2017), the Himalayas (e.g. Benn et al., 2001; Byers et al., 2019), and New Zealand (e.g. Davies et al., 2003; Goodsell et al., 2005). During the Quaternary, cataclysmic GLOFs resulted in large-scale landscape changes (e.g. Baker, 1973; Komatsu et al., 2009). The best-known example may be the repeated outbursts of glacial Missoula Lake at the southern margin of the Laurentide Ice Sheet in North America at the end of the Pleistocene, which created channeled scablands and many other large erosional and depositional landforms such as potholes, waterfalls, gravel bars etc. in eastern Washington (Baker, 1973). Other large lake outbursts, such as the freshwater outbursts from Agassiz Lake during the last deglaciation, may have caused regional climate change by altering the ocean's thermohaline circulation (Teller, 1995; Clarke et al., 2009).

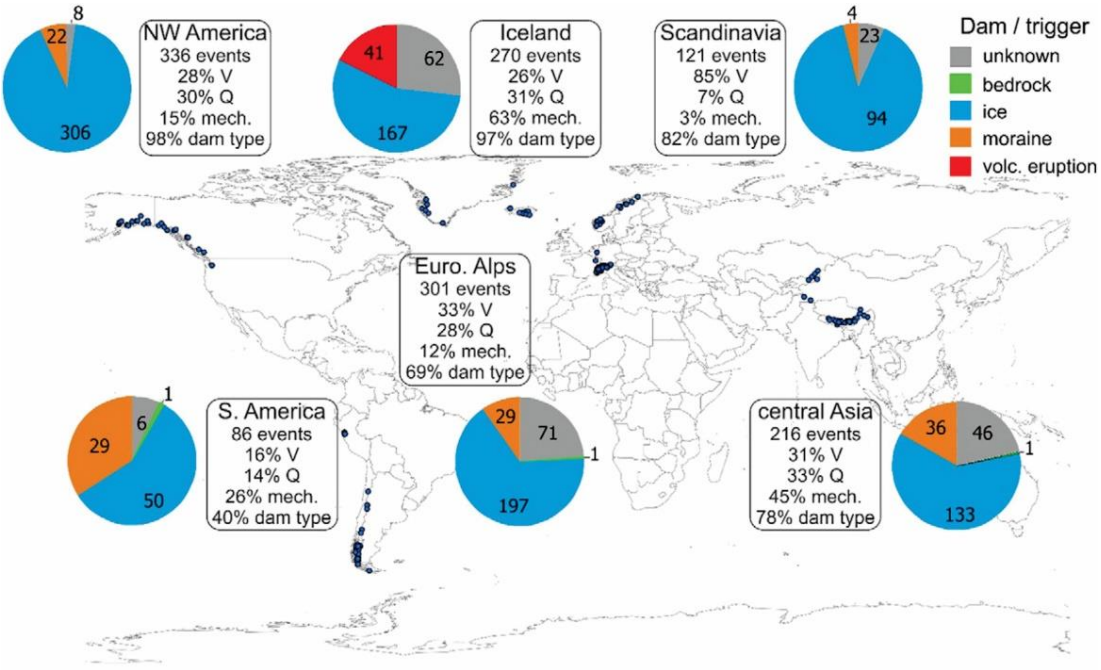

Figure 1.1. Overview by major region of the number of historical GLOFs per dam type/trigger (pie charts). The rectangles display the total number of events per region, and the proportion of GLOFs for which physical attributes (i.e. V: volume, Q: discharge, mech.: floodwater release and/or routing mechanisms, and dam type) are known (from Carrivick and Tweed, 2016).

GLOFs result from the drainage of ice- and moraine-dammed glacial lakes (Richardson and Reynolds, 2000). These lakes can be classified based on their topographic position and nature of the dam (Benn and Evans, 2010).

1.1.1. Moraine-dammed lakes

Moraine-dammed lakes occur between the glacier margin and frontal and/or lateral moraines (Clague and Evans, 2000) (Fig. 1.2). To form moraine-dammed lakes, the debris supply at the glacier margin should overcome the melt stream capacity for sediment transport, which is also referred to as a *decoupled margin* (Benn et al., 2003). The recent retreat of many mountain glaciers from their late Holocene positions, for example, resulted in the formation of moraine-dammed lakes (Clague and Evans, 2000; Richardson and Reynolds, 2000).

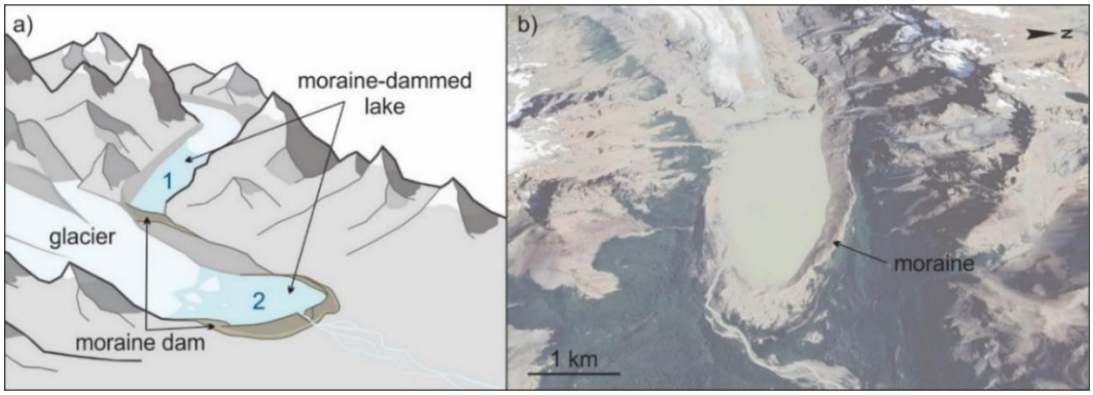

Figure 1.2. Moraine-dammed lakes. **(a)** Schematic figure showing possible locations of moraine-dammed lakes. (1) In a side valley, dammed by a lateral moraine. (2) Behind a terminal moraine. **(b)** Example of a moraine-dammed lake, i.e. Torre Lake, in front of the Grande Glacier along the Southern Patagonian Icefield (SPI), Argentina (49.3 °S) (Google Earth Image).

Lake drainage occurs when the moraine dam breaks. Moraine dam failure can be triggered by seiche or displacement waves generated by seismic activity, water discharge from supra-, en-, or subglacial lakes, dam settlement and/or piping, and ice and rock falls, rockslides or moraine failures into lakes (Richardson and Reynolds, 2000; Westoby et al., 2014) (Fig. 1.3). Climatically-induced triggers such as high-intensity precipitation or a snowmelt event, and the melting of ice cores in the moraine dam, can also lead to dam failure (Harrison et al., 2018) (Fig. 1.3). Once the waves overtop the sediment barrier, the dam breaching process is initiated and the erosive power of water discharge can lead to dam failure and eventually a GLOF (Westoby et al., 2014). The dam can break down completely and fully drain the lake or partially and leave behind a lower-level lake, in which case another GLOF can occur from the same lake in the future (Benn and Evans, 2010).

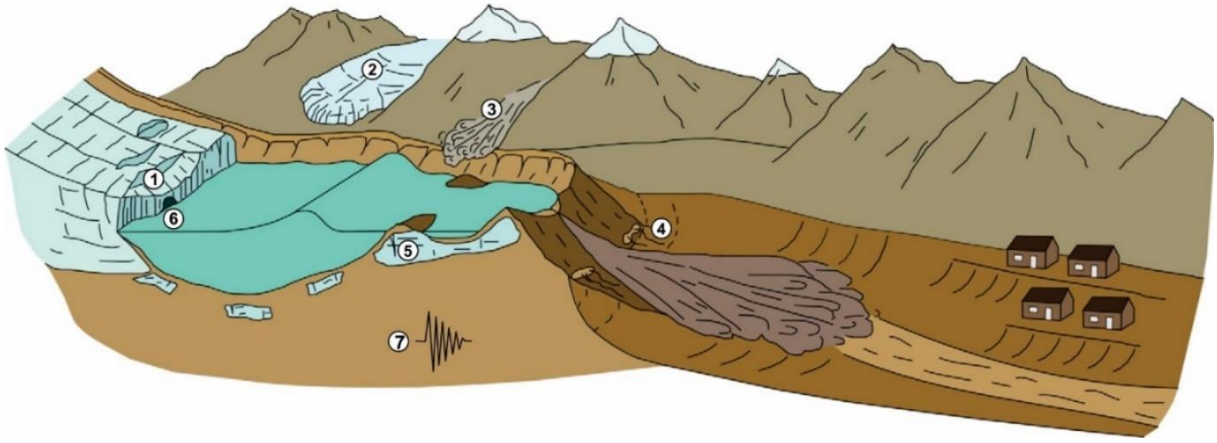

Figure 1.3. Schematic overview of the potential triggers of GLOFs from a moraine-dammed lake. Potential triggers include: (1) contact glacier calving, (2) icefall from hanging glacier, (3) rock/snow/ice avalanche, (4) dam settlement and/or piping, (5) degradation of ice-cored moraine, (6) water discharge by supra-, en-, or subglacial lakes, and (7) seismic activity (Figure modified from Westoby et al., 2014).

GLOFs induced by the drainage of moraine-dammed lakes are highly destructive as they induce a mixture of water, rocks, mud, ice, and other debris. The largest GLOF from a moraine-dammed lake reported in the literature is that of Cerro Largo Lake in March 1989 in Chile (47 °S), which released an estimated water volume of 140 x 10^6 m³ (Burton et al., 2020). Another well-known example of one of the most devastating moraine-dammed lake GLOFs is the 1941 event in Cordillera Blanca (Peru). This GLOF initiated from the drainage of Palcacocha Lake. It led to the complete drainage of a second moraine-dammed lake (Jircacocha Lake) downstream and destroyed part of the city of Huaráz, killing thousands of people and making it one of the deadliest outbursts ever documented (Lliboutry et al., 1977).

1.1.2. Ice-dammed lakes

Ice-dammed lakes form in similar topographic positions as moraine-dammed lakes but occur where local or regional drainage is prevented by a glacier (Fig. 1.4a). This can be where valleys are blocked by a glacier, or at the junction between two valley glaciers. Contrary to moraine-dammed lakes, ice-dammed lakes can experience repeated filling and draining cycles as ice dams form much faster compared to moraine dams. GLOFs from ice-dammed lakes can thus occur more frequently, e.g. on annual or longer timescales. Outbursts from ice-dammed lakes tend to result in lower flood discharges compared to moraine-dammed outbursts with a similar lake volume, as the enlargement of tunnels within ice is often a slower process than overtopping and incision of moraine dams (Costa and Schuster, 1988; Clague and Evans, 2000).

Although lake drainage occurs as the glacier recedes, drainage of an ice-dammed lake does not necessarily require complete dam destruction. Subglacial conduits, for example, result in lake drainage and can rapidly close again by ice creep after the GLOF occurred (e.g. Cachet 2 Lake, Chile; Dussaillant et al., 2010). Another example of repeated ice-dammed lake drainage is found at the Perito Moreno Glacier in Argentinian Patagonia. The Perito Moreno Glacier, i.e. an outlet glacier of the Southern Patagonian Icefield (SPI), is pushed across Argentino Lake and eventually divides the lake into two separate bodies of water, i.e. the Brazo Rico and the Témpanos Channel (Fig. 1.4b). As the Brazo Rico has no outlet, the water level in the Brazo Rico rises above the Témpanos Channel water level. Intermittently, water pressure from the Brazo Rico leads to rupture of the ice dam, releasing large amounts of water from the Brazo Rico to the Témpanos Channel to the north (Fig. 1.4c). This ice dam-rupture cycle occurs naturally between once a year to once every decade (Chinni and Warren, 2004).

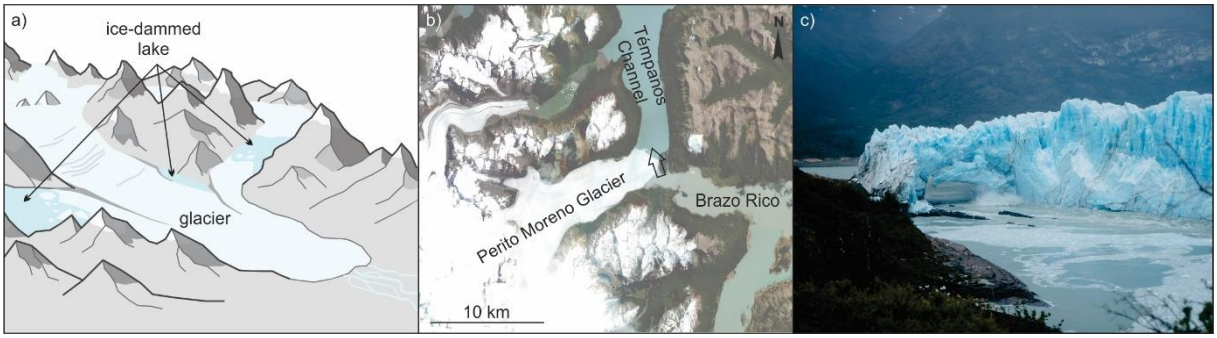

Figure 1.4. Ice-dammed lakes. **(a)** Schematic figure showing different settings of ice-dammed lakes. **(b)** Location of Argentino Lake in Argentinian Patagonia (50.5 °S), where the Perito Moreno Glacier splits the lake into the Brazo Rico to the south and the Témpanos Channel to the north (Global Mapper World Imagery). The arrow indicates water flow from the Brazo Rico during ruptures of the ice dam. **(c)** Ice chunks falling into Argentino Lake, at the tip of the Perito Moreno Glacier. Water flow erodes the ice and enlarges the tunnel until the bridge eventually collapses. Picture taken on 06/05/2016, facing the Brazo Rico (Photo Credit: Renée Lusano).

GLOFs from ice-dammed lakes are particularly frequent in Iceland due the concurrence of intense volcanic activity and glaciers. This type of GLOFs is related to geothermal heating or subglacial volcanic eruptions. They were initially referred to with the Icelandic term *jökulhlaups*, which is now widely accepted as synonym of GLOFs to describe any abrupt flood by the release of a glacial lake. Some of the best known and most spectacular examples of Icelandic GLOFs occur from Vatnajökull, an ice cap located in the southwestern part of Iceland, where GLOF peak discharges from the subglacial lake Grímsvötn reached up to 50 000 m^3/s at the glacier margin and where single events can last up to several weeks (Björnsson, 2002).

1.2. Worldwide GLOF occurrence

Glacial lake outbursts occur in most glacierized regions and have been documented worldwide for many centuries (Carrivick and Tweed, 2016) (Fig. 1.5). The oldest historical GLOF records are most abundant in the European Alps and Iceland, and they indicate that GLOF frequency seems to have decreased since the mid-1990s in every major world region (Fig. 1.5). Documented lake outbursts originated from 332 sites, and two thirds of the sources that have produced repeated GLOFs (i.e. > five floods) produce floods progressively earlier in the year, which might indicate a global climatic control (Carrivick and Tweed, 2016). Recorded GLOFs have predominantly (70 %) occurred from ice-dammed lakes, of which 36 % had recorded a societal impact. Only 9 % of GLOFs with a known trigger are from moraine-dammed lakes (Carrivick and Tweed, 2016) (Fig. 1.1).

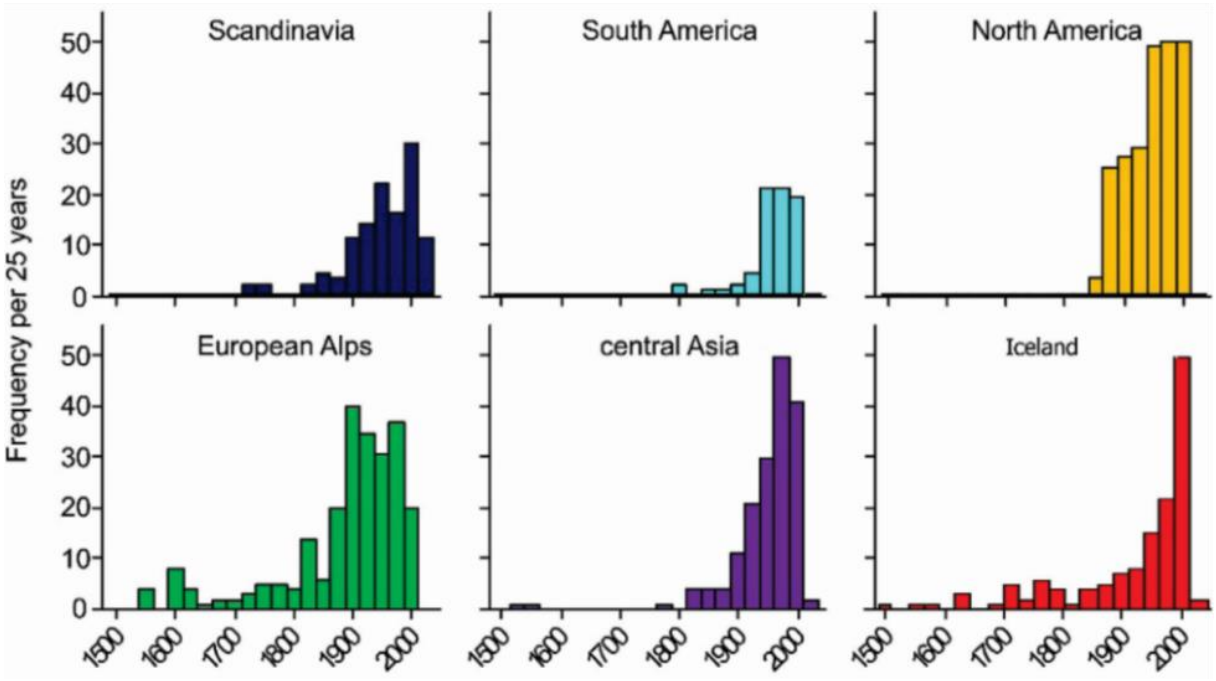

Figure 1.5. Recorded GLOF frequency, i.e. number of GLOFs per 25 years, for different regions over the past 500 years (Carrivick and Tweed, 2016).

The direct societal impact of GLOFs involves loss of lives and livestock, and damage to infrastructure, such as roads, buildings, bridges, hydropower facilities, etc. (Fig. 1.6). In addition, the erosive power of GLOFs can trigger landslides, or the release of high amounts of sediment, which, if it reaches fjords downstream, such as in west Greenland, can interrupt fishing activities, thus indirectly causing damage. Worldwide, GLOFs frequently occur in Iceland and Canada, with a relatively high number of events and sites. Yet, GLOF damage in these countries is often low. On the other hand, lake outbursts have caused the highest societal impact in South America and Asia, making them the most vulnerable regions to GLOFs worldwide (Carrivick and Tweed, 2016). Throughout recorded history, GLOFs have caused at least 7 deaths in Iceland, 393 deaths in the European Alps, 5745 deaths in South America, and 6300 deaths in central Asia (Carrivick and Tweed, 2016).

Figure 1.6. Damage caused by GLOFs worldwide. **(a)** The city of Huaráz (Peru) where a large area was swept away by the 1941 GLOF due the emptying of Palcacocha Lake. The aerial picture was taken six years after the event, on 24/06/1947 (Photo credit: Arnold Heim). **(b)** Aftermath of a landslide near Tatopani (Nepal) caused by the July 2016 GLOF in the Bhotekoshi/Sunkoshi River, Nepal (Photo credit: Christoff Andermann). **(c)** The Upper Bhote Koshi Hydroelectric Project intake dam (Nepal), which was partially destroyed by the same July 2016 GLOF in Nepal (Photo credit: Kristen Cook). **(d)** Flooding of the Skaftá River (Iceland) due to a glacial lake outburst in 2015 (Photo credit: Egill Aðalstainsson).

1.3. Relationship between GLOF occurrence and climate

The formation of ice-dammed and moraine-dammed lakes is inevitably linked to climate change via glacier mass balance (Carrivick and Tweed, 2013). The post-Little Ice Age (LIA) deglaciation, for example, resulted in an increase of glacial lakes worldwide, both in size and number (e.g. Paul et al., 2007; Wang et al., 2011; Davies and Glasser, 2012; Carrivick and Quincey, 2014; Aniya, 2017; Wilson et al., 2018; Shugar et al., 2020). A recent study that mapped glacial lakes around the world using satellite images and scaling relations estimates that global glacial lake volume increased by around 48 %, to 156.5 km^3, between 1990 and 2018 (Shugar et al., 2020). During this period, the number and total area of lakes increased by 53 and 51 %, respectively (Shugar et al., 2020), and their number and size will most likely continue to increase in most regions in the coming decades (IPCC, 2019).

In contrast to the number and size of glacial lakes worldwide, little is known about trends in the frequency and magnitude of glacial lake outburst floods over the past decades (Carrivick and Tweed, 2016; Harrison et al., 2018). Historical data suggest that GLOFs have occurred globally throughout recorded history (Carrivick and Tweed, 2016; Fig. 1.5), with only limited evidence that their frequency has changed (Seneviratne et al., 2012; IPCC, 2019). In the future, it is hypothesized that new lakes will

form close to unstable mountain slopes where lake outbursts might be more easily triggered by the impact of landslides (IPCC, 2019).

Despite the recent increase in glacial lakes and the assumption that GLOF frequency is currently increasing, the number of GLOFs from moraine-dammed lakes has actually been declining in the last 50 years in all major world regions (Carrivick and Tweed, 2016; Harrison et al., 2018). The global increase in GLOF frequency that occurred between 1930 and 1970 was associated with a delayed response to the warming that ended the Little Ice Age (Harrison et al., 2018). Afterwards, the frequency of GLOFs originating from the failure of moraine dams has been decreasing, despite glacier recession. The climate stabilization that followed the LIA is at the basis of this recent decline in moraine-dammed GLOF frequency and regularity (Harrison et al., 2018). Similarly, warming from the late 1800s until around 1940, and from 1965 to today destabilized moraine dams in North America (Clague and Evans, 2000). Finally, Veh et al. (2019) observed no significant increase in the number of GLOFs since the late 1980s in the Himalayas. It thus appears that, at the global scale, the frequency of GLOFs from moraine-dammed lakes stabilized or decreased during the last decades.

Likewise, GLOFs from ice-dammed lakes, which currently account for 70 % of the recorded lake outbursts, also seem to have decreased during the last decades (Carrivick and Tweed, 2016). Such GLOFs may increase during periods of glacier advance (Benn and Evans, 2010; Round et al., 2017), as observed during the LIA in the French Alps (Vivian, 2001). The situation is less clear in the Himalayas, where irregular, frequent and sudden advances of Karakorum glaciers in response to global warming have resulted in ice dam lake formation and subsequent outburst flooding throughout the region (Bazai et al., 2021).

Although many regionally-focused research papers on GLOFs exist, most GLOF studies have addressed glacial lake formation (e.g. Tweed and Russell, 1999), GLOF triggering mechanisms (e.g. Westoby et al., 2014), outburst susceptibility and prediction (e.g. Iribarren Anacona et al., 2014; Cook et al., 2016), hydraulic flow behavior (e.g. Walder and Costa, 1996; Cenderelli and Wohl, 2003), and landscape (e.g. Carrivick, 2007) and societal impacts (e.g. Carrivick and Tweed, 2016). Very few studies have investigated the possible link between climate variability and GLOF frequency (e.g. Chen et al., 2010; Harrison et al., 2018). Consequently, the global impact of climate change on GLOF occurrence throughout the Quaternary and the likely evolution of GLOFs under future climate change remains largely unclear. This is mainly due to a lack of continuous long-term flood records that extend beyond river-gauged datasets. In addition, the majority of publications on GLOF occurrence makes use of instrumental data or historical records. These records are therefore limited to the last centuries and the existing GLOF inventories might significantly underestimate the number of events (Carrivick and Tweed, 2016) (Fig. 1.5). Given the natural hazard potential of GLOFs worldwide, a comprehensive understanding about the link between climate and GLOF occurrence is key for future GLOF forecasting and to improve flood hazard assessments.

1.4. GLOFs in Patagonia

As in many other mountainous glacierized regions, GLOFs are also a well-known phenomenon around glacier margins in the Chilean Andes. Previous studies have reported GLOFs in Central Chile (e.g. Iribarren Anacona et al., 2014), and around the Northern Patagonian Icefield (NPI) (e.g. Harrison et al., 2006; Iribarren Anacona et al., 2014; Iribarren Anacona et al., 2015; Aniya, 2017) and SPI (e.g. Peña and Escobar, 1983; Chinni and Warren, 2004). Chilean Patagonia appears to be particularly vulnerable to

GLOFs, which is frequently described in the literature as a consequence of the rise in the number of glacial lakes related to the accelerated glacier recession in the southern Andes (Harrison et al., 2006; Lopez et al., 2010; Davies and Glasser, 2012; Wilson et al., 2018, 2019). Between 1945 and 2011, it is estimated that the glacial lake volume for the NPI has increased by 4.8 km³, with the largest increase after 1987 (Loriaux and Casassa, 2013). During the last decades, Patagonian glacial lakes, excluding the three largest lakes Argentino, Viedma, and San Martin, have more than doubled in volume (Shugar et al., 2020), and their number increased from 2926 to 4202 (43 %) (Wilson et al., 2018). Despite this increase in lake size and volume, it remains unclear whether GLOF frequency has changed during the last decades and centuries.

In Chilean Patagonia, GLOFs are particularly pronounced in the Baker River (47–48 °S), which drains most of the eastern side of the NPI (Fig. 1.7). Most of the recent Baker River GLOFs originated from the outburst of Cachet 2 Lake, which is located on the eastern margin of the Colonia Glacier (Figs. 1.7 and 1.8). Between April 2008 and November 2020, the ice-dammed Cachet 2 Lake generated 23 GLOFs (Dussaillant et al., 2010; Jacquet et al., 2017; Dirección General de Aguas, DGA, Chile). During these lake outbursts, water from Cachet 2 Lake spills into the Colonia River, a tributary of Baker River. This causes the Baker River to triple in discharge, sometimes reaching up to 4200 m³/s (DGA, Chile). At the confluence of Colonia and Baker rivers, the regular flow of Baker River towards the South is blocked and results in the inundation of large areas, e.g. the Valle Grande floodplain, upstream of the confluence with Colonia River (Fig. 1.7). Downstream, an estimated 1.0 to 1.5 x 10^5 tons of sediment per event is transported and deposited in Martínez Channel, which may contribute up to 5 % to the annual fine sediment load in the fjord (Quiroga et al., 2011).

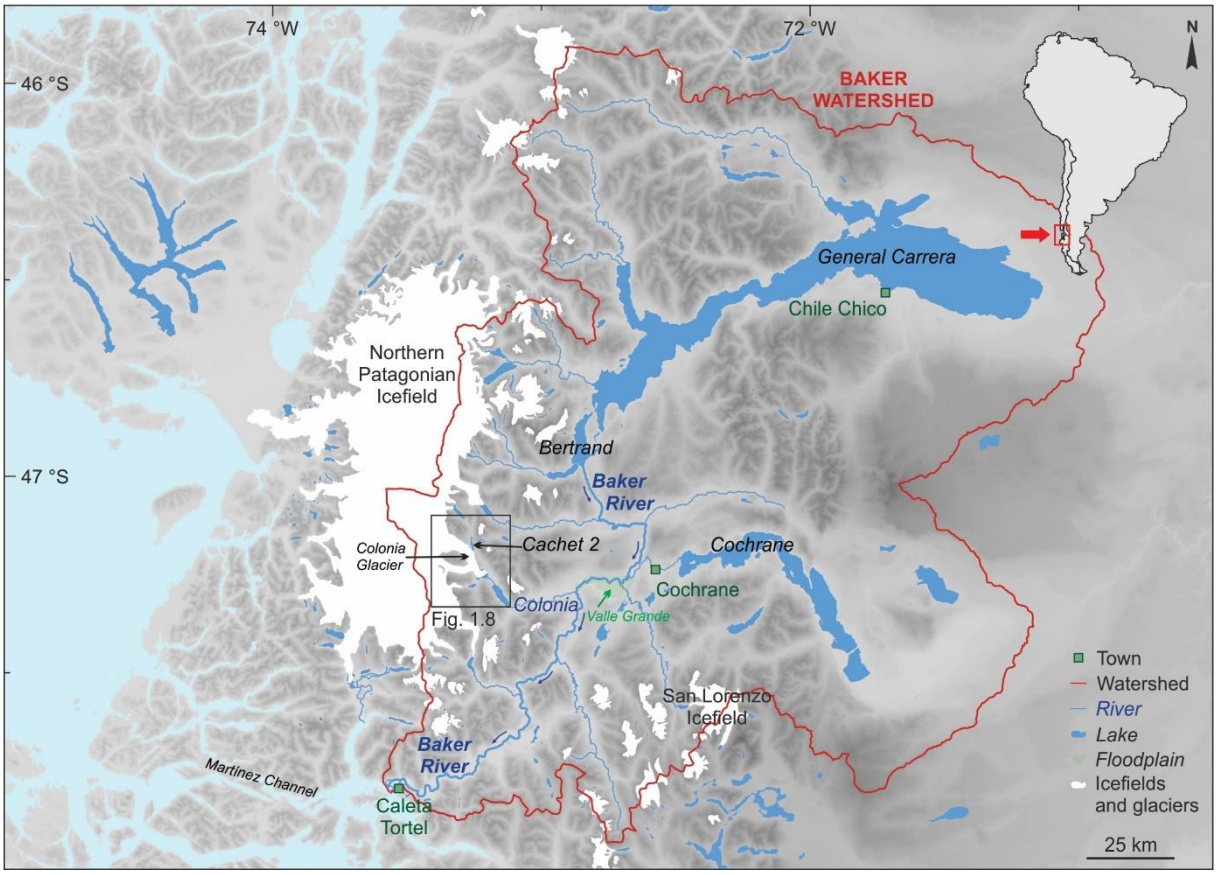

Figure 1.7. Location of Cachet 2 Lake and Colonia River in the Baker River watershed.

The 21st century Cachet 2 GLOFs were not the only GLOFs that affected the Baker River. Between 1881 and the 1960s, for example, the Colonia valley also experienced repeated GLOFs caused by water drainage from Arco Lake, which used to be dammed by Colonia Glacier (Fig. 1.8; Tanaka, 1980; Winchester and Harrison, 2000; Dussaillant et al., 2010; Jacquet et al., 2017). Arco GLOFs frequently occurred until a stable drainage path was established in the 1960s (Winchester and Harrison, 2000).

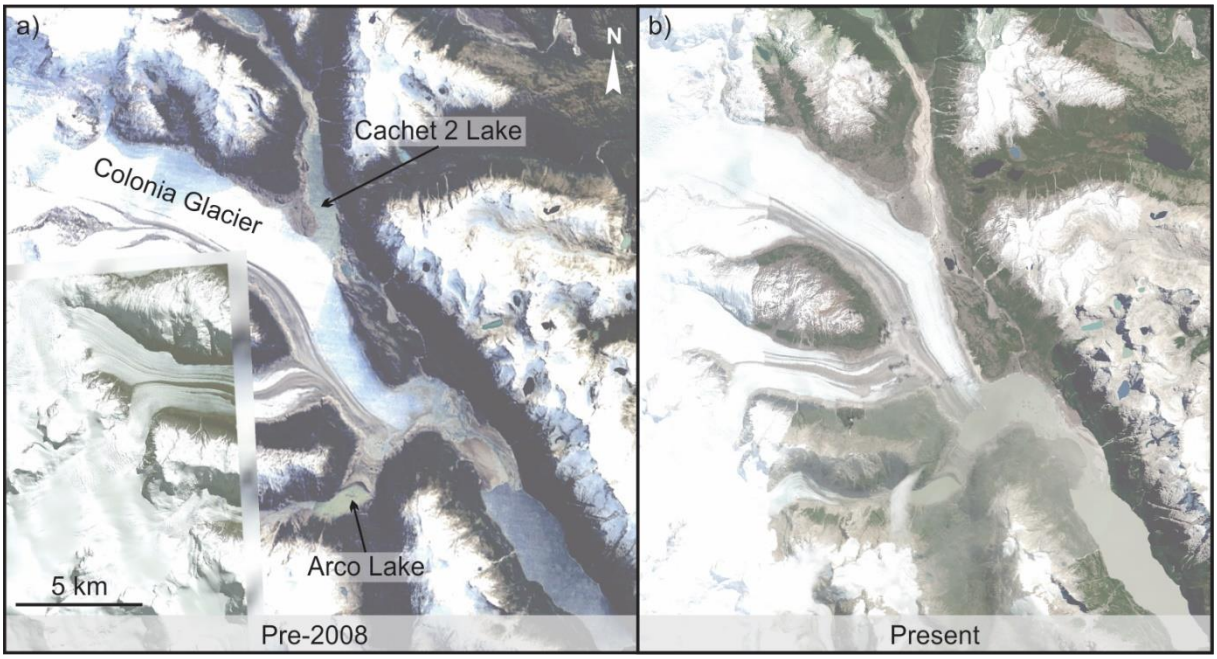

Figure 1.8. Recent GLOF occurrence in the Colonia valley (Chilean Patagonia, 47.3 °S). **(a)** Ice-dammed Cachet 2 Lake before the start of the 2008–2020 GLOF sequence (Landsat image; Global Mapper World Imagery). **(b)** Present day situation (Google Earth). The location of Arco Lake, which is at the origin of Colonia River GLOFs between 1881 and the 1960s, is also indicated.

Although the Baker River experienced 23 GLOFs between 2008 and 2020 due to the emptying of Cachet 2 Lake, no GLOFs were documented between the 1968 and 2008 (Dussaillant et al., 2010). Whether this apparent increase in GLOFs is real or simply the result of a lack of data and knowledge about GLOFs is currently unknown. The re-occurrence of GLOFs after an apparent 40-year long period of quiescence makes the Baker region particularly well suited to study the impact of climate change on GLOF frequency. This apparent increase has also reinvigorated discussions about the potential relationship between climate change and GLOF occurrence (Casassa et al., 2010; Kargel et al., 2012). However, there is currently no conclusive answer to how climate change and GLOF occurrence are linked to each other, mainly due to a lack of continuous flood records on long timescales.

1.5. Research questions

With this in mind, this thesis addresses three main research questions with the ultimate objective to understand if there is a relationship between GLOF occurrence and climate variability in Patagonia.

1. **How are Baker River GLOFs recorded in fjord sediments?**

GLOFs are amongst the most extreme discharge events in glacierized regions worldwide. Although their deposits have been investigated in lake settings (e.g. Xu et al., 2015; Røthe et al., 2019), how the sediment reaching and deposited in fjords during GLOFs differs from the background sediments remains

mostly unknown. In lakes, GLOFs result in event deposits that can be finer or coarser than the background sediment depending on the specific setting of each lake (e.g. Boes et al., 2018; Røthe et al., 2019). The only GLOF sediments that have been examined in a marine environment are those of Disenchantment Bay, an Alaskan tidewater glacier fjord, where the signature of the GLOF deposits is variable and ambiguous (Willems et al., 2011).

How Baker River GLOFs are recorded in fjord sediments is addressed in chapters 4 and 5. Chapter 4 presents the bathymetry of the head of Martínez Channel, i.e. the fjord at the outflow of the Baker River, and attempts to identify the processes that have shaped the fjord's subaquatic morphology. A suite of ten sediment cores collected in the same fjord is then examined to determine the GLOF signature in fjord sediments (Chapter 5).

2. How are Baker River GLOFs recorded in terrestrial and historical archives?

In addition to the fjord sediments investigated in the first question above, terrestrial and historical archives also have the potential to hold Baker River GLOF records. In the literature, the only existing data comprises fragmentary reports of GLOF occurrence in the Colonia valley (Oportus, 1928; De Agostini, 1945), dendrochronological, and lichenometric evidence (Tanaka, 1980; Winchester and Harrison, 2000), and discharge data of the Baker River, which only started to be monitored in 1963. In addition, slackwater deposits composed of light grey sand and silt have been used to identify the largest Baker River GLOFs that occurred after the Last Glacial Maximum (LGM) (Benito et al., 2014; 2021; Benito and Thorndycraft, 2020).

The potential of terrestrial and historical archives is addressed in chapters 6 and 7. In chapter 6, sediments from the Valle Grande floodplain along the upper Baker River are used to reconstruct GLOF occurrence during the late Holocene. In chapter 7, results from additional geological and historical archives are investigated and discussed.

3. Is there a relationship between GLOF occurrence and glacier and climate variability during the late Holocene?

To understand the possible impact of glacier variability, and ultimately climate change, on GLOF occurrence, our flood records are compared to existing multi-archive reconstructions of precipitation, temperature, and glacier variability. This third objective, which focuses on evaluating the potential link between GLOF occurrence and climate variability, is addressed in chapters 6 and 7.

References

Abram, N., Gattuso, J.-P., Prakash, A., Cheng, L., Chidichimo, M.P., Crate, S., Enomoto, H., Garschagen, M., Gruber, N., Harper, S., Holland, E., Kudela, R.M., Rice, J., Steffen, K., and von Schuckmann, K. (2019) Framing and Context of the Report. In: IPCC Special Report on the Ocean and Cryosphere in a Changing Climate [Pörtner, H.-O., Roberts, D.C., Masson-Delmotte, V., Zhai, P., Tignor, M., Poloczanska, E., Mintenbeck, K., Alegría, A., Nicolai, M., Okem, A., Petzold, J., Rama, B., Weyer, N.M. (eds.)], 60 pp.

Aniya, M. (2017) Glacier variations of Hielo Patagónico Norte, Chile, over 70 years from 1945 to 2015. *Bulletin of Glaciological Research*, **35**, 19 – 38.

Baker, V.R. (1973) Palaeohydrology and sedimentology of Lake Missoula flooding in eastern Washington. *Geological Society of America Special Publication*, **144**, 1 – 79.

Bazai, N.A., Cui, P., Carling, P.A., Wang, H., Hassan, J., Liu, D., Zhang, G., and Jin, W. (2021) Increasing glacial lake outburst flood hazard in response to surge glaciers in the Karakoram. *Earth-Science Reviews*, **212**, 103432.

Benito, G., Thorndycraft, V.R. Machado, M.J., Sancho, C., Dussaillant, A., and Meier, C.I. (2014). Magnitud y frecuencia de inundaciones Holocenas generadas por vaciamiento de lagos glaciares en el Rio Baker, Campo de Hielo, Patagonico Norte, Chile. In: Schnabel, S., Gutiérrez, Á.G. (Eds.), Sociedad Española de Geomorfología. Cáceres, Spain, pp. 24–27.

Benito, G., and Thorndycraft, V.R. (2020). Catastrophic glacial-lake outburst flooding of the Patagonian Ice Sheet. *Earth-Science Reviews,* **200**, 102996.

Benito, G., Thorndycraft, V.R., Medialdea, A., Machado, M.J., Sancho, C., and Dussaillant, A. (2021) Declining discharge of glacial lake outburst floods through the Holocene in central Patagonia. *Quaternary Science Reviews*, **265**, 106810.Benn, D.I., Wiseman, S., and Hands, K.A. (2001) Growth and drainage of supraglacial lakes on the debris-mantled Ngozumpa Glacier, Khumbu Himal, Nepal. *Journal of Glaciology*, **47**(159), 626 – 638.

Benn, D.I., Kirkbride, M.P., Owen, L.A., and Brazier, V. (2003) Glaciated valley landsystems. *In: Evans, D.J.A. (Ed.). Glacial landsystems*. Arnold, London, 372 – 406.

Benn, D.I., and Evans, D.J.A. (2010) Glacial lakes and outburst floods. *In: Glaciers and glaciation*. vol. 2 Hodder education, London, pp. 86 – 96.

Björnsson, H. (2002) Subglacial lakes and jökulhaups in Iceland. *Global and Planetary Change*, **35**, 255 – 271.

Boes, E., Van Daele, M., Moernaut, J., Schmidt, S., Jensen, B.J.L., Praet, N., Kaufman, D., Haeussler, P., Loso, M.G., and De Batist, M. (2018) Varve formation during the past three centuries in three large proglacial lakes in south-central Alaska. *Geological Society of America Bulletin*, **130**, 757 – 774.

Burton, J.W., Chambers, F.B., Sincavage, R., and Cross, M.D. (2020) Analysis of glacial lake outburst flood terrain and sedimentary deposits in valle soler, Northern Patagonia Icefield. *Physical Geography*

Byers, A.C., Rounce, D.R., Shugar, D.H., Lala, J.M., Byers, E.A., and Regmi, D. (2019) A rockfall-induced glacial lake outburst flood, Upper Barun Valley, Nepal. *Landslides*, **16**, 533 – 549.

Carrivick, J.L. (2007) Modelling coupled hydraulics and sediment transport of a high-magnitude flood and associated landscape change. *Annals of Glaciology*, **45**, 143 – 154.

Carrivick, J.L., and Tweed, F.S. (2013) Proglacial lakes: character, behavior and geological importance. *Quaternary Science Reviews*, **78**, 34 – 52.

Carrivick, J.L., and Quincey, D.J. (2014) Progressive increase in number and volume of ice-marginal lakes on the western margin of the Greenland Ice Sheet. *Global and Planetary Change*, **116**, 156 – 163.

Carrivick, J.L., and Tweed, F.S. (2016) A global assessment of the societal impacts of glacier outburst floods. *Global and Planetary Change*, **144**, 1 – 16.

Casassa, G., Wendt, J., Wendt, A., López, P., Schuler, T., Maas, H.G., Carrasco, J., and Rivera, A. (2010) Outburst floods of glacial lakes in Patagonia: is there an increasing trend? Geophysical Research Abstracts, **12**, EGU General Assembly.

Cenderelli, D.A., and Wohl, E.E. (2003) Flow hydraulics and geomorphic effects of glacial lake outburst floods in the Mount Everest region, Nepal. *Earth Surface Processes and Landforms*, **28**, 385 – 407.

Chen, Y., Xu, C., Chen, Y., Li, W., and Liu, J. (2010) Response of glacial-lake outburst floods to climate change in the Yarkant River basin on northern slope of Karakoram Mountains, China. *Quaternary International*, **226**, 75 – 81.

Chinni, G.A., and Warren, C.R. (2004) The 2004 outburst flood at Glaciar Perito Moreno, Argentina. *Journal of Glaciology*, **50**, 615 – 616.

Clague, J.J., and Evans, S.G. (2000) A review of catastrophic drainage of moraine-dammed lakes in British Columbia. *Quaternary Science Reviews*, **19**, 1763 – 1783.

Clarke, G.K., Bush, A.B., and Bush, J.W. (2009) Freshwater discharge, sediment transport, and modelled climate impacts of the final drainage of glacial Lake Agassiz. *Journal of Climate*, **22**, 2161 – 2180.

Cook, S.J., Kougkoulos, I., Edwards, L.A., Dortch, J., and Hoffmann, D. (2016) Glacier change and glacial lake outburst flood risk in the Bolivian Andes. *The Cryosphere*, **10**, 2399 – 2413.

Costa, J.E., and Schuster, R.L. (1988) The formation and failure of natural dams. *Geological Society of America Bulletin*, **100**, 1054 – 1068.

Craigmile, M.N. (2018) Climate change and GLOFs: A Multi-Locational Meta-Analysis on the Peak Discharge and Flood Volume of Glacial Lake Outburst Floods. *Senior Independent Study Theses.* Paper 7952.

Davies, T.R.H., Smart, C.C., and Turnbull, J.M. (2003) Water and sediment outbursts from advanced Franz Josef Glacier, New Zealand. *Earth Surface Processes and Landforms*, **28**, 1081 – 1096.

Davies, B.J., and Glasser, N.F. (2012) Accelerating shrinkage of Patagonian glaciers from the Little Ice Age (~AD 1870) to 2011. *Journal of Glaciology*, **58** (212), 1063 – 1084.

De Agostini, A.S.S. (1945) Andes Patagonicos, Viajes de exploración a la Cordillera Patagonica Austral. Segunda edición aumentada y corregida. Buenos Aires. 436 pp.

Dussaillant, A., Benito, G., Buytaert, W., Carling, P., Meier, C., and Espinoza, F. (2010) Repeated glacial-lake outburst floods in Patagonia: an increasing hazard? *Natural hazards*, **54**, 469 – 481.

Eisbacher, G.H., and Clague, J.J. (1984) Destructive mass movements in high mountains: hazards and management. *Geological Survey of Canada Paper*, 84 – 16, 230 pp.

Goodsell, B., Anderson, B., Lawson, W.J., and Owens, I.F. (2005) Outburst flooding at Franz Josef Glacier, South Westland, New Zealand. *New Zealand Journal of Geology and Geophysics*, 48, 95 – 104.

Haeberli, W. (1983) Frequency and characteristics of glacier Roods in the Swiss Alps. *Annuals of Glaciology*, 4, 85– 90.

Harrison, S., Glasser, N., Winchester, V., Haresign, E., Warren, C., and Jansson, K. (2006) A glacial lake outburst flood associated with recent mountain glacier retreat, Patagonian Andes. *The Holocene*, 16, 611 – 620.

Harrison, S., Kargel, J.S., Huggel, C., Reynolds, J., Shugar, D.H., Betts, R.A., Emmer, A., Glasser, N., Haritashya, U.K., Klimeš, J., Reinhardt, L., Schaub, Y., Wilshire, A., Regmi, D., and Vilímek, V. (2018) Climate change and the global pattern of moraine-dammed glacial lake outburst floods. *The Cryosphere*, 12, 1195 – 1209.

Hauser, A. (1993) Remociones en massa en Chile. *Servicio Nacional de Geología y Mineria de Chile Boletín*, 45, 75 pp.

IPCC (2014) Climate Change 2014: Synthesis Report. Contribution of Working Groups I, II, and III to the Fifth Assessment Report of the Intergovernmental Panel of Climate Change [Core Writing Team, Pachauri, R.K. and Meyer, L.A. (eds.)]. IPCC, Geneva, Switzerland, 151 pp.

IPCC (2018) Global warming of 1.5 °C. An IPCC Special Report on the impacts of global warming of 1.5°C above pre-industrial levels and related global greenhouse gas emission pathways, in the context of strengthening the global response to the threat of climate change, sustainable development, and efforts to eradicate poverty [Masson-Delmotte, V., P. Zhai, H.-O. Pörtner, D. Roberts, J. Skea, P.R. Shukla, A. Pirani, W. Moufouma-Okia, C. Péan, R. Pidcock, S. Connors, J.B.R. Matthews, Y. Chen, X. Zhou, M.I. Gomis, E. Lonnoy, T. Maycock, M. Tignor, and T. Waterfield (eds.)], 630 pp.

IPCC (2019) IPCC Special Report on the Ocean and Cryosphere in a Changing Climate. *Intergovernmental Panel on Climate Change*, 765 pp.

Iribarren Anacona, P., Norton, K.P., and Mackintosh, A. (2014) Moraine-dammed lake failures in Patagonia and assessment of outburst susceptibility in the Baker Basin. *Natural Hazards and Earth System Sciences*, 14, 3243 – 3259.

Iribarren Anacona, P., Mackintosh, A., and Norton, K (2015) Reconstruction of a glacial lake outburst flood (GLOF) in the Engaño Valley, Chilean Patagonia: Lessons for GLOF risk management. *Science of the Total Environment*, 527-528, 1 –11.

Jacquet, J., McCoy, S.W., McGrath, D., Nimick, D.A., Fahey, M., O'kuinghttons, J., Friesen, B.A., and Leidlich, J. (2017) Hydrologic and geomorphic changes resulting from episodic glacial lake outburst floods: Rio Colonia, Patagonia, Chile. *Geophyscial Research Letters*, 44, 854 – 864.

Kargel, J.S., Alho, P., Buytaert, W., Célleri, R., Cogley, J.G., Dussaillant, A., Guido, Z., Haeberli, W., Harrison, S., Leonard, G., Maxwell, A., Meier, C.I., Poveda, G., Reid, B., Reynolds, J.M., Portocarrero, C., Romero, H., and Schneider, J.F. (2012) Glaciers in Patagonia: Controversy and prospects. Eos Transactions American Geophysical Union, AGU 93 (22), 212.

Komatsu, G., Arzhannikov, S.G., Gillespie, A.R., Burke, R.M., Miyamoto, H., and Baker, V.R. (2009) Quaternary paleolake formation and cataclysmic flooding along the upper Yenisei River. *Geomorphology*, 104, 143–164.

Lliboutry, L. Morales, A.B., Pautre, A., and Schneider, B. (1977) Glaciological problems set by the control of dangerous lakes in Cordillera Blanca, Peru. Historic failures of morainic dams, their causes and prevention. *Journal of Glaciology*, 18, 239 – 254.

Lopez, P., Chevallier, P., Favier, V., Pouyaud, B., Ordenes, F., and Oerlemans, J. (2010) A regional view of fluctuations in glacier length in southern South America. *Global and Planetary Change*, 71, 85 – 108.

Loriaux, T., and Casassa, G. (2013) Evolution of glacial lakes from the Northern Patagonian Icefield and terrestrial water storage in a sea-level rise context. *Global and Planetary Change*, 102, 33 – 40.

Mayo, L.R. (1989) Advances of Hubbard Glacier and 1986 outburst of Russell Fjord, Alaska, U.S.A. *Annals of Glaciology*, 13, 189 – 194.

Nadeem, S., Elahi, I., Hadi, A., and Uddin, I. (2012) Traditional knowledge and local institutions support adaptation to water-induced hazards in Chitral, Pakistan. ICIMOD, Kathmandu, 51 pp.

Nerem, R.S., Beckley, B.D., Fasullo, J.T., Hamlington, B.D., Masters, D., and Mitchum, G.T. (2018) Climate-change-driven accelerated sea-level rise detected in the altimeter era. *Proceedings of the National Academy of Sciences*, 115, 201717312.

Oportus, C. (1928) Informe sobre el problema de colonización de la zona del río Baker. Departamento de Tierras y Colonización, Ministerio de Fomento, Santiago de Chile.

Oppenheimer, M., Glavovic , B.C., Hinkel, J., van de Wal, R., Magnan, A.K., Abd-Elgawad, A., Cai, R., Cifuentes-Jara, M., DeConto, R.M., Ghosh, T., Hay, J., Isla, F., Marzeion, B., Meyssignac, B., and Sebesvari, Z. (2019) Sea Level Rise and Implications for Low-Lying Islands, Coasts and Communities. In: IPCC Special Report on the Ocean and Cryosphere in a Changing Climate [Pörtner, H.-O., Roberts, D.C., Masson-Delmotte, V., Zhai, P., Tignor, M., Poloczanska, E., Mintenbeck, K., Alegría, A., Nicolai, M., Okem, A., Petzold, J., Rama, B., Weyer, N.M. (eds.)], 765 pp.

Paul, F., Kääb, A., and Haeberli, W. (2007) Recent glacier changes in the Alps observed by satellite: Consequences for future monitoring strategies. *Global and Planetary Change*, 56, 111 – 122.

Peña, H., and Escobar, F. (1983) Análisis de una crecida por vaciamiento de una represa glacial. *Actas, VI Congreso Nacional, Sociedad Chilena de Ingeniería Hidráulica*, 375 – 392.

Quiroga, E., Ortiz, P., Gerdes, D., Reid, B., Villagran, S., and Quiñones, R. (2011) Organic enrichment and structure of macrobenthic communities in the glacial Baker Fjord, Northern Patagonia, Chile. *Journal of the Marine Biologial Association of the United Kingdom*, 92(1), 73 – 83.

Richardson, S.D., and Reynolds, J.M. (2000) An overview of glacial hazards in the Himalayas. *Quaternary International*, 65/66, 31 – 47.

Røthe, T.O., Bakke, J., and Støren, E.W.N. (2019) Glacier outburst floods reconstructed from lake sediments and their implications for Holocene variations of the plateau glacier Folgefonna in western Norway. *Boreas*, 48, 616 – 634.

Round, V., Leinss, S., Huss, M., Haemmig, C., and Hajnsek, I. (2017) Surge dynamics and lake outbursts of Kyagar Glacier, Karakoram. *The Cryosphere*, **11**, 723 – 739.

Russell, A.J. (1989) A comparison of two recent jökulhaups from an ice-dammed lake, Søndre Strømfjord, West Greenland. *Journal of Glaciology*, **35**, 157 – 162.

Seneviratne, S.I., Nicholls, N., Easterling, D., Goodess, C.M., Kanae, S., Kossin, J., Luo, Y., Marengo, J., McInnes, K., Rahimi, M., Reichstein, M., Sorteberg, A., Vera, C., and Zhang, X. (2012) Changes in climate extremes and their impacts on the natural physical environment. In: Managing the Risks of Extreme Events and Disasters to Advance Climate Change Adaptation.A Special Report of Working Groups I and II of the Intergovernmental Panel on Climate Change [Field, C.B., Barros, V., Stocker, T.F., Qin, D., Dokken, D.J., Ebi, K.L., Mastrandrea, M.D., Mach, K.J., Plattner, G.-K., Allen, S.K., Tignor, M., and Midgley, P.M. (eds.)]. Cambridge University Press, Cambridge, UK and New York, NY, USA, 109-230 pp.

Shugar, D.H., Burr, A., Haritashya, U.K., Kargel, J.S., Watson, C.S., Kennedy, M.C., Bevington, A.R., Betts, R.A., Harrison, S., and Strattman, K. (2020) Rapid worldwide growth of glacial lakes since 1990. *Nature Climate Change*, **10**, 939 – 945.

Tanaka, K. (1980) Geographic contribution to a periglacial study of the Hielo Patagonico Norte with special reference to the glacial outburst originated from Glacier-Dammed Lago Arco, Chilean Patagonia. Centre Co Ltd, Tokyo, 97 pp.

Teller, J.T. (1995) The impact of large ice sheets on continental paleohydrology. In: Gregory, K., Baker, V., Starkel, L. (Eds.), Global Continental Paleohydrology. Wiley, New York, pp. 109–129

Thorarinsson, S. (1939) The ice-dammed lakes of Iceland with particular reference to their values as indicators of glacier oscillations. *Geografiska Annaler*, **21**, 216 – 242.

Tweed, F.S., and Russell, A.J. (1999) Controls on the formation and sudden drainage of glacier-impounded lakes: implications for jökulhlaup characteristics. *Progress in Physical Geography*, **23**, 79 – 110.

Veh, G., Korup, O., von Specht, S., Roessner, S., and Walz, A. (2019) Unchanged frequency of moraine-dammed glacial lake outburst floods in the Himalaya. *Nature Climate Change*, **9**, 379 – 383.

Velicogna, I., Mohajerani, Y.A.G., Landerer, F., Mouginot, J., Noel, B., Rignot, E., Sutterly, T., van den Broeke, M., van Wessem, M., and Wiese, D. (2020) Continuity of ice sheet mass loss in Greenland and Antarctica from the GRACE and GRACE Follow-On missions. *Geophysical Research Letters*, **47**, e2020GL087291.

Vivian, R. (2001) Des Glaciers du Faucigny aux Glaciers de Mont Blanc. La Fontaine de Siloe, Montmelian.

Walder, J.S., and Costa, J.E. (1996) Outburst floods from glacier-dammed lakes: the effect of mode of lake drainage on flood magnitude. *Earth Surface Processes and Landforms*, **21**, 701 – 723.

Wang, W., Yao, T., and Yang, X. (2011) Variations of glacial lakes and glaciers in the Boshula mountain range, southeast Tibet, from the 1970s to 2009. *Annuals of Glaciology*, **52**, 9 – 17.

Westoby, M.J., Glasser, N.F., Brasington, J., Hambrey, M.J., Quincey, D.J., and Reynolds, J.M. (2014) Modelling outburst floods from moraine-dammed glacial lakes. *Earth Science Reviews*, **134**, 137 – 159.

Willems, B.A., Powell, R.D., Cowan, E.A., and Jaeger, J.M. (2011) Glacial outburst flood sediments within Disenchantment Bay, Alaska: Implications of recognizing marine jökulhaup deposits in the stratigraphic record. *Marine Geology*, **284**, 1 – 12.

Wilson, R., Glasser, N.F., Reynolds, J.M., Harrison, S., Anacona, P.I., Schaefer, M., and Shannon, S. (2018) Glacial lakes of the Central and Patagonian Andes. *Global and Planetary Change*, **162**, 275 – 291.

Wilson, R., Harrison, S., Reynolds, J., Hubbard, A., Glasser, N.F., Wündrich, O., Iribarren Anacona, P., Mao, L., and Shannon, S. (2019) The 2015 Chileno Valley glacial lake outburst flood, Patagonia. *Geomorphology*, **332**, 51 – 65.

Winchester, V., and Harrison, S. (2000) Dendrochronology and lichenometry: colonization, growth rate and dating of geomorphological events on the east side of the North Patagonian Icefield, Chile. *Geomorphology*, **34**, 181 – 194.

Xu, M., Bogen, J., Wang, Z., Bønsnes, T.E., and Gytri, S. (2015) Pro-glacial lake sedimentation from jökulhaups (GLOF), Blåmannsisen, northern Norway. *Earth Surface Processes and Landforms*, **40**, 654 – 665.

Zalasiewicz, J., and Williams, M. (2016) Climate change through Earth's history. In: Letcher, T.M. (Ed.) Climate change, observed Impacts on Planet Earth, second edition. p. 3 – 17.

2. Setting

2.1. Baker River

The Baker River is located in Chilean Patagonia (47–48 °S; Fig. 2.1). It is the largest river in Chile in terms of mean annual discharge (~1100 m³/s; Dussaillant et al., 2012) and it drains most of the eastern side of the NPI. Its watershed, which runs across the border between Chile and Argentina, covers an area of approximately 30,000 km². The watershed can be divided in the upper and lower Baker River watersheds as most sediments in the upper Baker River watershed are trapped in lakes General Carrera and Cochrane and do not reach the Baker River itself.

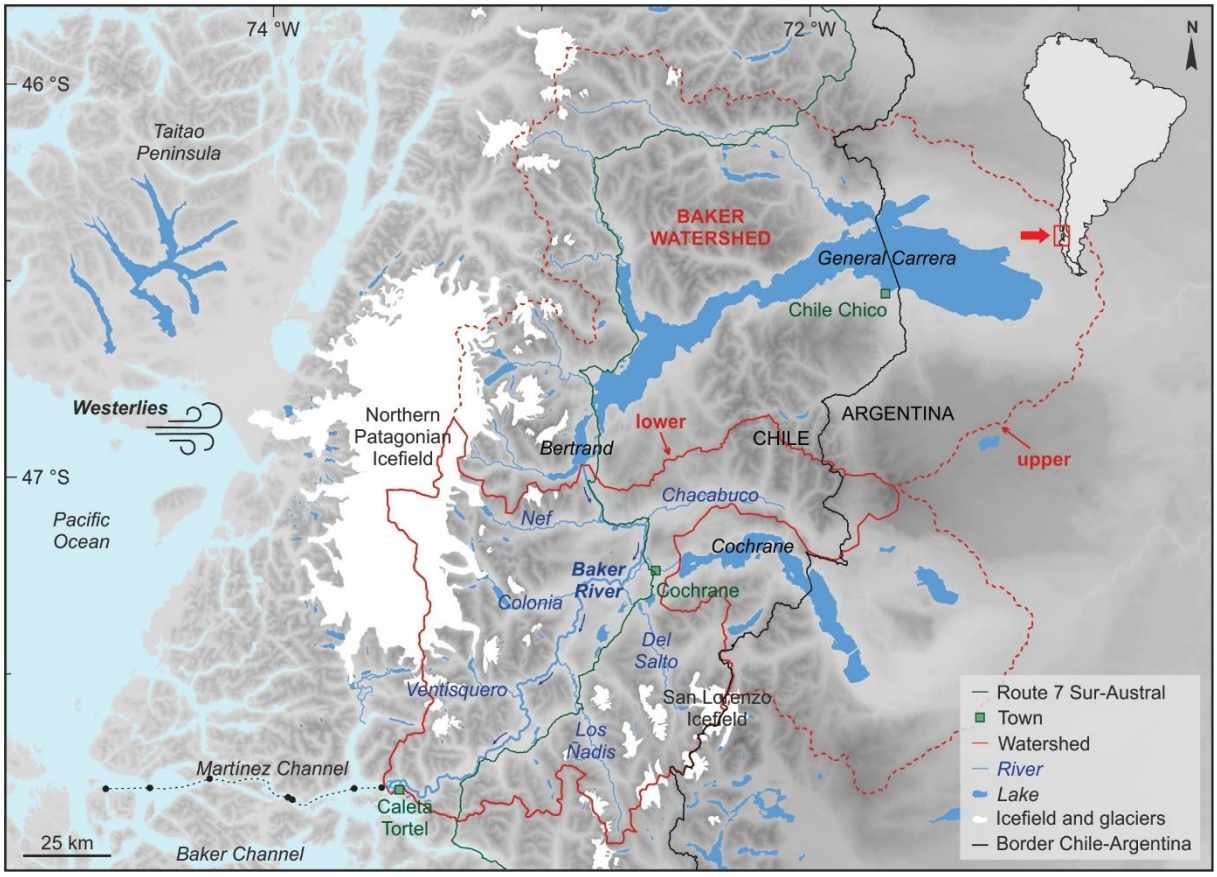

Figure 2.1. Location of the Baker River and its watershed in Chilean Patagonia along the eastern side of the NPI. The background image is a grey-scale SRTM digital elevation model. Dashed red lines and solid red lines represent the upper and lower Baker River watersheds, respectively. Locations of CTD stations in the Martínez Channel investigated during the October 2014 COPAS Sur-Austral campaign, which were used to construct cross-sections of temperature and salinity (shown in Fig. 2.2) (Rebolledo et al., 2019), are indicated with black dots.

The Baker River originates at Bertrand Lake, which is fed by General Carrera Lake, and continues to flow southwards along the NPI (Fig. 2.1). Its main tributaries are, from north to south, Nef, Chacabuco, Del Salto, Colonia, De Los Ñadis, and Ventisquero rivers. The proglacial rivers Nef, Colonia, and Ventisquero receive meltwater from NPI outlet glaciers on the western side of the watershed, whereas Chacabuco, Del Salto, and De Los Ñadis rivers drain the eastern part of the watershed, where the Del Salto and De Los Ñadis rivers receive meltwater from small mountain glaciers. The Baker River has a glacial regime due to the input of meltwater, and discharge varies seasonally between 600 m³/s in winter and 1200 m³/s in summer (Dussaillant et al., 2012). West of the town of Caleta Tortel, the Baker River flows into the Martínez Channel where a large fan-shaped delta, covering approximately 14 km², is formed. The

specific properties of the Baker River watershed, i.e. river originating at the large General Carrera Lake, mixture of glacial and non-glacial tributaries, varied topography, and temperate climate, make the hydrological regime of the Baker River relatively unique.

2.2. Oceanography of the Baker-Martínez fjord system

Oceanographic processes in the Baker-Martínez fjord system, which connects the terrestrial environments of Patagonia with the Pacific Ocean, are dominated by sharp vertical and horizontal gradients in both salinity and temperature (Sievers and Silva, 2008). Once the Baker River enters the Martínez Channel, it forms a relatively thin buoyant plume of low salinity waters on top of the salty warmer water mass from the Pacific Ocean (Fig. 2.2). The structure of this two-layer flow circulation that characterizes the Baker-Martínez fjord system varies seasonally according to river discharge, and the thickness and surface velocity of the buoyant plume increases, i.e. reaching up to 20–30 m (Sievers and Silva, 2008; Rebolledo et al., 2019) and 20 cm/s (Ross et al., 2014), respectively, during summer due to glacier and snowmelt (Iriarte et al., 2014).

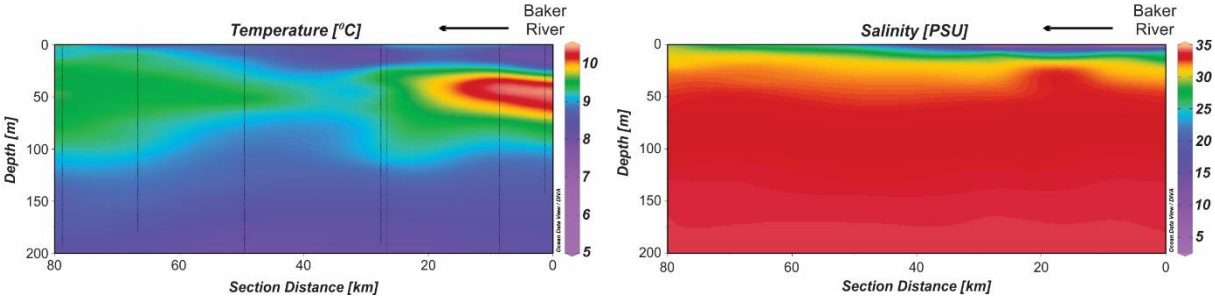

Figure 2.2. The two-layer flow circulation shown by cross-sections of temperature and salinity in Martínez Channel based on CTD measurements (see Fig. 2.1 for location) in October 2014 (austral spring; Rebolledo et al., 2019).

Studies in the Baker-Martínez fjord system have focused on marine biodiversity (e.g. Quiroga et al., 2016), and few studies have investigated sediment facies and accumulation through seismic profiling and sediment coring (e.g. DaSilva et al. 1997; Boldt, 2014). Therefore, very little is known about the sedimentary processes taking place in this fjord system, especially at the head of Martínez Channel. In fjord systems, the coarser bedload of the river is generally deposited onto the delta upon entering the fjord, whereas the finer particles transported in suspension are entrained in the buoyant plume where the sediment-laden water mixes with the salty water mass from the inward moving compensating current (Syvitski and Shaw, 1995). As the plume flows towards the ocean, suspended sediment settles in response to the increasing salinity, decreasing velocity, and due to flocculation, agglomeration, and palletization (Syvitski, 1991).

2.3. Present-day climate and vegetation

The climate of Patagonia is temperate with a strong seasonality in temperature and precipitation (Luebert and Pliscoff, 2006). Most precipitation in the Baker River watershed falls as snow during the austral fall and winter (Dussaillant et al., 2012). In the Baker River watershed, precipitation displays a strong longitudinal asymmetry driven by the orographic high of the Andes and the dominating humid Southern Westerly Wind Belt (SWWB) coming from the Pacific Ocean (Figs. 2.3 and 2.4a).

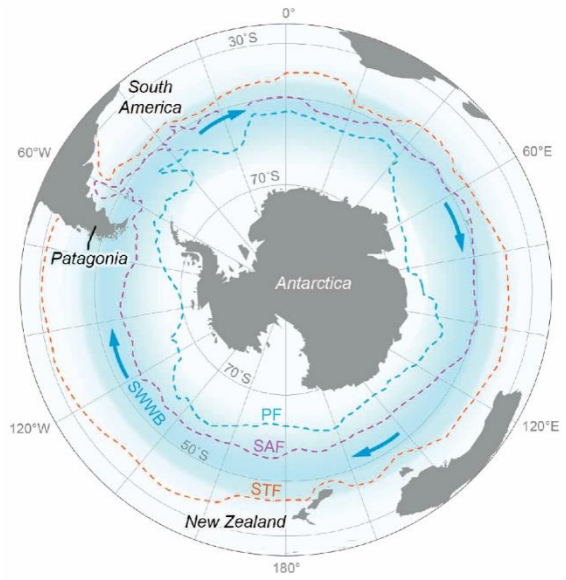

Figure 2.3. Map of the Southern Hemisphere with the approximate distribution of the Southern Westerly Wind Belt (SWWB) and oceanic polar fronts (PF: Polar Front, and SAF: sub-Antarctic Polar Front). The Subtropical Front (STF) is located at the northern limit of the SWWB (Davies et al., 2020).

On the western side of the Andes, a hyperhumid climate prevails due to the uplift of moist air originating from the Pacific with an annual precipitation up to 5000 mm (Miller, 1976; Garreaud et al., 2013). In contrast, forced subsidence rapidly decreases precipitation from up to 2000 mm/yr in the western part of the watershed to less than 300 mm/yr in the eastern part, where drier conditions prevail (Garreaud et al., 2013). The annual temperature in the Baker River watershed varies between 4 °C in austral winter (June to August) and 13 °C in austral summer (December to February) (Garreaud et al., 2013), and decreases with elevation (Fig. 2.4b).

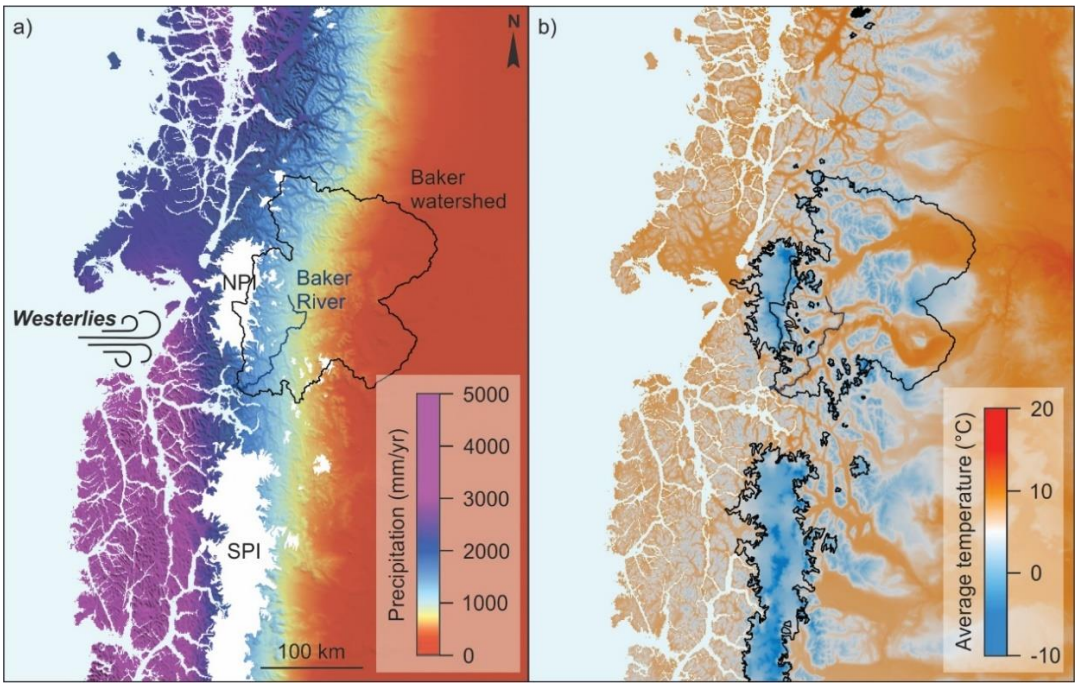

Figure 2.4. Climate in NW Patagonia. The two main icefields, i.e. NPI and SPI, and the Baker River and its catchment are indicated. **(a)** Annual precipitation and **(b)** average temperature between 1970–2000 (Fick and Hijmans, 2017).

Present-day vegetation distribution in the watershed mainly reflects the longitudinal precipitation gradient. In the western part of the watershed, vegetation is mainly composed of evergreen and deciduous forests with *Nothofagus betuloides* (Luebert and Pliscoff, 2006). At higher altitudes, vegetation is dominated by deciduous forest, consisting of *Nothofagus pumilio*. The arid landscape towards the east is dominated by gramineous steppe and shrubland with *Nothofagus antarctica* and *Festuca pallescens*.

2.4. Quaternary climate and glacier evolution of Patagonia

The mountainous region of Chilean Patagonia is characterized by a complex island and channel landscape that was formed by extensive glacial erosion. During the Quaternary, the NPI and SPI have contracted and expanded several times (Kaplan et al., 2004; Douglass et al., 2005; Harrison and Glasser, 2011), converging into the larger Patagonian Ice Sheet (PIS: 38–56 °S) during glacials (Caldenius, 1932). The PIS was at its maximum extent during the LGM, reaching the Pacific Ocean and extending far into the eastern forelands in Argentina (Fig. 2.5).

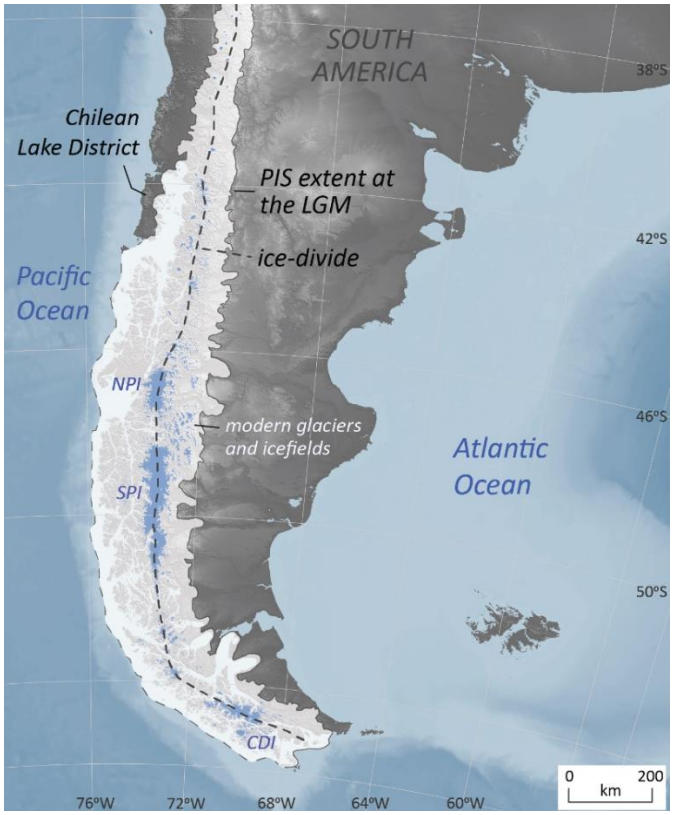

Figure 2.5. Modeled glacier cover of the PIS during the LGM compared to the present-day NPI, SPI, Cordillera Darwin Icefield (CDI), and other smaller glaciers, which are shown in light blue (Davies et al., 2020).

During the LGM, the Patagonian climate was about ~6 °C cooler (Kaplan et al., 2008), and Patagonian glacier fluctuations were controlled by variations in atmospheric temperature and precipitation, extent of Antarctic sea-ice cover, the internal characteristics of the icefields, atmospheric/oceanic coupling-induced climate variability, and latitudinal migration of the SWWB (Glasser et al., 2004).

Following the LGM, the SWWB and the warm Subtropical Front (STF) shifted southward towards Antarctica (Moreno et al., 2012; Lamy et al., 2007). At the same time, the temperature of coastal waters around Patagonia increased (Lamy et al., 2007) and precipitation decreased, resulting in the recession

of PIS glaciers around 18 cal kyr BP (Moreno et al., 2015; Bendle et al., 2019) (Fig. 2.6a–b). Towards the end of the deglaciation, the final phase of glacier recession and disintegration of the PIS into the NPI and SPI resulted in the opening of new drainage routes and the formation of many fjords and lakes (Figs. 2.5, 2.6a–b). Discharge of large quantities of ice and meltwater, which was initially directed eastwards into the Atlantic, was reorganized westwards towards the Pacific Ocean during a first drainage reversal prior to 15.3–15.0 cal kyr BP (Thorndycraft et al., 2019; Fig. 2.6b). Geomorphological records evidence that 10^3 km^3 of meltwater was released to the Pacific over at least six drainage events, where the final stages of lake drainage involved catastrophic outbursts along the Baker River valley (Thorndycraft et al., 2019; Benito and Thorndycraft, 2020; Fig. 2.6c–f).

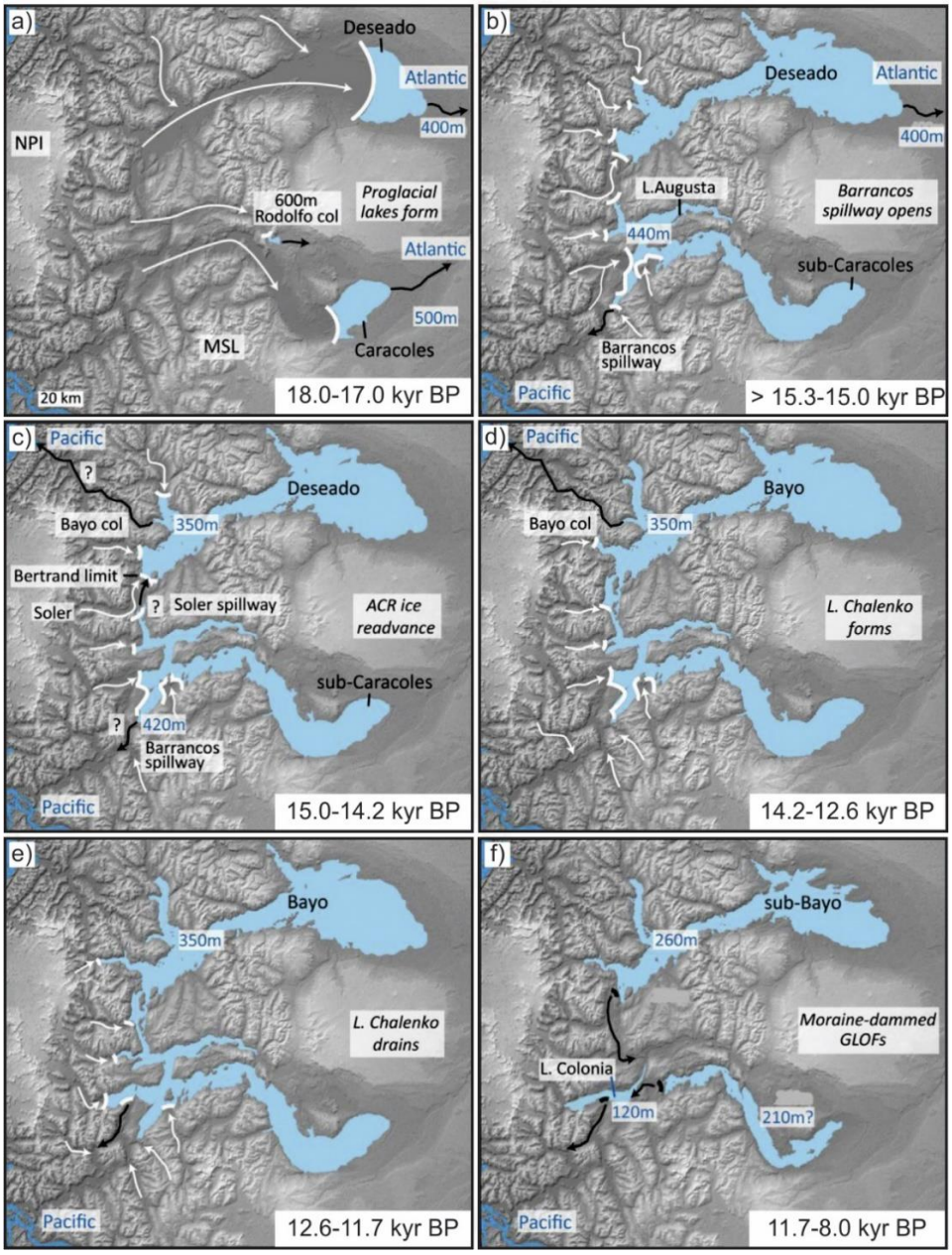

Figure 2.6. Paleolake evolution model during deglaciation of the NPI following the LGM (Modified after Thorndycraft et al., 2019). White and black arrows indicate main ice flow pathways and meltwater drainage routes, respectively. The glacier-lake margins and moraine-dam positions are shown with white and black lines, respectively.

Throughout the Holocene, it appears that both temperature and precipitation have significantly fluctuated (Glasser et al., 2004). Multiple proxy records indicate that the start of the Holocene in Chilean Patagonia was marked by an extended warm and dry period (e.g. Siani et al., 2010; Caniupán et al., 2011; Villa-Martinez et al., 2012; Mansilla et al., 2016; Moreno and Videla, 2016; Moreno et al., 2018a), coeval with a decrease in the strength of the SWWB (Moreno et al., 2018b). Atmospheric temperatures east of the Andes were about 2 °C above modern values in the period 8.5–6.5 cal kyr BP (Glasser et al., 2004). The period between 6.0–3.6 kyr cal BP on both sides of the Andes appears to have been colder and wetter than present (Glasser et al., 2004), coinciding with an increase in wind strength in central Patagonia (45 °S) (Van Daele et al., 2016), and with the onset of Holocene neoglaciations around 5.0 cal kyr BP (Glasser et al., 2004; Aniya, 2013; Moreno et al., 2018b). The late Holocene was generally characterized by centennial intervals of cold and wet climatic conditions, favorable for glacier growth (Moreno et al., 2018b), alternating with warmer and drier conditions (Davies et al., 2020).

Different chronologies of Holocene Neoglacial advances have been postulated (Fig. 2.7). The 'Mercer-type' identifies three Neoglacial advances at 5.2–4.5 cal kyr BP, 2.8–2.0 cal kyr BP, and the 17th–19th centuries, which is frequently associated with the LIA, based on dendrochronology and radiocarbon dates from moraines in front of SPI glacier margins and results from the Chilean Lake District, situated north of the Patagonian icefields (Mercer, 1982). According to Mercer (1970), the first Neoglacial advance between 5.2 and 4.5 cal kyr BP was the largest of the three Holocene advances. The 'Aniya-type' scheme contains four Neoglacial advances occurring around 4.0 cal kyr BP, 2.4–2.2 cal kyr BP, 1.6–0.9 cal kyr BP, and the 17th–19th centuries (Aniya, 1995, 1996). The latter scheme includes additional data from both SPI and NPI glaciers. Afterwards, a revised chronology was proposed by Aniya (2013), which included five Neoglaciations at 5.1–4.5 cal kyr BP, 4.0–3.6 cal kyr BP, 2.8–2.0 cal kyr BP, 1.6–0.9 cal kyr BP, and during the 17th–19th centuries.

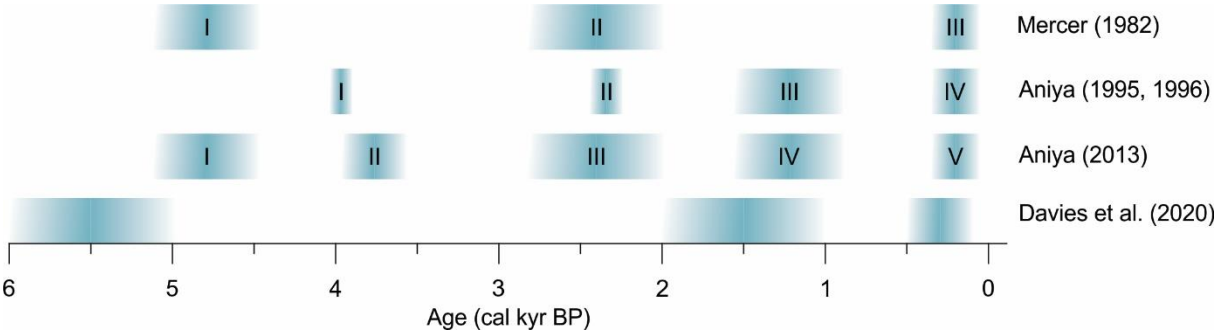

Figure 2.7. Neoglacial advances of Patagonian glaciers during the Mid- to Late Holocene, proposed by Mercer (1982), Aniya (1995, 1996), Aniya (2013) and Davies et al. (2020).

However, the existence of the Neoglaciation at 1.6–0.9 cal kyr BP has not yet been solidly confirmed in Patagonia, and its occurrence is only based on data from few study sites (three glaciers of the SPI and one glacier of the NPI; Aniya, 2013). Aniya (2013) stresses out that studies on the Holocene Neoglaciations of NPI glaciers in particular are very limited, and many moraines still have to be studied. Both the 'Mercer' and 'Aniya' chronologies are still considered equally valid, however, they should be regarded as broad regional trends as glacier advances have also been recorded outside these time periods (Glasser et al., 2004). Regional differences are expected to manifest. For example, the thorough review of glaciations of the Andes region during the past millennium by Masiokas et al. (2009) points out a regional contrast between the SPI and NPI: the maximum extent of NPI glaciers during Neoglaciation V occurred during the 19th century, whereas the maximum advance for SPI glaciers was

identified one to three centuries earlier. Since precipitation, which nourishes the icefields, is brought by the SWWB, the latitudinal shift and oscillations of the SWWB could explain the time lag between NPI and SPI glaciers (Aniya, 2013). The most recent review of Patagonian Ice Sheet evolution by Davies et al. (2020) suggests that Neoglacial advances or stabilizations occured at 6–5 cal kyr BP, 2–1 cal kyr BP, and 0.5–0.2 cal kyr BP (Fig. 2.7). Still, the NPI glacier Colonia shows evidence of an advance at 2.9 cal kyr BP (Nimick et al., 2016), which is in agreement with the 2.5 cal kyr BP-dated moraine formation of Leones glacier (NPI) (Harrison et al., 2008).

Although several re-advances have been identified after the last neoglaciation, a general recession of Patagonian glaciers has dominated this region until present times (Masiokas et al., 2009). Between 1870 and 2011, eastern NPI glaciers have lost an estimated 19.1 % of their total glacier surface area (Davies and Glasser, 2012). Similarly, smaller northern Patagonian mountain glaciers located to the East of the NPI that discharge into the Del Salto (e.g. San Lorenzo Icefield) and De Los Ñadis rivers (Fig. 2.1), generally retreated after the latest advance in the 17th–19th centuries (Davies and Glasser, 2012). Regional warming over most of the 20th century combined with a long-term decrease in precipitation have been proposed as possible forcing mechanisms behind the general recession trend (Rignot et al., 2003; Villalba et al., 2003).

2.5. Baker River floods

2.5.1. Late Quaternary GLOFs

The oldest evidence of GLOF occurrence in the Baker catchment dates back to ~12.6–11.7 cal kyr BP and is based on megaflood-type landform features (Benito and Thorndycraft, 2020). Following ice retreat after the Antarctic Cold Reversal (ACR), multiple catastrophic floods, with volumes around 100 km³, helped re-establish water discharge towards the Pacific Ocean via the Baker River (Turner et al., 2005; Glasser et al., 2016; Thorndycraft et al., 2019). These floods include the outburst of Chelenko Lake (~300 km³) (Fig. 2.6e), a palaeolake that unified General Carrera Lake and Cochrane Lake, and the final stages of lake drainage along the Baker valley (Thorndycraft et al., 2019; Benito and Thorndycraft, 2020; Fig. 2.6f). Slackwater deposits found immediately downstream the Baker Colonia confluence evidence the occurrence of additional paleofloods during the Holocene (Benito et al., 2014; Benito and Thorndycraft, 2020). At least eight floods were identified between 7.0 – 2.5 cal kyr BP, and at least three floods during the last 600 years, which were separated by a stable period between 2.5 – 0.6 cal kyr BP. Based on these slackwater deposits, Benito et al. (2021) suggested that flood magnitude decreased by two orders of magnitude throughout the Holocene.

2.5.2. Historical GLOFs

The first historical record of GLOF occurrence in the Baker River area starts from the early 1880s (Tanaka, 1980), and is related to the post-LIA retreat of Colonia Glacier between 1850 and 1880 (Harrison and Winchester, 2000). Due to this retreat, Arco Lake, which was dammed at the time by Colonia Glacier, abruptly emptied around 1881 and released approximately 265 x 10^6 m³ of water (Winchester and Harrison, 2000) (Fig. 2.8a). Afterwards, GLOFs regularly occurred due to outbursts from Arco Lake, with a minimum of 38 high lake levels, as suggested by a horizontal sequence of 38 sand and coarser sediments lining both valley sides (Winchester and Harrison, 2000). Based on dendrochronology and lichenometry, severe floods took place around 1896/1897, 1914/1917, 1944 and 1963 (Winchester and Harrison, 2000). In the late 1960s, a drainage path eventually established between Arco and Colonia lakes and outbursts appeared to have ceased (Winchester and Harrison, 2000; Dussaillant et al., 2010; Jacquet et al., 2017).

Figure 2.8. Photographic documentation of Arco Lake and Baker River GLOFs from the Colonia valley. **(a)** Oblique aerial view on Arco Lake in 1944 (Winchester and Harrison, 2000). **(b)** Evidence of an outburst event during the austral summer of 1945, which was able to uproot large trees and erode riverbanks of Colonia (De Agostini, 1945). **(c)** Aerial picture of the confluence of Colonia River and Baker River, taken two weeks after the abrupt drainage of Cachet 2 Lake in April 2008, which resulted in the inundation of the Valle Grande floodplain (Photo credit: Jonathan Leidich).

The Colonia GLOFs that occurred during the first half of the 20th century are documented and described in details by Carlos Oportus and Alberto M. de Agostini (Oportus, 1928; De Agostini, 1945) (Fig. 2.8b). These floods occurred regularly from January to February and formed a constant threat to the local communities and their cattle. During these GLOFs, originating from Arco Lake, the Baker River was pushed back 15 km upstream of the confluence with Colonia River due to the increased Colonia River discharge (Oportus, 1928; De Agostini, 1945). Within 24 hours, water levels in Baker River increased by at least 4 m and resulted in the complete inundation of the Valle Grande floodplain. Simultaneously with the Arco GLOF period, GLOFs from the Nef valley were also documented (Fig. 2.1) (Oportus, 1928; De Agostini, 1945). Although these outbursts also caused flooding of Valle Grande, the GLOFs from the Nef valley in the 1940s were of lower magnitude compared to those from the Colonia valley, and they only resulted in partial inundation of the floodplain (De Agostini, 1945). After an apparent 40-year long period of quiescence during which no Colonia GLOFs were documented, the Baker River experienced a new series of repeated GLOFs from the Colonia River since April 2008 (Dussaillant et al., 2010; Jacquet et al., 2017). All recent events resulted from the abrupt emptying of Cachet 2 Lake into the Colonia River, generally through a subglacial tunnel below the Colonia Glacier (Dussaillant et al., 2010; Friesen et al., 2015). Between GLOFs, the tunnel closes by ice creep, allowing the lake to refill (Dussaillant et al., 2010). During these lake outbursts, the Baker River discharge roughly triples, reaching between 3000 and 3800 m³/s, river water temperature drops by several degrees (Dussaillant et al., 2010) (Fig. 2.9), and large floodplains, including Valle Grande (Fig. 2.8c), inundate. Between April 2008 and November 2017, a total of 22 GLOFs have been recorded with a frequency of 1–3 per year (Jacquet et al., 2017; DGA, Chile). Another GLOF, yet relatively small, occurred in November 2020 due the emptying of Cachet 2 Lake, which resulted in an increase in Baker River discharge from around 700 to 1200 m³/s (DGA, Chile). Although most events (15 out of 23) occurred during spring and summer, and could potentially be related to increasing temperatures and ice melt, the exact trigger of these 21st century lake outbursts is still unclear.

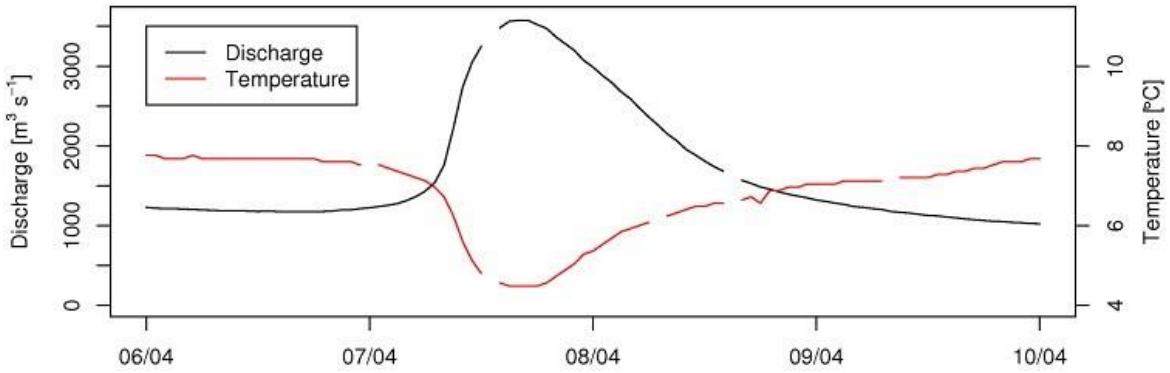

Figure 2.9. Discharge and water temperature just downstream the Baker-Colonia confluence during the April 2008 Cachet 2 GLOF (Figure from Dussaillant et al., 2010).

In addition to Arco and Cachet 2 lakes, a series of other proglacial lakes are also known to have triggered GLOFs in the Baker River watershed during the last decades. The most northern location of documented GLOF occurrence is Engaño Lake (Fig. 2.10a). In March 1977, the collapse of the moraine-dammed Engaño Lake released an estimated 12–13 x 10^6 m³ of water and debris, inundating the small village Bahía Murta Viejo, located 26 km downstream the failed lake (Iribarren Anacona et al., 2015). The 1977 Engaño GLOF destroyed many homes, farm and forestry land, and killed most livestock, forcing 126 inhabitants to move to the nearby, higher elevated, Bahía Murta Nuevo. Further south, the late 2000 GLOF in the Leones valley was triggered by rockfall in Calafate Lake that breached the moraine and displaced 2 x 10^6 m³ of debris downslope (Harrison et al., 2006) (Fig. 2.10b).

The largest moraine-dammed lake failure reported in the literature occurred in March 1989 by the outburst of Cerro Largo Lake, which spills into the Soler River (Hauser, 1993; Clague and Evans, 2000; Burton et al., 2020) (Fig. 2.10c). Its peak discharge was first estimated to be 1800–2000 m³/s (Hauser, 1993), however, Burton et al. (2020) estimate that this event resulted in a peak discharge of around 20 000 m³/s and that it released approximately 140 x 10^6 m³ of water and debris into the Soler valley.

In addition to glacial lakes along the NPI, smaller icefields located in the eastern part of the Baker River watershed may also have triggered GLOFs. The drainage of Las Lengas Lake into the Los Ñadis River, a tributary of Baker River, was previously identified using LANDSAT images, based on which it was dated 1987–1998 (Iribarren Anacona et al., 2014) (Fig. 2.10d). This GLOF released an estimated 4.36 x 10^6 m³ of water (Iribarren Anacona et al., 2014). Another river that discharges into the Baker River, i.e. Del Salto River, might have experienced GLOFs originating from glacial lakes in front of San Lorenzo glaciers (Fig. 2.10). However, there are no historical records of GLOFs originating from San Lorenzo proglacial lakes.

Finally, it should be noted that the 1977 Engaño GLOF and the 2000 Calafate GLOF occurred in the upper part of the Baker River watershed (Fig. 2.10), i.e. upstream of General Carrera Lake, and were therefore filtered and buffered before reaching Baker River. Likewise, the 1989 Cerro Largo Lake GLOF (Fig. 2.10) passed through Bertrand Lake before entering Baker River.

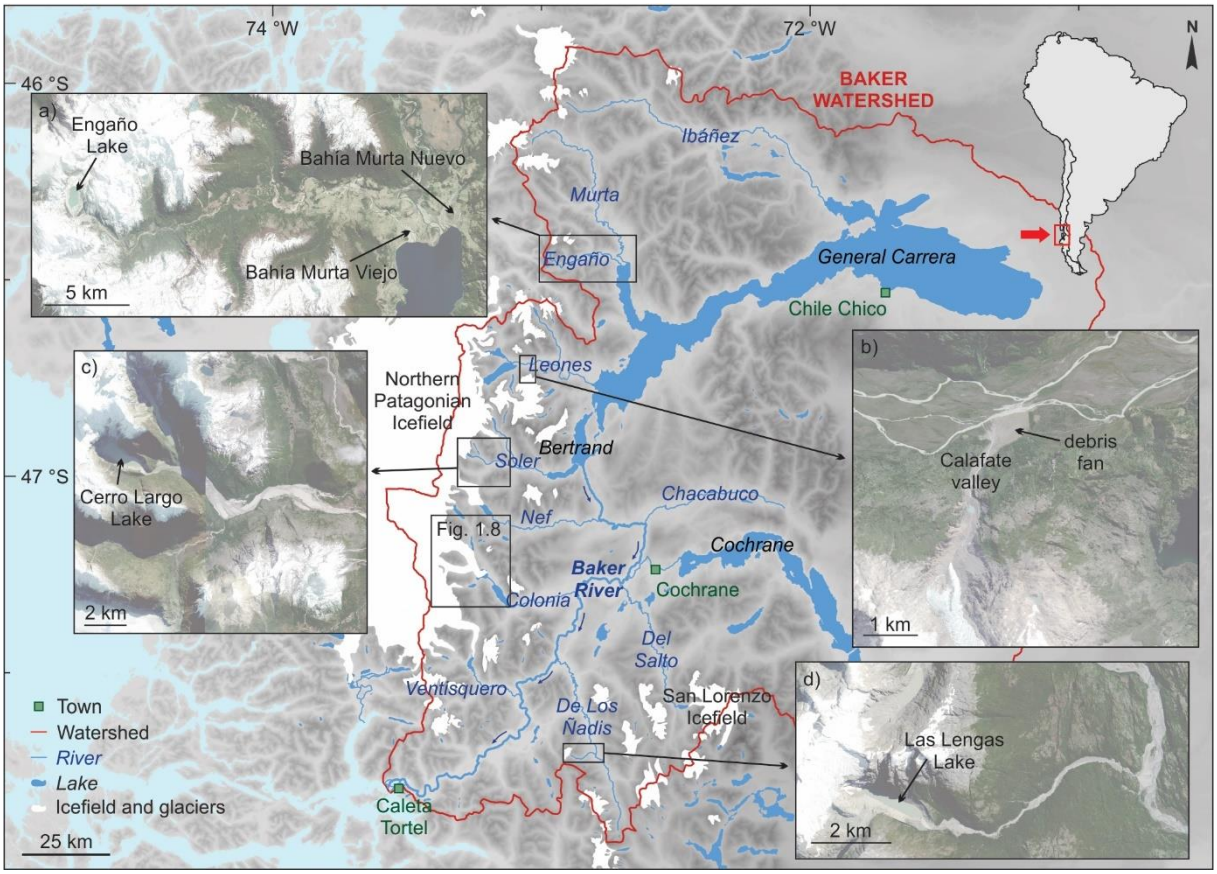

Figure 2.10. Location of documented GLOFs in the Baker River watershed. **(a)** Engaño Lake. Its outburst in 1977 destroyed large parts of Bahía Murta Viejo. **(b)** Remnants of Calafate Lake with the GLOF debris fan resulting from the 2000 Calafate Lake failure. **(c)** Cerro Largo Lake that partially drained during the 1989 GLOF. **(d)** Las Lengas Lake (Landsat images; Global Mapper World Imagery).

2.5.3. Meteorological floods

In addition to GLOFs, the Baker River watershed is also affected by meteorological floods, i.e. events induced by extreme precipitation or rain-on-snow. Such floods occur on an annual to decadal timescale, often during austral fall (Dussaillant et al., 2012). They can result in peak discharges comparable to the the 21st century Cachet 2 GLOFs. The largest historical rain-on-snow events occurred in December 1976 and December 1989 (Dussaillant et al., 2010; Benito et al., 2021).

References

Aniya, M. (1995) Holocene glacial chronology in Patagonia: Tyndall and Upsala glaciers. *Arctic Antarctic Alpine Research*, **27**, 311 – 322.

Aniya, M. (1996) Holocene variations of Ameghino Glacier, southern Patagonia. *The Holocene*, **6**, 247 – 252.

Aniya, M. (2013) Holocene glaciations of Hielo Patagónico (Patagonia Icefield), South America: A brief review. *Geochemical Journal*, **47**, 97 – 105.

Bendle, J.M., Palmer, A.P., Thorndycraft, V.R., and Matthews, I.P. (2019) Phased Patagonian Ice Sheet response to Southern Hemisphere atmospheric and oceanic warming between 18 and 17 ka. *Scientific Reports*, **9**, 4133.

Benito, G., Thorndycraft, V.R. Machado, M.J., Sancho, C., Dussaillant, A., and Meier, C.I. (2014). Magnitud y frecuencia de inundaciones Holocenas generadas por vaciamiento de lagos glaciares en el Rio Baker, Campo de Hielo, Patagonico Norte, Chile. In: Schnabel, S., Gutiérrez, Á.G. (Eds.), Sociedad Española de Geomorfología. Cáceres, Spain, 24–27 pp.

Benito, G., Thorndycraft, V.R., Medialdea, A., Machado, M.J., Sancho, C., and Dussaillant, A. (2021) Declining discharge of glacial lake outburst floods through the Holocene in central Patagonia. *Quaternary Science Reviews*, **265**, 106810.

Benito, G., and Thorndycraft, V.R. (2020). Catastrophic glacial-lake outburst flooding of the Patagonian Ice Sheet. *Earth-Science Reviews,* **200**, 102996.

Boldt, K.V. (2014) Fjord sedimentation during the rapid retreat of tidewater glaciers: observations and modeling. Doctoral dissertation, University of Washington, USA, 162 pp.

Burton, J.W., Chambers, F.B., Sincavage, R., and Cross, M.D. (2020) Analysis of glacial lake outburst flood terrain and sedimentary deposits in valle soler, Northern Patagonia Icefield. *Physical Geography*

Caldenius, C.C. (1932) Las glaciaciones cuaternarios en la Patagonia y Tierra del Fuego, *Geografiska Annaler*, **14**, 144 – 157.

Caniupán, M., Lamy, F., Lange, C.B., Kaiser, J., Arz, H., Kilian, R., Baeza Urrea, O., Aracena, C., Hebbeln, D., Kissel, C., Laj, C., Mollenhauer, G., and Tiedemann, R. (2011) Millennial-scale sea Surface temperatura and Patagonian Ice Sheet changes off southernmost Chile (53 °S) over the past ~60 kyr. *Paleoceanography*, **26** (3), PA3221.

Clague, J.J., and Evans, S.G. (2000) A review of catastrophic drainage of moraine-dammed lakes in British Columbia. *Quaternary Science Reviews*, **19**, 1763 – 1783.

DaSilva, J.L., Anderson, J.B., and Stravers, J. (1997) Seimic facies changes along a nearly continuous 24° latitudinal transect: the fjords of Chile and the northern Antarctic Peninsula. *Marine Geology*, **143**, 103 – 123.

Davies, B.J., and Glasser, N.F. (2012) Accelerating shrinkage of Patagonian glaciers from the Little Ice Age (~AD 1870) to 2011. *Journal of Glaciology*, **58** (212), 1063 – 1084.

Davies, B.J., Darvill, C.M., Lovell, H., Bendle, J.M., Dowdeswell, J.A., Fabel, D., García, J.-L., Geiger, A., Glasser, N.F., Gheorghiu, D.M., Harrison, S., Hein, A.S., Kaplan, M.R., Martin, J.R.V., Mendelova, M., Palmer, A., Pelto, M., Rodés, Á., Sagredo, E.A., Smedley, R.K., Smellie, J.L., and Thorndycraft,

V.R. (2020) The evolution of the Patagonian Ice Sheet from 35 ka to the present day (PATICE). *Earth-Science Reviews*, **204**, 103152.

De Agostini, A.S.S. (1945) Andes Patagonicos, Viajes de exploración a la Cordillera Patagonica Austral. Segunda edición aumentada y corregida. Buenos Aires. 436 pp.

Douglass, D.C., Singer, B.S., Kaplan, M.R., Ackert, R.P., Mickelson, D.M., and **Caffee, M.W.** (2005) Evidence of early Holocene glacial advances in southern South America from cosmogenic surface-exposure dating. *Geology*, **33**(3), 237 – 240.

Dussaillant, A., Benito, G., Buytaert, W., Carling, P., Meier, C., and **Espinoza, F.** (2010) Repeated glacial-lake outburst floods in Patagonia: an increasing hazard? *Natural hazards*, **54**, 469 – 481.

Dussaillant, A., Buytaert, W., Meier, C., and **Espinoza, F.** (2012) Hydrological regime of remote catchments with extreme gradients under accelerated change: the Baker basin in Patagonia. *Hydrological Sciences Journal*, **57**, 1530 – 1542.

Fick, S. E., and **Hijmans, R. J.** (2017) WorldClim 2: New 1-km spatial resolution climate surfaces for global land areas. *International Journal of Climatology,* **37**(12), 4302–4315.

Friesen, B.A., Cole, C.J., Nimick, D.A., Wilson, E.M., Fahey, M.J., McGrath, D., and **Leidich, J.** (2015) Using satellite images to monitor lake outburst floods—Lago Cachet Dos drainage, Chile. U.S. Geological Survey Scientific Investigations Map 3322, scale 1:15,000.

Garreaud, R., Lopez, P., Minvielle, M., and **Rojas, M.** (2013) Large-scale control on the Patagonian climate. *Journal of Climate*, **26**, 215 – 230.

Glasser, N.F., Harrison, S., Winchester, V., and **Aniya, M.** (2004) Late Pleistocene and Holocene palaeoclimate and glacier fluctuations in Patagonia. *Global and Planetary Change*, **43**, 79 – 101.

Glasser, N.F., Jansson, K.N., Duller, G.A.T., Singarayer, J., Holloway, M., and **Harrison, S.** (2016) Glacial lake drainage in Patagonia (13-8 kyr) and response of the adjacent Pacific Ocean. *Science Reports*, **6**, 21064.

Harrison, S., and **Winchester, V.** (2000) Nineteenth- and twentieth century glacier fluctuations and climate implications in the Arco and Colonia valleys, Hielo Patagónico Norte, Chile. *Arctic, Antarctic, and Alpine Research*, **32**, 55 – 63.

Harrison, S., Glasser, N., Winchester, V., Haresign, E., Warren, C., and **Jansson, K.** (2006) A glacial lake outburst flood associated with recent mountain glacier retreat, Patagonian Andes. *The Holocene*, **16**, 611 – 620.

Harrison, S., Glasser, N., Winchester, V., Haresign, E., Warren, C., Duller, G. A. T., Bailey, R., Ivy-Ochs, S., Jansson, K., and **Kubik, P.** (2008). Glaciar León, Chilean Patagonia: late-Holocene chronology and geomorphology. *The Holocene*, **18**(4), 643 – 652.

Harrison, S., and **Glasser, N.F.** (2011) The Pleistocene glaciations of Chile. *In: Ehlers, J., Gibbard, P.L., Hughes, P.D. (Eds.), Quaternary Glaciations – Extent and Chronology – A Closer Look.* Developments in Quaternary Sciences, vol. 15. Elsevier, Amsterdam, pp. 739 – 756.

Hauser, A. (1993) Remociones en massa en Chile. *Servicio Nacional de Geología y Mineria de Chile Boletín*, **45**, 75 pp.

Iriarte, J.L., Pantoja, S., and Daneri, D. (2014) Oceanographic processes in Chilean fjords of Patagonia: From small to large-scale studies. *Progress in Oceanography*, 129, 1 – 7.

Iribarren Anacona, P., Norton, K.P., and Mackintosh, A. (2014) Moraine-dammed lake failures in Patagonia and assessment of outburst susceptibility in the Baker Basin. *Natural Hazards and Earth System Sciences*, 14, 3243 – 3259.

Iribarren Anacona, P., Mackintosh, A., and Norton, K (2015) Reconstruction of a glacial lake outburst flood (GLOF) in the Engaño Valley, Chilean Patagonia: Lessons for GLOF risk management. *Science of the Total Environment*, 527-528, 1 –11.

Jacquet, J., McCoy, S.W., McGrath, D., Nimick, D.A., Fahey, M., O'kuinghttons, J., Friesen, B.A., and Leidlich, J. (2017) Hydrologic and geomorphic changes resulting from episodic glacial lake outburst floods: Rio Colonia, Patagonia, Chile. *Geophysical Research Letters*, 44, 854 – 864.

Kaplan, M.R., Ackert, R.P., Singer, B.S., Douglass, D.C., and Kurz, M.D. (2004) Cosmogenic nuclide chronology of millennial-scale glacial advances during O-isotope Stage 2 in Patagonia. *Bulletin of the Geological Society of America*, 116, 308 – 321.

Kaplan, M.R., Fogwill, C.J., Sugden, D.E., Hulton, N.R.J., Kubik, P.W., and Freeman, S.P.H.T. (2008) Southern Patagonian glacial chronology for the Last Glacial period and implications for Southern Ocean Climate. *Quaternary Science Reviews*, 27, 284 – 294.

Lamy, F., Kaiser, J., Arz, H.W., Hebbeln, D., Ninnemann, U., Timm, O., Timmermann, A. and Toggweiler, J.R. (2007) Modulation of the bipolar seesaw in the Southeast Pacific during Termination 1. *Earth and Planetary Science Letters*, 259, 400 – 413.

Luebert, F., and Pliscoff, P. (2006) Sinopsis bioclimática y vegetacional de Chile. *Editorial Universitaria*, Santiago.

Mansilla, C.A., McCulloch, R.D., and Morello, F. (2016) Palaeoenvironmental change in Southern Patagonia during the Late-glacial and Holocene: implications for forest refugia and climate reconstructions. *Palaeogeography, Palaeoclimatology, Palaeoecology*, 447, 1 – 11.

Masiokas, M.H., Rivera, A., Espizua, L.E., Villalba, R., Delgado, S., and Carlos Aravena, J. (2009) Glacier fluctuations in extratropical South America during the past 1000 years. *Palaeogeography, Palaeoclimatology, Palaeoecology*, 281, 242 – 268.

Mercer, J.H. (1970) Variations of some Patagonian glaciers since the Late Glacial: II. American *Journal of Science*, 269, 1 – 25.

Mercer, J.H. (1982) Holocene glacier variations in southern South America. *Striae*, 18, 35 – 40.

Miller, A. (1976) The climate of Chile. *In*: Schwerdtfeger, W. (ed.) *Climates of Central and South America*. Elsevier, Amsterdam, 113 – 145.

Moreno, P.I., Villa-Martínez, R., Cárdenas, M.L., and Sagredo, E.A. (2012) Deglacial changes of the southern margin of the southern westerly winds revealed by terrestrial records from SW Patagonia (52°S). *Quaternary Science Reviews*, 41, 1 – 21.

Moreno, P.I., Denton, G.H., Moreno, H., Lowell, T.V., Putnam, A.E., and Kaplan, M.R. (2015) Radiocarbon chronology of the last glacial maximum and its termination in northwestern Patagonia. *Quaternary Science Reviews*, 122, 233 – 249.

Moreno, P.I., and Videla, J. (2016) Centennial and millennial-scale hydroclimate changes in northwestern Patagonia since 16,000 yr BP. *Quaternary Science Reviews*, **149**, 326 – 337.

Moreno, P.I., Vilanova, I., Villa-Martinez, R., Dunbar, R.B., Mucciarone, D.A., Kaplan, M.R., Garreaud, R.D., Rojas, M., Moy, C.M., and De Pol-Holz, R. (2018a) Onset and evolution of southern annular mode-like changes at centennial timescale. *Scientific Reports*, **8**, 3458.

Moreno, P.I., Videla, J., Valero-Garces, B., Alloway, B.V., and Heusser, L.E. (2018b) A continuous record of vegetation, fire-regime and climatic changes in northwestern Patagonia spanning the last 25,000 years. *Quaternary Science Reviews*, **198**, 15 – 36.

Nimick, D.A., McGrath, D., Mahan, S.A., Friesen, B.A., and Leidich, J. (2016) Latest Pleistocene and Holocene glacial events in the Colonia valley, Northern Patagonian Icefield, southern Chile. *Journal of Quaternary Science*, **31**(6), 551 – 564.

Oportus, C. (1928) Informe sobre el problema de colonización de la zona del río Baker. Departamento de Tierras y Colonización, Ministerio de Fomento, Santiago de Chile, 120 pp.

Quiroga, E., Ortiz, P., González-Saldías, R., Reid, B., Tapia, F.J., Pérez-Santos, I., Rebolledo, L., Mansilla, R., Pineda, C., Cari, I., Salinas, N., Montiel, A., and Gerdes, D. (2016) Seasonal benthic patterns in a glacial Patagonian fjord: the role of suspended sediment and terrestrial organic matter. *Marine Ecology Progress Series*, **561**, 31 – 50.

Rebolledo, L., Bertrand, S., Lange, C.B., Quiroga, E., Troch, M., Silva, N., Cárdenas, P., and Pantoja, S. (2019) Compositional and biogeochemical variations of sediments across the terrestrial-marine continuum of the Baker-Martínez fjord system (Chile, 48°S). *Progress in Oceanography*, **174**, 89 – 104.

Rignot, E., Rivera, A., and Casassa, G. (2003) Contribution of the Patagonian icefields of South America to global sea level rise. *Science*, **302**, 434 – 437.

Ross, L., Perez-Santos, I., Valle-Levinson, A., and Schneider, W. (2014) Semidiurnal internal tides in a Patagonian fjord. *Progress in Oceanography*, **129**, 19 – 34.

Siani, G., Colin, C., Michel, E., Carel, M., Richter, T., Kissel, C., and Dewilde, F. (2010) Late Glacial to Holocene terrigenous sediment record in the Northern Patagonian margin: Paleoclimate implications. *Palaeogeography, Palaeoclimatology, Palaeoecology*, **297**, 26 – 36.

Sievers, H.A., and Silva, N. (2008) Progress in the oceanographic knowledge of Chilean interior waters, from Puerto Montt to Cape Horn. *Silva, N., and Palma, S. (Eds.)* Comité Oceanográfico Nacional – Pontificia Universidad Católica de Valparaíso, Valparaíso, pp. 53–58.

Syvitski, J.P.M. (1991) The changing microfabric of suspended particulate matter – the fluvial to marine transition: flocculation, agglomeration, and palletization. *In: Bennet, R.H., Bryant, W.R., and Hulbert, M.H. (Eds.)* Microstructure of fine-grained sediments. New York, Springer-Verlag, pp. 131 – 137.

Syvitski, J.P.M., and Shaw, J. (1995) Sedimentology and geomorphology of fjords. *In: Perillo, G.M.E. (Ed.)* Geomorphology and Sedimentology of Estuaries. Amsterdam, Elsevier, pp. 113 – 178.

Tanaka, K. (1980) Geographic contribution to a periglacial study of the Hielo Patagonico Norte with special reference to the glacial outburst originated from Glacier-Dammed Lago Arco, Chilean Patagonia. Centre Co Ltd, Tokyo, 97 pp.

Thorndycraft, V.R., Bendle, J.M., Benito, G., Davies, B.J., Sancho, C., Palmer, A.P., Fabel, D., Medialdea, A., and Martin, J.R.V. (2019) Glacial lake evolution and Atlantic-Pacific drainage reversals during deglaciation of the Patagonian Ice Sheet. *Quaternary Science Reviews*, **203**, 102 – 127.

Turner, K.J., Fogwill, C.J., McCulloch, R.D., and Sugden, D.E. (2005) Deglaciation of the eastern flank of the North Patagonian Icefield and associated continental-scale lake diversions. *Geografiska Annaler*, **87A**, 363 – 374.

Van Daele, M., Bertrand, S., Meyer, I., Moernaut, J., Vandoorne, W., Siani, G., Tanghe, N., Ghazoui, Z., Pino, M., and Urrutia, R. (2016) Late Quaternary evolution of Lago Castor (Chile, 45.6 °S): Timing of the deglaciation in northern Patagonia and evolution of the southern westerlies during the last 17 kyr. *Quaternary Science Reviews*, **133**, 130 – 146.

Villalba, R., Lara, A., Boninsegna, J.A., Masiokas, M., Delgado, S., Aravena, J.C., Roig, F.A., Schmelter, A., Wolodarsky, A., and Ripalta, A. (2003) Large-scale temperatura changes across the southern Andes: 20th-century variations in the context of the past 400 years. *Climatic Change*, **59**, 117 – 232.

Villa-Martinez, R., Moreno, P.I., and Valenzuela, M.A. (2012) Deglacial and postglacial vegetation changes on the eastern slopes of the central Patagonian Andes (47 °S). *Quaternary Science Reviews*, **32**, 86 – 99.

Winchester, V., and Harrison, S. (2000) Dendrochronology and lichenometry: colonization, growth rate and dating of geomorphological events on the east side of the North Patagonian Icefield, Chile. *Geomorphology*, **34**, 181 – 194.

3. Methods

3.1. Multibeam bathymetry

Multibeam bathymetry was used to map the seafloor morphology. This technique involves the emission of multiple sound waves in a fan shape from transducers attached to the vessel (Fig. 3.1a). The amount of time it takes for the acoustic pulses to be reflected by the ocean floor and to return to the receiver is used to determine the water depth. Prior to the survey, a bathymetric grid was constructed using SHOA bathymetric map #9100 (Canal Baker y Puertos Adyacentes), which is based on a series of manual depth soundings (SHOA, 2001). This map was used to plan the navigation route of the vessel to obtain a full coverage with 50 % overlap between swaths. The spacing between the navigation lines, which run parallel to the shoreline, were estimated based on the principle that spacing equals 2 x depth. The bathymetry was mapped with an ELAC Seabeam 1050 system installed on the *R/V Sur Austral* (COPAS Sur-Austral, Chile), where the frame, holding the two 50 kHz transducers at an angle of 120°, was mounted at the bow of the vessel (Fig. 3.1b).

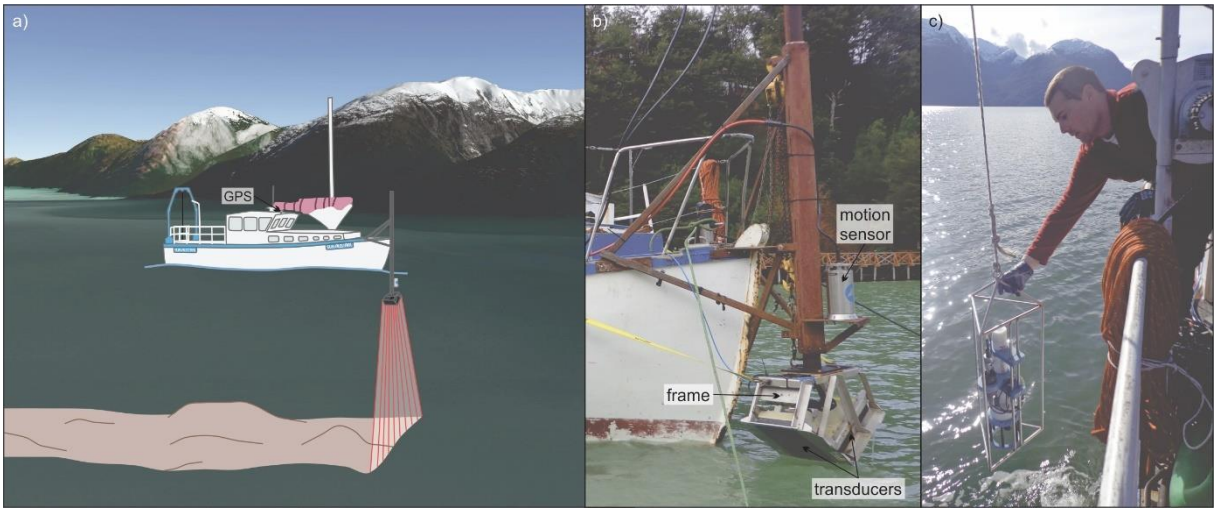

Figure 3.1. Data acquisition using the multibeam technique. **(a)** Schematic figure of the *R/V Sur Austral* mapping the bathymetry using the multibeam technique. **(b)** Bow of the *R/V Sur Austral* vessel to which the frame holding the two transducers and the motion sensor were attached. **(c)** RBR Maestro used to collect CTD profiles.

During data acquisition, the roll, pitch, and heave movements of the ship were simultaneously recorded by an Octans motion sensor (IXSEA). In addition, continuous Conductivity, Temperature, and Pressure (CTD) measurements were recorded at the water surface (~1 m depth) using a Valeport Modus CTD to correct for spatial changes in sound velocity. To correct for sound velocity changes with depth, vertical CTD profiles were taken on a daily basis with a RBR Maestro and were evenly distributed over the mapped area. This instrument was operated using an electrical winch (up and down speed: 1 m/s), and with a data acquisition rate of 6 Hz (Fig. 3.1c). The UNESCO algorithm (*Ruskin v1.13.1* software) was used to calculate sound velocities from CTD data. Positioning was based on GPS data acquired with a C-Nav2050G. For acquisition and navigation, the *Hydrostar v4.0.0* and *Fugawi v4.5* software were used, respectively. The multibeam data were processed using the *Caris HIPS and SIPS v9.1* software, where a time delay correction and tide correction was applied based on tide tables at Caleta Tortel, and the maps were created with *Fledermaus v7*.

3.2. Sediment sampling

Different techniques were used to collect sediment samples in the fjord and on floodplains. Samples in the fjord were retrieved via grab sampling and gravity coring. All sampling and coring locations were selected based on the results of the multibeam bathymetric data. Sampling on floodplains involved the use of U-shaped aluminum boxes and a Russian (or peat) corer.

3.2.1. Fjord

3.2.1.1. Grab sediment samples

Surface sediment samples were collected using a Van Veen grab sampler with a volume of 0.008 m^3 attached to a pneumatic winch aboard the *R/V Sur Austral* (Fig. 3.2a; Table S3A). Subsamples were collected with a small shovel. The samples were labeled GS17-XX, where GS stands for "grab sample", and 17 refers to the year of sampling (2017).

3.2.1.2. Gravity coring

Short gravity cores were taken with a 6.0 cm-inner diameter gravity corer aboard the *R/V Sur Austral* (Table S3A). For coring, empty PVC liners with a length of 1.5 m were placed into the corer (Fig. 3.2b). This system was lowered to the seafloor with the rubber valve in an open position and sunk into the sediments. While penetrating the sediment, the valve stayed in an open position, allowing unrestricted flow of water through the liner as long as the cable was slack. Upon retrieval of the corer, the valve turned into a sealed position and suction prevented the sediment from falling out of the PVC liner.

Figure 3.2. Sampling sediments in the fjords aboard the *R/V Sur Austral*. **(a)** Van Veen grab sampler to collect surface sediment samples. **(b)** Gravity corer equipped with an empty liner.

When the filled PVC liner was pulled out from the water and brought onto the deck, floral foam was pushed down and the liner was cut a few cm above the sediment-water interface. Finally, it was sealed with caps and tape, and labeled. Gravity cores were labeled FC17-XX, where FC stands for "fjord core", and 17 refers to the year of sampling (2017).

3.2.2. Floodplain

Sediment cores were collected on land in 50 cm-long sections using a Russian (or peat) corer. Sampling locations were selected based on their relative elevation above the Baker River, i.e. less than 6 m difference, as this corresponds to the water level rise of the Baker River during historical GLOFs (Table S3A). Prior to sampling, a gouge auger, which rapidly produces a profile with undisturbed sediment, was used to test the sites. During sampling, the Russian corer, which consists of a core chamber with a rotating steel blade with a cutting edge and a sharp end, was pushed into the sediment with the blade in a closed position (Fig. 3.3a). Extension rods (1 m length) were connected to core at greater depths. Upon the desired depth, the blade was rotated with a handle to collect uncompacted sediments into the core chamber. Once the corer was closed and pulled out of the sediment, the core chamber was opened to retrieve the sediment.

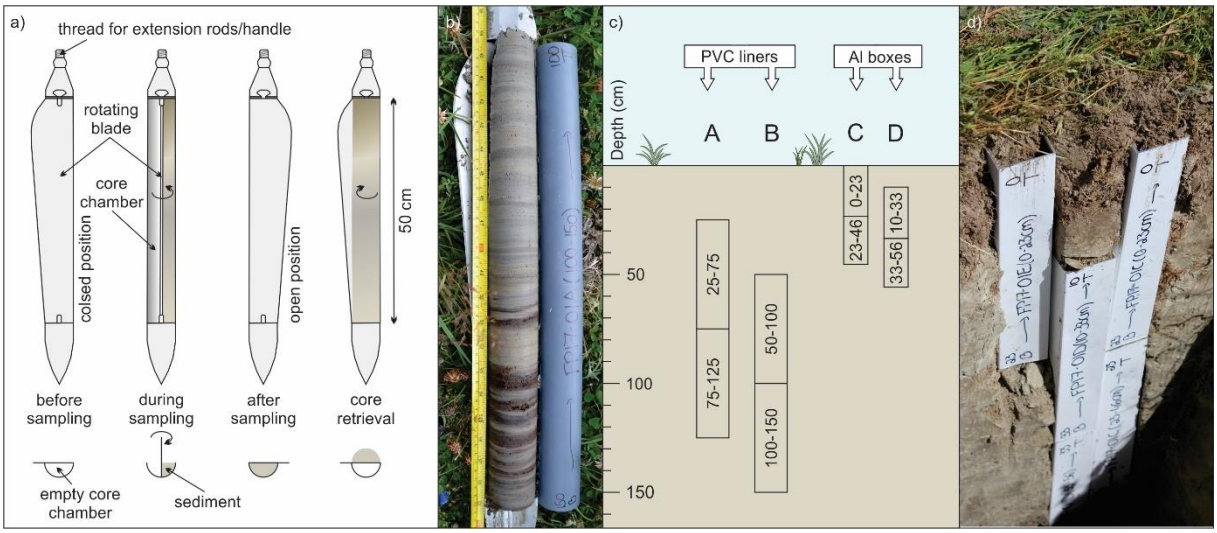

Figure 3.3. Schematic overview for sampling on land. **(a)** Different positions of the Russian corer during coring. **(b)** Example of a sediment core collected using the Russian corer. **(c)** Sampling strategy implemented on the field. **(d)** Sediments collected using U-shaped aluminum boxes.

All core sections were described, wrapped in plastic foil, stored in halved 5.0 cm-inner diameter PVC liners, and labeled (Fig. 3.3b). Sediment cores were retrieved in 50 cm overlapping steps from two parallel holes (A and B) to obtain a continuous composite core at each coring site (Fig. 3.3c). The upper part of the sediments, i.e. upper ~50 cm, were too consolidated for sampling with a Russian corer. To retrieve these sediments, 23 cm-long U-shaped aluminum boxes (4 x 4 cm) were pushed into a vertical profile created with a showel, at overlapping depth intervals and wrapped in plastic foil (Fig. 3.3c–d). Both the sediment cores and box samples were labeled FP17-XX, where FP stands for “floodplain”, and 17 refers to the year of sampling (2017).

3.2.3. River suspended sediment concentrations

The rivers discharging into the Baker River upstream (Nef, Chacabuco, Cochrane, Del Salto) and immediately downstream (Colonia) of Valle Grande were sampled prior to this thesis by Dr. Brian Reid (CIEP, Chile) for Suspended Sediment Concentration (SSC) measurements (Table S3A). Three sites were also sampled along the Baker River. The rivers were sampled throughout the year (n per river = 8–21) between 2008 and 2010. SSC values were obtained after manual filtration of 500 ml of river water on GFF filters.

3.3. Sediment analysis

All sediment samples were shipped from Coyhaique (Chile) to Ghent University (Belgium). An overview of the workflow applied to the samples collected in the fjord and on land is shown in figures 3.4 and 3.5, respectively. An overview of the resolution of each measurement is shown in Table 3.1.

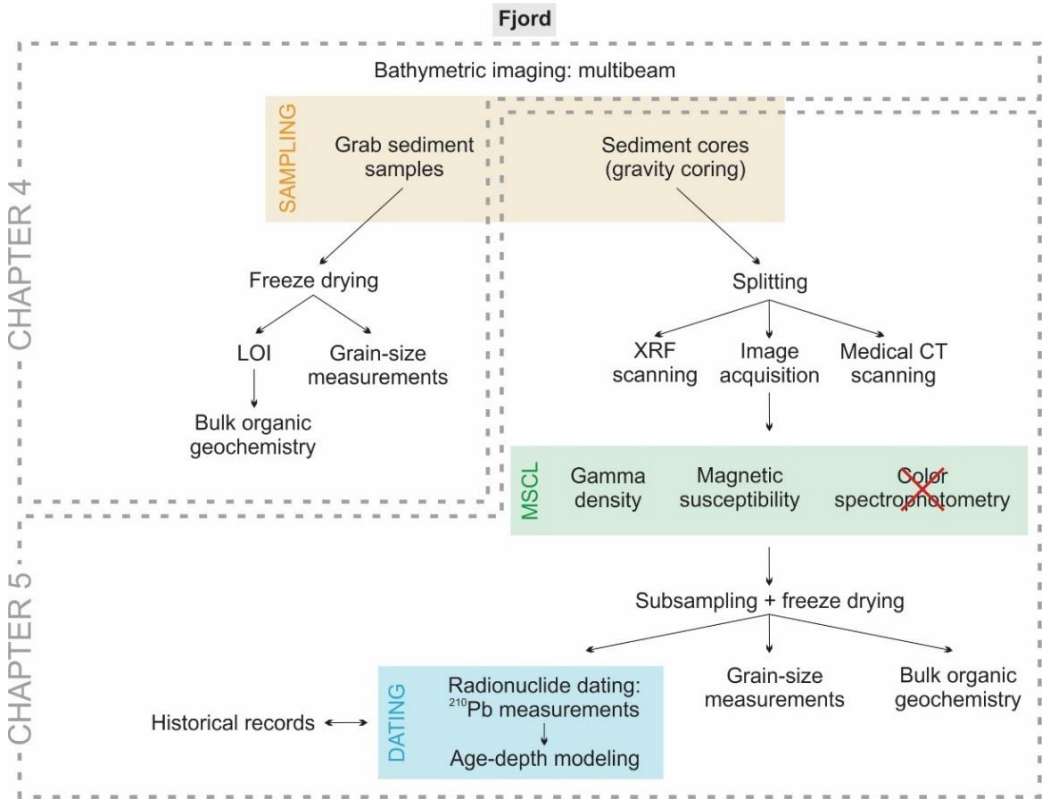

Figure 3.4. Workflow for the surface sediment samples and sediment cores collected in the fjord. The results of the multibeam bathymetric mapping and those obtained on the grab sediment samples are presented in chapter 4. Chapter 5 shows the results obtained on the fjord sediment cores. A red cross means that the results of this analysis were not used in this thesis.

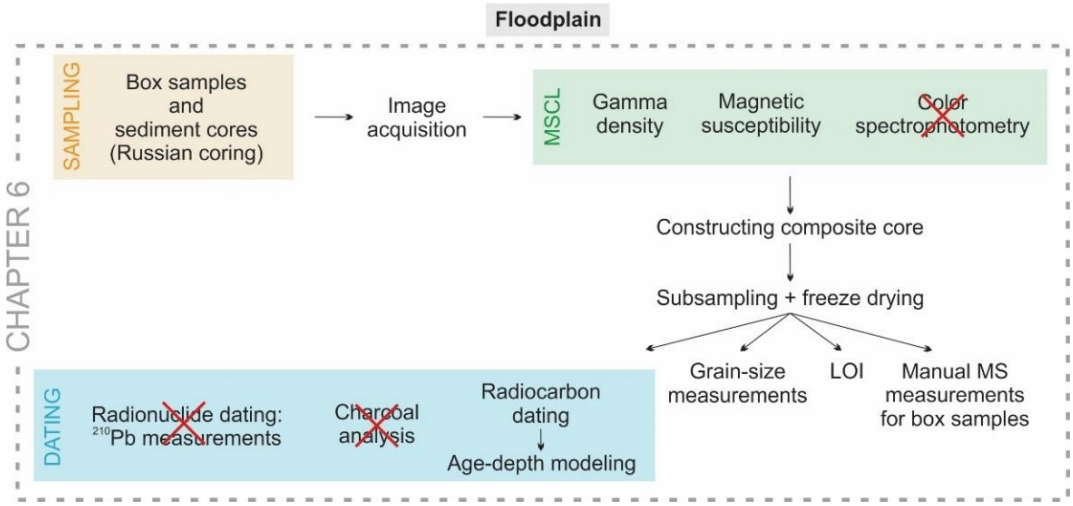

Figure 3.5. Workflow for the samples collected from the Valle Grande floodplain. Results obtained on these samples are presented in chapter 6. A red cross means that the results of this analysis were not used in this thesis.

3.3.1. Medical CT scanning

X-ray Computed Tomography (CT) scanning was performed with a SOMATOM Definition Flash CT-scanner (Siemens AG, Munich, Germany) at the Ghent University Hospital (Belgium) by Loïc Piret (UGent, Belgium) and Thomas Vandorpe (VLIZ, Belgium). X-ray CT scanning is based on X-ray attenuation, which depends on both material composition (effective atomic number) and density (Zatz, 1981; Cnudde et al., 2006), and produces cross-sectional (tomographic) images of the sediment core in a 3D way. This non-destructive visualization technique allows to identify changes in different sediment properties and structures (e.g. laminations, bioturbation, erosive features) that are not visible on core pictures. X-ray CT scanning was performed on the most promising fjord sediment cores (Table 3.1). The CT-scanner was operated at a voltage of 120 kV, an affective mAs of 200 and a pitch of 0.45. A voxel size of approximately 0.15 mm (X-Y direction or across core) by 0.60 mm (Z-direction or along core) was obtained after reconstruction. All CT-scan images were visualized using *VGStudio 2.2*.

3.3.2. Core splitting

The fjord sediment cores were split using a Geotek core splitter. This equipment operates two vibrating cutters that cut the plastic liners in two equal halves. A thin nylon wire was then used to cleanly split the sediment and two stainless steel blades were used to separate the two halves (archive [A] and working [W]).

3.3.3. Image acquisition

Split cores images of the working half were acquired immediately after splitting to prevent discoloration by oxidation. Split cores images were acquired with the Geotek Ltd. Geoscan IV Linescan Imaging system. A cleaned split core was placed on the rail and mechanically pushed below a light source and the Geoscan IV line scan camera (Fig. 3.6). Incoming light passes through a set of red, green, and blue filters, and the camera is equipped with a Nikon lens mount. As the core was pushed below the camera, single lines of image data were collected sequentially in a down-core direction. Core images were acquired at a 508 dpi resolution (200 pixels/cm) (Table 3.1).

3.3.4. Multi-Sensor Core Logging (MSCL)

The Geotek Ltd. Multi-Sensor Core Logger (MSCL) was used to measure different geophysical parameters along-core including gamma density, magnetic susceptibility (MS), and color spectrophotometry (Fig. 3.6). Before scanning, a thin plastic foil was placed on the sediment surface to avoid cross-contamination. Each core section was pushed past the sensors and measurements were collected at a downcore resolution of 2 mm (Table 3.1).

3.3.4.1. Gamma density

Gamma density was measured using a radioactive ^{137}Cs source, which emits a narrow beam of collimated gamma rays with energies of 0.662 MeV through the core. At this energy level, the primary mechanism for gamma ray attenuation is by Compton scattering, which results in partial energy loss of the scattered photons as they hit electrons in the core. The attenuation is thus directly linked to electron density and core thickness. With the help of a calibration piece, which consists of an aluminum scale of varying thickness installed in an empty liner, the gamma attenuation and the measured core thickness were used to estimate the wet density of the material. Different calibration pieces were used for the sediment cores collected on land and the gravity cores from the fjords as different liners were used and the density range of the sediment differs.

Table 3.1. Overview of the different analyses performed on sediment samples from the fjord and the floodplain with their downcore resolution. "–" means not measured.

Samples / Analysis	Fjord		Floodplain	
	Sediment grab samples	Gravity cores	Box samples	Sediment cores
CT scanning	–	0.06 mm[a]	–	–
Image acquisition	–	0.05 mm	0.05 mm	0.05 mm
MSCL	–	2 mm	2 mm	2 mm
XRF scanning	–	2 mm	–	–
Manual MS measurements	–	–	5 mm	–
Grain-size measurements	bulk	1 cm[b]	0.5, 1, or 2 cm[c]	0.5, 1, or 2 cm[c]
LOI	bulk	–	5 mm	5 mm
TOC	bulk	5 mm[d]	–	–
Charcoal counts	–	–	1 cm[e]	1 cm[e]
Radionuclide dating	–	10 cm[f]	10 cm[e]	10 cm[e]
Radiocarbon dating	–	–	–	selected samples

[a] Only on cores FC17-05, FC17-08, FC17-01, FC17-01A, and FC17-02

[b] Only on cores FC17-02 and FC17-08

[c] Only on core FP17-01

[d] Only on core FC17-08

[e] Only on cores FP17-01 and FP17-03

[f] Only on core FC17-02

3.3.4.2. Magnetic susceptibility

Magnetic Susceptibility (MS) is the direct measure of the degree of magnetization in response to an external magnetic field. MS was measured on the split core surface using a Bartington point sensor (MS2E) that is connected to a Bartington MS2 meter. An alternating magnetic field (2 kHz) is produced by an oscillator circuit in the sensor. Material close to the MS sensor will alter the oscillator frequency. If MS values are positive, the magnetic field is strengthened by the material, while material weakens the magnetic field in case of negative MS values. Higher MS values generally represent higher proportions of clastic material and/or coarser sediments. A measuring time of 10 s and precision of 1.0 SI x 10^{-5} was applied for the gravity cores. For the sediment cores collected in the floodplain, a measuring time of 10 s and precision of 0.1 SI x 10^{-5} was implemented. MS could not be measured on the box samples due to interference with the Aluminum of the boxes. Manual MS measurements were therefore performed on samples extracted from the boxes (see section 3.3.6).

3.3.4.3. Color spectrophotometry

The reflectance in the visible light spectrum (wavelengths 360–740 nm) was measured with a Konica Minolta color spectrophotometer. The data was calibrated using a calibration tile and color spaces are presented as luminosity L* (ranging from black, 0, to white, 100), a* (positive red, negative green), b* (positive yellow, negative blue), XYZ, and RGB values.

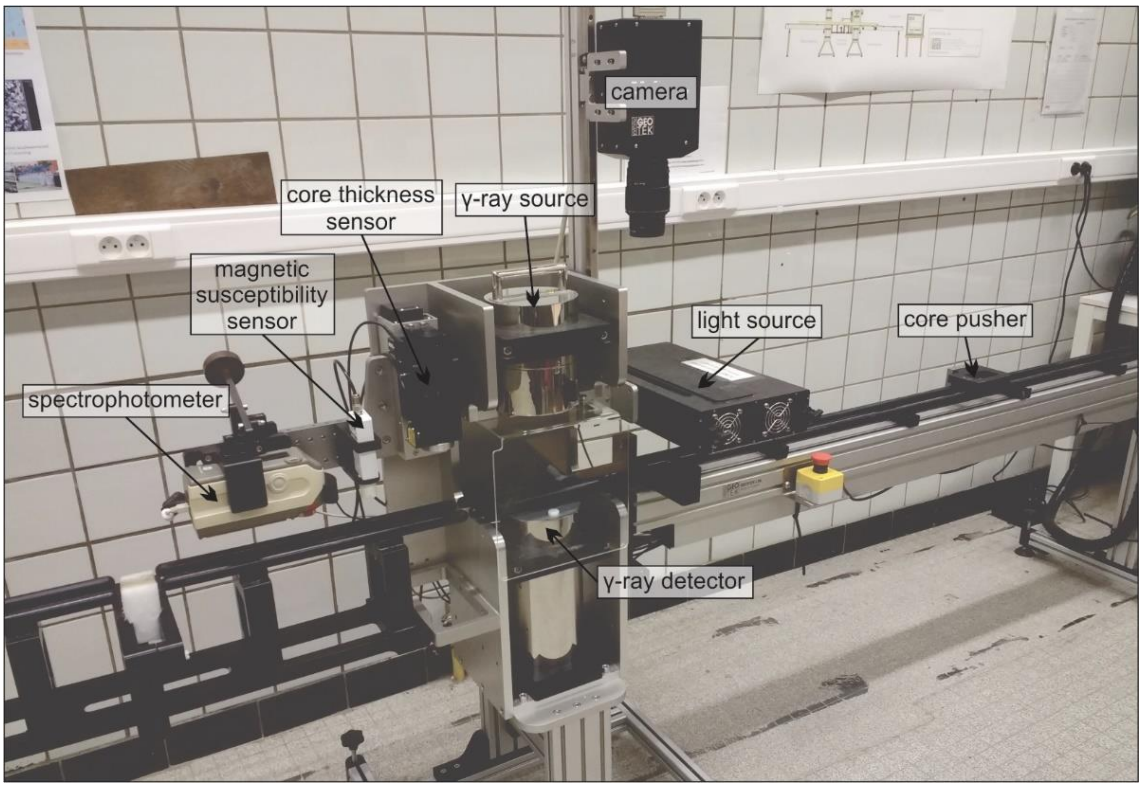

Figure 3.6. Photograph of the Multi-Sensor Core Logger (MSCL) at Ghent University with its different components labeled.

3.3.5. X-Ray Fluorescence (XRF) scanning

The elemental distribution of the fjord sediment cores was analyzed with an Itrax X-Ray Fluorescence (XRF) core scanner at Stockholm University (Stockholm, Sweden) by Loïc Piret (UGent, Belgium) and Dawei Liu (UGent, Belgium). Prior to core scanning, a 4-µm thin Chemplex 416 Prolene foil was placed on the sediment surface to prevent cross-contamination and drying of the sediments. During scanning, high-energetic X-rays are generated by heating a molybdenum tube. By targeting these high-energy X-rays towards the sediment, secondary (or fluorescent) X-rays are emitted from the material that has been excited. The energy of this emission is characteristic for the atoms present and can be used to determine the elemental composition of the sediment. Measurements were conducted with a molybdenum tube set at 30 kV and 50 mA, and data was collected at a downcore resolution of 2 mm during 25 seconds (Table 3.1). Afterwards, the *Q-spec* software was used to transform XRF spectra to individual counts. To avoid dilution effects, a centred log-ratio (CLR) transformation (Weltje et al., 2015) was applied. The CLR transformation was calculated using the following equation:

$$\text{CLR (x)} = \ln[\frac{x_1}{g(x)}, \frac{x_2}{g(x)}, \frac{x_3}{g(x)}, \ldots \frac{x_N}{g(x)}]$$

where x_N represents the counts of element N and $g(x)$ stands for the geometric mean of the composition, calculated as:

$$\text{g(x)} = \sqrt[n]{x_1 \cdot x_2 \cdot x_3 \cdot \ldots x_n}$$

The following elements (n=14) were used to calculate the geometric mean: Si, Cl, K, Ca, Ti, Mn, Fe, Zn, Br, Rb, Sr, Zr, Ba, and Pb. These elements are either the most abundant or those with a high raw count, i.e. > 5000.

3.3.6. Sub-sampling

Composite cores were constructed for the floodplain sediment cores based on core descriptions, images and MSCL data (Fig. 3.5). Afterwards, the composite core was continuously subsampled using a 5 mm-interval, and all samples were freeze-dried for two days using a LabConco 4.5 freeze dryer. Similarly, the grab sediment samples and subsamples of the fjord sediment cores were freeze-dried before analysis (Fig. 3.4).

3.3.7. Manual magnetic susceptibility measurements

Manual MS measurements were performed on the dried box samples using a Bartington MS2G Single Frequency (1.3 kHz) Sensor with a resolution of 1 x 10^{-6} SI volume-specific MS, attached to a Bartington MS3 meter. First, each sample was placed in a polythene vial with a diameter of 8 mm and a length of 30 mm, i.e. calibrated volume of 1 ml, and weighed. Blank measurements using an empty vial were conducted in-between each measurement to correct for drift, and measurements were repeated twice to increase the accuracy. Data was processed using *Bartsoft v4*. Finally, the mass-specific MS was calculated by dividing the volume-specific MS by the weight of the sample to eliminate the density-dependency of the volume-specific MS (Sandgren and Snowball, 2001).

3.3.8. Grain-size measurements

Grain-size measurements were conducted on samples from two fjord sediment cores, all sediment grab samples, and samples from one floodplain sediment core using the Malvern Mastersizer 3000, equipped with a Hydro MV dispersion module (Table 3.1). The Mastersizer 3000 measures the size of particles, ranging from 0.01 to 3500 µm, using the laser diffraction technique. The dispersed sample passes through the measurements lense, where a red and blue laser beam illuminates the particles. The intensity and the angle of light scattered by the particles as the laser beam passes through the sample is measured by a series of detectors and is used to calculate the distribution of particle size. In general, the smaller the particle, the wider the angle and the lower the intensity of the scattering.

An initial test was done to estimate the ideal amount of sample, as the obscuration level depends on the grain size. Prior to analysis, all samples were chemically treated to isolate the lithogenic fraction. First, the sediment was suspended in 10ml of de-ionized water. To remove organic matter, hydrogen peroxide (H_2O_2; 30 %) was added to the sample and set to boil until the reaction ended. Second, 1 ml of hydrogen chloride (HCl; 10 %) was added to the suspension to remove possible calcium carbonate. After neutralizing the pH by washing the solution, biogenic silica was removed by adding 1 ml of sodium hydroxide (NaOH; 2 N). Finally, the suspension was decanted again and treated with 1 ml of sodium hexametaphosphate (2 %) to avoid grain flocculation. The maximum measured grain size for the samples was restricted by using a 1 mm mesh sieve. A measuring time of 15 s with 10 % sonification was implemented. Each sample was measured at least three times to assure reproducibility. Grain-size distribution parameters were obtained using the *Gradistat v8* software (Blott and Pye, 2001), except for the grain-size mode, which was obtained directly from the *Mastersizer 3000* software for better precision.

3.3.9. Loss-On-Ignition

The organic and carbonate contents on the floodplain sediment cores was estimated using the Loss-On-Ignition (LOI) technique. This technique provides a fast and inexpensive means of determining the organic matter content of sediments and involves burning the sample at a specified temperature in a muffle furnace. During combustion, organic matter oxidizes to carbon dioxide and ash, and the resulting weight loss is closely related to the weight percentage of organic content (Dean, 1974; Bengtsson and Enell, 1986). First, the freeze-dried samples were additionally placed in the oven overnight at 105 °C to remove any remaining water from the samples. Approximately 0.25 g of dry sediment was placed in a pre-weighed crucible. Following Heiri et al. (2001), the dried samples were heated in the muffle oven for 4 hours at 550 °C. Afterwards, all samples were allowed to cool down in a desiccator for 30 minutes and re-weighed. LOI550 was calculated using the following equation:

$$\text{LOI550} = \frac{(DW_{105} - DW_{550})}{DW_{105}} \times 100$$

where DW_{105} represents the dry weight of the sample in g before heating, DW_{550} the dry weight of the sample in g after heating at 550 °C, and LOI550 the LOI at 550 °C in percentage dry weight. To estimate the carbonate content, samples were heated at 1000 °C for two hours. At 1000 °C, all carbonates are converted into oxides and carbon dioxide (Dean, 1974; Heiri et al., 2001). Afterwards, the samples are placed in a desiccator again for 30 minutes and weighed. LOI1000 was calculated using the following equation:

$$\text{LOI1000} = \frac{(DW_{550} - DW_{1000})}{DW_{550}} \times 100$$

where DW_{1000} represents the dry weight of the sample in g after heating.

3.3.10. Bulk organic geochemistry

To determine the total organic carbon (TOC) content of the grab sediment samples and samples from one fjord sediment core (Table 3.1), bulk organic geochemical analyses were performed using an elemental analyzer (EA) at the UCDavis Stable Isotope Facility (California, USA). The EA which was used to analyze the sample is a Micro Cube elemental analyzer (Elementar Analysensysteme GmbH, Hanau, Germany). Because of the limitations of the EA instrument, the total sample weight cannot exceed 75 mg, and the optimal amount of TOC for analysis is between 0.8 and 1 mg C, and should never exceed 1.2 mg. As the surface sediment samples are very poor in organic matter, sample sizes of 60 mg were used for the fjord sediment core. Samples were weighted and stored in silver (Ag) capsules. These were treated with sulfurous acid (1 N) to avoid the influence of inorganic carbon (Verardo et al., 1990), and dried using a ceramic heat lamp under a fume hood. Afterwards, samples were folded using tweezers to avoid any contamination and shipped to UCDavis for analysis.

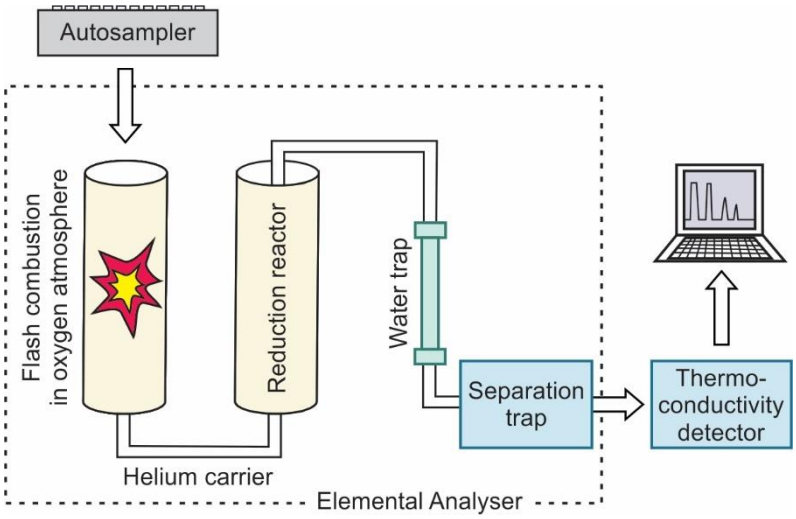

Figure 3.7. Simplified schematic diagram of the elemental analyzer (modified after Jasper et al., 2001 and Muccio and Jackson, 2009).

The Ag capsules containing the samples are first combusted in a reactor packed with copper oxide and lead chromate at a temperature of 1000 °C (Fig. 3.7). The combusted sample is then carried by a helium gas stream into a reduction reactor and a chemical trap (magnesium perchlorate) to remove excess oxides and water, respectively. Finally, N_2 and CO_2 are separated by a molecular sieve adsorption trap in the gas chromatograph before a thermoconductivity detector allows to determine elements.

3.4. Chronology

3.4.1. Radionuclide dating

To obtain a chronology of the fjord sediment cores, ^{210}Pb dating was used (Appleby and Oldfield, 1978). The isotope ^{210}Pb is part of the ^{238}U decay series, where ^{238}U decays to ^{226}Ra (half-life of 1622 years). In turn, ^{226}Ra decays to the inert gas ^{222}Rn (half-life of 3.82 days), which escapes from sediments to the atmosphere and decays via a series of short-lived daughters to ^{210}Pb (half-life of 22.26 years). ^{210}Pb gets deposited and can be used to date sediments on short timescales (up to 150 years). Aside from the natural ^{210}Pb atmospheric fallout (unsupported ^{210}Pb), ^{210}Pb is also naturally produced in sediments, i.e. supported ^{210}Pb. The unsupported ^{210}Pb activities are therefore calculated by subtracting the ^{226}Ra activity (or supported ^{210}Pb) from the total ^{210}Pb activity and are used for dating. Unsupported ^{210}Pb activities were measured by alpha spectrometry at the Australian Nuclear Science and Technology Organisation (ANSTO, Australia) following the methodology by Harrison et al. (2003) and McMinn et al. (1997).

The flux of unsupported ^{210}Pb to the sediment varies significantly depending on the sedimentation rate. In general, there are three standard models to determine the sedimentation rate from the unsupported ^{210}Pb activities: the CFCS (Constant Flux-Constant Sedimentation rate; Krishnaswamy et al., 1971), CRS (Constant Rate of Supply; Appleby and Oldfield, 1978), and CIC (Constant Initial Concentration; Robbins and Edgington, 1975; Goldberg et al., 1977) models. The CFCS and CRS models both assume that the atmospheric flux dominates the unsupported ^{210}Pb activities, and unsupported ^{210}Pb activities should therefore be comparable with natural fallout measurements when applying these models. The main difference between the two models is that the CRS model assumes a constant rate of ^{210}Pb supply to the sediments regardless of variations in the sedimentation rate, whereas the CFCS model assumes a constant ^{210}Pb atmospheric flux to the sediments and a constant sedimentation rate. The CIC model, on

the other hand, assumes that the initial value of unsupported ^{210}Pb was constant with time, i.e. a constant ratio of atmospheric and sediment flux, and is applied when the ^{210}Pb activities decline monotonically with depth. In this thesis, the CFCS model was used since (1) the unsupported ^{210}Pb activities did not reach background levels in the bottommost sample, and (2) the unsupported ^{210}Pb activities show a non-monotonous decreasing trend with depth. Errors on sediment ages were determined from uncertainties in the excess ^{210}Pb inventory.

3.4.2. Radiocarbon dating

Radiocarbon dating was used to establish a chronology for the floodplain sediment cores (Fig. 3.5; Table 3.1). The principle of radiocarbon dating is based on the radioactive decay of ^{14}C. In living plants or animals, the ^{14}C/^{12}C ratio is in equilibrium with the ^{14}C/^{12}C ratio in the atmosphere. When living material dies, radioactive decay sets in and ^{14}C decays to ^{14}N over time. Comparison between the isotopic composition of the sample and the ^{14}C/^{12}C ratio today allows to determine the age of the sample. As the amount of carbon in the atmosphere has not been constant through time, calibration is required. All ages in this thesis were calibrated using the latest calibration curve for the Southern Hemisphere (SHCal13; Hogg et al., 2013), and presented in calibrated years before present (cal yr BP), where "present" indicates AD 1950.

Samples for radiocarbon analysis were selected in organic-rich deposits near sharp lithological boundaries of the sediment cores. These samples were pretreated and examined by Dr. Dimitri Mauquoy (University of Aberdeen, UK) to identify macrofossils. Samples were first warmed in potassium hydroxide (KOH; 5 %) for 60 minutes, and then decanted into a petri dish containing de-mineralized water. The selected macrofossils were transferred into separate clean containers and cleaned thoroughly of any visible contamination (e.g. fungal hyphae, rootlets, or material introduced during laboratory work). During these steps a binocular microscope with 6X–50X magnification was used. After a first phase of selection and cleaning, samples were further cleaned. This procedure was repeated until the samples showed no visible contamination. The samples were then placed into clean vials with distilled water and some droplets of HCl (4 %) were added. Afterwards they were dried and placed into plastic vials. Consequently, the selection of monospecific plant macrofossils (e.g. leave bases) for radiocarbon analysis minimized the risk of age contamination due to plant roots for example. Measurements were made with an accelerator mass spectrometer at DirectAMS (USA). In addition, one bulk sediment sample was oven dried and analyzed at NOSAMS (USA).

Age-depth models were constructed based on calibrated radiocarbon ages to derive core chronologies. For this, the *BACON v2.3.6* software, which applies Bayesian statistics to reconstruct an age-depth model, was used (Blaauw and Christen, 2011). This algorithm is run as a script in R, a statistical software package, and divides the record into vertical sections to estimate the accumulation rate for each of these sections by applying many Markov Chain Monte Carlo (MCMC) iterations. Prior information on the accumulation rate (i.e. acc.mean and acc.shape) and its variability between neighboring depths (i.e. mem.mean, mem.strength) are inserted to constrain the accumulation rate. The average accumulation rate was estimated based on the age of the bulk sample at the bottom of the core, and low memory values were applied to the model because the sedimentation rate was assumed to vary significantly throughout the record depending on the lithology.

3.4.3. Charcoal analysis

Charcoal analysis was used to refine core chronologies of the floodplain sediment cores. This method relies on the comparison of charcoal concentrations with records of historical fire occurrences. Individual charcoal pieces, which are recognizable as opaque, angular and usually planar, black fragments (Whitlock and Larsen, 2001), were counted macroscopically by Dr. Dave McWethy at the Montana State University Paleoecology Laboratory (USA). Approximately 2 cc of sediment sample was analyzed at a 1 cm downcore resolution (Table 3.1). The size fraction of the pieces is > 125 µm as this size fraction represents atmospheric fall out within a short distance (1–3 km) of a local fire (e.g. Higuera et al., 2009). The data is presented as charcoal pieces per cm^3.

3.5. Historical records

To obtain an independent record of Baker River flood history over the past centuries, historical information on GLOFs was extracted from bibliographic sources, which include written and iconographic documents from early settlers and explorers in the Baker region (Table 3.2). In addition, interviews were conducted in the early settlements along the Baker River and its tributaries, between the towns of Cochrane and Caleta Tortel, by environmental historian Fernando Torrejón (Centro EULA, University of Concepción, Chile). To retrieve conversational evidence on the regional GLOF history, the oldest settlers were identified and a total of 14 people of both sexes were interviewed. Depending on the conversation, the individual interviews were divided into two categories: the open interviews, or so-called "life stories", and the semi-structured testimonies (Barela et al., 2004). It should be noted that three out of the 14 interviews did not provide relevant information regarding major Baker flood events. All conversational evidence was compared and processed to obtain a chronological and geographical record of extreme flood events in the Baker River basin since the mid-20th century. These testimonies and bibliographic sources were compiled and integrated with previously published data on flood events in the Baker watershed.

Table 3.2. Overview of the records used to reconstruct the Baker flood history.

Historical records	Time period
Bibliographic sources	
Oportus (1928)	late 1800s – 1928
De Agostini (1945)	first half 20th century
Conversational records	1950s – today
Published data on GLOFs	
Tanaka (1980)	1880s – 1958
Winchester and Harrison (2000)	1880s – 1960s
Harrison and Winchester (2000)	1880s – 1960s
Harrison et al. (2006)	Late 2000
Dussaillant et al. (2010)	2008 – 2009
Iribarren Anacona et al. (2014)	1977 – 2003
Iribarren Anacona et al. (2015)	1977
Friesen et al. (2015)	2011 – 2013
Jacquet et al. (2017)	2008 – 2016

3.6. Instrumental records

Despite the Baker River being located in a remote region, its watershed is relatively well equipped with river discharge stations (Fig. 3.8). Baker River hydrographs were obtained from DGA monitoring stations "Rio Baker en angostura Chacabuco" and "Rio Baker bajo Ñadis", which cover the last ~45 years (Fig. 3.9). For the last two decades, discharge data is also derived from station "Rio Baker en Colonia". The HidroAysén report (HidroAysén, 2010) was consulted to retrieve data on suspended sediment concentrations (SSC). The latter compiles daily SSC measurements downstream the Los Ñadis inflow between April 1976 and February 2003 (Fig. 3.8).

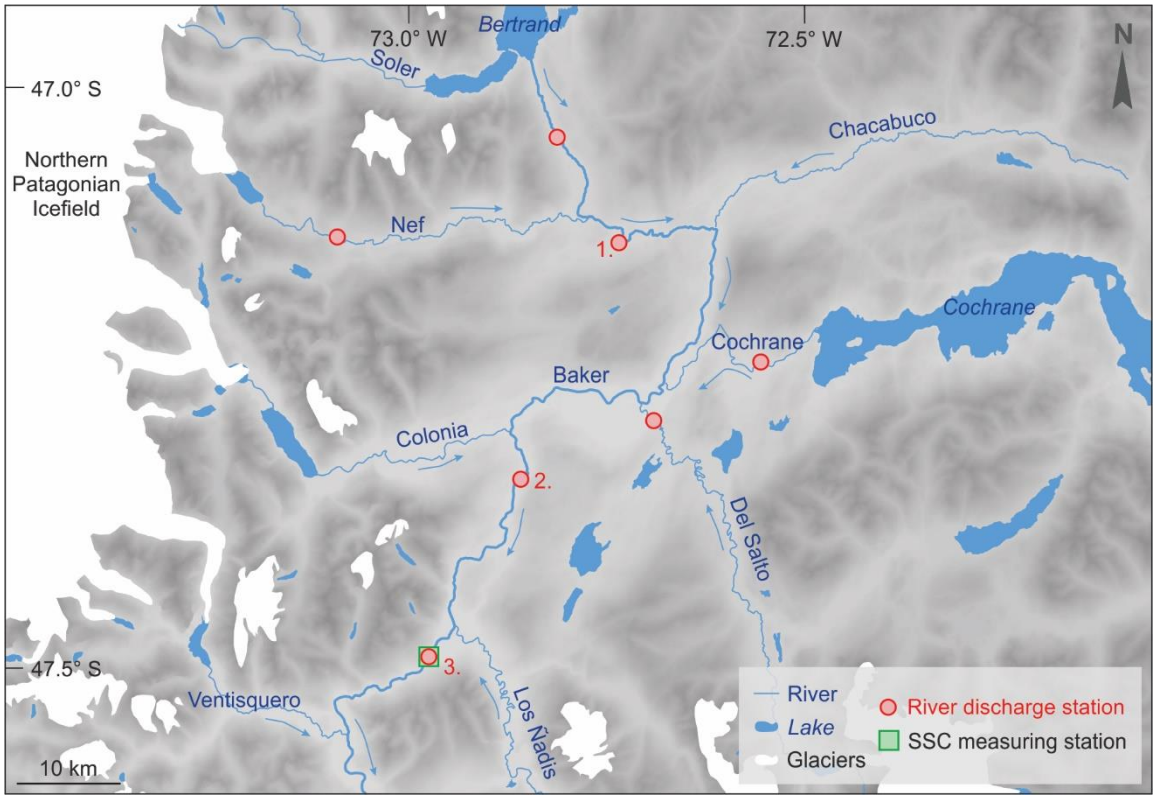

Figure 3.8. Hydrological stations in the lower Baker River watershed on a grey-scale SRTM digital elevation model background. The river discharge stations used in this thesis are 1. Rio Baker en angostura Chacabuco, 2. Rio Baker en Colonia, and 3. Rio Baker bajo Ñadis.

Discharge peaks were attributed a GLOF or meteorological origin based on their shape. GLOF hydrographs typically start more abruptly and generally last less than 48h (Fig. 3.10). Meteorological flood hydrographs, on the other hand, tend to last longer and are less abrupt, as they often result from several consecutive days of rainfall. Aside from their different hydrographs, meteorological floods can also be distinguished from GLOFs by comparing the river gauging data of different stations within the watershed. During meteorological floods, peaks in river discharge can be observed at all stations whereas GLOFs only cause discharge peaks at stations located downstream of the source lake. Moreover, as meteorological floods affect the entire Baker River watershed, their hydrographs tend to increase downstream along the Baker River. This is in contrast with GLOFs, whose hydrographs appear to decrease relatively fast downstream of the lake source (e.g. Jacquet et al., 2017). Finally, precipitation data were consulted to confirm the meteorological origin of the floods. For floods that occurred after 1979, daily gridded climate data integrated over the watershed were used to obtain precipitation data (Alvarez-Garretón et al., 2018).

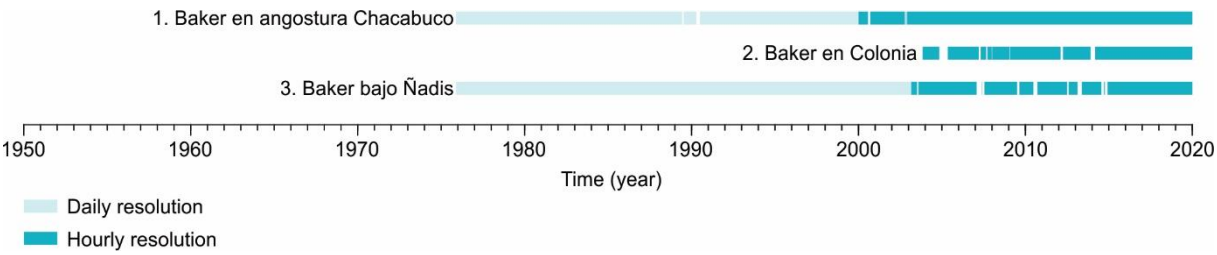

Figure 3.9. Overview of the hydrological data used in this PhD thesis (sources: ENDESA and DGA). See Fig. 3.8 for location. Older data from ENDESA exist for the "Baker en Colonia" station but they were not available to us.

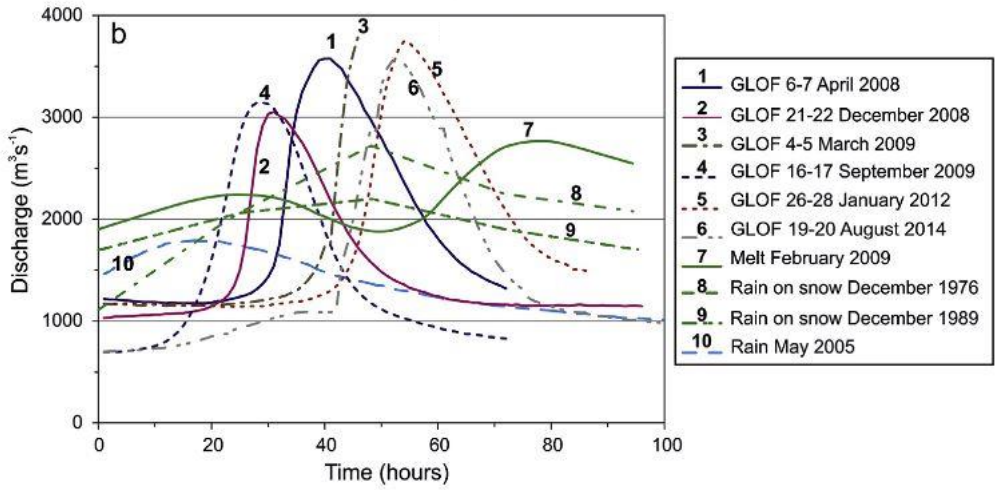

Figure 3.10. Comparison between hydrographs of GLOFs and meteorological floods (snowmelt, rain, or rain-on-snow). All hydrographs are from the river discharge station located immediately downstream of the Baker-Colonia confluence (Figure from Benito et al., 2021).

Finally, information on modern sediment accumulation rates at the head of Martínez Channel was obtained from a Technicap sequential PPS 4/3 sediment trap attached to a mooring. The sediment trap was installed 35m above the fjord bottom and it holds 24 bottles of 500ml. It sampled sediment from February 2017 to February 2020, at a 15-day resolution.

References

Alvarez-Garreton, C., Mendoza, P.A., Boisier, J.P., Addor, N., Galleguillos, M., Zambrano-Bigiarini, M., Lara, A., Puelma, C., Cortes, G., Garreaud, R., McPhee, J., and Ayala, A. (2018) The CAMELS-CL dataset: catchment attributes and meteorology for large sample studies – Chile dataset. *Hydrology and Earth System Sciences*, **22**, 5817 – 5846.

Appleby, P.G., and Oldfield, F. (1978) The calculation of lead-210 dates assuming a constant rate of supply of unsupported 210Pb to the sediment. *Catena*, **5**, 1 – 8.

Barela, L., Miguez, M., and García Conde, L. (2004) Algunos apuntes sobre historia oral. Buenos Aires, Argentina: Instituto Histórico de la Ciudad de Buenos Aires.

Bengtsson, L., and Enell, M. (1986) Chemical analysis. *In: Berglund, B.E. (Ed.), Handbook of Holocene Palaoecology and Palaeohydrlogy*. John Wiley & Sons Ldt., Chinchester, 423 – 451.

Blaauw, M., and Christen, J.A. (2011) Flexible paleoclimate age-depth models using an autoregressive gamma process. *Bayesian Analysis*, **6**, 457 – 474.

Blott, S.J., and Pye, K. (2001) GRADISTAT: a grain-size distribution and statistics package for the analysis of unconsolidated sediments. *Earth Surface Processes and Landforms*, **26**, 1237 – 1248.

Cnudde, V., Cnudde, J.P., Dupuis, C., and Jacobs, P.J.S. (2006) Recent progress in X-Ray CT as a Geosciences Tool. *Applied Geochemistry*, **21**, 826 – 832.

De Agostini, A.S.S. (1945) Andes Patagonicos, Viajes de exploración a la Cordillera Patagonica Austral. Segunda edición aumentada y corregida. Buenos Aires. 436 pp.

Dean, W.E., Jr. (1974) Determination of carbonate and organic matter in calcareous sediments and sedimentary rocks by loss on ignition: Comparison with other methods. *Journal of Sedimentary Petroleum*, **44**, 242 – 248.

Dussaillant, A., Benito, G., Buytaert, W., Carling, P., Meier, C., and Espinoza, F. (2010) Repeated glacial-lake outburst floods in Patagonia: an increasing hazard? *Natural hazards*, **54**, 469 – 481.

Friesen, B.A., Cole, C.J., Nimick, D.A., Wilson, E.M., Fahey, M.J., McGrath, D., and Leidich, J. (2015) Using satellite images to monitor lake outburst floods—Lago Cachet Dos drainage, Chile. U.S. Geological Survey Scientific Investigations Map 3322, scale 1:15,000.

Goldberg, E.D., Gambles, E., Griffin, J.J., and Koide, M. (1977) Pollution history in Narragansett Bay as recorded in its sediments. *Estuarine and Coastal Marine Science*, **5**, 549 – 561.

Harrison, J., Heijnis, H., and Caprarelli, G. (2003) Historical pollution variability from abandoned mie sites, Greater Blue Mountains World Heritage Area, New South Wales, Australia. *Environmental Geology*, **43**, 680 – 687.

Harrison, S., and Winchester, V. (2000) Nineteenth- and twentieth-century glacier fluctuations and climate implications in the Arco and Colonia valleys, Hielo Patagónico Norte, Chile. *Arctic, Antarctic, and Alpine Research*, **32**, 55 – 63.

Harrison, S., Glasser, N., Winchester, V., Haresign, E., Warren, C., and Jansson, K. (2006) A glacial lake outburst flood associated with recent mountain glacier retreat, Patagonian Andes. *The Holocene*, 16, 611 – 620.

Heiri, O., Lotter, A.F., and Lemcke, G. (2001) Loss on ignition as a method for estimating organic and carbonate content in sediments: reproducibility and comparability of results. *Journal of Paleolimnology*, 25, 101 – 110.

HidroAysén (2010) Centrales hidroeléctricas de Aysén S.A. – HidroAysén. Caracterización del régimen sedimentológico y efectos de la construcción de centrales del PHA. Anexo 2D, apéndice 4, parte 2, 687 pp.

Higuera, P.E., Brubaker, L.B., Anderson, P.M., Hu, F.S., and Brown, T.A. (2009) Vegetation mediated the impacts of postglacial climate change on fire regimes in the south-central Brooks Range, Alaska. *Ecological Monographs*, 97, 201 – 219.

Hogg, A.G., Hua, Q., Blackwell, P.G., Niu, M., Buck, C.E., Guilderson, T.P., Heaton, T.J., Palmer, J.G., Reimer, P.J., Reimer, R.W., Turney, C.S.M., and Zimmerman, S.R.H. (2013) SHCal13 southern hemisphere calibration, 0-50,000 years cal BP. *Radiocarbon*, 55, 1889 – 1903.

Iribarren Anacona, P., Norton, K.P., and Mackintosh, A. (2014) Moraine-dammed lake failures in Patagonia and assessment of outburst susceptibility in the Baker Basin. *Natural Hazards and Earth System Sciences*, 14, 3243 – 3259.

Iribarren Anacona, P., Mackintosh, A., and Norton, K (2015) Reconstruction of a glacial lake outburst flood (GLOF) in the Engaño Valley, Chilean Patagonia: Lessons for GLOF risk management. *Science of the Total Environment*, 527-528, 1 –11.

Jacquet, J., McCoy, S.W., McGrath, D., Nimick, D.A., Fahey, M., O'kuinghttons, J., Friesen, B.A., and Leidlich, J. (2017) Hydrologic and geomorphic changes resulting from episodic glacial lake outburst floods: Rio Colonia, Patagonia, Chile. *Geophysical Research Letters*, 44, 854 – 864.

Jasper, J.P., Fourel, F., Eaton, A., Morrison, J., and Phillips, A. (2001) Stable Isotopic Characterization of Analgesic Drugs. Abstract from the American Society of Mass Spectrometry, Chicago, USA.

Krishnaswamy, S., Lal, D., Martin, J., and Meybeck, M. (1971) Geochronology of lake sediments. *Earth and Planetary Science Letters*, 11, 407– 414.

McMinn, A., Hallegraeff, G.M., Thomson, P., Jenkinson, A.V., and Heijnis, H. (1997) Cyst and radionucleotide evidence for the recent introduction of the toxic dinoflagellate Gymnodinium catenatum into Tasmanian waters. *Marine Geology Progress Series*, 161, 165 – 172.

Muccio, Z., and Jackson, G.P. (2009) Isotope ratio mass spectrometry. *Analyst*, 134, 213 – 222.

Oportus, C. (1928) Informe sobre el problema de colonización de la zona del río Baker. Departamento de Tierras y Colonización, Ministerio de Fomento, Santiago de Chile, 120 pp.

Robbins, J.A., and Edgington, D.N. (1975) Determination of recent sedimentation rates in Lake Michigan using Pb-210 and CS-137. *Geochimica et Cosmochimica*, 39, 285 – 304.

Sandgren, P., and Snowball, I. (2001) Application of mineral magnetic techniques to paleolimnology. In *Tracking Environmental Change Using Lake Sediments Volume 2: Physical and Geochemical Methods (eds. Last, W.M. & Smol, J.P.)*. Dordrecht: Kluwer Academic Publishers. pp. 217–237

SHOA (2001) Servicio Hidrográfico y Oceanográfico de la Armada. *Canal Baker y puertos adyacentes*, 6th edition, 1:200000, Mercator projection. Valparaíso, Chile.

Tanaka, K. (1980) Geographic contribution to a periglacial study of the Hielo Patagonico Norte with special reference to the glacial outburst originated from Glacier-Dammed Lago Arco, Chilean Patagonia. Centre Co Ltd, Tokyo, 97 pp.

Verardo, D.J., Froelich, P.N., and McIntyre, A. (1990) Determination of organic carbon and nitrogen in marine sediments using the Carlo Erba NA-1500 Analyzer. *Deep-Sea Research*, **37**, 157 – 165.

Weltje, G., Bloemsma, M., Tjallingii, R., Heslop, D., Röhl, U., and Croudace, I. (2015) Prediction of Geochemical Composition from XRF Core Scanner Data: A new multivariate approach including automatic selection of calibration samples and quantification of uncertainties. *In: Croudace, I., Rothewell, R. (Eds.) Micro-XRF Studies of Sediment Cores. Developments in Paleoenvironmental Research*, vol. 17. Springer, Dordrecht, The Netherlands.

Whitlock, C., and Larsen, C. (2001) Charcoal as a fire proxy. *In: J. P. Smol, H. J. B. Birks & W. M. Last (Eds.) Tracking Environmental Change Using Lake Sediments, Terrestrial, Algal, and Siliceous Indicators*, vol. 3. KluwerAcademic Publishers, Dordrecht, The Netherlands.

Winchester, V., and Harrison, S. (2000) Dendrochronology and lichenometry: colonization, growth rate and dating of geomorphological events on the east side of the North Patagonian Icefield, Chile. *Geomorphology*, **34**, 181 – 194.

Zatz, L.M. (1981) Basic principles of computed tomography scanning. *In: Newton, T.H. and Potts, D.G. (Eds.), Technical Aspects of Computed Tomography.* Mosby, St. Louis, MO.

Table S3A. Overview of the samples used in this PhD thesis.

	Latitude (° S)	Longitude (° E)	Date (dd/mm/yyyy)	Length (cm)
Fjord				
Gravity cores				
FC17-01	47.8004	73.66169	07/02/2017	113
FC17-01A	47.80235	73.66129	06/02/2017	116
FC17-02	47.80512	73.65194	07/02/2017	127
FC17-03	47.79840	73.73300	07/02/2017	138
FC17-04A	47.77211	73.69180	06/02/2017	72
FC17-05	47.78693	73.65629	06/02/2017	117
FC17-06	47.78669	73.64903	06/02/2017	116
FC17-07	47.78583	73.64362	06/02/2017	102
FC17-08	47.79242	73.63994	06/02/2017	107
FC17-09	47.79023	73.62998	06/02/2017	76
FC17-10	47.78444	73.61631	06/02/2017	87
FC17-17	47.78753	73.60652	07/02/2017	104
Sediment grab samples				
GS17-01a	47.63783	73.65421	05/02/2017	–
GS17-01	47.63909	73.65773	05/02/2017	–
GS17-02a	47.64055	73.66252	05/02/2017	–
GS17-02	47.64175	73.66740	05/02/2017	–
GS17-03	47.64261	73.67298	05/02/2017	–
GS17-04	47.64263	73.68776	05/02/2017	–
GS17-05	47.65177	73.68108	05/02/2017	–
GS17-06	47.65273	73.69947	05/02/2017	–
GS17-07	47.67320	73.71278	05/02/2017	–
GS17-08	47.68835	73.71938	05/02/2017	–
GS17-09	47.70908	73.71408	05/02/2017	–
GS17-10	47.72381	73.70324	05/02/2017	–
GS17-11	47.74270	73.69878	05/02/2017	–
GS17-12	47.76129	73.69342	05/02/2017	–
GS17-13	47.78909	73.62663	05/02/2017	–
GS17-14	47.78399	73.61241	05/02/2017	–
GS17-15	47.79111	73.60480	05/02/2017	–
GS17-16	47.79500	73.59974	05/02/2017	–
GS17-17	47.79063	73.59333	05/02/2017	–
GS17-18	47.79034	73.60009	05/02/2017	–
GS17-19	47.78557	73.61646	06/02/2017	–
GS17-20	47.78533	73.62568	06/02/2017	–
GS17-21	47.78915	73.63958	06/02/2017	–
GS17-22	47.79290	73.63686	06/02/2017	–
GS17-23	47.78233	73.60341	06/02/2017	–
GS17-24	47.79066	73.78233	06/02/2017	–
GS17-25	47.79516	73.58971	07/02/2017	–

GS17-26	47.65553	73.69476	08/02/2017	–
GS17-27	47.66309	73.70060	08/02/2017	–
GS17-28	47.67361	73.70182	08/02/2017	–
GS17-29	47.67754	73.70576	08/02/2017	–
GS17-30	47.68130	73.70930	08/02/2017	–
GS17-31	47.68931	73.71352	08/02/2017	–
GS17-32	47.69913	73.71220	08/02/2017	–
GS17-33	47.70747	73.70996	08/02/2017	–
GS17-34	47.71692	73.71207	08/02/2017	–
GS17-35	47.65144	73.70441	08/02/2017	–
GS17-36	47.65191	73.70258	08/02/2017	–
GS17-37	47.65253	73.70115	08/02/2017	–
GS17-38	47.67365	73.69809	08/02/2017	–
GS17-39	47.65744	73.68986	08/02/2017	–
GS17-40	47.65502	73.69685	08/02/2017	–
GS17-41	47.65815	73.68826	08/02/2017	–
GS17-42	47.65128	73.69161	08/02/2017	–
GS17-43	47.65038	73.67554	08/02/2017	–
Floodplain				
FP17-01	47.27748	72.77005	29/01/2017	362
FP17-02	47.26964	72.82353	30/01/2017	200
FP17-03	47.26752	72.75880	30/01/2017	500
FP17-04	47.26841	72.72092	31/01/2017	454
River samples				
Baker	47.0517	72.8137	Aug 2008 – Jun 2010	–
	47.2053	72.6307	Aug 2008 – May 2010	–
	47.2953	72.8698	Nov 2008 – May 2010	–
Nef	47.1226	72.7869	Dec 2008 – May 2010	–
Chacabuco	47.1157	72.6061	Aug 2008 – May 2010	–
Cochrane	47.2776	72.6928	Aug 2008 – May 2010	–
Del Salto	47.2835	72.7075	Aug 2008 – May 2010	–
Colonia	47.3063	72.8807	Nov 2008 – Jan 2010	–

4. Modern sedimentary processes at the heads of Martínez Channel and Steffen Fjord, Chilean Patagonia

This chapter is based on:

Vandekerkhove, E., Bertrand, S., Crescenzi Lanna, E., Reid, B., and **Pantoja, S.** (2020) Modern sedimentary processes at the heads of Martínez Channel and Steffen Fjord, Chilean Patagonia. *Marine Geology*, **419**, 106076.

Author contributions: EV and SB acquired the multibeam data and EV and ECL processed them. EV and ECL analyzed the surface sediment samples. EV and SB interpreted the results and wrote the paper, with contributions from BR and SP.

Abstract: Chilean fjord sediments constitute high-resolution archives of climate and environmental change in the southern Andes. To interpret such records accurately, it is crucial to understand how sediment is transported and deposited within these basins. This issue is of particular importance in glaciofluvial Martínez Channel and Steffen Fjord (48°S), due to the increasing occurrence of Glacial Lake Outburst Floods (GLOFs) originating from outlet glaciers of the Northern Patagonian Icefield. Hence, the bathymetry of the head of Martínez Channel and Steffen Fjord was mapped at high resolution and the grain size and organic carbon content of grab sediment samples were examined. Results show that the subaquatic deltas of Baker and Huemules rivers at the head of Martínez Channel and Steffen Fjord, respectively, are deeply incised (up to 36 m) by sinuous channels. The presence of sediment waves and coarser sediments within these channels imply recent activity and sediment transport by turbidity currents. Although several potential triggering processes are plausible, we argue that elevated river discharge and the associated high suspended sediment loads is the main cause for the occurrence of turbidity currents at the head of these fjords and are of key importance in shaping the fjord's subaquatic morphology. This study shows that the heads of Martínez Channel and Steffen Fjord are dynamic sedimentary environments with rapidly migrating channels. It highlights the importance of site selection and multi-coring in any future project aimed at reconstructing environmental change using the sediments of either fjord.

4.1. Introduction

Fjords are sensitive environments at the interface between the ocean and the adjacent mountainous land masses. They occur in mid to high latitude regions and their sediment infill is, or was, closely related to glacier activity (e.g. Syvitski et al., 1987). Consequently, fjords can hold important sediment records of these changing glacial conditions during the Holocene. Patagonian fjord sediments, in particular, are increasingly recognized as high-resolution archives of climate and environmental changes. Previous studies have used these sediment archives to reconstruct past changes in glacier variability (Bertrand et al., 2012, 2017), sea surface temperature (Sepúlveda et al., 2009; Caniupán et al., 2014), precipitation (Lamy et al., 2010; Bertrand et al., 2014), and seismic activity (Piret et al., 2017a; Wils et al., 2018).

A fjord area that is increasingly attracting the attention of scientists working in Patagonia is the Baker-Martínez fjord system (48°S), particularly due to the increasing occurrence of Glacial Lake Outburst Floods (GLOFs) originating from the rapidly retreating outlet glaciers of the Northern Patagonian Icefield (NPI; Harrison et al., 2007; Lopez et al., 2010; Dussaillant et al., 2010; Davies and Glasser, 2012; Wilson et al., 2018). Although the impact of modern GLOFs on the hydrography and ecology of the Baker-

Martínez fjord system has recently received a fair amount of attention (e.g. Marin et al., 2013; Meerhoff et al., 2018), the sedimentary processes taking place in the fjords during GLOFs remain mostly unknown. This is largely due to the lack of a detailed bathymetric map, for which only few manual depth soundings have been acquired by the Chilean Navy Hydrographic and Oceanographic Service (Servicio Hidrográfico y Oceanográfico de la Armada, 2001). Detailed bathymetric data is particularly of interest for future research on how GLOFs influence the fjord's morphology and how they are recorded in its sediments, which is of both scientific and societal interest since this may allow generating long sediment archives of GLOF variability, as well as affect important decisions regarding the future development of the region (e.g. subsea infrastructure, town expansion).

General fjord sedimentation models indicate that the sediment entering a fjord is separated into two components: (1) a coarser bedload which gets deposited quickly onto the delta, and (2) a buoyant hypopycnal plume which flows on top of a salty, warmer, water mass, creating a two-layer flow typical for fjord systems (Syvitski and Shaw, 1995). As rivers in Chilean Patagonia discharge large amounts of sediment-laden freshwater into the fjords, the two-layer circulation varies seasonally according to river discharge, which increases in summer due to glacier and snowmelt (Iriarte et al., 2014). As the buoyant plume flows towards the ocean, suspended sediment settles in response to the decreasing velocity, increasing salinity, and due to flocculation, agglomeration, and palletization of finer particles (Syvitski, 1991). Previous studies have shown the diverse morphologies existing in Patagonian fjords and how different glaciofluvial sedimentary processes are important in shaping the morphology of the fjord bottoms (e.g. DaSilva et al., 1997; Boyd et al., 2008; Rodrigo, 2008; Araya Vergara, 2011; Dowdeswell et al., 2013).

To better understand the sedimentary processes taking place at the heads of Martínez Channel and Steffen Fjord (48°S), this paper presents approximately 100 km² of new high-resolution multibeam bathymetry acquired in 2016. The distinctive morphological features are then thoroughly described and discussed. In addition, grab sediment samples are examined for their physical properties and organic carbon content to understand recent fjord sedimentary processes related to the discharge of water and sediments by the main rivers entering the fjords.

4.2. Setting

Martínez Channel and Steffen Fjord are located in Chilean Patagonia (47.8°S – 73.6°W; Fig. 4.1a), between the Northern Patagonian Icefield (NPI) and the Southern Patagonian Icefield (SPI). This mountainous region is characterized by a complex island and channel landscape that was formed by extensive glacial erosion. During the Quaternary, the NPI and SPI have contracted and expanded several times (Kaplan et al., 2004; Douglass et al., 2005; Harrison and Glasser, 2011), converging during glacial periods into the larger Patagonian Ice Sheet (PIS: 38–56°S; Caldenius, 1932). After the Last Glacial Maximum (LGM), PIS glaciers started to shrink and new drainage routes opened (Harrison & Glasser, 2011; Garcia et al., 2012; Glasser et al., 2012; Glasser et al., 2016), eventually leading to the formation of many fjords and lakes. Discharge of large quantities of ice and meltwater was reorganized westwards towards the Pacific Ocean from 10 kyr onwards (Glasser et al., 2016), or earlier (13.5 kyr ago; Hubbard et al., 2005).

The glacierized region of Chilean Patagonia is increasingly prone to GLOFs due to the rapid retreat of most NPI outlet glaciers (Harrison et al., 2007; Lopez et al., 2010; Davies and Glasser, 2012; Wilson et al., 2017). Most current GLOFs in the region originate from the Colonia river valley (Dussaillant et al.,

2010; Fig. 4.1a), where previous studies have provided evidence for flooding events in 1896–1897, 1914–1917, 1944, and 1963 (Lliboutry, 1956; Tanaka, 1980; Winchester and Harrison, 2000). Since April 2008, the Colonia river valley experiences repeated GLOFs related to the abrupt emptying of Cachet 2 Lake (Dussaillant et al., 2010; Jacquet et al., 2017). During such GLOF events, Baker River triples in discharge (Dussaillant et al., 2010) and river suspended sediment concentrations increase 8-fold due to erosion of lake-bed and valley-fill deposits in the watershed (Bastianon et al., 2012). Similar flood events also occurred in the Huemules river valley, where 10 GLOFs were documented between 1985 and 2013 (Aniya, 2014).

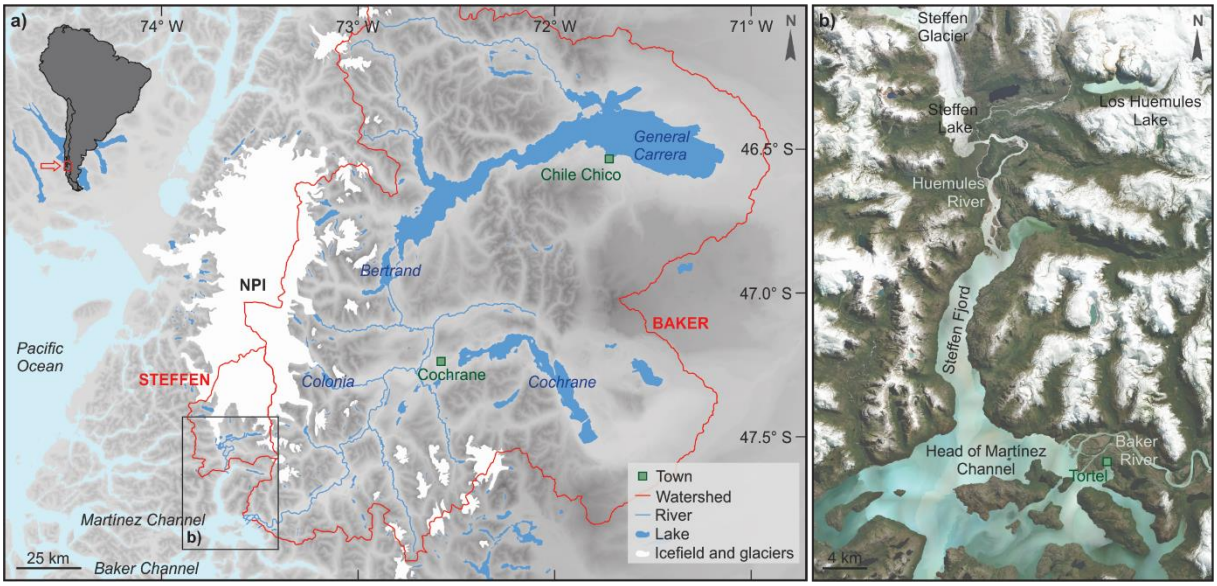

Figure 4.1. Location of Steffen Fjord and the head of Martínez Channel in Chilean Patagonia. **(a)** Watersheds of Huemules and Baker rivers (in red), which are the main tributaries of Steffen Fjord and Martínez Channel, respectively. The limits of the watersheds under the Northern Patagonian Icefield (NPI) are from Lopez et al. (2010). **(b)** Location of Baker and Huemules rivers at the heads of Martínez Channel and Steffen Fjord, respectively (Global Mapper World Imagery). The white patches correspond to snow and ice.

The Baker-Martínez fjord system connects the western terrestrial environments of Patagonia with the Pacific Ocean (Fig. 4.1a). Its main tributary is Baker River, which drains most of the eastern side of the NPI and constitutes the largest river in Chile in terms of volume of water. The river starts at Bertrand Lake, which is fed by General Carrera Lake, and continues to flow southwards. Baker River discharge ranges from 600 (winter) to 1200 (summer) m^3/s, and it reaches up to 4200 m^3/s during GLOFs (Dirección General de Aguas, DGA, Chile; Jacquet et al., 2017). According to Quiroga et al. (2012), some of the GLOFs carry an estimated 1.0 to 1.5 x 10^5 tons of sediment to the fjord and may contribute up to 5 % of the annual fine sediment load. Baker River discharges at the head of Martínez Channel near the town of Caleta Tortel, where it splits into one main and two smaller outlet channels (Fig. 4.1b). On the fan-shaped aerial delta, which covers approximately 14 km^2, several smaller abandoned channels are visible.

Steffen Fjord is situated immediately to the south of the NPI and it is mainly fed by meltwater from Steffen Glacier via Huemules River. It is an elongated north-south orientated basin, with a total length of approximately 20 km and an average width of 2.5 km (Fig. 4.1b). Steffen Glacier is the third largest glacier of the NPI with a surface area of 428.3 km^2 (Lopez et al., 2010), which drains most of the southern part of the icefield (Fig. 4.1a). Over the past decades, the frontal retreat of Steffen Glacier has

accelerated from 0.5 km²/yr (1979–2001) to 1.2 km²/yr (2001–2011), resulting in an ice surface loss of 12 km² between 2001 and 2011 (López and Casassa, 2011). Similar to Baker River, Huemules River has a glacial regime due to the large input of meltwater from Steffen Glacier. At the mouth of Huemules River, water flows into Steffen Fjord through one main channel, forming a ~3.6 km² fan-shaped delta that encompasses the entire width of the fjord. To the south, surface waters from Steffen Fjord join Martínez Channel and continue flowing westwards towards the Pacific Ocean. Although GLOFs have been documented along Huemules River (Aniya, 2014; DGA, 2019), the river is not equipped with a permanent discharge monitoring station. The exact hydrological conditions during GLOFs are therefore not known.

4.3. Material and methods

4.3.1. Multibeam bathymetry

The bathymetry of the head of Martínez Channel and of Steffen Fjord was mapped with an ELAC Seabeam 1050 system in austral winter 2016 to avoid the influence of large sound velocity variations by variable freshwater input. A mounting frame holding the two 50 kHz transducers at a 120° angle, was installed at the bow of the *R/V Sur-Austral* (COPAS Sur-Austral, Chile). In order to correct for roll, pitch, and heave movements, an Octans Motion Sensor (IXSEA) was placed on the mounting pole above the transducers. CTD measurements were continuously recorded at the water surface (approximately 1 m depth) using a Valeport Modus CTD. To correct for sound velocity changes with depth, a total of 24 vertical CTD profiles were taken with an RBR Maestro, operating at a sampling rate of 6 Hz and vertical speed of 1 m/s. These CTD profiles were collected on a daily basis and were evenly distributed over the mapped area (Supplementary Fig. S4A). The multibeam data were processed with *Caris HIPS and SIPS v9.1*, including tide correction based on tide tables at Caleta Tortel (maximum tidal range of 1.9 m). The final bathymetric maps have a grid resolution of 5 m and were created using *Fledermaus v7*.

4.3.2. Grab sediment samples

A total of 45 surface sediment samples were collected in February 2017 aboard the *R/V Sur-Austral,* using a Van Veen grab sampler (0.008 m³) attached to a pneumatic winch. A small shovel was used to collect subsamples. All samples were freeze dried. Grain-size measurements of the lithogenic fraction were conducted with a Malvern Mastersizer 3000 particle size analyzer (Ghent University, Belgium). In order to remove organic matter, all samples were pre-treated with 2 ml of a 30 % hydrogen peroxide (H_2O_2) solution added to 10 ml of demineralized water containing the suspended sample. Additionally, 1 ml of a 10 % hydrochloric acid (HCl) solution and 1 ml of a 2N sodium hydroxide (NaOH) solution were added to remove carbonate and biogenic silica, respectively. After rinsing the sample, grain flocculation was avoided by shortly boiling the samples with sodium hexametaphosphate (calgon). Measuring times of 12 s with 10 % sonification were used. Total Organic Carbon (TOC) content was determined by analyzing the samples with an elemental analyzer at the Stable Isotope Facility (UC Davis, California, USA). To remove possible inorganic carbon, all samples were treated with 1N sulfurous acid prior to analysis (Verardo et al., 1990).

4.4. Results

4.4.1. Basin morphology

The swath bathymetry imagery indicates that the basin floor (where Steffen Fjord and Martínez Channel merge) is relatively flat, varying on average from 280 to 285 m depth, with a maximum measured water depth of 290 m. Steep-walled fjord slopes (up to 75°) occur close to the shorelines (Fig. 4.2). Two seamounts are also visible on the flat basin floor. Closer to the river mouths, the bathymetry shows well-

developed deltas with several subaquatic morphological features. These features are presented separately for the head of Martínez Channel and Steffen Fjord below.

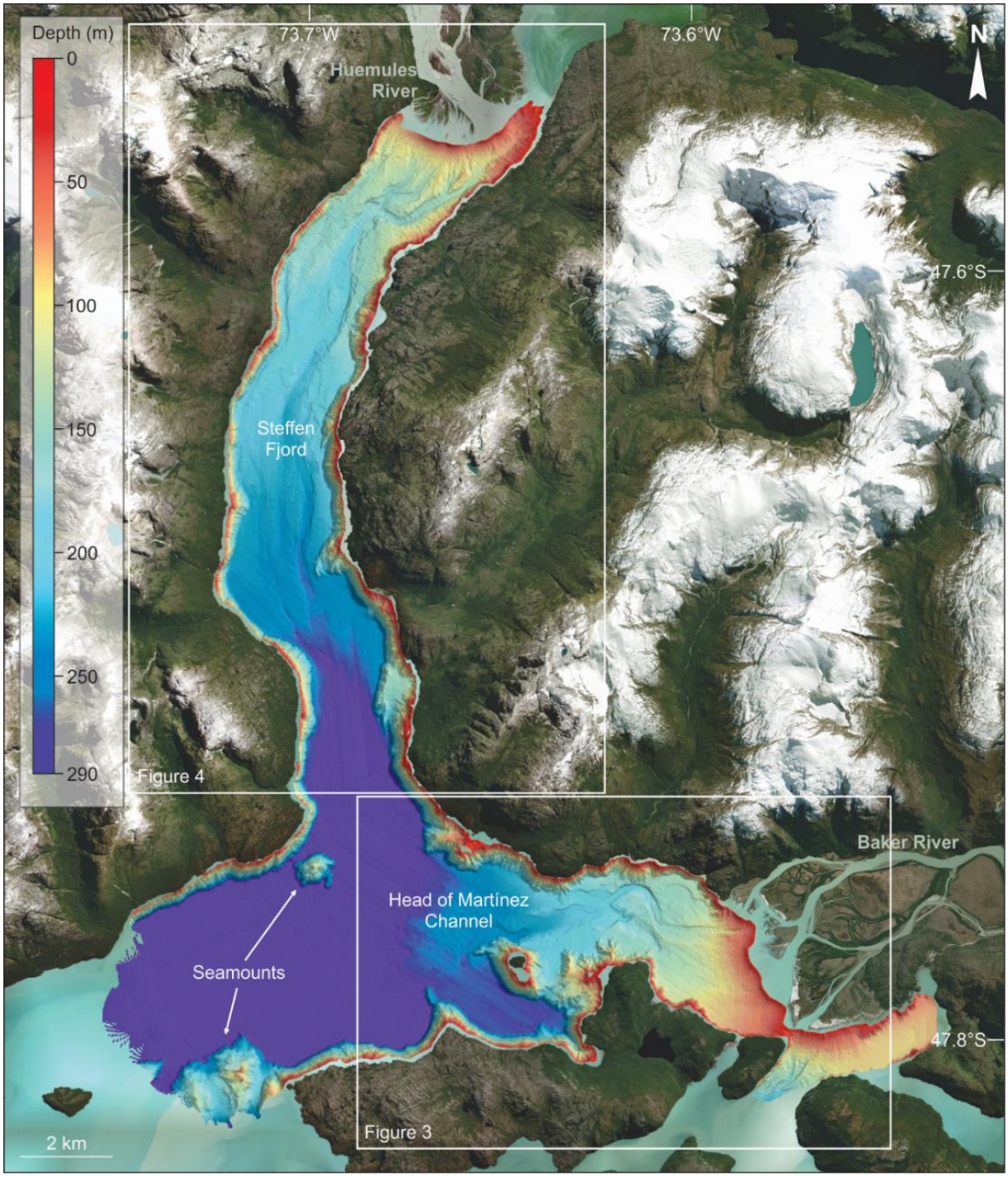

Figure 4.2. Bathymetry of Steffen Fjord and of the head of Martínez Channel.

4.4.1.1. The head of Martínez Channel: morphological features

The morphology in front of Baker River mouth is characterized by a large subaquatic delta, with depths that gradually increase from 0 to 266 m (Fig. 4.3). The proximity of islands in front of the delta obstructs the development of a complete subaquatic delta. The delta slope has a concave profile with a slightly higher slope gradient in the shallower part of the delta (3.4° up to 2 km from the Baker River mouth) compared to the mid-slope region (2°; Figs. 4.3 and 4.4). The maximum extent of the submarine delta

is located approximately 7.9 km west of the delta margin where a distributary fan can be observed (Fig. 4.3b). The submarine delta is incised by two prominent channels that are bounded by elevated sediment ridges or levees in the upper slope as well as in the mid-slope delta region (Fig. 4.3b). The meandering channel west of the main river mouth cuts up to 26 m deep in the sediment and has a total length of approximately 8 km. It has an average width of 140 m and measures 400 m at its widest point (Fig. 4.4a-c). The channel deviates counterclockwise along-slope Vigía Island and it terminates at a 266 m-deep flat fjord bottom where a lobe-shaped depositional fan is formed (Fig. 4.3).

The secondary channel is smaller and located in front of the southern branch of Baker River, confined between Morgan and Barrios Islands, where several smaller submarine chutes and channels converge into one single channel. The latter has an average incision depth of 6 m and an average width of 160 m. Bathymetric data for this channel is incomplete so its southern limit is unknown.

Within the axial channels of the head of Martínez Channel, crescent-shaped transverse bedforms are present (Fig. 4.3b-c). These bedforms occur at regular intervals from a depth of 70 m and continue down to 175 m depth. The wavelength of the ridges increase with distance from the delta margin, from 22.5 m at a depth of 60 m to 115 m at a depth of 172 m. The slope of their steeply dipping lee side is on average 13° but can go up to 21° (Fig. 4.4d). Similar bedforms, although more irregularly shaped, appear in the unchannelized region on the upper slope of the delta, parallel to the delta margin (Figs. 4.3b, d). These creep-like features of scours and ridges continue downslope approximately 1.7 km from the Baker delta lip to a depth of 138 m (Figs. 4.3b and 4.4a). They cover an area of 3.6 km² and occur where the slope gradient is between 5 to 15°. The ridges are 1.5 to 5.5 m high and measure up to 700 m in width. In addition, distinctive erosive features, i.e., gullies and remnant channel walls, are visible on the subaquatic part of the delta (Fig. 4.3b). At the margin of the San Martin river inlet, situated west of Baker River, a smaller fluvial-fed depocenter can be observed (Fig. 4.3b). It is incised with several gullies and terminates at the western channel. Finally, a head scarp just north of Vigía Island, with a slope angle of 80°, suggests the occurrence of a submarine slope failure (Fig. 4.3).

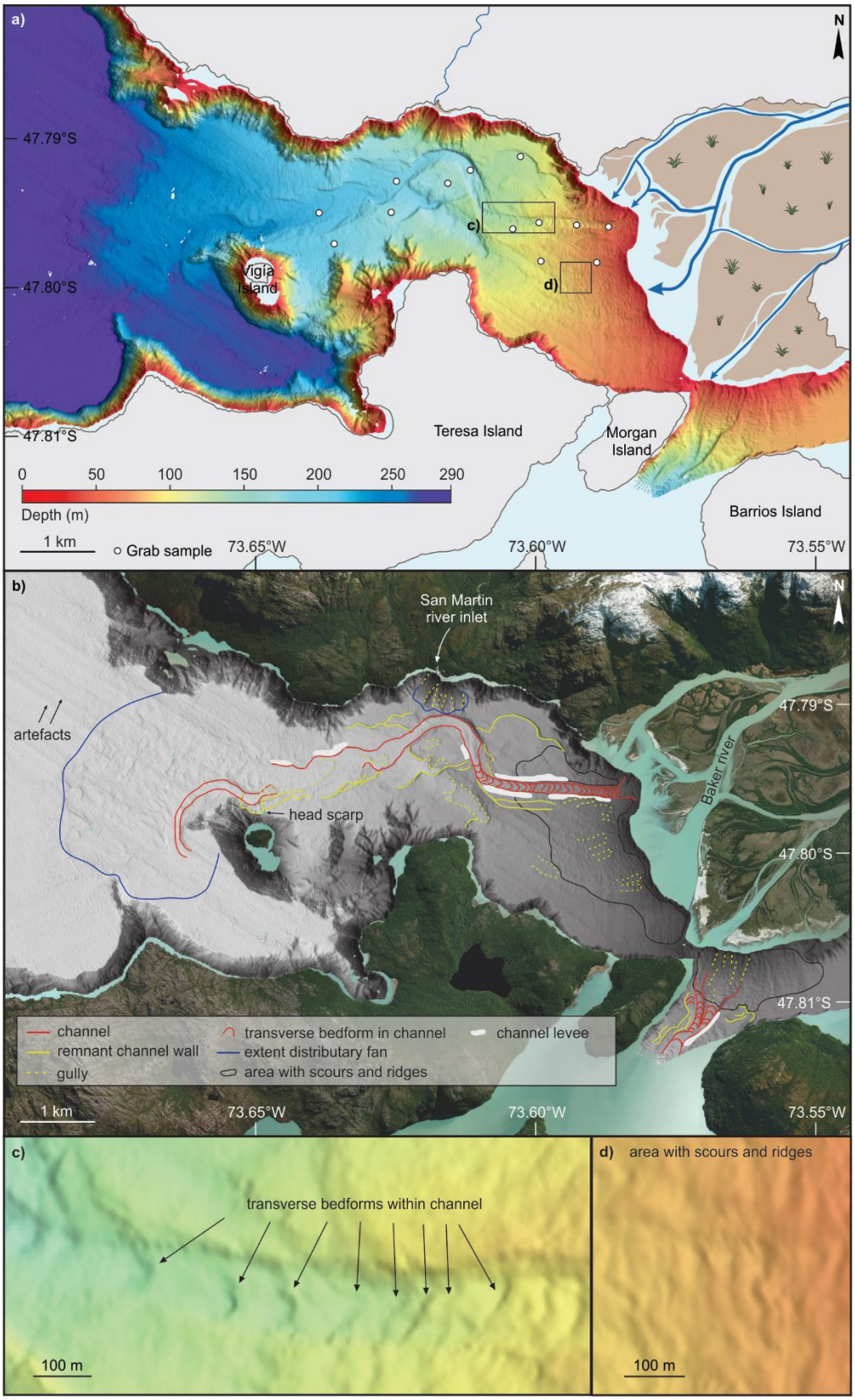

Figure 4.3. Bathymetry of the Baker River delta and delta front at the head of Martínez Channel. **(a)** Bathymetric map and location of the grab sediment samples (white circles). **(b)** Grey shaded-relief bathymetry with indication of the main morphological features identified from the bathymetric data. **(c)** Enlargement of the transverse bedforms within the channel. **(d)** Enlargement of the non-channelized area with sinuous scours and ridges.

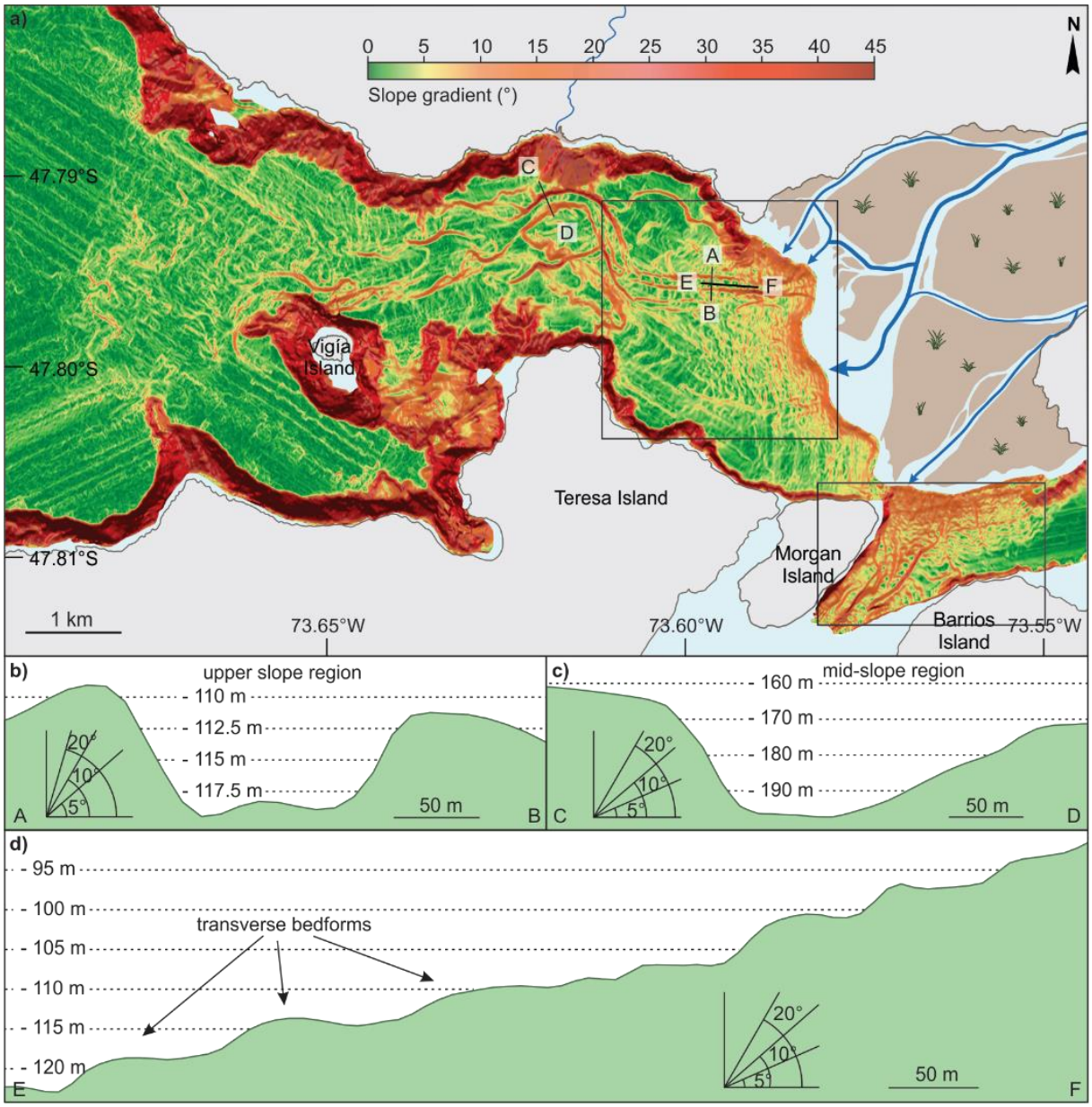

Figure 4.4. (a) Slope map of the Baker River delta and prodelta at the head of Martínez Channel. **(b–d)** Cross-sections (see (a) for location) of the main channel in the upper slope region (b) and in the mid-slope area (c), and of the crescent-shaped transverse bedforms observed in the channel (d).

4.4.1.2. Steffen Fjord: morphological features

The upper part of the Huemules subaquatic delta is characterized by several gullies that converge into one well-developed channel (Figs. 4.5 and 4.6). This channel extends up to 11.5 km to the south in Steffen Fjord and it opens into a flat basin at a depth of 265 m. It has an average width of 185 m and measures 550 m at it widest point. The maximum incision depth is 36 m and channel levees can be observed in the mid-slope region (Fig. 4.6b). At approximately 3.6 km from the Huemules river mouth, the channel deviates slightly around a subaquatic feature. As at the head of Martínez Channel, crescent-shaped ridges or transverse bedforms are visible within the gullies and channel, although to a lesser extent (Figs. 4.5 and 4.6c). These ridges are observed up to 2 km from the Huemules delta lip down to a depth of 165 m. The steep lee side of the ridges has an average slope gradient of 13° and a maximum of 26° and show no relation with depth. In terms of wavelengths, the distance between the ridges is

slightly more irregular than at the head of Martínez Channel and measures on average 105 m. Several gullies and remnant channel walls are visible along the channel. The unchannelized region on the upper delta slope also shows irregular bedforms consisting of sinuous scours and ridges. They cover a surface area of 1.7 km² and continue down to a depth of 115 m (Figs. 4.5b and 4.6c). Here, the ridges occur on a 5 to 10° slope.

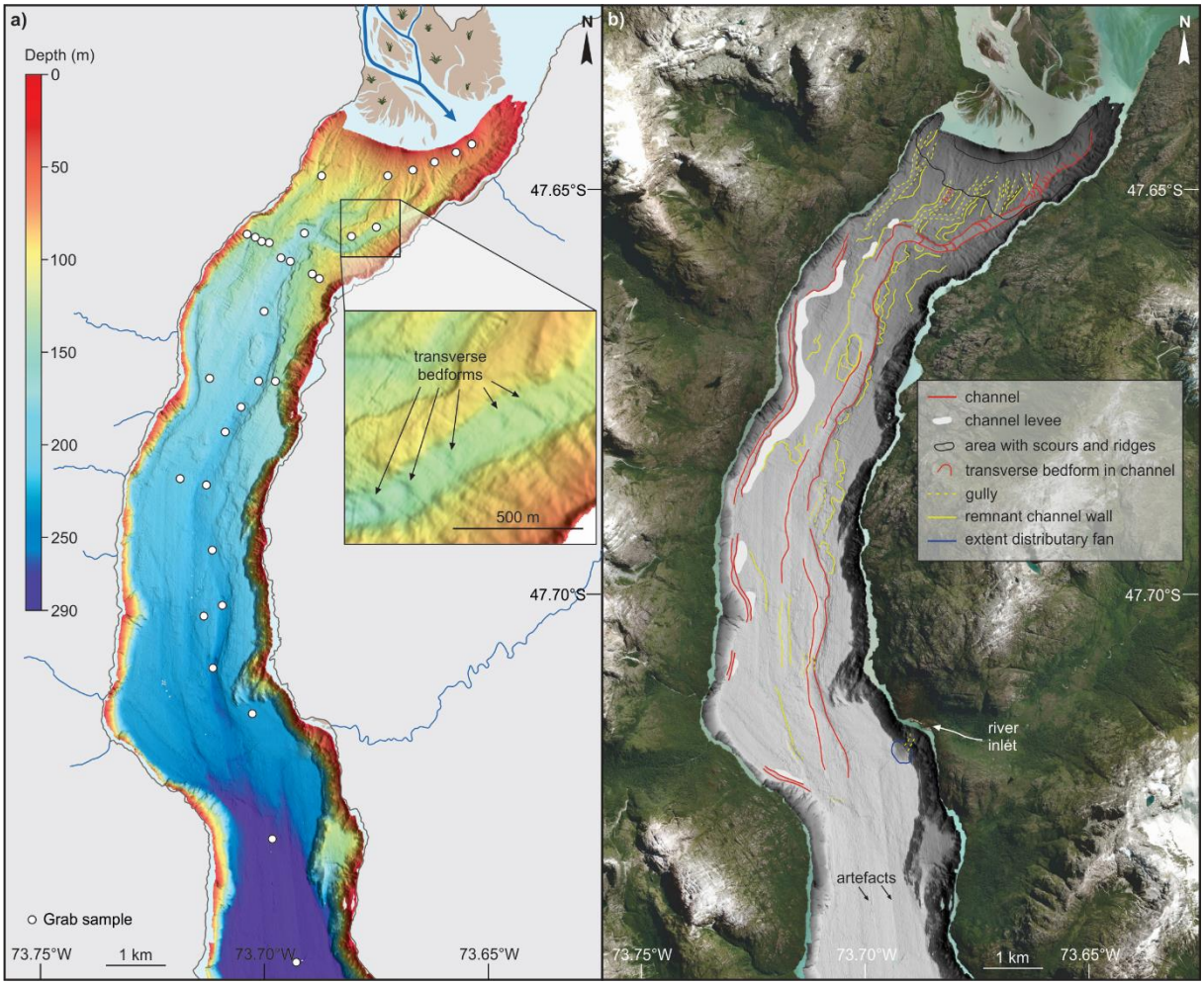

Figure 4.5. Bathymetry of Steffen Fjord. **(a)** Grab sediment samples locations are indicated with white circles. The enlargement displays the transverse bedforms within the channel. **(b)** Grey shaded-relief bathymetry of Steffen Fjord with indication of the main morphological features identified from the bathymetric data.

Along the western shoreline of Steffen Fjord, a 7.5 km-long sinuous channel, with slightly elevated levees towards the central axis of the fjord, can be observed at the slope break (Figs. 4.5b and 4.6d). The maximum height difference between the bottom of the channel and the top of its levee is 18 m. Finally, a smaller subaquatic delta with a lobe-shaped fan is visible near a river inlet along the eastern shoreline of the fjord (Fig. 4.5b).

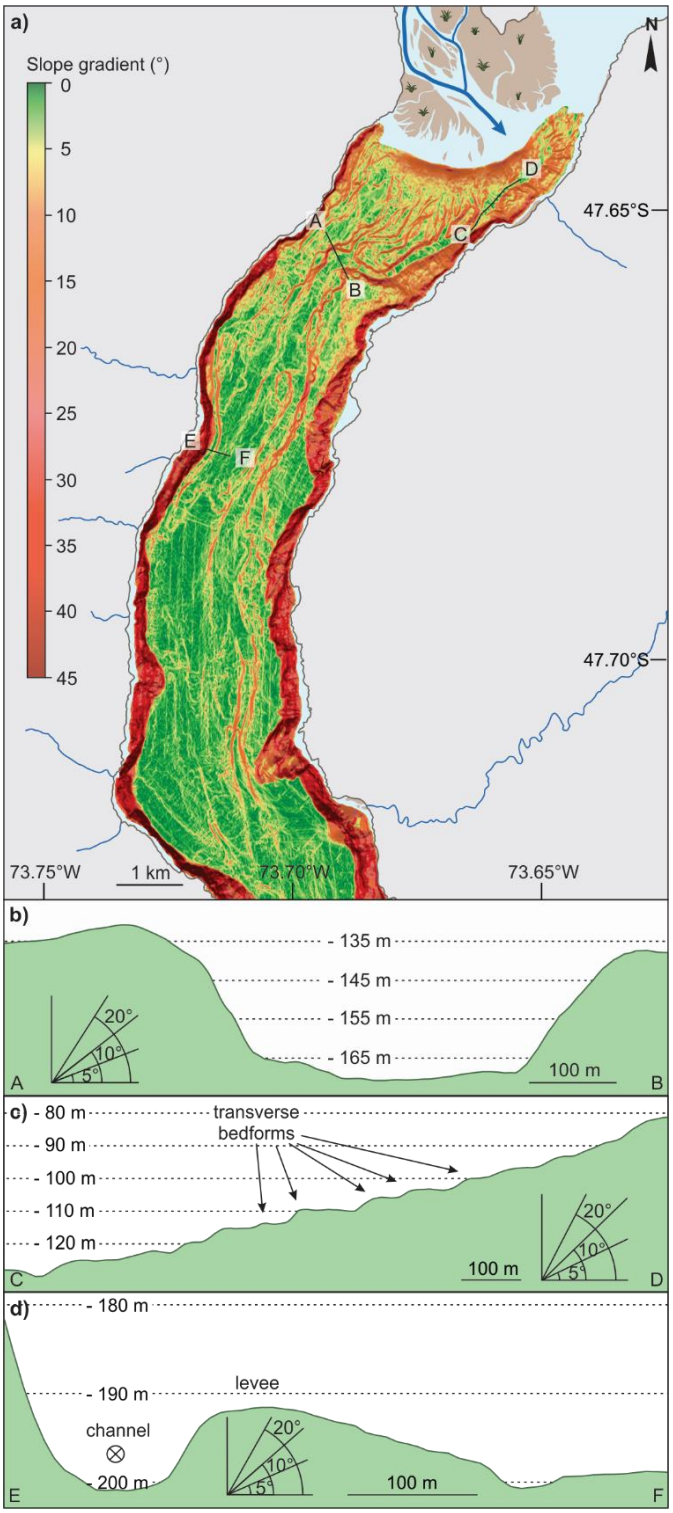

Figure 4.6. (a) Slope map of Steffen Fjord. **(b–d)** Cross-section (see (a) for location) through the main channel in the upper slope region (b), the crescent-shaped transverse bedforms observed within the channel (c), and the channel along the western shoreline (d).

4.4.2. Sediment properties

4.4.2.1. Grain size

Mean sediment grain-size values at the head of Martínez Channel vary from 11.46 to 87.39 µm whereas samples from Steffen Fjord have mean grain-size values ranging from 6.09 to 411.66 µm. At the head of

Martínez Channel, the majority of the samples are composed of fine to medium silt and most grain-size distributions are bimodal, whether the samples are from the channel or not (Figs. 4.7a and 4.7b). Samples located close to the delta lip are coarser and consist of coarse silt to fine sand. Similar to the head of Martínez Channel, samples situated near the delta margin of Steffen Fjord are slightly coarser (medium silt to medium sand) compared to samples further downslope (fine to medium silt) (Figs. 4.7c and 4.7d). In addition, the latter are better sorted compared to samples at the delta lip.

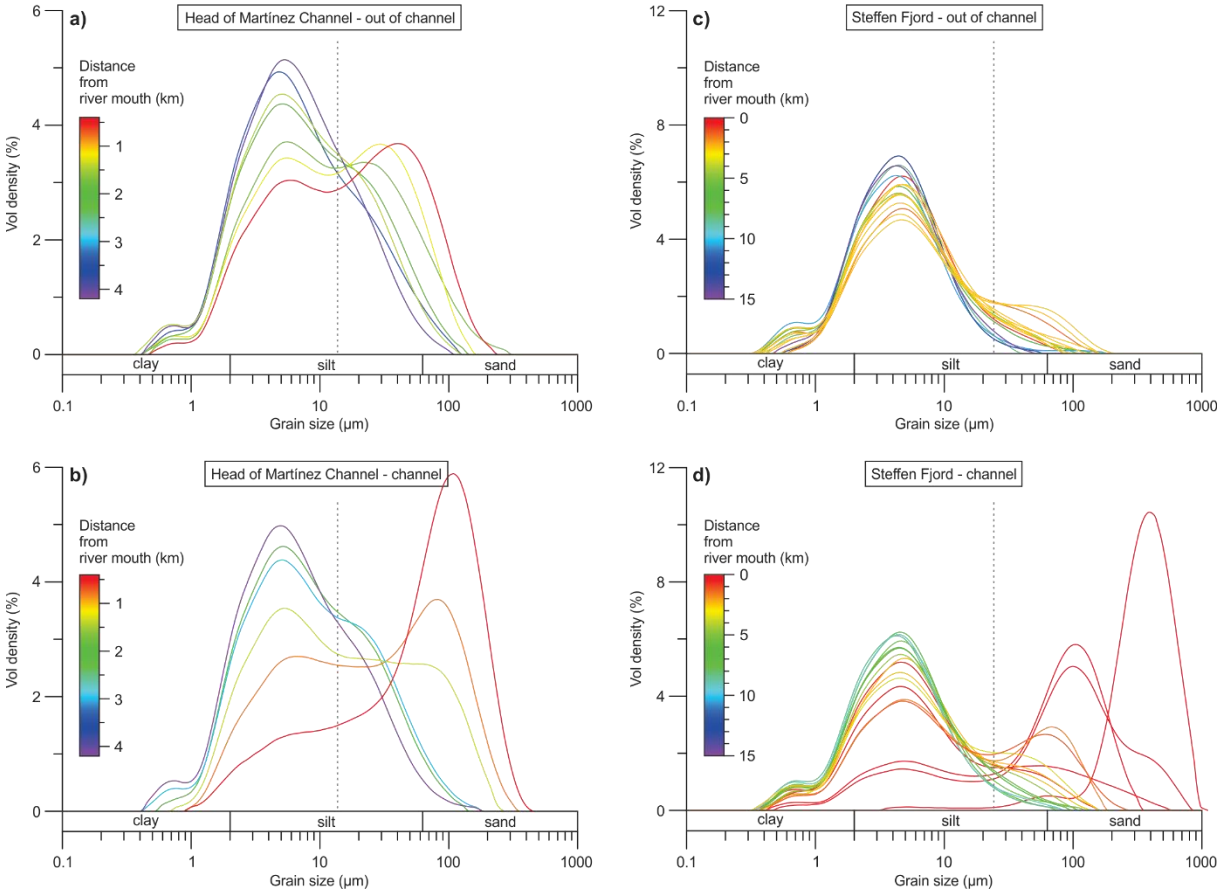

Figure 4.7. Grain-size distribution of the grab sediment samples from the **(a)** non-channelized region and **(b)** channels at the head of Martínez Channel. **(c–d)** Same but for Steffen Fjord. Colors vary according to the distance from the river mouth. For the Martínez Channel and Steffen Fjord, a grain-size boundary (inter-modal minimum) was set at 14.5 and 24.1 µm, respectively, to distinguish between the fine and coarse fractions (see also Fig. 4.8).

A clear difference in grain-size appears when comparing samples collected within the channels to samples from non-channelized regions, especially close to the shallow part of the delta. As displayed in Figs. 4.7b (head of Martínez Channel) and 4.7d (Steffen Fjord), samples in the channels are consistently coarser compared to locations out of the channels at the same distance from the river mouth. To compare the amount of coarse particles between samples from the channel and from the non-channelized region, a boundary, i.e., the minimum between the two grain-size distinct modes, was selected for both the head of Martínez Channel (14.5 µm) and Steffen Fjord (24.1 µm). This coarse particle percentage was calculated for each sample and represented in Fig. 4.8. In both the head of Martínez Channel (Fig. 4.8a) and Steffen Fjord (Fig. 4.8b), results show a decreasing trend in the amount of coarse particles with increasing distance from the river mouths, and samples in the channels have

consistently more coarse particles than samples outside of the channel, i.e., 44.3 versus 34.2 % at the head of Martínez Channel and 24.6 versus 7.2 % in Steffen Fjord.

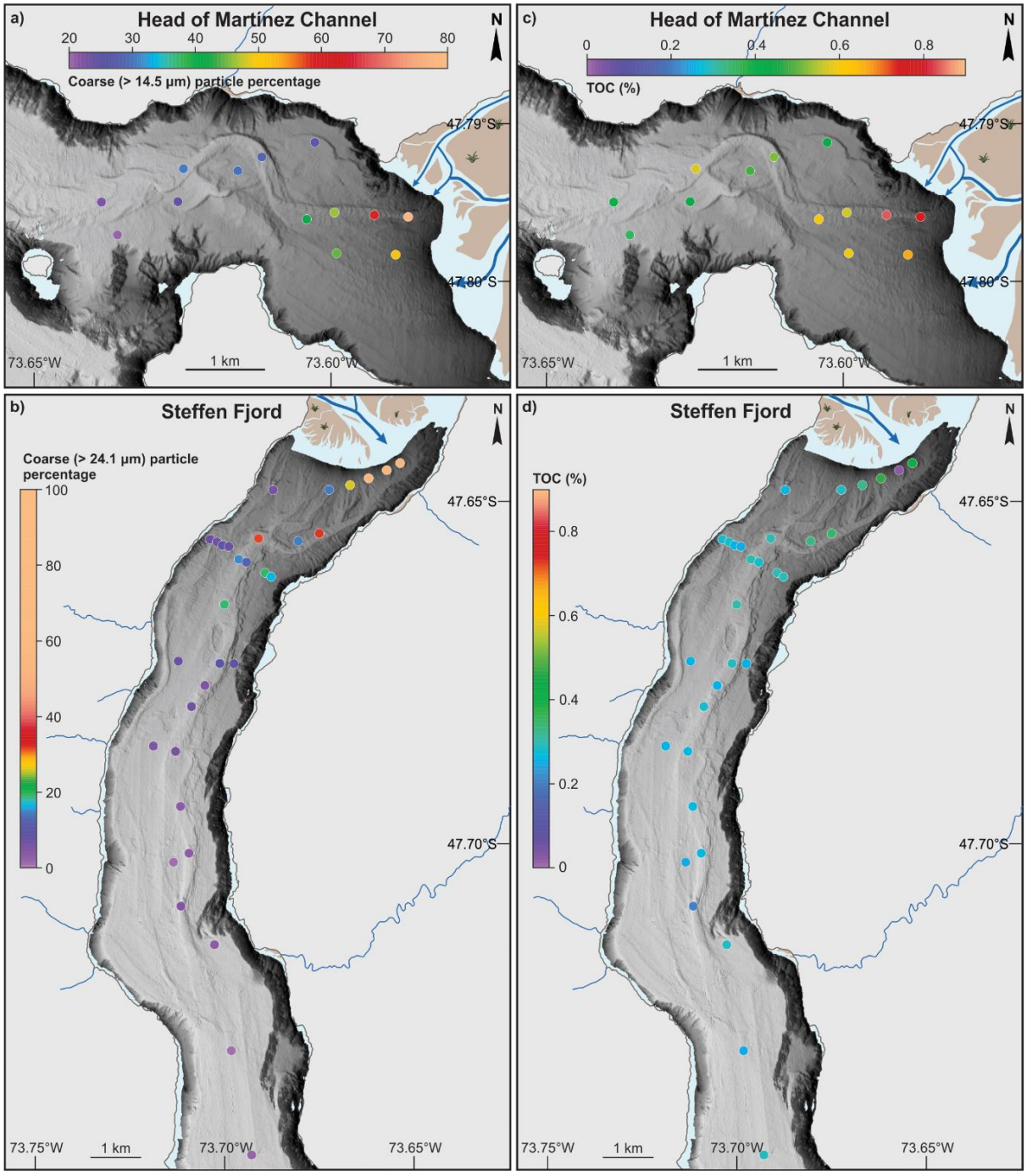

Figure 4.8. Grain size and organic carbon content in the delta region of the head of Martínez Channel and in Steffen Fjord. Coarse particle percentage of the grab sediment samples from **(a)** the head of Martínez Channel and **(b)** Steffen Fjord. **(c–d)** Same but for TOC. The grain-size boundaries used to calculate the coarse particle percentage were set at 14.5 and 24.1 µm for the head of Martínez Channel and Steffen Fjord, respectively (see Fig. 4.7 for rationale).

4.4.2.2. Organic carbon content

Overall, TOC contents are low in both fjords, with average values higher at the head of Martínez Channel (0.56 ± 0.14 %; Fig. 4.8c) than in Steffen Fjord (0.27 ± 0.07 %; Fig. 4.8d). In Steffen Fjord, TOC does not

vary with distance from the river mouth, depth, or location compared to the channel. In contrast, TOC values from the head of Martínez Channel display a general decreasing trend with depth, and they are systematically higher in the channels (0.61 %) than in the non-channelized part of the delta (0.51 %) (Fig. 4.8c).

4.5. Interpretation and discussion

4.5.1. Submarine channel systems

4.5.1.1. Channel activity

Channels in both the head of Martínez Channel and Steffen Fjord are deeply incised into their respective subaquatic deltas (Figs. 4.3 and 4.5). The presence of well-developed levees adjacent to the channels (Figs. 4.3b and 4.5b), implies recent channel activity, as the levees result from overspill during turbidity current activity within the channels. If the channels had not been active recently, these features would be buried under sediment settled from the surface plume and their morphology would become increasingly obscured. This is in agreement with the location of the channels in front of the river mouths, where large amounts of sediment is supplied to the fjords (Figs. 4.3 and 4.5).

Another clear indicator of recent channel activity is the presence of crescent-shaped ridges within the axial channels of both the head of Martínez Channel and Steffen Fjord (Figs. 4.4d and 4.6c). These bedforms occur at similar depths (70–85 to 170–180 m) in both fjords (Figs. 4.3b and 4.5b), where the average slope at these water depths is 2.9° for the head of Martínez Channel and 1.6° for Steffen Fjord. Such ridges, which are often referred to as sediment waves (e.g. Smith et al., 2005; Babonneau et al., 2013; Mazières et al., 2014; Dietrich et al., 2016; Normandeau et al., 2016b; Normandeau et al., 2019), are generally interpreted as a series of slowly migrating bedforms, where each lee side of the bedform is formed by a steeply dropping flow passing through a hydraulic jump before re-accelerating on the stoss side (Cartigny et al., 2011). They are regularly found in the proximal part of submarine channel systems, such as the Monterey Canyon in California (Paull et al., 2010), Canadian fjords (Prior et al., 1987; Conway et al., 2012; Normandeau et al., 2016a; Stacey and Hill, 2016), and the Fraser river delta (Hill, 2012). Depending on their geometry, internal structure, and grain-size distribution, channelized sediment waves can be classified into down-slope migrating (dunes) or up-slope migrating (cyclic steps, antidunes, chutes and pools) sediment waves (Cartigny et al., 2011). Channelized sediment waves with wavelengths and crest heights similar to those observed at the head of Martínez Channel and in Steffen Fjord have been interpreted as cyclic steps which migrate upslope and were hypothesized to be formed by supercritical dense underflows in the upper slope region (Hill, 2012; Babonneau et al., 2013; Hughes Clarke, 2016; Normandeau et al., 2016a; Stacey and Hill, 2016). The upslope orientation of the concave face of the sediment waves observed at the head of Martínez Channel and in Steffen Fjord suggests that the sediment waves are up-slope migrating cyclic steps (Hughes Clarke et al., 2012; Normandeau et al., 2016a; Stacey et al., 2018). In addition, the wavelengths of the bedforms at the head of Martínez Channel increase with distance from the delta margin. This indicates that due to decreasing slopes and increasing density flow specific discharge, the distance required for a turbidity current to become supercritical following a hydraulic jump increases (Fricke et al., 2015; Normandeau et al., 2016a). The latter might thus also explain why the distance between ridges increases downslope and ridges disappear in the lower slope region of the head of Martínez Channel and of Steffen Fjord. Compared to the well-developed ridges at the head of Martínez Channel, the ridges in Steffen Fjord are less pronounced and more irregular (Fig. 4.5). Given the recent retreat of Steffen Glacier and subsequent expansion of proglacial Steffen Lake (López and Casassa, 2011), turbidity current activity could have

decreased in recent times due to the lake's filtering effect (e.g. Normandeau et al., 2019). Finally, the steep slope angle of the Baker and Huemules river deltas promotes supercritical density flows, which is an additional argument for the up-slope migration of the ridges (Cartigny et al., 2011). Although the origin of channelized sediment waves is still debated, it is generally accepted that their formation involves flows at or close to the basin floor and can be associated with recent sediment transport (Wynn and Stow, 2002; Cartigny et al., 2011).

At the head of Martínez Channel, the presence of a head scarp north of Vigía Island (Fig. 4.3b) also implies recent channel activity. This scar feature represents a submarine slope failure which most likely occurred due to active scouring of the island's northern subaquatic slope by the channel. The absence of morphological evidence for landslide deposits within the channel and the observation that the channel is not yet buried implies the presence of eroding currents.

Recent channel activity at the head of Martínez Channel and in Steffen Fjord is additionally supported by data obtained on the grab sediment samples. Indeed, sediment within the channels is consistently coarser than in the non-channelized parts of the fjords and can thus be linked to a higher energetic environment (Figs. 4.7, 4.8a and b). It should however be noted that local variations in sediment grain size within the channels could also reflect the exact sampling location as sediments are generally coarser in the troughs than on the stoss of transverse bedforms (Postma and Cartigny, 2014). Although TOC values in Steffen Fjord are overall low due to the glacial nature of the sediment entering the fjord and do not show any significant difference between channels and the non-channelized region, samples from the head of Martínez Channel contain more organic matter, reflecting higher vegetation density in the watershed of Baker River. At the head of Martínez Channel, samples from the channels display higher TOC values compared to its non-channelized region due to the increased supply of terrestrial organic matter during periods of channel activity (Fig. 4.8c). The channels at the head of Martínez Channel and in Steffen Fjord can thus be interpreted as currently-active conduits for river sediment transport towards the deeper parts of the basins (Figs. 4.3 and 4.4).

The non-channelized region of the subaquatic deltas also displays sinuous-shaped scar features, but unlike the active channels, they do not cut deep into the subaquatic delta (Figs. 4.3b and 4.5b). These scars are most likely remnants of paleo-channels, which is supported by the relatively fine grain size of the corresponding sediment samples in both fjords (Figs. 4.8a and 4.8b). These channels were probably abandoned during an intense turbidity event and subsequently buried by fine-grained sediment settling from the buoyant surface layer.

4.5.1.2. Possible triggering mechanisms

Subaquatic channel systems similar to those observed at the heads of Martínez Channel and in Steffen Fjord have been described in many other regions such as the Chilean fjords adjacent to the SPI (Dowdeswell et al., 2013) and glaciofluvial fjords in the Northern Hemisphere (Prior et al., 1986; Syvitski et al., 1987; Conway et al., 2012; Hill, 2012; Stacey and Hill, 2016; Gales et al., 2019). They have also been identified in lake basins (Corella et al., 2016; Normandeau et al., 2016a) and on island slope and continental margins (Wynn et al., 2002; Smith et al., 2005; Migeon et al., 2012; Babonneau et al., 2013).

In lake basins, most channel systems are related to turbidity currents forming at river mouths. In those systems, the density contrast between the inflowing sediment-laden water and the receiving freshwater basin favors sediment transport by turbidity currents (Mulder and Syvitski, 1995). These turbidity currents are a key factor in controlling the morphology of active channels (e.g. Corella et al., 2016) but

they can also manifest as non-channelized undulating bedforms on the delta slope in the case of dilute and low density flows (e.g. Normandeau et al., 2016b). When rivers enter into a fjord or marine system, on the other hand, coarse sediment is deposited on the delta slope and most fine particles propagate as a buoyant plume due to the strong salinity, temperature, and therefore density, stratification of the water column (Syvitski and Shaw, 1995). Still, turbidity currents can develop in fjords due to repeated slope failures near the river inflow, or discharge of high suspended loads by rivers (Syvitski, 1989).

During slope failures at the delta front, sediment bodies can disintegrate and continue downslope as turbidity currents (Felix and Peakall, 2006; Hughes Clarke et al., 2012). Several mechanisms can trigger submarine slope collapses, including sediment remobilization by seismic shaking, internal waves and/or tidal changes, and in case of organic-rich sediments, slides can also be triggered by the combination of tidal drawdown and gas compressibility effects (e.g. Smith et al., 1990). At the head of Martínez Channel and in Steffen Fjord, earthquake-triggered slope failure is considered unlikely since the study region is located just south of the Chile Triple Junction, in the so-called Patagonian Volcanic Gap, where seismic hazard is low compared to other regions along the Chilean coastline (Hayes et al., 2015). This is supported by the lack of registered earthquakes of magnitude M > 3 within 250 km of Tortel during the last 100 years (USGS earthquake catalog). Tidal drawdown processes are also considered unlikely due to the low tidal range (< 2 m) at the head of Martínez Channel and in Steffen Fjord compared to the Squamish Delta (British Columbia) and Sept-Îles (St-Lawrence Gulf), where tidal ranges of 3–5 m have been shown to result in sediment unloading (e.g. Clare et al., 2016; Dietrich et al., 2016). Tidal drawdown processes at the head of Martínez Channel and in Steffen Fjord might however be able to enhance slope failures during periods of peak discharge. Likewise, internal tides at the head of Martínez Channel appear to be correlated to high discharge pulses of Baker River (Ross et al., 2014), particularly in summer when river discharge exceeds 1200 m^3/s. Similar to tidal drawdown processes, internal tides occurring during periods of elevated river discharge might enhance slope failures but internal tides alone are likely not able to generate slope failures. Given the overall low TOC values in both fjords compared to other fjords where turbidity currents triggered by gas compression have been observed (Fraser Delta, Christian et al., 1997), gas compressibility is not considered a possible mechanism.

A far more likely mechanism for triggering turbidity currents at the heads of Martínez Channel and Steffen Fjord is the discharge of high suspended loads by Baker and Huemules rivers, respectively. Such a mechanism has been observed in the channel system of Bute Inlet (Canada), for example, where a large-scale turbidity event was associated with a major river flood due to heavy snowmelt (Prior et al., 1987). In other glaciofluvial dominated fjords in Canada, large-scale turbidity events responsible for the formation of submarine channels have also been related to river discharge peaks due to the rapid inflow of meltwater in summer (Conway et al., 2012; Hughes Clarke et al., 2012).

High discharge of sediment-laden river waters can create turbidity currents in fjords either directly (plunging of river waters, sediment settling from the river plume; Hizzett et al., 2018) or indirectly (rapid sediment accumulation at the delta-lip resulting in slope instability and eventually submarine slides). At the Squamish delta (British Columbia), for example, detailed monitoring revealed that delta-lip failures occurred with a delay of several hours after peak discharge due to cumulative sedimentation at the delta top and tidally-induced pore pressure changes (Clare et al., 2016). Delta slope failures seem to happen rather frequently to maintain maximum slope stability (Syvitski and Shaw, 1995). The plunging of river waters during floods represents a more direct hyperpycnal flow triggering mechanism (Mulder and Syvtiski, 1995; Mulder et al., 2003). When sediment-laden river material entering the fjord is dense

enough, it plunges and evolves into a hyperpycnal flow (e.g. Dietrich et al., 2016). Finally, turbidity currents resulting from high suspended sediment loads, can also be triggered locally by sediment settling from the river plume (Parsons et al., 2001). These so-called "plume-triggered events" or "settling plume events" (Hizzett et al., 2018) are still poorly examined phenomena and only a few studies have described this process (e.g. Kineke et al., 2000; Hughes Clarke et al., 2014; Hizzett et al., 2018). Turbidity currents formed by plume-triggered events are more dilute compared to slope failures, and are able to maintain turbulence for longer periods of time, eventually leading to long runouts (Hizzett et al., 2018). At the Squamish delta (British Columbia), plume-triggered events dominate the triggering of underflows and contribute the majority of sediment to the depositional lobe, causing most of the seafloor changes on sub-annual timescales (Hizzett et al., 2018).

Theoretically, forming such underflows in fjords requires suspended sediment concentrations of 30–40 g/l at the active river plume (Syvitski, 1989; Syvitski and Shaw, 1995) to overcome density contrasts between river water and sea water. Such high sediment concentrations have rarely been measured but flocculation within brackish waters has been suggested to enhance particle settling (Syvitski and Shaw, 1995), and experiments revealed that plume-triggered events can occur at sediment concentrations as low as 0.5 g/l (Parsons et al., 2001). Still, a recent study at the Squamish delta (British Columbia) also showed that very dilute river plumes with sediment concentrations as low as 0.07 g/l were able to generate fast and short-lived turbidity currents (Hage et al., 2019). This study proposes a new mechanism where turbidity currents occur when fine-sediment, accumulating in a tidal turbidity maximum, is released during spring tide.

Like other glaciofluvial fjord systems, the hydrography of Martínez Channel and Steffen Fjord is highly influenced by the hydrological cycle of inflowing rivers. During the melt season in summer, the discharge of Baker River doubles (DGA, Chile), and total suspended sediment concentrations reach on average 0.08 g/l (Supplementary Table S4A). Aside from seasonal increases, discharge and related suspended sediment concentrations can also peak during short-lived floods associated with either extreme precipitation (e.g. rain-on-snow events) or GLOFs. During GLOFs, suspended sediment concentrations in Baker River increase up to at least 0.78 g/l (Supplementary Table S4A), and water temperature drops by ~3 °C, causing a densification of the fjord surface waters near the river mouth.

The morphology of the subaquatic deltas described at the head of Martínez Channel and in Steffen Fjord resemble that of well-studied fjord systems in British Columbia (Gales et al., 2019), for which suspended sediment concentrations at the river outflow during the meltwater season ranges between 0.04–0.7 g/l. Monitoring studies show that the subaquatic channel systems of these deltas are highly active, especially during elevated river discharge in summer (Hage et al., 2018). In addition, the recently proposed mechanism for turbidite triggering by Hage et al. (2019) does not require a fixed sediment threshold to be exceeded and implies more frequent generation of turbidity currents at a wider range of locations than previously thought. By comparison with these well-studied systems, we posit that the channel systems identified at the head of Martínez Channel and in Steffen Fjord are also predominantly shaped by turbidity currents induced by elevated river discharge and the associated high amounts of suspended sediment. Such floods could include seasonal events during the meltwater season, rain-on-snow events, or GLOFs, and they may be able to trigger turbidity currents through direct plunging of the river plume or by the occurrence of plume-triggered events.

Deciphering between these three types of floods without detailed monitoring of river discharge and channel activity is almost impossible. The ability of GLOFs to trigger turbidity currents is particularly unclear at this stage due to the competing effects of high suspended sediment concentrations and low water temperature and salinity. On the one hand, suspended sediment concentrations measured during the GLOFs that occurred within the last 10 years are one order of magnitude higher than during the meltwater season (Supplementary Table S4A), which significantly increases water density. The increased meltwater input during GLOFs, on the other hand, increases fjord stratification, which may prevent the formation of hyperpycnal flows. GLOFs of the magnitude of those observed within the last decade may therefore not be able to trigger turbidity currents in the fjord. It is possible that only the extreme GLOFs, i.e., those with exceptional suspended sediment concentrations, are able to create turbidity currents, possibly resulting in channel migration.

One observation that seems to favor the occurrence of plume-triggered turbidity currents (Hizzett et al., 2018) rather than direct plunging is the apparent lack of connection between the location of the head of the main (western) submarine channel at the head of Martínez Channel and that of the main Baker River channel (Fig. 4.3). Instead of being located immediately in front of the main present-day river branch, the submarine channel starts about 1.5 km to the north, suggesting that direct river plunging does not occur or is not able to carve deep subaquatic channels on the Baker River delta. This observation could however also reflect recent avulsion at the river mouth, which is supported by historical maps from the 1900s that show a better developed river channel on the northern side of the river delta (Nef, 1907; Supplementary Information Fig. S4B) immediately in front of the head of the subaquatic channel. The presence of abandoned channels on the subaquatic delta of Baker River may also reflect past avulsion (Fig. 4.3). The southern submarine channel being located immediately in front of the southern branch of Baker River (Fig. 4.3) supports this recent avulsion hypothesis. Such channel avulsions most likely occur during extreme discharge events, which have the potential to induce vigorous turbidity events, resulting in a complete re-organization of the subaquatic bedforms and channels (e.g. Kremer et al., 2015). A recently described process in which very dilute river plumes are able to trigger turbidity currents and seafloor erosion initiates approximately 100 m downstream of the river mouth (Hage et al., 2019), could similarly explain our observations.

Taken together, the presence of turbidity currents carving channels through the deltas at the head of Martínez Channel and Steffen Fjord is most likely associated with elevated river discharge and with the associated input of high amounts of suspended sediments that occur during floods. Although detailed monitoring of the subaquatic deltas is required to investigate the exact triggering process(es), we expect direct plunging of the river plume, plume-triggered events, and/or slope failures at the delta lip, enhanced by tidal drawdown processes and/or internal waves, to be the main geomorphic agents of the submarine delta at the head of Martínez Channel and Steffen Fjord.

4.5.2. Other morphological features

4.5.2.1. Along-slope channel in Steffen Fjord

The N-S oriented channel along the western shore of Steffen Fjord does not seem to be directly connected to the delta (Fig. 4.5b). Although it is interrupted at certain locations, this channel cuts deeply (up to 10 m) into the sediments at the bottom of the slope and recent activity is very likely given the clear morphology of the channel. The channel morphology also seems to be more pronounced at sharp turns along the shoreline, probably due to increasing flow velocity (Fig. 4.6d). There are two possible explanations for this channel feature. A first hypothesis is that this channel represents an abandoned

turbidity channel with levee formation. It could have been disconnected from the delta during a recent major turbidity event. On the other hand, the along-slope channel geometry and the presence of 10-m high mounds along the channel tend to suggest its formation by bottom currents deflected by the western margin of the fjord, i.e., a sediment drift (Rebesco et al., 2014). Since the two-layer flow circulation in Steffen Fjord is composed of a hypopycnal cold brackish water surface layer flowing southwards and a salty warmer layer of deeper Pacific Ocean water (Sievers and Silva, 2008; Moffat, 2014; Silva and Vargas, 2014), the bottom currents forming the sediment drift would most likely be directed northwards. Because this north-flowing bottom current originates at the outer fjord, it re-distributes fine-grained sediment, which explains why samples collected within this channel display grain-size values that are similar to the non-channelized areas (see the NW-SE grain-size transect in Fig. 8b). Due to the Coriolis effect, bottom currents flow parallel to the western steep fjord slope and the mounds are formed towards the central axis of the fjord, as currents are deflected counterclockwise. This effect might also be re-enforced by the prevailing westerly winds, which push surface waters towards the eastern side of the fjord, and therefore bottom waters towards the west.

Similar sediment drifts were described in lakes influenced by the southern westerlies, where they were interpreted as the result of wind-driven bottom currents (Gilli et al., 2005; Anselmetti et al., 2009; Heirman et al., 2012; Van Daele et al., 2016). However, both turbidity channels and sediment drifts result in very similar morphological features (e.g. mounded geometry) and it is not possible to identify the exact origin of this channel solely based on multibeam bathymetry.

4.5.2.2. Unchannelized sediment waves

Aside from the sediment waves within the axial channels, sinuous ridge and scour bedforms can also be observed on the non-channelized deltas of both the head of Martínez Channel and Steffen Fjord. These features only occur on the upper slope, where gradients range from 5 to 15° (Figs. 4.3b and 4.5b). Similar bedforms have previously been observed at the Fraser delta (British Columbia), where they were interpreted as migrating sediment waves formed by unconfined turbidity currents on the delta slope (Hill, 2012). Other studies in lake basins have also linked the occurrence of non-channelized sediment waves on delta slopes, similar to those within the channels at the head of Martínez Channel and Steffen Fjord, to turbidity current activity (Normandeau et al., 2016a; Normandeau et al., 2016b). The sediment waves observed in the non-channelized upper flow regime of both the head of Martínez Channel and Steffen Fjord (Figs. 4.3 – 4.6), could therefore imply similar unconfined turbidity currents occurring on the delta slope. According to Howe et al. (2010), such sediment waves are an indicator of current reworking and bedload transport resulting from high sediment supply at river inflows in fjords.

In addition, the gullies observed in the non-channelized upper slope region at the head of Martínez Channel (Fig. 4.3b) also suggest the occurrence of high concentration turbidity currents (Syvitski et al., 1987). For example, the emplacement of cyclic steps on the upper foresets of a proglacial sandur delta were hypothesized to originate from river-derived hyperpycnal flows in a delta-front setting (Dietrich et al., 2016). The occurrence of unchannelized sediment waves at the head of Martínez Channel and Steffen Fjord is therefore an extra argument for non-channelized sediment migration or channel shifting due to the occurrence of large-scale turbidity events rather than slope failures.

4.5.2.3. Delta plain morphology: absence of moraines

Fjords are the product of glacial erosion. Therefore, fjord sediments generally preserve glaciomarine fans, and terminal and/or recessional moraines corresponding to glacier variations during the

Quaternary (Howe et al., 2010). In Chilean fjords, Holocene moraines are generally well preserved (e.g. Rodrigo, 2008; Dowdeswell et al., 2013; Lastras and Dowdeswell, 2016). It is not surprising that no moraine features were observed at the head of Martínez Channel, since the fjord deglaciated over 8 kyr ago (Glasser et al., 2016). The lack of evidence of ice retreat in Steffen Fjord, however, is more surprising since the terminus of Steffen Glacier is located only twelve km landwards. The absence of a subaquatic moraine in Steffen Fjord supports the interpretation of Glasser et al. (2011) and Mardones et al. (2018) that Steffen Glacier remained land-based during the Little Ice Age advance. Neoglacial moraines could exist at the bottom of the fjord but would have been buried and are therefore no longer visible in the subaquatic morphology, as in other fjords of Chilean Patagonia (DaSilva et al., 1997; Moffat, 2014; Piret et al., 2017b). Given the depth of the fjord, it is also possible that Steffen Glacier was calving, instead of grounded, which could also explain the absence of subaquatic moraines in Steffen Fjord.

4.5.3. Implications for paleoclimate and paleoenvironmental research: site selection

The presence of channels actively carving through the deltas at the head of Martínez Channel and Steffen Fjord has important implications for the selection of coring sites for future paleoclimate and paleoenvironmental research. Our results show that the processes of sediment transport and deposition at the head of these fjords can vary within a few hundreds of meters, which makes proper site selection crucial. In both fjords, the channels act as conduits for the transport of relatively coarse river sediments to the prodelta areas. At these locations, sediment preservation is expected to be very low due to strong erosional processes (e.g. Vendetuolli et al., 2019). This implies that ideal coring sites for paleohydrological reconstructions (extreme events) should be located on the distal fan lobe, out of the channel axis. It should however be noted that sedimentation in the distal region of river/delta systems dominated by subaquatic channels is directly linked to the activity of the channels, i.e. the location of the river mouth and the delta slope morphology (Kremer et al., 2015). Channel shifts at the head of Martínez Channel and in Steffen Fjord, which are very likely to have occurred in the past, can thus result in significant lithological changes and caution should be exercised when interpreting long sediment records in terms of past flood occurrence. To account for channel migration, a multi-core approach, and possibly the acquisition of seismic data, are recommended. At distal locations, large floods are expected to be recorded as turbidites intercalated within finer sediment settling from the surficial plume. Sites located closer to the delta will likely register more floods compared to sampling sites further away, which will only contain evidence of the largest or most extreme events.

4.6. Conclusions

High-resolution bathymetric imagery of the heads of Martínez Channel and Steffen Fjord reveal that the fjords' geomorphology is characterized by large subaquatic deltas incised by up-to-36m deep submarine channels. The presence of these channels, together with the occurrence of channelized sediment waves and coarser sediments within the channels, reflect recent sediment transport by turbidity currents. Although detailed monitoring is required to pinpoint the exact triggering mechanism(s) of the turbidity currents in these two fjords, we argue that these currents are related to periods of elevated discharge of Baker and Huemules rivers and to the associated high suspended sediment loads, irrespective of the flood's origin (seasonal increase, high precipitation event, or GLOFs). These turbidity currents may be triggered by direct plunging of the river plume, plume-triggered events, and/or slope failures at the delta lip, potentially enhanced by tidal drawdown processes and/or internal waves. Increased river discharge during meltwater events and intense precipitation are hypothesized to be of key importance for shaping the submarine channels and thus the geomorphology of the heads of Martínez Channel and

Steffen Fjord. Our results also highlight the importance of high-resolution bathymetric mapping before any sediment coring activities. Avoiding blind coring is especially important at fjord heads, where delta morphology is highly influenced by active channel processes. Future sediment-based paleoclimate and paleoenvironmental reconstructions at the head of Martínez Channel and in Steffen Fjord should therefore highly benefit from the bathymetric map presented in this paper.

4.7. Data availability

The bathymetric map related to this article can be found on Marine Geoscience Data System (MGDS; DOI 10.1594/IEDA/324731, 324732, 324733, 324734).

Acknowledgements

We thank Koen De Rycker, Helena Pryer, Loïc Piret, Fernando Torrejón, and the staff of Centro de Investigación en Ecosistemas de la Patagonia (CIEP, Chile) for their help with data acquisition and sample collection. We are also thankful to the captain (Rodrigo Mansilla) and crew of the *R/V Sur-Austral* (COPAS Sur-Austral, Tortel, Chile). Philipp Kempf, Thomas Vandorpe, and Nore Praet are thanked for their help with data processing. We wish to thank Romina San Martín (University of Concepción, Chile) for easing the administration and Carlos Moffat (University of Delaware, USA) for providing the tide files. We are grateful to Loïc Piret and Benjamin Amann for providing constructive comments on an earlier version of this manuscript. The Flanders Marine Institute (VLIZ) is acknowledged for providing the *Caris* software and QPS is thanked for the academic discount on the *Fledermaus* software. Finally, we acknowledge the Chilean Navy Hydrographic and Oceanographic Service (SHOA) for the authorization to map the fjords (permit number 13270/24/235/Vrs). The research presented here was funded by the Flemish Research Foundation (FWO, Belgium) Paleo-GLOFs project G0D7916N and by UGent BOF project HYDROPROX (01N02216). The authors wish to thank three anonymous reviewers for their constructive comments that improved an earlier version of this manuscript.

References

Aniya, M. (2014) GLOF of a side-lake, Laguna de los Témpanos, of Glaciar Steffen, Hielo Patagónico Norte, South America (in Japanese). *Proceedings of JSSI & JSSE Joint Conference – 2014/Hachinohe*, A1 – 7.

Anselmetti, F.S., Ariztegui, D., De Batist, M., Gebhardt, A.C., Haberzettl, T., Niessen, F., Ohlendorf, C., and Zolitschka, B. (2009) Environmental history of southern Patagonia unravelled by the seismic stratigraphy of Laguna Potrok Aike. *Sedimentology*, **56**, 873 – 892.

Araya Vergara, J.F. (2011) Submarine failures in the bottom of the Aysén fjord, Northern Patagonia, Chile. *Investig. Geogr.*, **43**, 17 – 34.

Babonneau, N., Delacourt, C., Cancouët, R., Sisavath, E., Bachèlery, P., Mazuel, A., Jorry, S.J., Deschamps, A., Ammann, J., and Villeneuve, N. (2013) Direct sediment transfer from land to deep-sea: Insights into shallow multibeam bathymetry at La Réunion Island. *Marine Geology*, **346**, 47 – 57.

Bastianon, E., Bertoldi, W., and Dussaillant, A. (2012) Glacial-lake outburst flood effects on Colonia River morphology, Chilean Patagonia. River Flow 2012, CRC Press, pp. 573 – 579.

Bertrand, S., Hughen, K.A., Lamy, F., Stuut, J.-B.W., Torrejón, F., and Lange, C.B. (2012) Precipitation as the main driver of Neoglacial fluctuations of Gualas glacier, Northern Patagonian Icefield. *Climate of the Past*, **8**, 519 – 534.

Bertrand, S., Hughen, K., Sepúlveda, J., and Pantoja, S. (2014) Late Holocene covariability of the southern westerlies and sea surface temperature in northern Chilean Patagonia. *Quaternary Science Reviews*, **105**, 195 – 208.

Bertrand, S., Lange, C.B., Pantoja, S., Hughen, K., Van Tornhout, E., and Smith Wellner, J. (2017) Postglacial fluctuations of Cordillera Darwin glaciers (southernmost Patagonia) reconstructed from Almirantazgo fjord sediments. *Quaternary Science Reviews*, **177**, 265 – 275.

Boyd, B.L., Anderson, J.B., Wellner, J.S., and Fernández, R.A. (2008) The sedimentary record of glacial retreat, Marinelli Fjord, Patagonia: Regional correlations and climate ties. *Marine Geology*, **255**, 165 – 178.

Caldenius, C.C. (1932) Las glaciaciones cuaternarios en la Patagonia y Tierra del Fuego, *Geografiska Annaler*, **14**, 144 – 157.

Caniupán, M., Lamy, F., Lange, C., Kaiser, J., Kilian, R., Arz, H.W., León, T., Mollenhauer, G., Sandoval, S., De Pol-Holz, R., Pantoja, S., Wellner, J., and Tiedemann, R. (2014) Holocene sea-surface temperature variability in the Chilean fjord region. *Quaternary Research*, **82**, 342 – 353.

Cartigny, M.J.B., Postma, G., van den Berg, J.H., and Mastbergen, D.R. (2011) A comparative study of sediment waves and cyclic steps based on geometries, internal structures and numerical modeling. *Marine Geology*, **280**, 40 – 56.

Clare, M.A., Hughes Clarke, J.E., Talling, P.J., Cartigny, M.J.B., and Pratomo, D.G. (2016) Preconditioning and triggering of offshore slope failures and turbidity currents revealed by most detailed monitoring yet at a fjord-head delta. *Earth and Planetary Science Letters*, **450**, 208 – 220.

Conway, K.W., Barrie, J.V., Picard, K., and Bornhold, B.D. (2012) Submarine channel evolution: active channels in fjords, British Columbia, Canada. *Geo-Marine Letters*, **32**, 301 – 312.

Corella, J.P., Loizeau, J.-L., Kremer, K., Hilbe, M., Gerard, J., le Dantec, N., Stark, N., González-Quijano, M., and Girardclos, S. (2016) The role of mass-transport deposits and turbidites in shaping modern lacustrine deepwater channels. *Marine and Petroleum Geology*, **77**, 515 – 525.

DaSilva, J.L., Anderson, J.B., and Stravers, J. (1997) Seismic facies changes along a nearly continuous 24° latitudinal transect: the fjords of Chile and the northern Antarctic Peninsula. *Marine Geology*, **143**, 103 – 123.

Davies, B.J., and Glasser, N.F. (2012) Accelerating shrinkage of Patagonian glaciers from the Little Ice Age (~AD 1870) to 2011. *Journal of Glaciology*, **58** (212), 1063 – 1084.

DGA (2019) Minuta Tecnica N° 1, 22 de enero de 2019, Inundación río Huemules Superior, sector Estero Steffen. 7 pp.

Dietrich, P., Ghienne, J.-F., Normandeau, A., and Lajeunesse, P. (2016) Upslope-migrating bedforms in a proglacial sandur delta: cyclic steps from river-derived underflows? *Journal of Sedimentary Research*, **86**, 112 – 122.

Douglass, D.C., Singer, B.S., Kaplan, M.R., Ackert, R.P., Mickelson, D.M., and Caffee, M.W. (2005) Evidence of early Holocene glacial advances in southern South America from cosmogenic surface-exposure dating. *Geology*, **33** (3), 237 – 240.

Dowdeswell, J.A., and Vásquez, M. (2013) Submarine landforms in the fjords of southern Chile: implications for glacimarine processes and sedimentation in a mild glacier-influenced environment. *Quaternary Science Reviews*, **64**, 1 – 19.

Dussaillant, A., Benito, G., Buytaert, W., Carling, P., Meier, C., and Espinoza, F. (2010) Repeated glacial-lake outburst floods in Patagonia: an increasing hazard? *Natural hazards*, **54**, 469 – 481.

Felix, M., and Peakall, J. (2006) Transformation of debris flows into turbidity currents: Mechanisms inferred from laboratory experiments. *Sedimentology*, **53**(1), 107 – 123.

Fricke, A.T., Sheets, B.A., Nittrouer, C.A., Allison, M.A., and Ogston, A.S. (2015) An examination of Froude-supercritical flows and cyclic steps on a subaqueous lacustrine delta, Lake Chelan, Washington, U.S.A. *Journal of Sedimentary Research*, **85**, 754 – 767.

Gales, J.A., Talling, P.J., Cartigny, M.J.B., Hughes Clarke, J., Lintern, G., Stacey, C., and Clare, M.A. (2019) What controls submarine channel development and the morphology of deltas entering deep-water fjords? *Earth Surface Processes and Landforms*, **44**, 535 – 551.

García, J.L., Kaplan, M.R., Hall, B.L., Schaefer, J.M., Vega, R.M., Schwartz, R., and Finkel, R. (2012) Glacier expansion in southern Patagonia throughout the Antarctic cold reversal. *Geology*, **40**, 859 – 862.

Gilli, A., Anselmetti, F.S., Ariztegui, D., Beres, M., McKenzie, J.A., and Markgraf V. (2005) Seismic stratigraphy, buried beach ridges and contourite drifts: the Late Quaternary history of the closed Lago Cardiel basin, Argentina (49 °S). *Sedimentology*, **52**, 1 – 23.

Glasser, N.F., Harrison, S., Jansson, K.N., Anderson, K., and Cowley, A. (2011) Global sea-level contribution from the Patagonian Icefields since the Little Ice Age maximum. *Nature Geoscience*, **4**, 303 – 307.

Glasser, N.F., Harrison, S., Schnabel, C., Fabel, D., and Jansson, K.N. (2012) Younger Dryas and early Holocene age glacier advances in Patagonia. *Quaternary Science Reviews*, **58**, 7 – 17.

Glasser, N.F., Jansson, K.N., Duller, G.A.T., Singarayer, J., Holloway, M., and Harrison, S. (2016) Glacial lake drainage in Patagonia (13-8 kyr) and response of the adjacent Pacific Ocean. *Science Reports*, **6**, 21064.

Hage, S., Cartigny, M.J.B., Clare, M.A., Sumner, E.J., Vendettuoli, D., Hughes Clarke, J.E., Hubbard, S.M., Talling, P.J., Lintern, D.G., Stacey, C.D., Englert, R.G., Vardy, M.E., Hunt, J.E., Yokokawa, M., Parsons, D.R., Hizzett, J.L., Azpiroz-Zabala, M., and Vellinga, A.J. (2018) How to recognize crescentic bedforms formed by supercritical turbidity currents in the geologic record: Insights from active submarine channels. *Geology*, **46**, 563 – 566.

Hage, S., Cartigny, M.J.B., Sumner, E.J., Clare, M.A., Hughes Clarke, J.E., Talling, P.J., Lintern, D.G., Simmons, S.M., Silva Jacinto, R., Vellinga, A.J., Allin, J.R., Azpiroz-Zabala, M., Gales, J.A., Hizzett, J.L., Hunt, J.E., Mozzato, A., Parsons, D.R., Pope, E.L., Stacey, C.D., Symons, W.O., Vardy, M.E., and Watts, C. (2019) Direct monitoring reveals initiation of turbidity currents from extremely dilute river plumes. *Geophysical Research Letters,* **46**, 11310 – 11320.

Harrison, S., Winchester, V., and Glasser, N. (2007) The timing and nature of recession of outlet glaciers of Hielo Patagónico Norte, Chile, from their Neoglacial IV (Little Ice Age) maximum positions. *Global and Planetary Change*, **59**, 67 – 78.

Harrison, S., and Glasser, N.F. (2011) The Pleistocene glaciations of Chile. *In: Ehlers, J., Gibbard, P.L., Hughes, P.D. (Eds.), Quaternary Glaciations – Extent and Chronology – A Closer Look.* Developments in Quaternary Sciences, vol. 15. Elsevier, Amsterdam, pp. 739 – 756.

Hayes, G.P., Smoczyk, G.M., Benz, H.M., Villaseñor, A., and Furlong, K.P. (2015) Seismicity of the Earth 1900–2013, Seismotectonics of South America (Nazca Plate Region): U.S. Geological Survey Open-File Report 2015–1031-E, 1 sheet, scale 1:14 000 000.

Heirman, K., De Batist, M., Arnaud, F., and De Beaulieu, J.-L. (2012) Seismic stratigraphy of the late Quaternary sedimentary infill of Lac d'Armor (Kerguelen archipelago): a record of glacier retreat, sedimentary mass wasting and southern Westerly intensification. *Antarctic Science*, **24**, 608 – 618.

Hill, P.R. (2012) Changes in submarine channel morphology and slope sedimentation patterns from repeat multibeam surveys in the Fraser River delta, western Canada. *International Association of Sedimentologists Special Publications*, **44**, 47 – 70.

Hizzett, J.L., Hughes Clarke, J.E., Sumner, E.J., Cartigny, M.J.B., Talling, P.J., and Clare, M.A. (2018) Which triggers produce the most erosive, frequent, and longest runout turbidity currents on deltas? *Geophysical Research Letters*, **45**(2), 855 – 863.

Howe, J.A., Austin, W.E.N., Forwick, M., Paetzel, M., Harland, R., and Cage, A.G. (2010) Fjord systems and archives: a review. *In: Howe, J.A., Austin, W.E.N., Forwick, M., Paetzel, M. (Eds.), Fjord Systems and Archives*. Geological Society, London, Special Publications, 344, pp. 5 – 15.

Hubbard, A., Hein, A.S., Kaplan, M.R., Hulton, N.R.J., and Glasser, N. (2005) A modelling reconstruction of the Last Glacial Maximum Ice Sheet and its deglaciation in the vicinity of the Northern Patagonian Icefield, South America. *Geografiska Annaler*, **87 A** (2), 375 – 391.

Hughes Clarke, J.E., Brucker, S., Muggah, J., Hamilton, T., Cartwright, D., Church, I., and Kuus, P. (2012) Temporal progression and spatial extent of mass wasting events on the Squamish prodelta

slope. In *Landslides and engineered slopes: Protecting society through improved understanding* (Vol. 122, pp. 1091 – 1096). London: Taylor and Francis Group.

Hughes Clarke, J.E., Marques, C.R.V., and Pratomo, D. (2014) *Imaging active mass-wasting and sediment flows on a fjord delta* (pp. 249 – 260). Squamish, British Columbia: Springer International Publishing.

Hughes Clarke, J.E. (2016) First wide-angle view of channelized turbidity currents links migrating cyclic steps to flow characteristics. *Nature communications*, 7, 11896.

Iriarte, J.L., Pantoja, S., and Daneri, D. (2014) Oceanographic processes in Chilean fjords of Patagonia: From small to large-scale studies. *Progress in Oceanography*, 129, 1 – 7.

Jacquet, J., McCoy, S.W., McGrath, D., Nimick, D.A., Fahey, M., O'kuinghttons, J., Friesen, B.A., and Leidlich, J. (2017) Hydrologic and geomorphic changes resulting from episodic glacial lake outburst floods: Rio Colonia, Patagonia, Chile. *Geophysical Research Letters*, 44, 854 – 864.

Kaplan, M.R., Ackert, R.P. Jr, Singer, B.S., Douglass, D.C., and Kurz, M.D. (2004) Cosmogenic nuclide chronology of millennial-scale glacial advances during O-isotope stage 2 in Patagonia. *Geological Society of America Bulletin*, 116 (3/4), 308 – 321.

Kineke, G.C., Woolfe, K.J., Kuehl, S.A., Milliman, J.D., Dellapenna, T.M., and Purdon, R.G. (2000) Sediment export from the Sepik River, Papua New Guinea: Evidence for a divergent sediment plume. *Continental Shelf Research*, 20, 2239 – 2266.

Kremer, K., Corella, J.P., Hilbe, M., Marillier, F., Dupuy, D., Zenhäusern, G., and Girardclos, S. (2015) Changes in distal sedimentation regime of the Rhone delta systems controlled by subaquatic channels (Lake Geneva, Switzerland/France). *Marine Geology*, 370, 125 – 135.

Lamy, F., Kilian, R., Arz, H.W., Francois, J.-P., Kaiser, J., Prange, M., and Steinke, T. (2010) Holocene changes in the position and intensity of the southern westerly wind belt. *Nature Geoscience*, 3, 695 – 699.

Lastras, G., and Dowdeswell, J.A. (2016) Terminal and recessional moraines in the fjords of southern Chile. *In: Dowdeswell, J.A., Canals, M., Jakobsson, M., Todd, B.J., Dowdeswell, E.K., and Hogan, E.K. (Eds.)* Atlas of Submarine Glacial Landforms: Modern, Quaternary and Ancient. Geological Society, London, Memoirs, 46, 65 – 66.

Lliboutry, L. (1965) Nieves y Glaciars de Chile, fundamento de glaciologia, Chile. Ediciones de la Universidad de Chile, 417 pp.

Lopez, P., Chevallier, P., Favier, V., Pouyaud, B., Ordenes, F., and Oerlemans, J. (2010) A regional view of fluctuations in glacier length in southern South America. *Global and Planetary Change*, 71, 85 – 108.

López, P., and Casassa, G. (2011) Recent acceleration of ice loss in the Northern Patagonian Icefield. *The Cryosphere Discussions*, 5, 3323 – 3381.

Mardones, M., Aguayo, M.A., Smith, E.A., and Ruiz, P.L. (2018) Retroceso glacial reciente en al Campo de Hielo Norte, región de Aysén: relación con variaciones climáticas. *Revista de geografía Norte Grande*, 69, 121 – 147.

Marin, V.H., Tironi, A., Paredes, M.A., and Contreras, M. (2013) Modeling suspended solids in a Northern Chilean Patagonia glacier-fed fjord: GLOF scenarios under climate change conditions. *Ecological Modelling*, 264, 7 – 16.

Mazières, A., Gillet, H., Castelle, B., Mulder, T., Guyot, C., Garlan, T., and Mallet, C. (2014) High-resolution morphobathymetric analysis and evolution of Capbreton submarine canyon head (Southeast Bay of Biscay – French Atlantic Coast) over the last decade using descriptive and numerical modeling. *Marine Geology*, 351, 1 – 12.

Meerhoff, E., Castro, L.R., Tapia, F.J., and Pérez-Santos, I. (2018) Hydrographic and biological impacts of a Glacial Lake Outburst Flood (GLOF) in a Patagonian fjord. *Estuaries and Coasts*, 42, 132 – 143.

Migeon, S., Mulder, T., Savoye, B., and Sage, F. (2012) Hydrodynamic processes, velocity structure and stratification in natural turbidity currents: Results inferred from field data in the Var Turbidite System. *Sedimentary Geology*, 245-246, 48 – 62.

Moffat, C. (2014) Wind-driven modulation of warm water supply to a proglacial fjord, Jorge Montt Glacier, Patagonia. *Geophysical Research Letters*, 41, 3943 – 3950.

Mulder, T., and Syvitski, J.P.M. (1995) Turbidity currents generated at river mouths during exceptional discharges to the world oceans. *Journal of Geology*, 103, 285 – 299.

Mulder, T., Syvitski, J.P.M., Migeon, S., Faugères, J.-C., and Savoye, B. (2003) Marine hyperpycnal flows: initiation, behavior and related deposits. A review. *Marine and Petroleum Geology*, 20, 861 – 882.

Nef, F. (1907) *Estuario Canal Baker*, 1:200000, Chile.

Normandeau, A., Lajeunesse, P., Poiré, A.G., and Francus, P. (2016a) Morphological expression of bedforms formed by supercritical sediment density flows on four fjord-lake deltas of the south-eastern Canadian Shield (Eastern Canada). *Sedimentology*, 63, 2106 – 2129.

Normandeau, A., Lamoureux, S.F., Lajeunesse, P., and Francus, P. (2016b) Sediment dynamics in paired High Arctic lakes revealed from high-resolution swath bathymetry and acoustic stratigraphy surveys. *Journal of Geophysical Research: Earth Surface*, 121, 1676 – 1696.

Normandeau, A., Dietrich, P., Hughes Clarke, J., Van Wychen, W., Lajeunesse, P., Burgess, D., and Ghienne, J.-F. (2019) Retreat pattern of glaciers controls the occurrence of turbidity currents on high-latitude fjord deltas (eastern Baffin Island). *Journal of Geophysical Research: Earth Surface*, 124, 1559 – 1571.

Paull, C.K., Ussler III, W., Caress, D.W., Lundsten, E., Covault, J.A., Maier, K.L., Xu, J., and Augenstein, S. (2010) Origins of large crescent-shaped bedforms within the axial channel of Monterey Canyon, offshore California. *Geosphere*, 6, 755 – 774.

Parsons, J.D., Bush, J.W.M., and Syvitski, J.P.M. (2001) Hyperpycnal plume formation from riverine outflows with small sediment concentrations. *Sedimentology*, 48, 465 – 478.

Piret, L., Bertrand, S., Kissel, C., De Pol-Holz, R., Tamayo Hernando, A., and Van Daele, M. (2017a) First evidence of a mid-Holocene earthquake-triggered megaturbidite south of the Chile Triple Junction. *Sedimentary Geology*, 375, 120 – 133.

Piret, L., Bertrand, S., Vandekerkhove, E., Harada, N., Moffat, C., and Rivera, A. (2017b) Gridded bathymetry of the Baker-Martinez fjord complex (Chile, 48°S) v1. Figshare. Fileset.

Postma, G., and Cartigny, J.B. (2014) Supercritical and subcritical turbidite currents and their deposits – A synthesis. *Geology*, **42**, 987 – 990.

Prior, D.B., Bornhold, B.D., and Johns, M.W. (1986) Active sand transport along a fjord-bottom channel, Bute Inlet, British Colombia. *Geology*, **14**, 581 – 584.

Prior, D.B., Bornhold, B.D., Wiseman, W.J., and Lowe, Jr.D.R. (1987) Turbidity current activity in a British Columbia fjord. *Science*, **237**, 1330 – 1333.

Quiroga, E., Ortiz, P., Gerdes, D., Reid, B., Villagran, S., and Quiñones, R. (2012) Organic enrichment and structure of macrobenthic communities in the glacial Baker fjord, Northern Patagonia, Chile. *Journal of the Marine Biological Association of the United Kingdom*, **92** (1), 73 – 83.

Rodrigo, C. (2008) Submarine topography in the Chilean North Patagonian channels. *In: Silva, N., and Palma, S. (Eds.)* Progress in the oceanographic knowledge of Chilean interior waters, from Puerto Montt to Cape Horn. Comité Oceanográfico Nacional – Pontificia Universidad Católica de Valparaíso, Valparaíso, pp. 19 – 23.

Ross, L., Pérez-Santos, I., Valle-Levinson, A., and Schneider, W. (2014) Semidiurnal internal tides in a Patagonian fjord. *Progress in Oceanography*, **129**, 19 – 34.

Sepúlveda, J., Pantoja, S., Hughen, K.A., Bertrand, S., Figueroa, D., León, T., Drenzek, N.J., and Lange, C. (2009) Late Holocene sea-surface temperature and precipitation variability in northern Patagonia, Chile (Jacaf Fjord, 44°S). *Quaternary Research*, **72**, 400 – 409.

Servicio Hidrográfico y Oceanográfico de la Armada (2001) *Canal Baker*, 6th edition, 1:200000, Valparaíso, Chile.

Sievers, H.A., and Silva, N. (2008) Water masses and circulation in austral Chilean channels and fjords. *In: Silva, N., and Palma, S. (Eds.)* Progress in the oceanographic knowledge of Chilean interior waters, from Puerto Montt to Cape Horn. Comité Oceanográfico Nacional – Pontificia Universidad Católica de Valparaíso, Valparaíso, pp. 53 – 58.

Silva, N., and Vargas, C.A. (2014) Hypoxia in Chilean Patagonian Fjords. *Progress in Oceanography*, **129**, 62 – 74.

Smith, N.D., Phillips, A.C., and Powell, R.D. (1990) Tidal drawdown: A mechanism for producing cyclic sediment laminations in glaciomarine deltas. *Geology*, **18**, 10 – 13.

Smith, D.P., Ruiz, G., Kvitek, R., and Iampietro, P.J. (2005) Semiannual patterns of erosion and deposition in upper Monterey Canyon from serial multibeam bathymetry. *GSA Bulletin*, **117**, 1123 – 1133.

Stacey, C.D., and Hill, P.R. (2016) Cyclic steps on a glacifluvial delta, Howe Sound, British Colombia. *In: Dowdeswell, J.A., Canals, M., Jakobsson, M., Todd, B.J., Dowdeswell, E.K., and Hogan, E.K. (Eds.)* Atlas of Submarine Glacial Landforms: Modern, Quaternary and Ancient. Geological Society, London, Memoirs, **46**, 93 – 94.

Stacey, C.D., Hill, P.R., Talling, P.J., Enkin, R.J., Hughes Clarke, J.H., and Lintern, D.G. (2018) How turbidity current frequency and character varies down a fjord-delta system: Combining direct monitoring, deposits and seismic data. *Sedimentology*, **66**, 1 – 31.

Syvitski, J.P.M., Burrell, D.C., and Skei, J.M. (1987) Fjords: Processes and Products. Springer, Berlin.

Syvitski, J.P.M. (1989) On the deposition of sediment within glacier-influenced fjords: Oceanographic controls. *Marine Geology*, **85**, 301 – 329.

Syvitski, J.P.M. (1991) The changing microfabric of suspended particulate matter – the fluvial to marine transition: flocculation, agglomeration, and palletization. *In: Bennet, R.H., Bryant, W.R., and Hulbert, M.H. (Eds.)* Microstructure of fine-grained sediments. New York, Springer-Verlag, pp. 131 – 137.

Syvitski, J.P.M., and Shaw, J. (1995) Sedimentology and geomorphology of fjords. *In: Perillo, G.M.E. (Ed.)* Geomorphology and Sedimentology of Estuaries. Amsterdam, Elsevier, pp. 113 – 178.

Tanaka, K. (1980) Geographic Contribution to a Periglacial Study of the Hielo Patagónico Norte with Special Reference to the Glacial Outburst Originated from Glacier-Dammed Lago Arco, Chilean Patagonia. Center Company, Tokyo, 97 pp.

Van Daele, M., Bertrand, S., Meyer, I., Moernaut, J., Vandoorne, W., Siani, G., Tanghe, N., Ghazoui, Z., Pino, M., Urrutia, R., and De Batist, M. (2016) Late Quaternary evolution of Lago Castor (Chile, 45.6 °S): Timing of the deglaciation in northern Patagonia and evolution of the southern westerlies during the last 17 kyr. *Quaternary Science Reviews,* **133**, 130 – 146.

Vendettuoli, D., Clare, M.A., Hughes Clarke, J.E., Vellinga, A., Hizzet, J., Hage, S., Cartigny, M.J.B., Talling, P.J., Waltham, D., Hubbard, S.M., Stacey, C., and Lintern, D.G. (2019) Daily bathymetric surveys document how stratigraphy is built and its extreme incompleteness in submarine channels. *Earth and Planetary Science Letters*, **515**, 231 – 247.

Verardo, D.J., Froelich, P.N. and McIntyre, A. (1990) Determination of organic carbon and nitrogen in marine sediments using the Carlo Erba NA-1500 Analyzer. *Deep-sea Research*, **37** (1), 157 – 190.

Wils, K., Van Daele, M., Lastras, G., Kissel, C., Lamy, F., and Siani, G. (2018) Holocene event record of Aysén fjord (Chilean Patagonia): an interplay of volcanic eruptions, crustal and megathrust earthquakes. *Journal of Geophysical Research: Solid Earth*, **123**(1), 324 – 343.

Wilson, R., Glasser, N.F., Reynolds, J.M., Harrison, S., Anacona, P.I., Schaefer, M., and Shannon, S. (2018) Glacial lakes of the Central and Patagonian Andes. *Global and Planetary Change*, **162**, 275 – 291.

Winchester, V., and Harrison, S. (2000) Dendrochronology and lichenometry: colonization, growth rates and dating of geomorphogical events on the east side of the North Patagonian Icefield, Chile. *Geomorphology*, **34**, 181 – 194.

Wynn, R.B., Piper, D.J.W., and Gee, M.J.R. (2002) Generation and migration of coarse-grained sediment waves in turbidity current channels and channel-lobe transition zones. *Marine Geology*, **192**, 59 – 78.

Wynn, R.B., and Stow, D.A.V. (2002) Classification and characterisation of deep-water sediment waves. *Marine Geology*, **192**, 7 – 22.

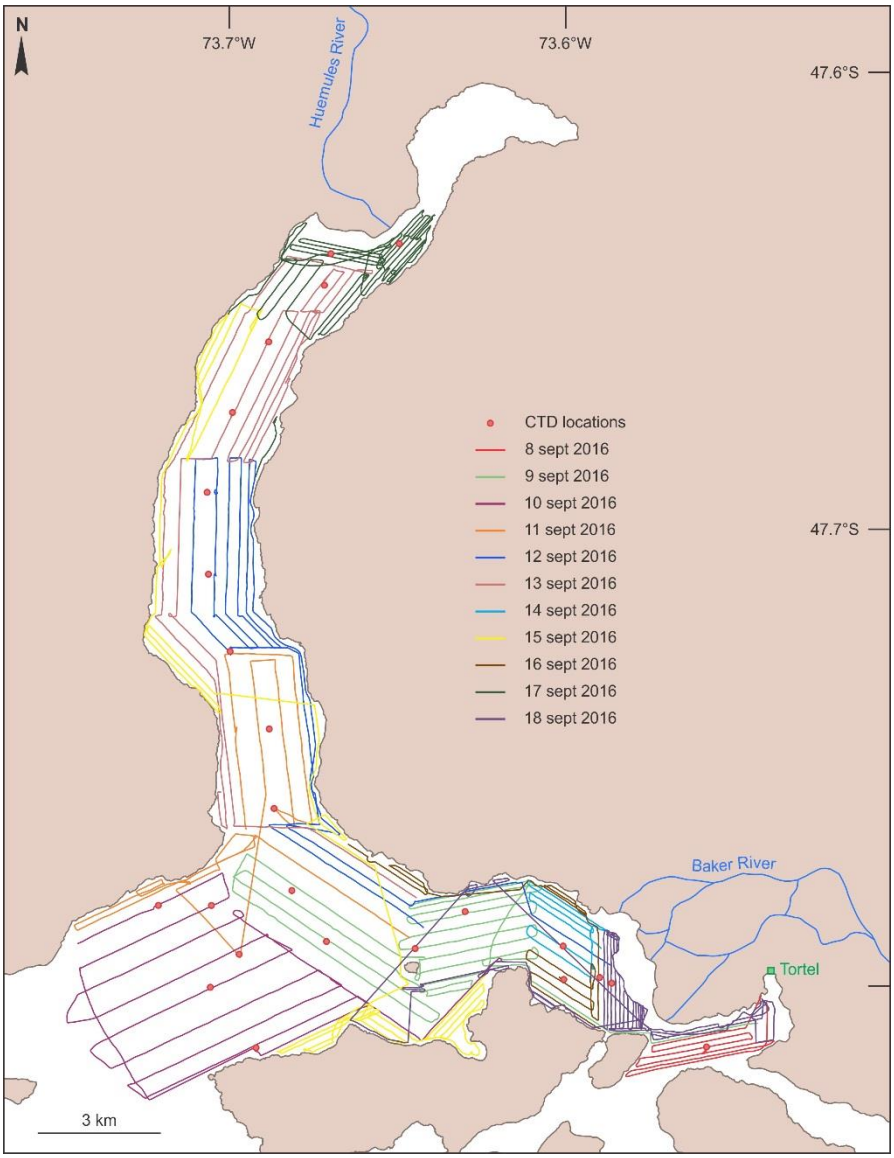

Figure S4A. Tracklines of the multibeam survey in September 2016. Different survey days are represented by different colors. The locations of the CTD casts used to calculate sound velocity profiles are indicated as red dots.

Table S4A. Suspended sediment concentrations (SSC) measured in Baker River, just upstream of the area of tidal freshwater influence (47.7991 °S – 73.3915 °W). Mean daily discharge was measured at the Baker bajo Ñadis station (DGA, Chile). The elevated suspended sediment concentrations on 22/12/08 and 17/09/09 (in bold) are associated with GLOFs triggered on 21/12/08 and 16/09/09, respectively. SSC values were obtained by filtration through 47 mm GFF filters.

Date (dd/mm/yy)	Time	SSC (mg/l)	Mean daily discharge (m^3/sec)	Season
02/11/08		122.6	659	Spring
02/12/08	13:10	90.8	1040	Summer
22/12/08	**20:00**	**780.6**	**2262**	**Summer**
04/02/09	14:45	76.3	1152	Summer
18/04/09	12:30	102.8	1206	Autumn
17/06/09	12:05	21.8	917	Winter
20/08/09	16:45	14.0	Not available	Winter
16/09/09	16:15	33.3	Not available	Spring
17/09/09	**11:00**	**574.5**	**Not available**	**Spring**
11/10/09	18:00	32.3	688	Spring
16/11/09	12:30	20.1	676	Spring
22/12/09	13:15	77.4	1088	Summer
17/01/10	18:25	96.5	1752	Summer
07/02/10	15:00	73.7	1449	Summer
20/03/10	20:00	67.3	1357	Autumn
24/04/10	18:00	17.2	803	Autumn
29/05/10	11:10	20.2	852	Autumn
28/06/10	12:20	26.3	1279	Winter
08/03/14	11:10	26.4	1077	Autumn
09/03/14	12:32	17.2	1051	Autumn
10/03/14	12:15	21.8	968	Autumn
11/03/14	12:30	9.5	992	Autumn
12/03/14	13:04	20.9	988	Autumn
14/03/14	11:53	28.0	935	Autumn
15/03/14	12:24	11.4	890	Autumn
16/03/14	11:47	19.7	874	Autumn
17/03/14	10:56	10.9	846	Autumn
19/01/15	10:20	65.7	1693	Summer
20/01/15	10:20	62.1	1637	Summer
21/01/15	09:00	55.3	1570	Summer
22/01/15	10:30	52.4	1522	Summer
23/01/15	09:30	49.3	1534	Summer
24/01/15	10:20	51.7	1609	Summer
25/01/15	09:30	55.8	1670	Summer
26/01/15	09:30	66.7	1637	Summer
27/01/15	10:00	60.9	1649	Summer
28/01/15	09:20	63.3	1567	Summer

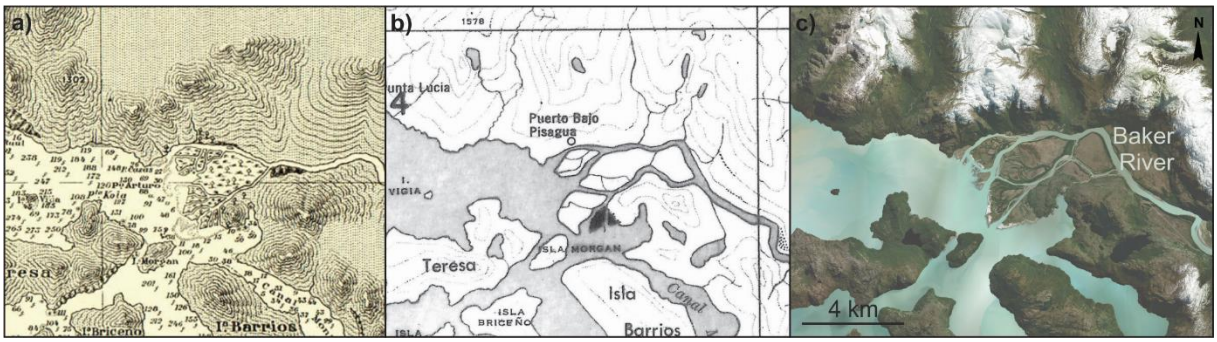

Figure S4B. The Baker river delta in (a) 1900 (Nef, 1907) and (b) 1944/1945 (Instituto Geográfico Militar de Chile, 1953) compared to (c) its current morphology (Global Mapper World Imagery). Note that in 1900, the northern river branch was better developed than at present.

References

Instituto Geográfico Militar de Chile (1953) *Rio Baker N° 4773*, 1:250000, compiled from trimetrogon photographs, Santiago, Chile.

Nef, F. (1907) *Estuario Canal Baker*, 1:200000, Chile.

5. Signature of modern glacial lake outburst floods in fjord sediments (Baker River, Chile)

This chapter is based on:

Vandekerkhove, E., Bertrand, S., Torrejón, F., Kylander, M., and **Saunders, K.M.** (accepted) Signature of modern Glacial Lake Outburst Floods in fjord sediments (Baker River, Chile). *Sedimentology*

Author contributions: EV and SB collected the sediment cores. EV conducted the sediment analyses, and FT collected historical data. KMS and MK performed the ^{210}Pb measurements, and XRF analysis, respectively. EV and SB wrote the paper, with contributions from FT, MK, and KMS.

Abstract: Glacial Lake Outburst Floods (GLOFs) constitute a major hazard in glacierized regions. They are particularly pronounced in the Baker River watershed (Chilean Patagonia, 48°S), where 23 events occurred between 2008 and 2020. Although GLOF deposits have previously been studied in lake settings, how modern GLOFs are recorded in fjord sediments remains mostly unknown. To address this issue, ten sediment cores collected in the fjord immediately downstream of the Baker River (Martínez Channel) were investigated and compared to the recent GLOF history of the river. Results show that sediments accumulate at 2.0–3.4 cm year^{-1} and that GLOF deposits can be distinguished from background sediments by their finer grain size (5.98 ± 0.82 µm) and lower organic carbon content (0.31 ± 0.06 %), reflecting the release and transport in suspension of high amounts of glacial rock flour during GLOFs. Although 21 GLOFs from Cachet 2 Lake occurred between 2008 and 2017, the first events left a stronger imprint in the sediment, suggesting that more sediment of glacial origin was released during those initial events, possibly due to lake-bed erosion. An older GLOF deposit was tentatively linked to the outburst of Las Lengas Lake in 1988. The sediment cores also contain fine-grained turbidites, especially in the prodelta area. These turbidites confirm recent channel activity, but most of them seem to have been triggered by processes other than GLOFs. Overall, our results suggest that GLOF deposits are distinct from typical flood turbidites. They are best identified by their low grain size and TOC contents, and best archived on the delta slope, away from any submarine channel influence. Finally, our results highlight the potential of fjord sediment archives to establish pre-historical GLOF records and ultimately improve GLOF hazard assessments.

5.1. Introduction

Glacial Lake Outburst Floods (GLOFs) are catastrophic events that occur when a lake dammed by a glacier or moraine suddenly empties, resulting in the abrupt flooding of downstream environments. They constitute a major threat in glacierized regions and often cause damage to infrastructure and/or result in the loss of human lives and livestock (Carrivick and Tweed, 2016). It is generally assumed that GLOF frequency is currently increasing due to accelerating glacier retreat and thinning rates (e.g., Iribarren Anacona et al., 2014; Wilson et al., 2018). However, recent studies suggest that the frequency of GLOFs from moraine dam failures has been declining since the mid-1990s (Carrivick and Tweed, 2016; Harrison et al., 2018). Likewise, the frequency of GLOFs from ice-dammed lakes seems to have decreased globally over the last 50 years (Carrivick and Tweed, 2016), despite an increase in the size and number of glacial lakes worldwide (Shugar et al., 2020).

Chilean Patagonia is particularly vulnerable to GLOFs. There, the recent increase in GLOF frequency is generally seen as a possible consequence of the rise in the number of glacial lakes related to the

accelerated retreat of glaciers in the southern Andes (Wilson et al., 2018, 2019). In Chilean Patagonia, GLOFs are especially pronounced in the Baker region (47–48°S), where 23 events have been documented between April 2008 and November 2020 (Dussaillant et al., 2010; Jacquet et al., 2017). Historical information suggests the occurrence of additional GLOFs from various proglacial lakes from as early as 1881 (Tanaka, 1980; Winchester and Harrison, 2000; Dussaillant et al., 2010; Jacquet et al., 2017).

Due to the relative lack of instrumental data in Patagonia, however, little is known about GLOF occurrence on longer timescales, and geological records are needed to extend the flood record to pre-historical timescales. One of the most promising types of geological archives is fjord sediments, which are increasingly recognized as high-resolution recorders of climate and environmental change (Bianchi et al., 2020). Fjord sediments are particularly promising in the Baker River area since Baker River discharges into the Baker-Martínez Fjord System, where GLOFs are known to affect the stratification of the water column and suspended sediment concentrations (Marín et al., 2013, Meerhoff et al., 2019).

Although previous studies have investigated GLOF deposits in lake settings (e.g. Xu et al., 2015; Røthe et al., 2019), little is known about how GLOFs are recorded in fjord sediments. The only GLOF deposits that have been described in marine sediments are those of Disenchantment Bay (Alaska) (Willems et al., 2011), which are composed of stratified mud, sand, and diamicton, formed by sediment gravity flows and hypopycnal plume sedimentation. GLOF deposits in this tidewater glacier fjord are difficult to identify from background sediments (Willems et al., 2011), and the sediment sequence deposited by the 1986 outburst flood, for example, is vertically and laterally heterogenous (Cowan et al., 1996). In lakes, GLOFs are able to create rapidly deposited layers or event deposits but their sedimentological properties are rather variable (e.g. Xu et al., 2015; Boes et al., 2018; Røthe et al., 2019). In Rundvatnet Lake in Norway, for example, GLOFs are recorded as clear sand layers embedded in a finer-grained background matrix (Xu et al., 2015). In Buarvatnet Lake (Norway), however, GLOFs are recorded as fine-grained deposits, which was explained by sediment filtration in lakes located along the course of the river (Røthe et al., 2019). Aside from intermediate lakes, which are able to trap sediments, the nature of the glacial lake dam (i.e. ice vs moraine) can also influence the GLOF properties (Benn and Evans, 2010). For example, GLOFs originating from ice-dammed lakes generally result in lower peak discharges compared to GLOFs from moraine-dammed lakes with a comparable lake volume, as the enlargement of ice tunnels is often a slower process than the overtopping and incision of moraines (Costa and Schuster, 1988; Clague and Evans, 2000). Finally, other factors, such as triggering mechanism, dam-failure mechanism, and hydraulic flow behavior, might also influence GLOF hydrology (Walder and Costa, 1996; Benn and Evans, 2010; Westoby et al., 2014), and therefore their signature in downstream sediments.

In this paper, we examine ten sediment cores from the head of Martínez Channel to understand how modern GLOFs are recorded in fjord sediments. Since previous results have shown the presence of rapidly migrating channels at the fjord head (Vandekerkhove et al., 2020a), a multi-core and multi-proxy approach was used to test whether sediments deposited during GLOFs can be distinguished from the background sediments and from other event deposits. The interpretation of the sediment data is based on the recent GLOF history of Baker River, which is derived from gauged river-flow datasets, historical records, and testimonies.

5.2. Setting

5.2.1. Baker River

The Baker River is situated in Chilean Patagonia (47–48°S), where it drains most of the eastern part of the Northern Patagonian Icefield (NPI; Fig. 1A). It is the largest river in Chile in terms of mean annual discharge (Dussaillant et al., 2012). The river originates at Bertrand Lake, which is fed by General Carrera Lake, and continues to flow southwards along the NPI. Its main tributaries are, from north to south, proglacial rivers Nef, Colonia, and Ventisquero, which originate from NPI outlet glaciers, and rivers Chacabuco, Del Salto, and Los Ñadis, which drain the eastern part of the watershed. Del Salto and Los Ñadis rivers both receive meltwater from mountain glaciers on the eastern side of the Baker watershed. Due to the large input of glacial meltwater, the discharge of Baker River varies seasonally from 600 m^3 s^{-1} in winter to 1200 m^3 s^{-1} in summer (Dussaillant et al., 2012). To the south, the Baker River flows into the Martínez Channel, where it forms a large fan-shaped delta near the town of Caleta Tortel (Fig. 1A).

5.2.2. Martínez Channel

Upon entering the fjord, the sediment-laden freshwater from Baker River continues to flow as a buoyant hypopycnal plume on top of the salty, warmer, water mass from the Pacific Ocean (Iriarte et al., 2014), creating a two-layer flow typical of fjord systems (Syvitski and Shaw, 1995). The vertical structure of this two-layer circulation varies seasonally in relation to Baker River discharge, which increases in summer due to an increased meltwater contribution from snow and glaciers (Iriarte et al., 2014). Recent multibeam data of the head of Martínez Channel shows that the subaquatic delta is incised by well-developed channels (Fig. 1B; Vandekerkhove et al., 2020a), which implies the presence of turbidity currents that are able to transport sediments to the ~280 m deep prodelta area. Vandekerkhove et al. (2020a) hypothesized that these dense underflows are most likely formed during sporadic Baker River floods, due to extreme precipitation, rain-on-snow events, or GLOFs, without being able to decipher between these three possibilities.

5.2.3. Baker River GLOFs

Recent GLOFs in the Baker River watershed all initiated from the emptying of Cachet 2 Lake into the Colonia River, a tributary of the Baker River (Fig. 1A). During such events, the Baker River triples in discharge and river water temperature drops by 3 to 4 °C due to the input of glacial meltwater (Dussaillant et al., 2010). Floodplains located immediately upstream of the confluence with the Colonia River inundate (Vandekerkhove et al., 2020b), while downstream of the confluence, Baker River suspended sediment concentrations increase 8-fold, mostly due to the erosion of lake-bed and valley-fill deposits in the upper watershed (Quiroga et al., 2012; Bastianon et al., 2012). Cachet 2 Lake is not the only one triggering GLOFs in the Colonia valley. Arco Lake, which used to be dammed by the Colonia Glacier, caused GLOFs by repeated water discharge between 1881 and the 1960s (Tanaka, 1980; Winchester and Harrison, 2000; Dussaillant et al., 2010; Jacquet et al., 2017). Other more recent examples of GLOFs in the Baker watershed are the 1977 collapse of the moraine-dammed Engaño Lake that resulted in the inundation of a small village located 26 km downstream of the failed lake (Iribarren Anacona et al., 2015), and the outburst of Laguna del Cerro Largo in March 1989 that resulted in an estimated peak discharge of around 20 000 m^3 s^{-1} and spilled approximately 140 x 10^{-6} m^3 of water and debris into the Soler Valley (Burton et al., 2021) (Fig. 1A). Finally, the late 2000 rockfall in Calafate Lake breached the lake terminal moraine and triggered a GLOF that displaced 2 x 10^6 m^3 of debris downslope in the Leones valley (Harrison et al., 2006). In addition to GLOFs, the Baker River region also experiences

meteorological floods resulting from long-lasting (several days) extreme precipitation events (Dussaillant et al., 2012; Vandekerkhove et al., 2020b).

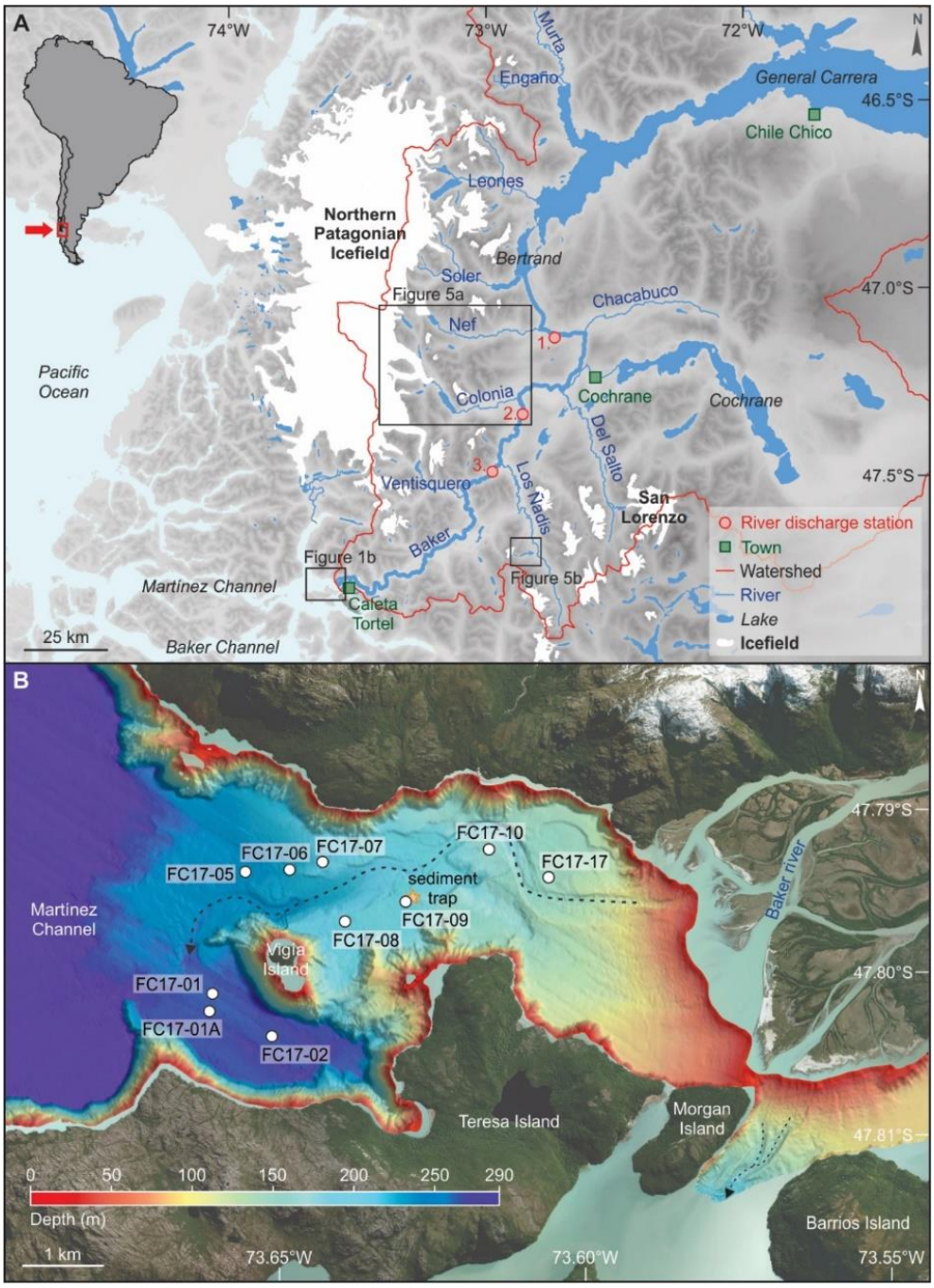

Figure 5.1. Location of the lower Baker River watershed and of the Baker River delta at the head of Martínez Channel. (A) Location of the Baker River along the eastern side of the Northern Patagonian Icefield (NPI). The background image is a grey-scale SRTM digital elevation model. The DGA river discharge stations along Baker River are 1. Rio Baker en angostura Chacabuco; 2. Rio Baker en Colonia; and 3. Rio Baker bajo Ñadis. Note that the first station is located upstream of the Colonia River, whereas the other two are downstream. (B) Subaerial (Global Mapper World Imagery) and subaquatic (Vandekerkhove et al., 2020a) topography of the Baker River delta, which extends down to a depth of 280 m in Martínez Channel. The white dots indicate the location of the sediment cores. The submarine channels are highlighted with dashed arrows and the location of the sediment trap is displayed with an orange star.

5.2.4. Present-day climate

Chilean Patagonia displays a strong longitudinal precipitation gradient driven by the orographic high of the Andes and the dominating humid southern westerlies. On the western side of the Andes and on top of the NPI, a hyperhumid climate prevails due to the uplift of moist air originating from the Pacific Ocean, with annual precipitation varying from 5000 to 10 000 mm (Garreaud et al., 2013). In contrast, forced subsidence results in dry conditions on the eastern side, where precipitation rapidly decreases to less than 300 mm $year^{-1}$ (Garreaud et al., 2013). The west-east temperature gradient is not as pronounced as for precipitation. The annual temperature varies between 4 °C in austral winter (June to August) and 13 °C in austral summer (December to February) and freezing levels are generally above 1 km a.s.l. Present-day vegetation distribution in the Baker River region mainly reflects the longitudinal precipitation gradient, with evergreen north Patagonian rainforests in the southwestern part of the watershed and grass steppe near the border with Argentina (Luebert and Pliscoff, 2006).

5.3. Material and methods

5.3.1. Sedimentologial and geophysical analysis

Ten sediment cores were retrieved from Martínez Channel using a gravity corer with 1.5 m-long transparent liners operated from the R/V Sur Austral (Fig. 1B). All sediment cores were described, imaged (linescan) and logged with a Geotek Multi-Sensor Core Logger (MSCL) at Ghent University, Belgium. Magnetic susceptibility (MS; Bartington MS2E point sensor) was logged at a downcore resolution of 2 mm.

The elemental composition of the sediment cores was analyzed with a 2 mm step-size using an Itrax X-Ray Fluorescence (XRF) core scanner at Stockholm University (Stockholm, Sweden). Data were acquired for 25 seconds using a molybdenum tube set at 30 kV and 50 mA. Zr was used as a grain-size proxy as this element is often associated with heavy minerals and enriched in coarser material (e.g. Bertrand et al., 2012; Davies et al., 2015; Liu et al., 2019). A centered log-ratio (CLR) transformation (Weltje et al., 2015) was applied to the Zr counts to avoid dilution effects. It was calculated using the following equation:

$$\text{CLR Zr} = \ln\left[\frac{Zr\ counts\ (z)}{g(z)}\right]$$

where *Zr counts (z)* stands for the Zr counts measured at depth z and *g(z)* represents the geometric mean of the composition at depth z, calculated as:

$$g(z) = \sqrt[n]{counts_{element\ 1} \cdot counts_{element\ 2} \cdot \ldots counts_{element\ n}}$$

The following elements (n=14) were used to calculate the geometric mean: Si, Cl, K, Ca, Ti, Mn, Fe, Zn, Br, Rb, Sr, Zr, Ba, and Pb.

The two most promising sediment cores, i.e. FC17-02 and FC17-08, were selected for further analysis based on their location, length, and distinctive lithology. X-ray Computed Tomography (CT) scanning was performed on these two cores using a Siemens SOMATOM Definition Flash CT-scanner at Ghent University Hospital (Belgium). The CT-scanner was operated at a voltage of 120 kV, an effective mAs of 200 and a pitch of 0.45. After reconstruction, a voxel size of approximately 0.15 mm (X-Y direction, across core) by 0.60 mm (Z-direction, along core) was obtained. The data were visualized and studied using the VGStudio 2.2 software.

Grain-size measurements were conducted on sediment cores FC17-02 and FC17-08 at 1 cm resolution using a Malvern Mastersizer 3000, equipped with a Hydro MV dispersion module. In order to remove organic matter, all samples were pre-treated by adding H_2O_2 (30 %) to the sediment suspended in 10 ml of deionized water. The suspension was then set to boil until the reaction ended. Afterwards, 1 ml of HCl (10 %) was added to the sample to remove possible calcium carbonate. After neutralizing the solution, biogenic silica was removed by adding 1 ml of NaOH (2N). Finally, all samples were decanted again before 1 ml of sodium hexametaphosphate (2 %) was added to the sample to avoid grain flocculation. A measuring time of 12 seconds with 10 % sonification was used.

Total Organic Carbon (TOC) content was determined continuously at a 0.5 cm-interval on sediment core FC17-08. Samples were analyzed on a Micro Cube elemental analyzer at the Stable Isotope Facility (UCDavis, California, USA). To remove possible inorganic carbon, all samples were treated with 1N sulfurous acid prior to analysis (Verardo et al., 1990).

5.3.2. Chronology

A chronology was established on the longest sediment core (FC17-02) using ^{210}Pb. Unsupported ^{210}Pb activities were calculated by subtracting ^{226}Ra activities from ^{210}Pb activities (Atahan et al., 2014; Mabit et al., 2014). Both isotopes were measured using alpha spectrometry at the Australian Nuclear Science and Technology Organisation (ANSTO, Australia) following the methodology of McMinn et al. (1997) and Harrison et al. (2003). One-cm-thick bulk sediment samples collected at a 10 cm-interval were measured, avoiding the event deposits. The Constant Flux-Constant Sedimentation (CFCS) model was applied to obtain a chronology as unsupported ^{210}Pb activity did not reach background levels in the bottommost sample and that the activities did not show a monotonous decrease. Errors on sediment ages were determined from uncertainties in the excess ^{210}Pb activities. The age-depth model of core FC17-02 was projected onto core FC17-08 using lithological correlations.

5.3.3. Historical and instrumental records

Historical information on past GLOF occurrence was extracted from bibliographic sources, which include written and iconographic documents from explorers and early settlers in the Baker region. In addition, field interviews were conducted in some of the early settlements along the Baker River and its tributaries to obtain independent testimonies of the Baker River flood history. These data were integrated with previously published information on flood events in the Baker watershed (Iribarren Anacona et al., 2014).

Baker River discharge data were obtained from two DGA (Chilean Water Directorate) monitoring stations: Rio Baker en angostura Chacabuco and Rio Baker bajo Ñadis (Fig. 1A). Discharge data from the DGA station Rio Baker en Colonia from 2003–2018 were also used. Discharge peaks were attributed a GLOF or intense precipitation origin by comparing discharge upstream and downstream of the confluence with proglacial rivers. Discharge peaks interpreted as resulting from intense precipitation were corroborated using precipitation data integrated over the respective station watersheds (Alvarez-Garreton et al., 2018).

5.4. Results

5.4.1. Lithology

Three major distinctive lithological facies, labeled A, B, and T, are defined in the fjord sediment cores based on their sedimentological properties and Zr variability (Fig. 2).

The type A facies represents the dominant lithology in most cores and can be regarded as background sediments (Fig. 2). These deposits are composed of greenish-grey silt. Their average mean grain size is 6.02 ± 0.67 µm (1σ) and 7.32 ± 0.65 µm, in cores FC17-02 and FC17-08, respectively (Fig. 3). The TOC values of the A facies vary around 0.36 ± 0.04 % in core FC17-08. A distinction can be made between type A1 and A2 sediments, where A2 sediments appear darker and slightly coarser than the A1 sediments (Fig. 2). The relatively coarser nature of facies A2 is confirmed by grain-size measurements (the A2 facies is on average 1 µm coarser than the A1 facies; Fig. S1) and Zr values, which are significantly positively correlated ($r = 0.66$, $p < 0.001$) to grain size (Fig. 3). The A2 facies is most abundant in the sediment cores closest to the Baker River outflow, i.e. FC17-17, FC17-10, and FC17-09, and at the base of most cores (Fig. 2).

Type B facies is composed of light-colored green-grey fine silt and mainly occurs, with few exceptions, in the upper ~35 cm of all cores (Fig. 2). Compared to the A facies, type B sediments are finer-grained, i.e. 5.20 ± 0.47 µm and 5.98 ± 0.82 µm, in cores FC17-02 and FC17-08, respectively (Fig. 3), and they display lower Zr values (Fig. 2). Moreover, these sediments show slightly lower TOC values, i.e. 0.31 ± 0.06 % (Fig. 3). A distinction between B1 and B2 facies is made based on grain size, with type B1 sediments being finer (average mean grain size in cores FC17-02 and FC17-08: 4.57 ± 0.02 µm) than B2 sediments (5.81 ± 0.72 µm), and a grain-size distribution that is more skewed towards the finer grain-size fraction (Fig. 3; Fig. S1).

A third facies, i.e. T facies or turbidite facies, occurs in all sediment cores (Fig. 2). This facies can be distinguished based on the typical fining-upward trends of turbidites, as shown by the Zr, MS, and grain-size values (Figs. 2 and 3). Most of the sediment cores on the delta slope (FC17-17 to FC17-05; Fig. 2) show only one clear turbidite at a depth of approximately 70 cm. Core FC17-05 contains an additional turbidite at the top. On the other hand, turbidites are abundant in the sediment cores located in the prodelta near the channel mouth (FC17-01, FC17-01A, and FC17-02; Fig. 2). In all cores, the base of the turbidites consists of coarse silt to coarse sand. In general, two types of turbidites can be distinguished based on color: light (T1) and dark (T2). The TOC results from core FC17-08 show that the T2 turbidite has distinctly higher TOC values (0.57 ± 0.10 %) than the background sediments (Fig. 3). The few T1 turbidites do not appear enriched in organic matter and are only found in the upper 30 cm of the most distal cores (FC17-05, FC17-01, FC17-01A, and FC17-02), and at a depth of 67 cm in FC17-02 (Fig. 2).

The various sediment facies can be relatively easily distinguished in a TOC versus Zr biplot (Fig. 4). The biplot confirms that the A2 facies is slightly coarser, i.e., enriched in Zr, than the A1 deposits. It also shows that the B facies, especially B1, clearly stands out from the background sediments (A facies) due to its finer nature. The dark T2 turbidite in core FC17-08 plots on the coarse side of the graph and displays higher TOC values than any other facies.

CT scans reveal that the laminations are extensively deformed throughout cores FC17-02 and FC17-08, due to bioturbation (Figs. 3, S2). However, turbidites and the B facies are generally not bioturbated. Laminations remain particularly visible in the B1 facies (Fig. S2).

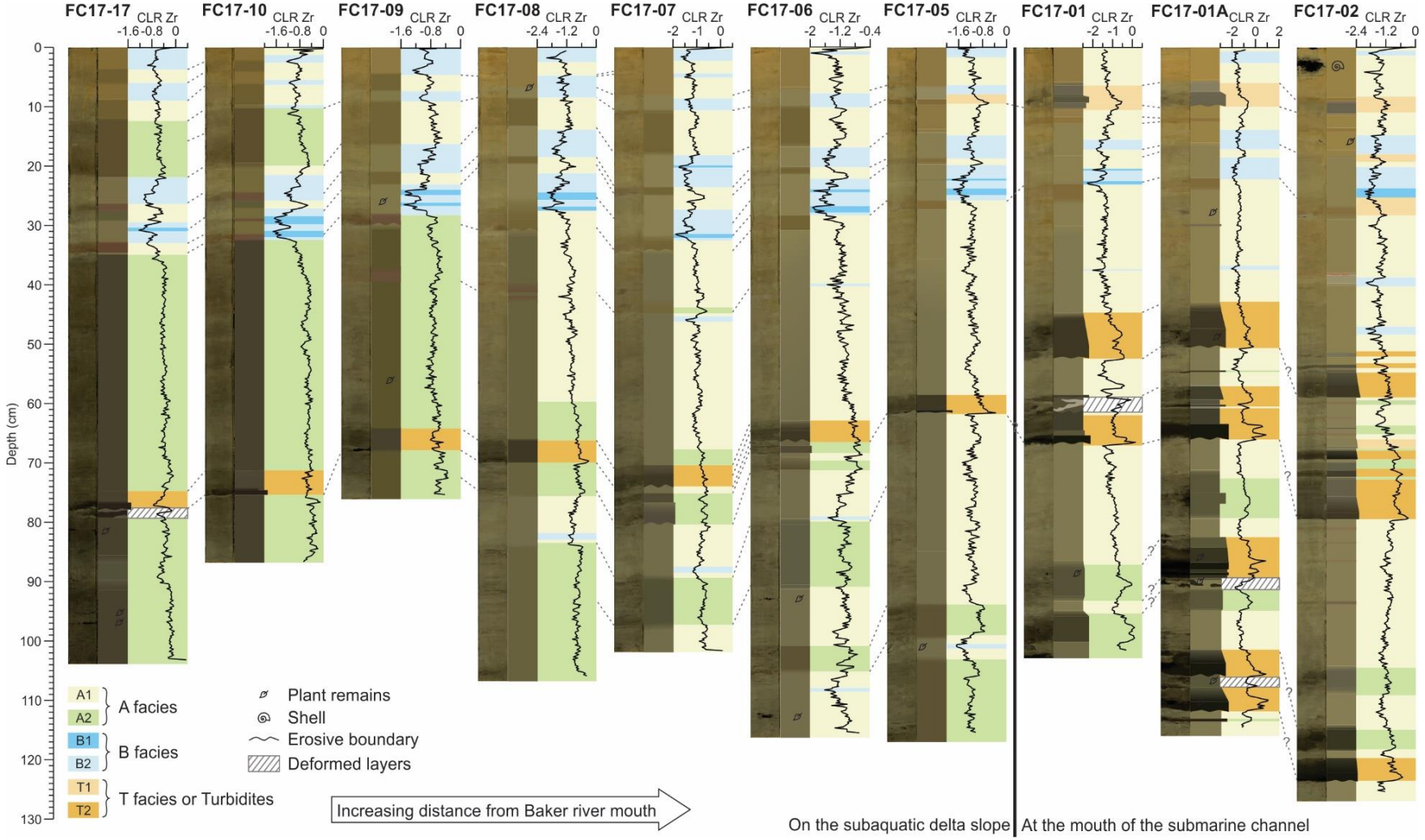

Figure 5.2. Lithology of sediment cores collected at the head of Martínez Channel with increasing distance from Baker River mouth to the right. The last three cores (FC17-01 to 02) are located on the prodelta in front of the main submarine channel, whereas the others were collected on the subaquatic delta slope (see Fig. 1B for exact location). Photographs are on the left and lithologs are displayed on the right. For all cores, Centered Log Ratio (CLR)-transformed Zr counts are displayed and used as a proxy for grain size. Lithological correlations are indicated using grey dashed lines.

5.4.2. Age-depth model

Unsupported ^{210}Pb concentrations in core FC17-02 show an overall decrease with depth (Fig. S3). The sample at 10–11 cm depth, which corresponds to a T1 turbidite (Fig. 3) was discarded from the model. The resulting age-depth model shows that the core covers a time span of 41 ± 9 years (Fig. 3), i.e. that the sediment record starts in 1976 ± 9 CE. The average sedimentation rate, excluding the turbidites, is 2.46 ± 0.06 cm year^{-1}, and it is slightly higher at the top of the core (2.52 cm year^{-1}) than at the bottom (2.40 cm year^{-1}).

This age-depth model was projected onto sediment core FC17-08 using relative variations in the thickness of sediment packages that are clearly correlated between cores FC17-02 and FC17-08 (Fig. S4). Turbidites were excised from the logs prior to calculating thickness differences. Results show that core FC17-08 covers 35 ± 8 years, and that the bottom of the core corresponds to 1982 ± 8 CE (Fig. 3). The accumulation rate of the turbidite-free deposits is 2.95 cm year^{-1}. As for FC17-02, it is higher at the top of the core (3.03 cm year^{-1}) than at the bottom (2.88 cm year^{-1}).

Correlations based on the lithological boundaries between the cores show that sediment accumulation rates in the other cores is relatively similar, with core average values for the turbidite-free sediments ranging from 3.39 cm year^{-1} near the river mouth (FC17-17) to 2.02 cm year^{-1} to the southwest of Vigía Island (FC17-01A) (Fig. S4).

The calculated accumulation rate is in accordance with results obtained from a sediment trap located near coring site FC17-09, i.e. 2.3 km to the northeast of FC17-02 (Fig. 1B), which gave accumulation rates of 3.08, 2.57, and 2.68 cm year^{-1} for the periods of 2017–2018, 2018–2019, and 2019–2020, respectively. Using correlations between cores FC17-09 and FC17-02 to account for spatial variations in sediment accumulation (Fig. S4) yields a projected accumulation rate of 2.35 ± 0.46 cm year^{-1} at site FC17-02 for years 2017–2020, which is in excellent agreement with the core average background sedimentation rate of 2.46 ± 0.06 cm year^{-1}.

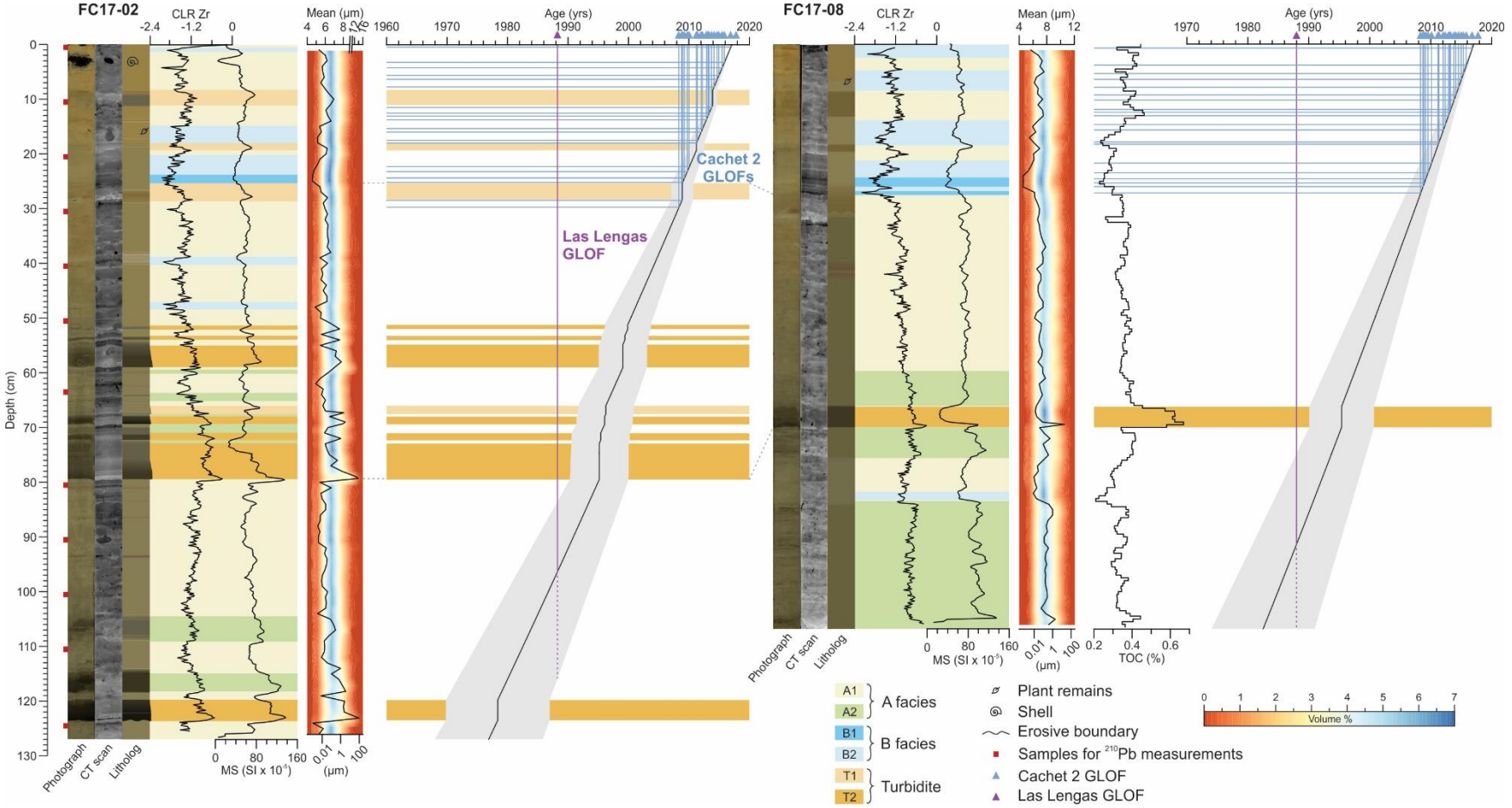

Figure 5.3. Lithology, high-resolution grain-size, and chronology of sediment cores FC17-02 and FC17-08 (see Fig. 1B for location). For the CT scans, denser material is represented by lighter colors and vice versa. The samples used for radionuclide analysis (core FC17-02) were taken at a 10-cm interval and are indicated by red squares. The CFCS age model is displayed, with error envelopes shown in grey. Turbidites, which are shown in orange, were considered as instantaneous deposits and subtracted for the construction of the model (see Fig. S3). The overall turbidite-free sedimentation rate at site FC17-02 is 2.46 ± 0.06 cm/yr. The age-depth model of FC17-08 was established by multiplying the ages obtained for FC17-02 by 1.20 ± 0.12, which represents the ratio between turbidite-free sediment thickness in FC17-08 versus FC17-02, as calculated from core correlations (shown with grey dashed lines; Fig. S4). For both cores, grain-size distributions and mean grain size (1 cm resolution) are shown. In addition, TOC values (5 mm resolution) are plotted for FC17-08. The Cachet 2 and Las Lengas GLOFs are represented using blue and purple triangles and lines, respectively.

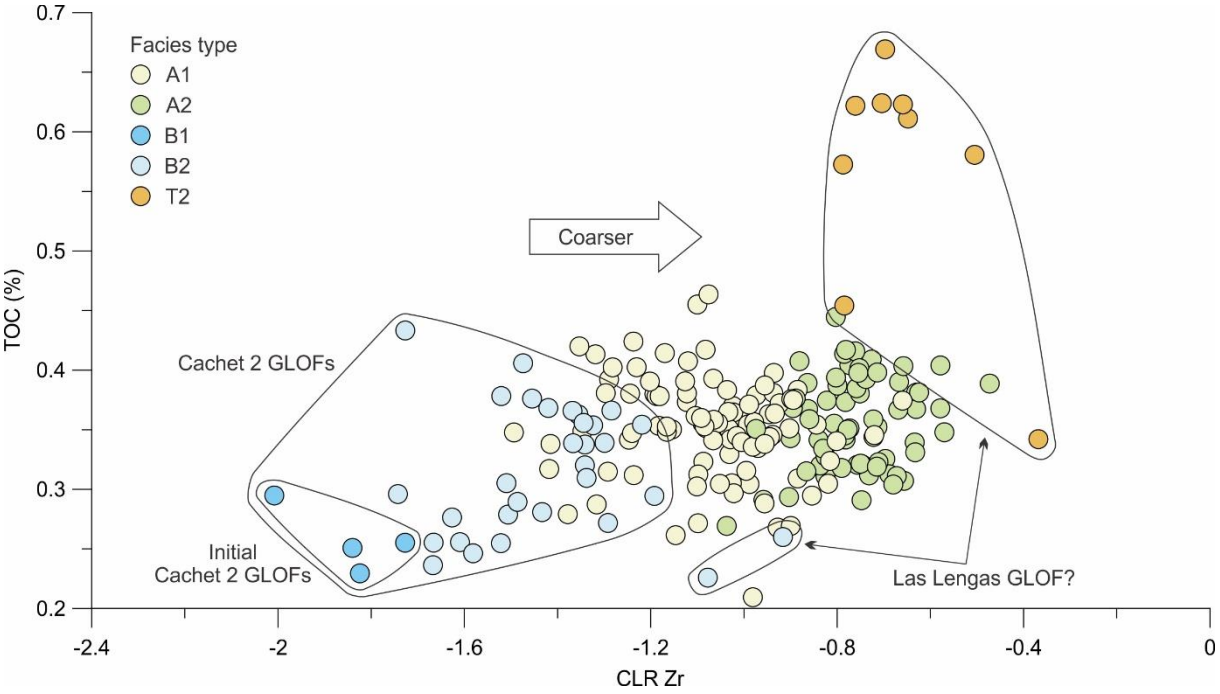

Figure 5.4. Identification of the sediment facies occurring in sediment core FC17-08 based on TOC contents and Centered Log Ratio (CLR)-transformed Zr counts (which reflect grain size). Samples from different sediment facies are distinguished using the color-scale used in Figs. 2 and 3. Samples corresponding to the 21st century Cachet 2 GLOFs and possibly to the 1988 Las Lengas GLOF are highlighted. Note that T1 facies is not represented since it is absent from sediment core FC17-08.

5.4.3. Historical Baker River GLOFs

The Baker River GLOF history was reconstructed from 1965 onwards (Table 1), using instrumental records, previously published data (Iribarren Anacona et al., 2014; Jacquet et al., 2017), and testimonies (Table S1). This time-window corresponds to the maximum period of time covered by the sediment cores. During this period, GLOFs in the Baker River appear to have originated from only two tributaries, i.e. the Colonia and Los Ñadis rivers (Fig. 1A). The 1977 and 2000 GLOFs from the moraine-dammed Engaño and Calafate lakes are not included as these events occurred upstream of the much larger General Carrera Lake (>3 orders of magnitude more voluminous than the GLOFs) and were therefore filtered and buffered before reaching Baker River (Fig. 1A). Likewise, the 1989 Laguna del Cerro Largo GLOF is discarded since it passed through Bertrand Lake before entering Baker River.

5.4.3.1. Colonia

Between April 2008 and November 2020, a total of 23 GLOFs occurred from the emptying of Cachet 2 Lake (Table 1, Fig. 5A–B; see section 2.3). Aside from the recent Cachet 2 GLOFs, it appears that all previous Colonia River GLOFs occurred prior to 1965 (Table 1).

Table 5.1. Overview of Baker River GLOFs since 1965 based on instrumental data, historical records and testimonies (Table S1). Discharge data are from two DGA (Chilean Water Directorate) stations located immediately downstream of the confluence with Colonia and Los Ñadis rivers (see Fig. 1 for location). The drained volume was calculated using hourly discharge data from these two stations. Cachet 2 Lake levels are from DGA station "Lago Cachet 2 en Glaciar Colonia", which was installed in May 2009. *Peak discharge and drained lake volume for the Las Lengas GLOF were calculated by Iribarren Anacona et al. (2014) based on the change in lake area. "–" means not measured and "?" indicates a lack of data.

Date (dd/mm/yyyy)	Source(s)	Lake	Peak discharge ($m^3 s^{-1}$)		Drained volume (x 10^6 m^3)		Maximum lake level (m)
			Rio Baker en Colonia	Rio Baker bajo Ñadis	Rio Baker en Colonia	Rio Baker bajo Ñadis	
17/11/2020	DGA	Cachet 2	1202	1329	46	72	–
07/11/2017	DGA	Cachet 2	1364	1497	240	273	22.14
28/11/2016	DGA	Cachet 2	2012	2166	198	227	30.97
14/11/2015	DGA	Cachet 2	2650	3007	121	168	–
16/06/2015	DGA	Cachet 2	3363	–	241	?	–
05/12/2014	DGA	Cachet 2	2866	–	137	?	–
18/08/2014	DGA	Cachet 2	3570	–	251	?	34.02
01/02/2014	DGA	Cachet 2	–	4240	?	253	39.63
23/09/2013	DGA	Cachet 2	>2532	2844	>137	197	28.71
10/04/2013	DGA	Cachet 2	2654	–	125	?	19.52
08/02/2013	DGA	Cachet 2	3598	–	173	?	38.14
07/11/2012	DGA	Cachet 2	3307	3557	>88	182	38.34
02/04/2012	DGA	Cachet 2	3538	3350	168	170	–
26/01/2012	DGA	Cachet 2	3747	3680	>198	245	–
29/05/2011	DGA	Cachet 2	2753	2834	162	168	–
04/03/2011	DGA	Cachet 2	2916	3128	192	211	–
06/10/2010	DGA	Cachet 2	733	?	?	?	–
05/01/2010	DGA	Cachet 2	2941	2912	101	103	–
16/09/2009	DGA	Cachet 2	3144	–	191	?	–
05/03/2009	DGA	Cachet 2	>3812	3516	?	195	–
21/12/2008	DGA	Cachet 2	2866	–	137	?	–
08/10/2008	DGA	Cachet 2	3007	2715	188	176	–
07/04/2008	DGA	Cachet 2	3575	3378	186	186	–
1988	Testimonies; Iribarren Anacona et al., 2014	Las Lengas	1301*		4.36*		–

5.4.3.1. Los Ñadis

Further downstream, the Baker River also experienced flooding from the Los Ñadis River (Fig. 1A). Conversations with local settlers reveal that Las Lengas Lake abruptly emptied sometime between 1985 and 1992, triggering a GLOF in the Los Ñadis River (Fig. 5C; records f to l in Table S1). Most interviewees mention the year 1988 and two of them recall that the GLOF occurred at the beginning of March following an unusually warm and dry summer (records I and k in Table S1). This event was previously identified using LANDSAT images, based on which it was dated 1987–1998 (Iribarren Anacona et al., 2014). According to testimonies, the flooding only lasted for a few hours, but it increased the Los Ñadis River water level by two meters. Further downstream, areas located seven meters above the Los Ñadis River level inundated (record h in Table S1). Due to the large inflow of meltwater from the Las Lengas River, the Los Ñadis River was backed up at least 1 km upstream (record k in Table S1). After the flood, water withdrew and the areas that had flooded were draped with white-colored mud, i.e. glacial rock flour. The Las Lengas Lake, which used to host a calving glacier, almost completely emptied.

5.5. Discussion

5.5.1. Sedimentological interpretation

5.5.1.1. A facies

The A facies is the most prominent lithology in all sediment cores and can be interpreted as background sediment (Fig. 2). Its low grain size (6.67 ± 0.66 µm) and TOC values (0.36 ± 0.04 %) are typical for a proglacial fjord environment (Syvitski, 1989; Syvitski and Shaw, 1995). The A2 facies, which is coarser and darker than A1, is more abundant in the cores located closer to the river mouth (Fig. 2), in agreement with observations made on surface sediment samples by Vandekerkhove et al. (2020a). These authors attributed the decreasing grain size with increasing distance from the river mouth as the result of gradual settling from the suspended sediment plume.

5.5.1.2. B facies

The B facies displays a lower mean grain size (5.68 ± 0.80 µm) than the background sediment (6.67 ± 0.66 µm, i.e. A facies), due to a significant increase in the relative amount of clay-size particles (Figs. 2, 3, 4 and S1). The B facies is also marked by a significant drop in TOC values (0.31 ± 0.06 %) compared to the background sediments (0.36 ± 0.04 %), which is particularly marked for the B1 deposits (0.26 ± 0.02 %; Figs. 3 and 4).

The B facies is present in all cores and aside from a few exceptions, it mostly occurs within the upper 35 cm of the sediment. According to the ^{210}Pb chronology, these sediments were deposited after 2008 ± 2 CE (Fig. 3). This timing corresponds remarkably well to the beginning of the 21st century GLOFs from Cachet 2 Lake, which occurred from April 2008 to November 2020 (Fig. 3). The fine-grained and low organic signature of the B facies, which is typical for sediments of glacial origin (e.g. Benn and Evans, 2010), supports this association. These B sediments are therefore interpreted as the signature of Cachet 2 GLOFs in Martínez Channel, and they most likely reflect the large amounts of very fine silt that is transported in suspension in Baker River during GLOFs (Fig. 5B). These sediments most likely originate from the erosion of the Cachet 2 lake bed, as observed by Jacquet et al. (2017). These authors estimate that between 2008 and 2015, GLOFs and the subsequent periods of free drainage removed approximately 25 x 10^6 m³ of sediment from the lake basin.

Although the B facies in the upper part of the cores is typically fine-grained and organic-poor, these indicators seem more extreme between 2008–2010, i.e. in the B1 facies, than afterwards (Figs. 3 and

4). The B1 facies therefore seems to be the signature of the initial Cachet 2 GLOF event(s), although individual sediment layer-to-GLOF association is not possible. Another remarkable characteristic of the B1 facies compared to B2, and to the rest of the cores, is the absence of bioturbation, which is represented as a clear layering on the CT scan images and implies rapid deposition (Figs. 3 and S2). It appears that the initial Cachet 2 Lake outburst events resulted in the deposition of a larger amount of sediments of glacial origin at the fjord head than the subsequent events. It is hypothesized that the lower input of glacial rock flour by the Cachet 2 GLOFs that occurred after ~2010 represents a decrease in the amount of sediment available for erosion at the bottom of Cachet 2 Lake, in agreement with the erosion rate estimates of Jacquet et al. (2017). Therefore, the post-2010 Cachet 2 GLOF deposits (B2 facies) do not display a glacial signal that is as clear as during the initial event(s) (B1 facies) (Figs. 2, 3, and 4). The B2 facies likely represents glacial rock flour diluted in background fjord sediments, which would explain why the decrease in TOC is only clearly marked in the initial Cachet 2 GLOF deposits (B1 facies; Fig. 4).

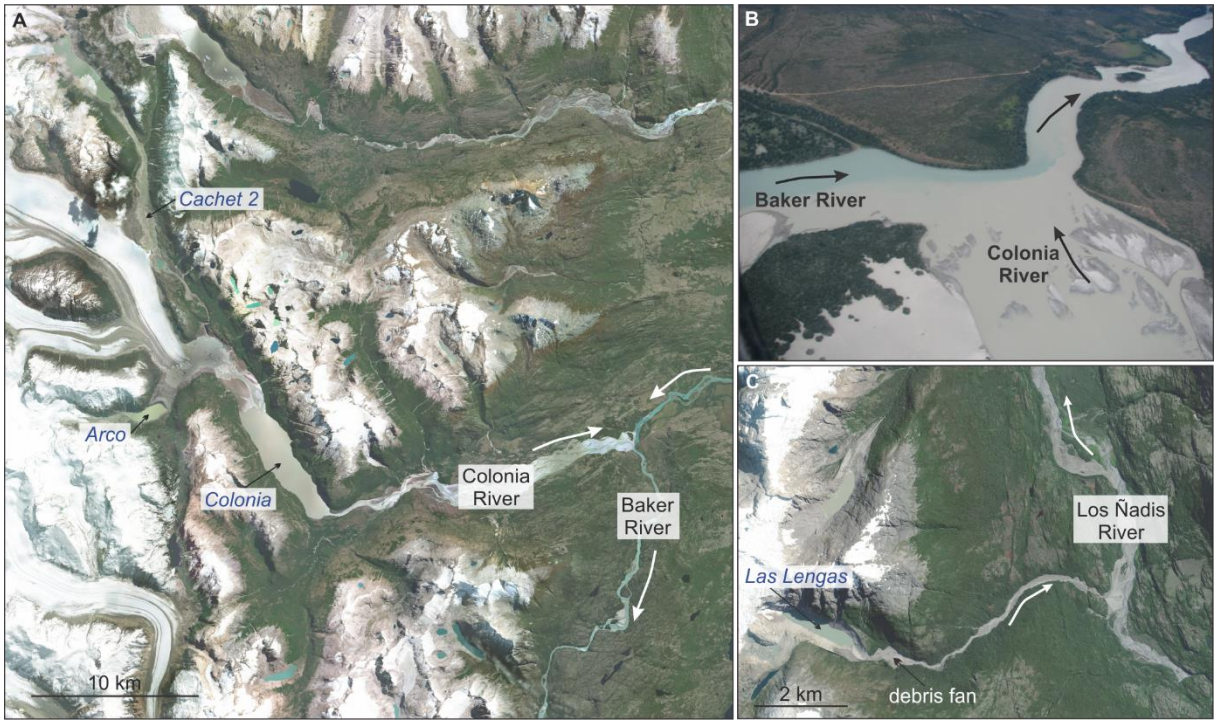

Figure 5.5. Proglacial lakes at the origin of modern Baker River GLOFs. (A) Cachet 2 Lake, which triggered Baker River GLOFs in 1976 and 2008–2017 (Global Mapper World Imagery). See figure 1A for location within the Baker watershed. (B) Aerial photograph of the confluence of Colonia River with Baker River during the December 2008 GLOF, showing large amounts of sediment released to the Baker River (photo credit: Paulina Rojas). As a reference scale, the width of the Colonia River at its outflow is ~500 m. (C) Las Lengas Lake, which triggered a GLOF in 1988 (Global Mapper World Imagery).

Aside from the recently deposited B-type sediments that are present in the upper 35 cm of all sediment cores, other B-type layers occur deeper in the cores and could thus represent older GLOF events (Figs. 2, 3, and 4). For instance, type B sediments are found in both FC17-05 and FC17-06 at a depth of 101 and 108 cm, which correspond to 1980 ± 10 CE and 1981 ± 11 CE, respectively (Fig. 2). No Baker River GLOFs were reported during this time window. These sediments could thus potentially be linked to the 1977 flood that was mentioned by two interviewees (records m and n in Table S1). This event is supported by Baker River discharge data, which show an abrupt increase to at least 2720 $m^3 s^{-1}$ from

the 28th to the 30th of December 1976 (Fig. 6A). One interviewee specifically recalls that the lower part of the Baker River was flooded on the 7th of January 1977, and that the flood lasted for about one week (record n in Table S1). According to Dussaillant et al. (2012) and Benito et al. (2021), this flood represents a rain-on-snow event resulting from several consecutive days of heavy rainfall and higher-than-average temperatures. Based on hydrographs, it seems to have mainly affected the western, glacier-covered, part of the watershed, which explains its glacial signature, i.e. sediments that are finer and less organic than background sediments.

In addition, three cores, i.e. FC17-06, FC17-07, and FC17-08, display B-type sediments between 79 and 89 cm (Fig. 2), with an age of 1991 ± 8 CE, corresponding in timing with the Las Lengas GLOF that occurred in 1988 (Table 1). In FC17-08, these sediments show a drop in TOC values (0.24 ± 0.03 %) that is similar to those observed in the B1 deposits representing the 2008–2017 Cachet 2 GLOFs (Figs. 3 and 4). Although B layers with an age of 1988 were only described in cores FC17-06, FC17-07, and FC17-08, a slight drop in grain size is visible in FC17-02 at a depth of 91 cm (corresponding to 1990 ± 6 CE) (Fig. 3). The 1988 Las Lengas GLOF was described as a catastrophic event that lasted 3 to 6 hours (records f to l in Table S1). Although, it is not clearly captured in Baker River discharge data downstream of the confluence with Los Ñadis River (Fig. 6A), this may reflect its short duration compared to the temporal resolution of the older river discharge measurements (daily). No peak in discharge was observed at the beginning of March 1988, although this date was clearly mentioned by two interviewees (records i and k in Table S1). Two candidates exist on the 3rd of November 1988 (discharge doubled) and on the 24th of August 1992 (discharge quadrupled) but both events seem to coincide with several consecutive days of higher-than-average precipitation. The existence of a GLOF from Las Lengas Lake in 1988 is therefore very likely, but whether this event was large enough to have a real impact on downstream sedimentation or not remains uncertain.

Other more recent B-type layers are found in cores FC17-01, FC17-01A, and FC17-02, between 37 and 49 cm, where they correspond to 2002 ± 3 CE, 2001 ± 4 CE, and 2001 ± 4 CE, respectively (Figs. 2 and 3). These deposits are, however, very thin and they do not correspond to any known Baker River GLOF, nor can they be linked to any major peak in the Baker River discharge during that time period (Fig. 6). Finally, cores FC17-02, FC17-06, and FC17-07 also display type B sediments between 39 and 46 cm that have an age of 2004 ± 3 CE (Fig. 2). Although one conversational record refers to a Baker River flood in 2005 (record c in Table S1), discharge data reveal no clear GLOFs during this period. These sediments could however represent minor, e.g. seasonal, increases in meltwater input.

5.5.1.3. T facies

Turbidites predominantly occur in the three cores located on the prodelta in front of the main submarine channel (FC17-01, FC17-01A, and FC17-02) (Figs. 1 and 2). They confirm that the main submarine channel has been active during the last ~40 years and subjected to sediment transport by dense turbidity currents.

A clear distinction arises when looking at the depth or age distribution of the T1 facies compared to the T2 facies (Figs. 2 and 3). Three of the four T1 turbidites occur in the upper 30 cm of the cores, i.e. during the 2008–2017 time interval, which corresponds in timing to the 21st century Cachet 2 GLOFs (Fig. 2). In cores FC17-02 and FC17-05, some of these T1 deposits seem to immediately precede B-type sediments (Fig. 2), suggesting a link between T1 turbidites and GLOF occurrence. This association is supported by the relatively fine and organic-poor nature of the T1 facies, which is similar to the glacial

rock flour nature of the B deposits. The T1 facies might thus represent turbidity currents triggered by the rapid settling of large amounts of sediments of glacial origin from the fjord plume immediately after GLOFs, i.e. plume-triggered events (Hizzett et al., 2018). The age of the most recent T1 turbidite (2014 ± 1 CE), which is found in all of the prodelta cores (FC17-01, FC17-01A, and FC17-02) as well as in core FC17-05, does seem to match a period during which Baker River discharge and GLOF frequency were higher than average (2012–2014; Table 1). Similarly, the other T1 turbidites found in the upper 30 cm of FC17-02 are dated 2009 ± 2 CE and 2011 ± 1 CE, and most likely represent relatively high magnitude GLOFs that occurred during the first half of the 2008–2017 sequence. T1 turbidites could thus represent the signature of high-magnitude GLOFs in the prodelta area. However, not all T1 turbidites appear to represent GLOFs since one of them occurs at 67 cm in core FC17-02 (1996 ± 5 CE), at a time during which no GLOF has been reported (Fig. 3). Finally, it is important to note that, as the majority of the recent Cachet 2 GLOFs are not represented by T1 turbidites, the T1 facies cannot be used as a reliable signature of GLOFs in fjord sediments.

By comparison, none of the T2 turbidites seem to correspond in age to any of the historical Baker River GLOFs (Fig. 3). This suggests that these turbidites were triggered by events other than GLOFs, supporting the explanation of Vandekerkhove et al. (2020a) that the increased fjord stratification produced by the additional input of low-density meltwater (compared to the fjord's saltier water) during GLOFs prevents the formation of underflows. Although suspended sediment concentrations at the Baker River outflow during recent GLOFs were one order of magnitude higher compared to values during the meltwater season (Vandekerkhove et al., 2020a), it appears that the density contrast was not high enough to trigger turbidity currents. In contrast to sediments of glacial origin, T2 turbidites are characterized by coarse and organic-rich sediments (0.57 ± 0.10 %, Fig. 4), which most likely represent sediment eroded from riverbanks, particularly in the lower Baker watershed, by intense precipitation, rain-on-snow events, or possibly high seasonal meltwater discharge. The peak discharge and thus erosion capability of meteorologically-triggered floods tends to increase downstream, as the contributing catchment area increases. This was for example the case of the 1976 rain-on-snow event, which caused major damage along the Baker River, especially at its outflow near the town of Caleta Tortel where several boats and other infrastructure were destroyed (records m and n in Table S1). This is in contrast with GLOFs, whose hydrographs tend to attenuate downstream (Cenderelli and Wohl, 2001, 2003). Indeed, peak Baker River discharges measured approximately 40 km downstream the lake during the recent Cachet 2 GLOFs ranged between 1500 and 4000 $m^3 s^{-1}$ (Table 1), whereas calculated GLOF peak discharges at Cachet 2 Lake had a median of approximately 4300 $m^3 s^{-1}$ and a maximum that exceeded 10 000 $m^3 s^{-1}$ (Jacquet et al., 2017). The organic-rich nature of turbidites is also a typical characteristic of meteorologically-triggered flood deposits in lake settings (e.g. Simonneau et al., 2013; Vannière et al., 2013; Wilhelm et al., 2013; Howarth et al., 2014), which supports our interpretation that the T2 facies is not related to GLOFs. Finally, these turbidites might also represent delta collapses, possibly triggered by extreme discharge events such as intense rainfall or rain-on-snow, with regards to the similar sedimentological signature as the background sediment in cores located in the upper slope region, i.e. FC17-17 and FC17-10 (Fig. 2). Delta collapses can indeed entrain reworked material from the upper slope to the prodelta region by turbidity currents. A seismic trigger is however unlikely since the fjord is located just south of the Chile Triple Junction, where seismic activity is low (Hayes et al., 2015; USGS earthquake catalog).

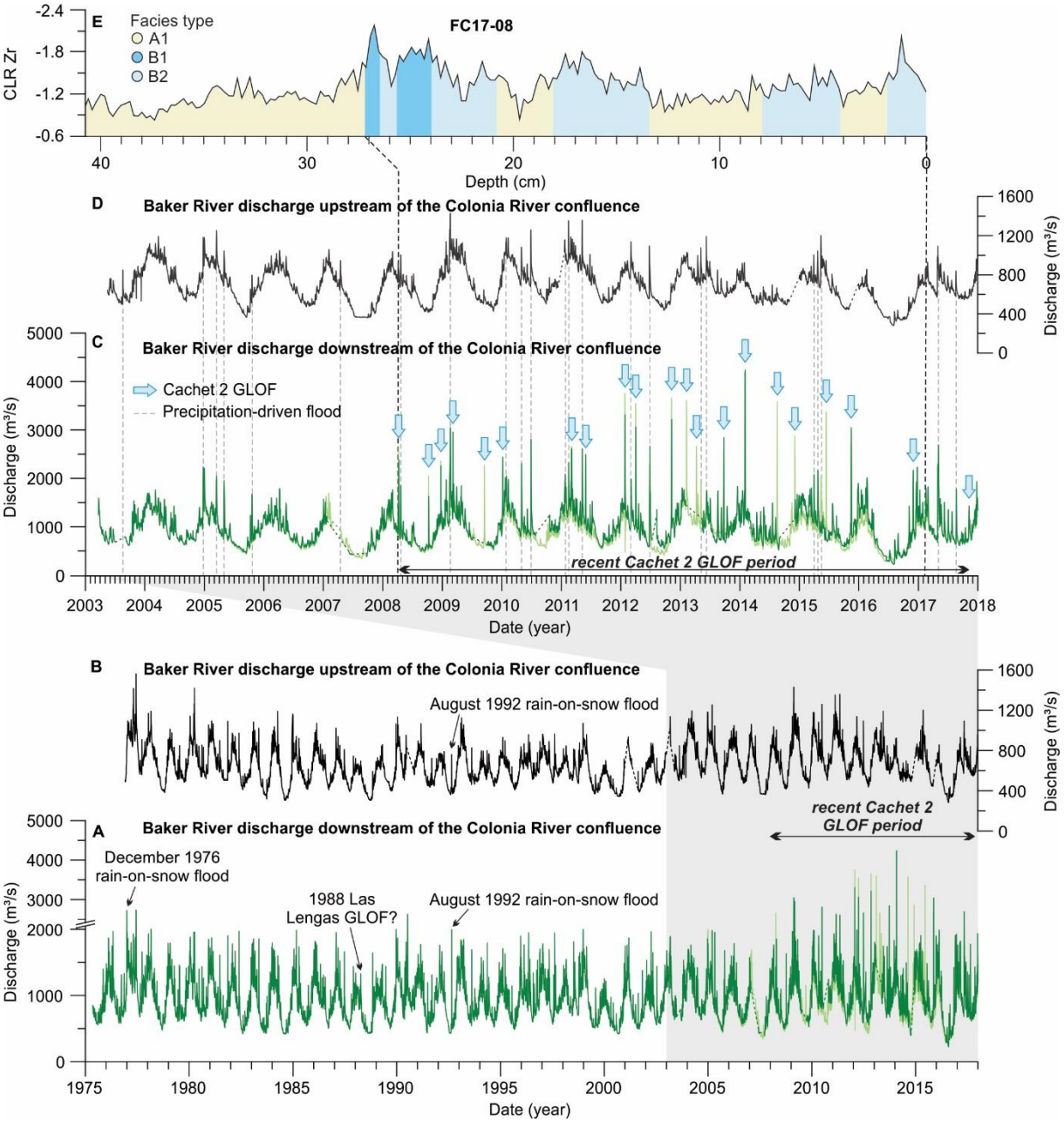

Figure 5.6. Baker River discharge downstream (A) and upstream (B) of the confluence with Colonia River, with 2003–2018 enlarged in graphs (C) and (D), and compared to the Centered Log Ratio (CLR)-transformed Zr counts of the upper 41 cm of sediment core FC17-08 (E). The DGA Baker River discharge station upstream of the Colonia River confluence, i.e. Rio Baker en angostura Chacabuco, is presented with a black line. The DGA Baker River discharge stations downstream of the Colonia River confluence, i.e. Rio Baker en Colonia and Rio Baker bajo Ñadis, are presented with light green and green lines, respectively. The locations of the discharge stations are shown in Fig. 1A. The Cachet 2 GLOFs are highlighted with blue arrows. The precipitation-driven floods, which are highlighted with grey dashed lines, were identified by comparison between discharge stations upstream and downstream of the Colonia River and were confirmed using precipitation data (Alvarez-Garretón et al., 2018). In (E) the different lithologies observed in core FC17-08 are also indicated.

Although most T2 turbidites are limited to cores from the prodelta area, one of them appears at a depth of around 70 cm in all cores, including those collected on the delta slope (Fig. 2). Based on the age-depth model, this T2 turbidite was deposited in 1995 ± 5 CE (Fig. 3). Considering that this turbidite extends beyond the limits of the main subaquatic channel, it likely represents a major event that was

able to trigger a large turbidity current overtopping the channel levees. The only flood event that was mentioned by interviewees near that time window, however, is the 1988 Las Lengas GLOF, which is not visible in the Baker River hydrographs. It is therefore unlikely to be at the origin of this widespread turbidite. A possible candidate is the extreme discharge event that occurred on the 24th of August 1992, during which Baker River discharge quadrupled in just two days to reach 1995 m^3 s^{-1} at the lowermost hydrological station (DGA, Chile) (Fig. 6A–B). Based on CR2MET precipitation data (Alvarez-Garreton et al., 2018), this event appears to be linked to two consecutive days of heavy rainfall. Since it occurred in winter, it most likely represents a rain-on-snow event. Consequently, this T2 turbidite could also represent a precipitation-driven flood, in agreement with its high TOC signature (Figs. 3 and 4), but contrary to the floods that triggered the many turbidites observed in the delta plain cores, this event must have been larger in magnitude to allow the overtopping of the channel levees.

5.5.2. Signature of the 1976 Cachet 2 and 1988 Las Lengas GLOFs

The sedimentary signature of the 2008–2017 Cachet 2 GLOFs in the sediments of Martínez Channel is relatively clear. They are represented by thin fine-grained and organic-poor layers in all cores, and the largest events might also be recorded as T1 turbidites in the sediment cores collected in the prodelta area. Between 1965 and the 21st century sequence of Cachet 2 GLOFs, however, another GLOF occurred in the Baker River watershed. It originated from the emptying of Las Lengas Lake in 1988 (Table 1). The signature of this event in the fjord's sediments is less clear.

The 1988 Las Lengas GLOF could correspond to the 1995 ± 5 CE T2 turbidite that occurs in all cores, or to the B2 layer that is visible at 79–89 cm in cores FC17-06, FC17-07, and FC17-08, which was dated 1991 ± 6 CE (Fig. 2). A third possibility is that this event was not recorded in the fjord's sediments. Several arguments favor its association with the B2 layer dated 1991 ± 6 CE. First, its modeled age is in perfect agreement with the age of the GLOF reported by several interviewees. Second, its lithology corresponds to the GLOF deposits that are clearly associated to the 21st century Cachet 2 GLOFs. And third, its TOC values in FC17-08 correspond to that of other deposits clearly associated to GLOFs (Figs. 3 and 4). The reason that this GLOF is only recorded in three of the ten sediment cores could represent its relatively low volume (4.36 x 10^6 m^3) and therefore low peak discharge in Baker River, especially compared to the large volume of the Cachet 2 GLOFs (101–251 x 10^6 m^3; Dussaillant et al., 2010; Table 1). Although the 1988 event is the only historical GLOF that is known to have originated from Las Lengas Lake and that initial GLOFs tend to have higher sediment loads (Jacquet et al., 2017), the overall meltwater and sediment contribution of this GLOF to the Baker River was likely too limited to leave a clear impact on the daily Baker River discharge values, and ultimately in the downstream fjord sediments.

The association of the widespread T2 turbidite dated 1995 ± 5 CE with the 1988 Las Lengas GLOF is less likely since it would imply a significant overestimation of the sedimentation rate in the lower half of the cores. The coarser sedimentary signature of this event compared to the Cachet 2 GLOFs, however, could reflect the absence of any intermediate lake, trapping sediments, between Las Lengas Lake and Martínez Channel. Coarse sediment availability is additionally supported by the moraine dam breach origin of this GLOF as outbursts from moraine-dammed lakes release highly destructive mixtures of water, rock, mud, glacial ice and other debris, often enhanced by bank erosion along the flood path (Benn and Evans, 2010). This is shown by the presence of a debris fan containing numerous large boulders at the outflow of Las Lengas Lake (Fig. 5C). Since the 1988 Las Lengas GLOF was a single event, it could have eroded large parts of the Los Ñadis riverbanks, explaining the relatively organic-rich signature of the turbidite. If the widespread T2 turbidite indeed represents the 1988 Las Lengas GLOF,

the difference in the sedimentary signature of Cachet 2 vs Las Lengas GLOFs could reflect the different nature of the GLOF (i.e. moraine-dammed versus ice-dammed), the absence of intermediate lake(s), and/or the lack of previous outbursts.

Based on the criteria at our disposal, and on the likely association of the widespread T2 turbidite with an intense rainfall event that occurred in August 1992, we suggest that the sedimentary signature of the 1988 Las Lengas GLOF is similar to that of the Cachet 2 GLOFs, i.e. that this event corresponds to the B2 layers at 79–89 cm in cores FC17-06, FC17-07, and FC17-08. Although we cannot fully discard the possibility that the 1988 Las Lengas GLOF triggered the widespread T2 turbidite or simply did not leave any imprint in the fjord's sediments, this is relatively unlikely.

5.5.3. GLOF signature in fjord sediments

GLOFs from the ice-dammed Cachet 2 Lake, and in particular the event(s) that initiated the 2008–2017 sequence, can be identified in the downstream fjord sediments as fine-grained and organic-poor, i.e. type B, deposits (Figs. 3 and 4). These deposits represent sediment of glacial origin, settling from the buoyant plume, and ultimately draping the fjord bottom relatively independently of the bathymetry. Some of the largest GLOFs might also be recorded as T1 turbidites underlying the B layers at the prodelta sites, likely representing events that were able to generate a plume-triggered turbidity current. Most GLOFs, however, were apparently not able to trigger a turbidity current, even though suspended sediment concentrations at the Baker River outflow increased by one order of magnitude during the recent GLOFs compared to the meltwater season (Vandekerkhove et al., 2020a). These events were likely unable to disrupt the stratification of the water column, probably due to the low density of the sediment-laden upper freshwater water mass compared to the deeper salty waters. T1 turbidites can therefore not be used to identify GLOF deposits.

Although the B facies clearly represents GLOFs, their fine-grained signature is somewhat counterintuitive. In sediments, extreme discharge events such as floods are generally recorded as coarse-grained deposits, due to the extreme hydraulic conditions. Indeed, the typical signature of floods in sediments is an organic-rich turbidite with a relatively coarse sandy base (e.g. Simonneau et al., 2013; Vannière et al., 2013; Sabatier et al., 2017). Similarly, GLOF deposits in Rundvatnet Lake in Norway were also described as distinct sand layers with normal grading embedded in a silt-clay matrix (Xu et al., 2015). The Cachet 2 GLOF deposits, however, are systematically finer than the background fjord sediments, reflecting the glacial nature of the source material. This fine grain size may also reflect the filtering of coarse particles by Colonia Lake, which is immediately downstream of Cachet 2 Lake (Fig. 5A), as suggested for other glaciated basins (e.g. Boes et al., 2018; Røthe et al., 2019; Piret et al., 2021). In such settings, GLOF deposits were also represented as deposits that are finer than the background sediments (Røthe et al., 2019).

Aside from their fine grain size, the Cachet 2 GLOF deposits are also marked by a significant drop in TOC values, which is particularly clear in the B1 facies at the beginning of the 2008–2017 sequence (Fig. 3). The latter most likely also reflects the glacial nature of the source sediment, which is typically characterized by TOC values around 0.2 % (e.g. Rebolledo et al., 2019). This is in contrast with the slightly higher TOC values of the background deposits, which reflect the higher vegetation density of the lower Baker watershed. This observation is similar to the GLOF deposits identified in Rundvatnet Lake (Norway), which also contained less organic material than the background sediments (Xu et al., 2015).

Although GLOFs resulted in the deposition of B-type sediments, we were not able to discern individual GLOF events in the sediment cores. During the 2008–2017 sequence, for instance, a total of 21 GLOFs occurred from Cachet 2 Lake. These individual events cannot be identified in the sediment records, which only show four periods rich in GLOFs during the same time interval (Fig. 6E). This likely represents the short time lapse between individual GLOF events (as short as two months), which did not allow enough background sediment to accumulate in between the B layers. This means that, for such GLOFs occurring at high frequency, it is not possible to use the B layers to determine flood frequency. Comparing the characteristics of the B layers with peak river discharge during the Cachet 2 GLOFs does not reveal any sediment property that could be used to estimate flood magnitude either (Table 1, Fig. 6). For example, although the highest magnitude Cachet 2 GLOFs occurred in 2012–2014, with peak discharge exceeding 3500 $m^3 s^{-1}$, the B layers corresponding to that time window are not particularly fine-grained or poor in TOC (Figs. 3 and 6). The finest and most organic-poor B layers (B1 facies) represent the Cachet 2 GLOFs that occurred at the beginning of the 2008–2017 sequence, suggesting that sediment availability plays a more important role than flood magnitude in controlling the characteristics of the B deposits. This implies that flood magnitude cannot be reconstructed.

Finally, it should be noted that not all type B deposits represent GLOFs. Intense meltwater events, such as the one induced by rain-on-snow in 1976, might also increase the input of sediment of glacial origin to the fjord, resulting in the deposition of type B sediments. Their sedimentological characteristics, however, suggest that these deposits are not entirely composed of glacial rock flour. Their signature is less pronounced than most other B layers, especially compared to the B1 facies associated with the initial GLOFs from Cachet 2 Lake.

5.5.4. Implications for site selection

Our results suggest that the deposits that best reflect GLOFs in fjord sediments are the B layers, which are deposited by settling from the buoyant plume. Although these deposits are relatively ubiquitous in the subaquatic delta and prodelta areas, we argue that the most suited sites to reconstruct the GLOF history of Baker River are located on the delta slope, away from the channels, and relatively close to the river mouth. One of the main advantages of these sites (e.g. FC17-07 to 09; Fig. 2) is that they are characterized by relatively high accumulation rates, which improves the odds of discerning individual GLOF layers. These sites are also where the contrast between the B layers and the background sediments is the largest since the TOC and grain size of the background sediments decrease with distance from the delta lip (Vandekerkhove et al., 2020a). Further away from the delta lip (e.g. sites FC17-06 and FC17-05), the composition of the B deposits and background sediment becomes relatively similar, rendering the identification of the B layers more difficult. Locations too close to the river mouth should however be avoided since they may be prone to erosion due to channel migration, and the increasingly higher accumulation rates mean that longer sediment cores will need to be acquired. Locations in the prodelta area in front of the submarine channels (e.g. FC17-01, FC17-01A, and FC17-02; Fig. 2) should also be avoided as these are subjected to turbidites, most of which are not related to GLOFs but result from other extreme events. In addition, sampling strategies should consider multi-coring since our results suggest that lower magnitude GLOFs, such as the 1988 Las Lengas GLOF, may only be recorded at specific locations. A multi-coring approach should thus be adopted to reconstruct a relatively complete GLOF history. To reconstruct GLOFs on longer time scales, acquiring seismic data prior to coring is crucial to detect paleo-channels and therefore to facilitate the selection of sites relatively unaffected by erosion.

Our results also have implications for GLOF reconstructions in fjords located in different climate and environmental settings. As a rule of thumb, one should focus on fjords where the background sediment is relatively organic, i.e. fjords that are not directly and/or solely fed by the proglacial river of interest. In truly proglacial fjords, identifying GLOF deposits will be particularly challenging due to similarities between the composition of the GLOF deposits and that of the background sediments. As such, the Baker River system is particularly unique and well-suited since a significant part of the Baker River watershed is vegetated, resulting in the deposition of background sediments that are not entirely glacial in nature. Therefore, the sediments of temperate fjords constitute more promising GLOF archives than those deposited in polar fjords.

In addition, the contrast between GLOF deposits and background sediments might have varied in the past due to changes in glacier cover, presence of proglacial lakes, vegetation density, precipitation, and temperature. For example, the GLOF signal is expected to be less distinct when background sediments are finer and less organic, due to, e.g., increased glacier cover and lower vegetation density. On the contrary, decreased meltwater input, higher rainfall, and higher vegetation density result in coarser background sediments and therefore enhance the contrast between GLOF deposits and background sediments. The ability to identify GLOF deposits in fjord sediments is thus always relative to the composition of the background sediments.

5.6. Conclusions

The 21st century Baker River GLOFs that originated from Cachet 2 Lake are recorded in the downstream fjord sediments as fine-grained and organic-poor deposits intercalated in slightly coarser and organic background sediments. A similar deposit was tentatively attributed to a 1988 GLOF from Las Lengas Lake. The composition of these deposits represents the input of large amounts of material of glacial origin during GLOFs, which likely originates from lake-bed erosion.

GLOF deposits are relatively easy to identify using lithological descriptions and Zr counts measured by XRF core scanning, which is a proxy for grain size. TOC measurements or any high-resolution proxy for organic matter content can help to confirm their glacial origin. Although some fine-grained and organic-poor turbidites may also be related to GLOFs, these deposits cannot be used to reconstruct GLOF occurrence since (a) they only represent a fraction of the GLOFs that occurred in the Baker River watershed, and (b) some of these turbidites are not related to any known GLOF event. Therefore, the most promising deposits to reconstruct the Baker GLOF history are fine-grained and organic-poor sediments deposited at the fjord head. However, not all sites have the same paleohydrological potential. The ideal coring sites are located on the delta slope, relatively far away from the submarine channels, but close enough to the river mouth to enhance the contrast between GLOF deposits and background sediments. Sites located in the prodelta area immediately in front of the channels should be avoided as they contain frequent turbidites that are unrelated to GLOFs.

Although our results clearly show that GLOFs are recorded as fine-grained and organic-poor deposits, they also suggest that these deposits may not always be appropriate to reconstruct changes in GLOF frequency. Repeated GLOFs, i.e. events occurring less than one year apart, are not recorded as individual events but rather as clusters of events. The latter likely results from the insufficient background sedimentation between the GLOF deposits. Likewise, our results suggest that some particularly intense rain-on-snow events may also be recorded as fine-grained and organic-poor deposits, especially if they affect glacier-covered areas. This means that fine-grained and organic-poor deposits do not

systematically represent GLOFs. Finally, our results show that GLOF magnitude is not represented by any of the sediment properties. Rather, the deposits with the lowest grain size and TOC values represent GLOFs that occurred at the beginning of the 2008–2017 sequence, suggesting that sediment availability plays a more important role than flood magnitude in controlling the characteristics of the GLOF deposits.

The sediment cores investigated in this study allowed us to identify the signature of the Baker River GLOFs that occurred during the last 40 years. Acquiring longer sediment cores would allow us to examine the signature of the higher-magnitude GLOFs that occurred between the 1880s and 1960s (De Agostini, 1945; Table S1), and they could eventually provide a record of pre-historical Baker River GLOFs. Although a late Holocene GLOF reconstruction of Baker River GLOFs was recently achieved from floodplain sediments (Vandekerkhove et al., 2020b), fjord sediments would certainly provide a higher temporal resolution. However, identifying GLOF deposits from background sediments may be more challenging during colder periods, e.g., neoglaciations, during which vegetation density, and therefore organic matter content in background sediments, was likely reduced.

Finally, the findings from this study should also be applicable to other fjord systems under the influence of GLOFs, particularly those located in temperate regions. Based on our results, we suggest that the most reliable GLOF archives are those from fjords that are not directly and/or solely fed by the proglacial river of interest.

Acknowledgements

We thank the captain (Rodrigo Mansilla) and the crew of the R/V Sur-Austral (COPAS Sur-Austral, Tortel, Chile), and Eleonora Crescenzi Lanna, Helena Pryer, and Loic Piret for their help with sample collection. Thomas Vandorpe and Loic Piret are thanked for CT scanning the cores. We are grateful to Alejandro Dussaillant for sharing the Baker River discharge data that were not readily available from the DGA. We are also thankful to Silvio Pantoja and Romina San Martín at the University of Concepción (Chile), and to the staff of Centro de Investigación en Ecosistemas de la Patagonia (CIEP, Chile). We acknowledge the Chilean Navy Hydrographic and Oceanographic Service (SHOA; permit number 13270/24/235/Vrs) for authorizing this sampling expedition. Anita Abarzua (Universidad Austral, Valdivia, Chile) is thanked for providing the gravity corer. Benjamin Amann, Loic Piret, Dawei Liu, Matthias Troch, and Gerardo Benito provided valuable comments on an earlier version of this manuscript. Finally, we thank Pierre Sabatier and one anonymous reviewer for their constructive comments. This research was funded by the Flemish Research Foundation (FWO, Belgium) Paleo-GLOFs project G0D7916N.

References

Alvarez-Garreton, C., Mendoza, P.A., Boisier, J.P., Addor, N., Galleguillos, M., Zambrano-Bigiarini, M., Lara, A., Puelma, C., Cortes, G., Garreaud, R., McPhee, J., and Ayala, A. (2018) The CAMELS-CL dataset: catchment attributes and meteorology for large sample studies – Chile dataset. *Hydrology and Earth System Sciences*, **22**, 5817 – 5846.

Bastianon, E., Bertoldi, W., and Dussaillant, A. (2012) Glacial-lake outburst flood effects on Colonia River morphology, Chilean Patagonia. River Flow 2012, CRC Press, 573 – 579.

Benn, D.I., and Evans, D.J.A. (2010) Glacial lakes and outburst floods. *In: Glaciers and glaciation*. vol. 2 Hodder education, London, 428 pp.

Benito, G., Thorndycraft, V.R., Medialdea, A., Machado, M.J., Sancho, C., and Dussaillant, A. (2021) Declining discharge of glacial lake outburst floods through the Holocene in central Patagonia. *Quaternary Science Reviews*, **265**, 106810.

Bertrand, S., Hughen, K.A., Sepúlveda, J., and Pantoja, S. (2012) Geochemistry of surface sediments from the fjords of Northern Chilean Patagonia (44–47°S): Spatial variability and implications for paleoclimate reconstructions. *Geochimica et Cosmochimica Acta*, **76**, 125 – 146.

Bianchi, T.S., Arndt, S., Austin, W.E.N., Benn, D.I., Bertrand, S., Cui, X., Faust, J.C., Koziorowska-Makuch, K., Moy, C.M., Savage, C., Smeaton, C., Smith, RW., and Syvitski, J. (2020) Fjords as Aquatic Critical Zones (ACZs). *Earth-Science Reviews*, **203**, 103145.

Boes, E., Van Daele, M., Moernaut, J., Schmidt, S., Jensen, B.J.L., Praet, N., Kaufman, D., Haeussler, P., Loso, M.G., and De Batist, M. (2018) Varve formation during the past three centuries in three large proglacial lakes in south-central Alaska. *Geological Society of America Bulletin*, **130**, 757 – 774.

Burton, J.W., Chambers, F.B., Sincavage, R., and Cross, M.D. (2021) Analysis of glacial lake outburst flood terrain and sedimentary deposits in valle soler, Northern Patagonia Icefield. *Physical Geography*

Carrivick, J.L., and Tweed, F.S. (2016) A global assessment of the societal impacts of glacier outburst floods. *Global and Planetary Change*, **144**, 1 – 16.

Cenderelli, D.A., and Wohl, E.E. (2001) Peak discharge estimates of glacial lake outburst floods and 'normal' climatic floods in the Mount Everest region, Nepal. *Geomorphology*, **40**, 57 – 90.

Cenderelli, D.A., and Wohl, E.E. (2003) Flow hydraulics and geomorphic effects of glacial lake outburst floods in the Mount Everest region, Nepal. *Earth Surface Processes and Landforms*, **28**, 385 – 407.

Clague, J.J., and Evans, S.G. (2000) A review of catastrophic drainage of moraine-dammed lakes in British Columbia. *Quaternary Science Reviews*, **19**, 1763 – 1783.

Costa, J.E., and Schuster, R.L. (1988) The formation and failure of natural dams. *Geological Society of America Bulletin*, **100**, 1054 – 1068.

Cowan, E.A., Carlson, P.R., and Powell, R.D. (1996) The marine record of the Russell Fiord outburst flood, Alaska, U.S.A. *Annals of Glaciology*, **22**, 194 – 199.

Davies, B.J., and Glasser, N.F. (2012) Accelerating shrinkage of Patagonian glaciers from the Little Ice Age (~AD 1870) to 2011. *Journal of Glaciology*, **58** (212), 1063 – 1084.

Davies, S.J., Lamb, H.F., and Roberts, S.J. (2015) Micro-XRF core scanning in palaeolimnology: recent developments. *In: Croudace, I.W., and Rothwell, R.G. (Eds.), Mirco-XRF Studies of Sediment Cores: Applications of a non-destructive tool for the environmental sciences.* Springer, Dordrecht, the Netherlands, pp. 189 – 226.

De Agostini, A.S.S. (1945) Andes Patagonicos, Viajes de exploración a la Cordillera Patagonica Austral. Segunda edición aumentada y corregida. Buenos Aires. 436 pp.

Dussaillant, A., Benito, G., Buytaert, W., Carling, P., Meier, C., and Espinoza, F. (2010) Repeated glacial-lake outburst floods in Patagonia: an increasing hazard? *Natural hazards*, **54**, 469 – 481.

Dussaillant, A., Buytaert, W., Meier, C., and Espinoza, F. (2012) Hydrological regime of remote catchments with extreme gradients under accelerated change: the Baker basin in Patagonia. *Hydrological Sciences Journal*, **57**, 1530 – 1542.

Garreaud, R., Lopez, P., Minvielle, M., and Rojas, M. (2013) Large-scale control on the Patagonian climate. *Journal of Climate*, **26**, 215 – 230.

Harrison, J., Heijnis, H., and Caprarelli, G. (2003) Historical pollution variability from abandoned mine sites, Greater Blue Mountains World Heritage Area, New South Wales, Australia. *Environmental Geology*, **43**, 680 – 687.

Harrison, S., Glasser, N., Winchester, V., Haresign, E., Warren, C., and Jansson, K. (2006) A glacial lake outburst flood associated with recent mountain glacier retreat, Patagonian Andes. *The Holocene*, **16**, 611 – 620.

Harrison, S., Kargel, J.S., Huggel, C., Reynolds, J., Shugar, D.H., Betts, R.A., Emmer, A., Glasser, N., Haritashya, U.K., Klimeš, J., Reinhardt, L., Schaub, Y., Wiltshire, A., Regmi, D., and Vilímek, V. (2018) Climate change and the global pattern of moraine-dammed glacial lake outburst floods. *The Cryosphere*, **12**, 1195 – 1209.

Hizzett, J.L., Hughes Clarke, J.E., Sumner, E.J., Cartigny, M.J.B., Talling, P.J., and Clare, M.A. (2018) Which triggers produce the most erosive, frequent, and longest runout turbidity currents on deltas? *Geophysical Research Letters*, **45**(2), 855 – 863.

Howarth, J.D., Fitzsimons, S.J., Norris, R.J. and Jacobsen, G.E. (2014) Lake sediments record high intensity shaking that provides insight into the location and rupture length of large earthquakes on the Alpine Fault, New Zealand. *Earth and Planetary Science Letters*, **403**, 340 – 351.

Iriarte, J.L., Pantoja, S., and Daneri, D. (2014) Oceanographic processes in Chilean fjords of Patagonia: From small to large-scale studies. *Progress in Oceanography*, **129**, 1 – 7.

Iribarren Anacona, P., Norton, K.P., and Mackintosh, A. (2014) Moraine-dammed lake failures in Patagonia and assessment of outburst susceptibility in the Baker Basin. *Natural Hazards and Earth System Sciences*, **14**, 3243 – 3259.

Iribarren Anacona, P., Mackintosh, A., and Norton, K (2015) Reconstruction of a glacial lake outburst flood (GLOF) in the Engaño Valley, Chilean Patagonia: Lessons for GLOF risk management. *Science of the Total Environment*, **527-528**, 1 –11.

Jacquet, J., McCoy, S.W., McGrath, D., Nimick, D.A., Fahey, M., O'kuinghttons, J., Friesen, B.A., and Leidlich, J. (2017) Hydrologic and geomorphic changes resulting from episodic glacial lake outburst floods: Rio Colonia, Patagonia, Chile. *Geophysical Research Letters*, **44**, 854 – 864.

Liu, D., Bertrand, S., and Weltje, G.J. (2019) An empirical method to predict sediment grain size from inorganic geochemical measurements. *Geochemistry, Geophysics, Geosystems*, **20**, 3690 – 3704.

Lopez, P., Chevallier, P., Favier, V., Pouyaud, B., Ordenes, F., and Oerlemans, J. (2010) A regional view of fluctuations in glacier length in southern South America. *Global and Planetary Change*, **71**, 85 – 108.

Luebert, F., and Pliscoff, P. (2006) Sinopsis bioclimática y vegetacional de Chile. *Editorial Universitaria*, Santiago.

Marín, V.H., Tironi, A., Paredes, M.A., and Contreras, M. (2013) Modeling suspended solids in a Northern Chilean Patagonia glacier-fed fjord: GLOF scenarios under climate change conditions. *Ecological Modelling*, **264**, 7 – 16.

McMinn, A., Hallegraeff, G.M., Thomson, P., Jenkinson, A.V., and Heijnis, H. (1997) Cyst and radionucleotide evidence for the recent introduction of the toxic dinoflagellate Gymnodinium catenatum into Tasmanian waters. *Marine Ecology Progress Series*, **161**, 165 – 172.

Meerhoff, E., Castro, L.R., Tapia, F., and Pérez-Santos, I. (2019) Hydrographic and biological impacts of a Glacial Lake Outburst Flood (GLOF) in a Patagonian Fjord. *Estuaries and Coasts*, **42**, 132 – 143.

Piret, L., Bertrand, S., Hawkings, J., Kylander, M., Torrejón, F., Amann, B., and Wadham, J. (2021) High-resolution fjord sediment record of a retreating glacier with growing intermediate proglacial lake (Steffen Fjord, Chile). *Earth Surface Processes and Landforms*, **46**, 239 – 251.

Quiroga, E., Ortiz, P., Gerdes, D., Reid, B., Villagran, S., and Quiñones, R. (2012) Organic enrichment and structure of macrobenthic communities in the glacial Baker Fjord, Northern Patagonia, Chile. *Journal of the Marine Biologial Association of the United Kingdom*, **92**(1), 73 – 83.

Rebolledo, L., Bertrand, S., Lange, C.B., Tapia, F.J., Quiroga, E., Troch, M., Silva, N., Cárdenas, P., and Pantoja, S. (2019) Compositional and biogeochemical variations of sediments across the terrestrial-marine continuum of the Baker-Martínez fjord system (Chile, 48 °S). *Progress in Oceanography*, **174**, 89 – 104.

Røthe, T.O., Bakke, J., and Støren, E.W.N. (2019) Glacier outburst floods reconstructed from lake sediments and their implications for Holocene variations of the plateau glacier Folgefonna in western Norway. *Boreas*, **48**, 616 – 634.

Sabatier, P., Wilhelm, B., Ficetola, G.F., Moiroux, F., Poulenard, J., Develle, A.L., Bichet, A., Chen, W., Pignol, C., Reyss, J.L., Gielly, L., Bajard, M., Perrette, Y., Malet, E., Taberlet, P., and Arnaud, F. (2017) 6-kyr record of flood frequency and intensity in the western Mediterranean Alps – Interplay of solar and temperature forcing. *Quaternary Science Reviews*, **170**, 121 – 135.

Simonneau, A., Chapron, E., Vannière, B., Wirth, S.B., Gilli, A., Di Giovanni, C., Anselmetti, F.S., Desmet, M. and Magny, M. (2013) Mass-movement and flood-induced deposits in Lake Ledro, southern Alps, Italy: implications for Holocene palaeohydrology and natural hazards. *Climate of the Past*, **9**, 825 – 840.

Syvitski, J.P.M. (1989) On the deposition of sediment within glacier-influenced fjords: Oceanographic controls. *Marine Geology*, **85**, 301 – 329.

Syvitski, J.P.M., and Shaw, J. (1995) Sedimentology and geomorphology of fjords. *In: Perillo, G.M.E. (Ed.)* Geomorphology and Sedimentology of Estuaries. Amsterdam, Elsevier, pp. 113 – 178.

Tanaka, K. (1980) Geographic contribution to a periglacial study of the Hielo Patagonico Norte with special reference to the glacial outburst originated from Glacier-Dammed Lago Arco, Chilean Patagonia. Centre Co Ltd, Tokyo, 97 pp.

Vandekerkhove, E., Bertrand, S., Crescenzi Lanna, E., Reid, B., and Pantoja, S. (2020a) Modern sedimentary processes at the heads of Martínez Channel and Steffen Fjord, Chilean Patagonia. *Marine Geology*, **419**, 106076.

Vandekerkhove, E., Bertrand, S., Mauquoy, D., McWethy, D., Reid, B., Stammen, S., Saunders, K.M., and Torrejón, F. (2020b) Neoglacial increase in high-magnitude Glacial Lake Outburst Flood Frequency, upper Baker River, Chilean Patagonia (47°S). *Quaternary Science Reviews*, **248**, 106572.

Vannière, B., Magny, M., Joannin, S., Simonneau, A., Wirth, S.B., Hamann, Y., Chapron, E., Gilli, A., Desmet, M., and Anselmetti, F.S. (2013) Orbital changes, variation in solar activity and increased anthropogenic activities: controls on the Holocene flood frequency in the Lake Ledro area, northern Italy. *Climate of the Past*, **9**, 1193 – 1209.

Verardo, D.J., Froelich, P.N. and McIntyre, A. (1990) Determination of organic carbon and nitrogen in marine sediments using the Carlo Erba NA-1500 Analyzer. *Deep-sea Research*, **37** (1), 157 – 165.

Weltje, G., Bloemsma, M., Tjallingii, R., Heslop, D., Röhl, U., and Croudace, I. (2015) Prediction of Geochemical Composition from XRF Core Scanner Data: A new multivariate approach including automatic selection of calibration samples and quantification of uncertainties. *In: Croudace, I., Rothewell, R. (Eds.)* Micro-XRF Studies of Sediment Cores. Developments in Paleoenvironmental Research, vol. 17. Springer, Dordrecht.

Wilhelm, B., Arnaud, F., Sabatier, P., Magand, O., Chapron, E., Courp, T., Tachikawa, K., Fanget, B., Malet, E., Pignol, C., Bard, E., and Delannoy, J.J. (2013) Paleoflood activity and climatic changes over the last 1400 years from lake sediments of the NW European Alps. *Journal of Quaternary Science*, **28** (2), 189 – 199.

Willems, B.A., Powell, R.D., Cowan, E.A., and Jaeger, J.M. (2011) Glacial outburst flood sediments within Disenchantment Bay, Alaska: Implications of recognizing marine jökulhaup deposits in the stratigraphic record. *Marine Geology*, **284**, 1 – 12.

Wilson, R., Glasser, N.F., Reynolds, J.M., Harrison, S., Anacona, P.I., Schaefer, M., and Shannon, S. (2018) Glacial lakes of the Central and Patagonian Andes. *Global and Planetary Change*, **162**, 275 – 291.

Wilson, R., Harrison, S., Reynolds, J., Hubbard, A., Glasser, N.F., Wündrich, O., Iribarren Anacona, P., Mao, L., and Shannon, S. (2019) The 2015 Chileno Valley glacial lake outburst flood, Patagonia. *Geomorphology*, **332**, 51 – 65.

Winchester, V., and Harrison, S. (2000) Dendrochronology and lichenometry: colonization, growth rate and dating of geomorphological events on the east side of the North Patagonian Icefield, Chile. *Geomorphology*, **34**, 181 – 194.

Xu, M., Bogen, J., Wang, Z., Bønsnes, T.E., and **Gytri, S.** (2015) Pro-glacial lake sedimentation from jökulhaups (GLOF), Blåmannsisen, northern Norway. *Earth Surface Processes and Landforms*, **40**, 654 – 665.

Supplementary Information

Table S5A. Conversational records based on field interviews conducted by Fernando Torrejón from the 25th until the 31st of January 2019, and written archives regarding Baker River GLOFs (in Spanish).

Conversational records	
Colonia River floods	
Interviewee	Record
(a) Luzmira Muñoz	*Doña Luzmira nació en 1951 en el sector los Ñadis a orillas del río Baker, cuando ella tenía 9 meses de edad habría ocurrido una "gran crecida del Colonia" (1951 ó 1952), de acuerdo a lo que le habría contado su mamá. Agrega, "en esa crecida se ahogó el papá de Segundo Quinto…, salió a buscar sus ovejas y entonces lo alcanzó la crecida".* *De acuerdo a su relato, cuando ella tenía 6 años (posiblemente en 1957) "se produjo una tremenda creciente del río Colonia que mató muchos animales" y a algunos colonos de la zona. Indica, "siempre había trueno cuando iba a venir la creciente… Venía una avalancha grande y después todo se recogía". Después cuando el Baker retomaba su normalidad "los árboles quedaban todos blanquitos de arenilla", refiriéndose al sedimento que cubría sus ramas y hojas.* *Finalmente relata que "todos los años habían crecidas en el Baker" y después de las crecidas, cuando salían a recolectar calafates (Berberis sp) todas las "matas de calafates estaban de color gris por la tierra", en grandes zonas ribereñas, refiriéndose muy probablemente al fino sedimento glaciar que las cubría después de cada avenida del río. Otro dato interesante entregado por Luzmira es que el sector de la "tapera de Jaque", ubicado a unos 200 ó 300 metros aguas abajo de la confluencia del Colonia en el Baker, "se inundaba completamente".*
(b) Leoncio Escobar Montecino	*A la edad de 30 años (1962), don Leoncio ya trabajaba en Valle Grande "como peón de Enrique Villalobos Ramírez, quien tenía un gran campo allí". Fue en esa época cuando presenció una "inmensa creciente" del río Colonia y Baker "entre el 1 de diciembre y el 5 de enero cuando era la creciente".* *Describe que cuando se producía la inundación "el Baker empezaba a enaltar y se sostenía, subía 10 metros, después 15 metros…, no se notaba la crecida". "En 24 horas se inundaba todo, se tapaba todo el Valle Grande…, el Baker era un sólo lago, hasta la orilla de la pasarela del Salto". (Se trataba de la antigua pasarela que estaba como a 100 metros de la actual pasarela según el mismo comentó). Agrega don Leoncio: "la creciente tenía 1000 metros de anchura cuando reventaba…, salía por arriba y debajo de los nevados…, duró como un mes todo" En este caso se refiere a la avenida del río Colonia.* *Como se sabía que el Baker tenía grandes crecidas, durante el período en que estas podían ocurrir, don Leoncio debía recorrer el campo "día y noche para vigilar los animales y sacarlos antes que se produjera la creciente…, entonces había como 1000*

	yeguas en el Valle Grande". Según relata el mismo, en 1962, "el patrón y su hermano estaban en el campo y me dijo que le avisará cuando se viniera la creciente". *Siguiendo las instrucciones recibidas, cuando empezó la inundación, don Leoncio le dio aviso a su patrón y les ensilló dos caballos para ir a "verla desde unos motecitos". "A las 5 (AM) ya se estaba produciendo la creciente, venía un oleaje suave…, una ola tras otra, hasta que venía una grande y arrasaba con todo".* *Don Leoncio también presenció otras inundaciones del Baker antes y después de 1962, pero éstas, según recuerda, fueron de menor magnitud a la del 62, alcanzando "sólo hasta la mitad del Valle Grande".*
(c) Cristián Arratia Vidal	*Don Cristián recuerda crecidas del Baker desde 1955 a la década de 1960, que "tapaban todo el Valle Grande hasta cerca del Valle Castillo, quedaban sólo pedacitos de cercos donde se podían ver los alambres…, lo que agarraba lo mataba todo…, los animales quedaban arriba de los ñirres".* *Menciona que "una gran creciente en los años 1962 ó 1963 inundó todo el sector del lago Vargas", su señora Rosa Vargas, presente en la entrevista, contradice las fechas indicando, con mucha seguridad, que dicha creciente "fue en 1966…".* *En aquel entonces don Cristián se encontraba en su campo del río Ventisquero señalando que: "el agua se metió adentro de la casa, estaba con mi mamá en el fogón [cocina]…, deben haber sido las 9 de la noche, pues aún no me acostaba, cuando fue el golpe de agua grande…, una caja con una gallina con pollos flotaba en el fogón…, abrí la puerta y se me entró toda el agua.... Con el agua más arriba de la cintura salí a buscar mis animales que estaban en el bajo…, los saqué. Desde el corte San Carlos hacia abajo la creciente tapó todo".* *Aquella crecida (1966) "tapó todos los campos bajos en el sector de lago Vargas, alcanzando cerca de mi casa" (que corresponde a su actual vivienda muy cercana a la Ruta 7). "Los animales muertos iban quedando melgados por las orillas del Baker…, río abajo del corte, el río arrastraba tremendas palizadas y barro". Después de esta gran crecida del Baker don Cristián cambio su población en el campo de río Ventisquero "como 300 metros más arriba, porque en lo plano se tapa todo con el agua".* *Don Cristian también menciona una gran creciente del río Baker en el año 2005, atribuida al vaciamiento repentino del lago Cachet, narrando que en el sector de la confluencia del los ríos Vargas y Baker "donde está el muelle, el río iba tapadito de palos…, espeso de palos…, el agua llena de barro, no se podía andar ni en bote…, después han venido crecientes pero más chicas". Añade finalmente: "antes de las grandes crecidas el Baker corría más encajonado".*
(d) Arnoldo Agustín Cárdenas	*Don Arnoldo sólo menciona que entre los años 1961-1962 se produjo una "gran creciente del Colonia…, esa inundación se extendía río arriba por el Baker hasta el sector de Valle Grande…, cuando bajaba la creciente, las vacas quedaban enredadas*

	arriba de las lengas y ñires a cinco o seis metros". Añade, "en el sector de Tortel no causó mucho daño".
Nef River floods	
Interviewee	Record
(e) Leoncio Escobar Montecino	*Refiriéndose a las crecidas del río Baker, don Leoncio entrega un importante dato, señalando que las crecidas que inundan el Valle Castillo, a continuación de Valle Grande aguas arriba, vienen directamente desde el Baker, posiblemente por avenidas del río Nef.*
Los Ñadis River floods	
Interviewee	Record
(f) Luzmira Muñoz	*Doña Luzmira llama a la gran crecida del río Los Ñadis "el reventón del Ñadis…" y aunque no recuerda bien la fecha exacta dice que ocurrió en el verano, entre los años 1988-1990. Añade que aquella "crecida duró como 3 horas... Se perdieron yeguarizos y otros animales que quedaban enganchados arriba de los ñirres" (se refiere a la especie arbórea Nothofagus antárctica). "Quedó una gran palizada y mucho barro en las riberas del río cuando bajó la creciente". Recuerda además que la crecida dañó las dos pasarelas del río Ñadis "una la dobló y otra la cortó".* *Don Arturo Arriagada, esposo de Luzmira, presente en la entrevista, agrega que su antigua casa, hoy desaparecida, que se ubicaba al costado de la actual Ruta 7, en un lugar aún reconocible, "quedó rodeada de agua y palos…, yo iba poniendo cañas para ver como subía el nivel de la creciente". La hermana de don Arturo, que también vivía en las cercanías "amaneció en una balsa con el agua hasta las rodillas". Señala finalmente que "el Ñadis crecía todos los años…, pero nunca se había visto una tan grande".*
(g) Ramón Ángel Caucamán Tabares	*"… don Pablo Pizarro Ganga, antiguo poblador del sector (hoy fallecido), quien le contó de la gran crecida del Ñadis entre 1988 y 1990, había ocurrido por causa del "reventón del arroyo Las Lengas" (afluente del Ñadis) ubicado frente al campo de ese poblador, que hizo que "el río Ñadis alcanzara dos metros de altura…, en partes menos en partes más". Tanto en el lecho del río Los Ñadis como en sus riberas se pueden observar esparcidos antiguos restos de troncos de árboles, muchos de los cuales, según don Ramón, corresponderían a aquellos "arrastrados por la creciente del Ñadis".*
(h) Marisol Pizarro Ganga	*Según recuerda la crecida del río "habría sido entre 1990-1992". Entonces "el lago se desforonó [sic] en el fundo El Triste", nombre del campo de su hermano Pablo (ya fallecido) que estaba en la ribera norte del río Los Ñadis, frente al estero Las Lengas.* *Llamaremos también lago Las Lengas al relativamente pequeño lago pro-glaciar que menciona doña Marisol y que se vació repentinamente sobre el estero del mismo nombre, generándose el evento que llevó al desbordamiento catastrófico del*

	río Los Ñadis. Marisol continua relatando: "tiró mucha arena…, donde vivía Pablo, tapó todo de arena…, la crecida llegó a casi dos metros de su casa". "El lago tenía un cerrito en el centro, que ya no estaba después que se vació. La crecida del Ñadis salió con todo…, se vino con lengas, arrasó con los potreros, animales, cercos…, desaparecieron varias casas en Ñadis bajo, en esa parte la crecida habría alcanzado los 7 metros en lo plano…, depositó barro en los campos que duró como tres años. El potrero de mi mamá desapareció todo…, perdió todos los chivos…, los yeguarizos quedaron encajados en los árboles".
(i) Misael Maldonado	*En referencia a la crecida del río Los Ñadis comenta que: "habría sido entre los días 6-8 de marzo…, entre 1985-1987", pero su esposa, presente también en la conversación señala que "fue después…", sin precisar el año, tomando como referencia la fecha de nacimiento de uno de sus hijos.* *Cuenta don Misael: "fue una crecida rápida…, duró desde las 5 hasta las 11 de la noche, dejó todo lleno de barro…, traía grandes palos y lengas" (Nothofagus pumilio). En el sector Los Canelos, curso medio del río Los Ñadis, donde se ubica su campo, la altura de la crecida alcanzó aproximadamente "los 4 metros…, me llevó unos terneros, tapó valles con arena". Comenta que "entre octubre y noviembre el Ñadis siempre iba crecido, para pasar a caballo había que esperar 1 ó 2 días a que bajara, pero nunca había crecido tanto el río".* *Don Misael también hace algunas alusiones a las "crecientes del Colonia", pero sin aportar datos de mayor relevancia, diciendo eso si que "el Colonia se le atravesaba al Baker, haciendo que la creciente llegaba hasta el Valle Castillo".*
(j) Nilda Pizarro Ganga	*"puede haber sido el año 1988 ó el 89…, el arroyo Las Lengas se desbordó en el río Ñadis…, en Los Canelos lo limpió todo, a los árboles les sacó la corteza". Los Canelos es el sector donde se encuentra el campo de don Misael Maldonado.* *En el campo de su mamá, sector bajo Ñadis, cuenta que el río "comenzó a crecer rápido, viejito del puesto salió con el agua al cuello…, el potrero donde estaba el puesto se lo llevó todo, se llevó los chivos de la mamá…, quedó tapado con barro y greda gris, pero en la primavera salió pasto. Después de la crecida doma Nilda dice que "el río bajó super-rápido, en casi dos horas…, las yeguas quedaron arriba de los ñirres, desde el puente nuevo [Ruta 7] hasta la pasarela [Ñadis bajo], se veían los animales colgando de los ñirres y mucha palería".*
(k) Orfelina Casanova Muñoz	*Doña Orfelina fue testigo presencial de la inusual crecida del río Ñadis, ocurrida "los primeros días de marzo de 1988…, mi hija Sofía tenía 3 años".* *Según nos relata, de acuerdo a lo que le contaba su esposo Pablo, al lago (Las Lengas) le caían témpanos del ventisquero "que estaba allí encima…"; en la actualidad, el aludido ventisquero o glaciar se encontraría más alejado del lago. "Ese verano fue bastante caluroso y seco, el río [Los Ñadis] venía bajo; como a las 10 de la mañana empezó a crecer un poquito y en las orillas se juntaron muchas hojitas y una espuma blanca…, Pablo me dijo que rara la crecida del río".*

	Orfelina cuenta que fue a buscar cebollas a la huerta que tenía en el bajo cerca del río, mientras tanto la crecida del estero Las Lengas, que desembocaba en la ribera sur del río Los Ñadis, frente a su campo "estaba formando una represa de palos". Cerca de las 11 de la mañana aquella represa acumuló tanta agua que "reventó, se empezó a venir toda esa cuestión…, se vino de un golpe". Un poco antes Pablo había ido al "potrero del bajo a sacar unos chivos…, entonces reventó ese inmenso montón de palos y el golpe de agua los tiró para afuera" (se refiere a Pablo y sus animales). *La violenta crecida del estero Las Lengas, según el relato de Orfelina, "volvió para atrás el Ñadis, unos mil metros más o menos…, todo lo que estaba emplayado [sic] quedó tapado de agua". La crecida llegó a metros de su casa, mientras sacaban las cosas más importantes y las llevaban al cerro donde se refugió Pablo Orfelina y sus 3 hijas. La altura a la que llegó el agua en su campo habría alcanzado entre los "10 ó 15" metros" según nos cuenta, "a un coigüe grande del bajo le llegó el agua hasta la copa…, quedó blanquito", (sería por (sedimento acarreado por la crecida); "la anchura del río se desparramó". "El ruido que produjo todo eso fue impresionante".* *A las cuatro de la tarde el Ñadis tenía el caudal previo a la gran crecida dice Orfelina, "el río iba bajito, bajito…". En las riberas del "Ñadis quedó un puro barrial hasta mismo abajo, quedó pura arena, era de color plomo como yeso…, después se secaba y era un polvillo. Las lengas quedaron blanquitas". La crecida que arrastró todo este sedimento glaciar descortezó los árboles ribereños "les sacó toda la cáscara".* *Río abajo se rellenaron muchos bajos en ambas riberas del Ñadis: "se formaron potreros planitos donde creció mucho pasto…, como en Los Canelos donde Misael Maldonado". Allí la mayor intensidad de la crecida se manifestó alrededor de los 5 de la tarde, cuenta doña Orfelina, mientras que en el curso inferior del Ñadis "la crecida pasó como a las 11 de la noche" arrasando con animales y casas cuyos pobladores debieron refugiarse en pequeños cerros donde "se amanecieron…, como la familia de Rosa Quinto". En las riberas del curso inferior del Ñadis quedaron "animales colgados de los árboles, yeguarizos colgados de las patas".* *Con posterioridad al evento, unos cuantos día después de ocurrido el evento el esposo de doña Orfelina fue a explorar la zona llegando al lago del que nacía el estero Las Lengas, comentándole que éste habría quedado vacío, según sus palabras, Pablo de dijo: "el lago quedó seco".*
(l) Cristián Arratia Vidal	*Don Cristián también recordó la gran crecida del río Los Ñadis, al preguntarle si esta habría ocurrido en 1988, respondió: "por ahí tuvo que ser…, deje mis caballos y aperos en un puesto en Ñadis bajo, las riendas y espuelas las colgué en un árbol…, cuando vino la crecida en la noche el puestero alcanzó a soltar mis caballos…, cuando regresé sólo recuperé las riendas y las espuelas…, las monturas y lo demás se perdió todo; a los días después aparecieron los caballos". "Esa creciente fue tan fuerte que dio vuelta la pasarela de donde la señora Rosa Quinto", refiriéndose a la pasarela que se encontraba en el sector Ñadis bajo, que aún existe.*

Baker River floods with unknown source	
Interviewee	Record
(m) René Vargas Sandoval	*"en 1977 se produjo la última creciente grande del Baker, a la casa de mi mamá le llegó el agua…, se le inundó toda la huerta y parte del campo". El campo de doña Julia Sandoval, su madre, se ubica a orillas del Baker en el sector del mismo lago Vargas.* *"el Baker antes tenía menos cauce, ahora es más ancho, el Baker…, cuanto campo se ha comido". Se refiere, con mucha probabilidad, a que antiguamente la caja del río era más angosta*
(n) José Becerra Vidal	*Don José recuerda una gran crecida del Baker ocurrida "el 7 de enero 1977…, es la más grande que he visto". Cuenta que, "el Baker venía de lado a lado, tapo todo, playas, barrancas…, sólo se veía la parte de arriba del monte"; se refiere a que solo quedaban visibles las copas de los árboles del bosque ribereño. El sector las Brisas (Tortel), "estaba todo tapado de agua".* *Cuenta don José que la inundación bajó paulatinamente durante una semana hasta que el río alcanzó nuevamente su nivel normal. Recuerda muy bien dicha crecida del Baker pues en ella se ahogaron su cuñado y sobrinos que venían en una balsa, comenta "yo con mi papá veníamos en otra balsa y nos salvamos…". La crecida "arrasaba con todo en Tortel, chalanas y botes…, si uno tenía maderas y animales se lo llevaba todo; días después, cuando salía a buscar leña en bote, encontraba animales flotando, todos hinchados" en el fiordo Baker.*

Historical documents	
Source	Record
Oportus (1928)	No puede utilizarse para colonización el hermoso mallín de unas 5 mil hectáreas situado entre le Sección La Colonia y la desembocadura del río Cochrane, en el Baker, porque la crecida de este río, que se verifica una vez en al año lo inunda completamente subiendo el agua hasta unos cuatro metros sobre el nivel premanente del río. Esta crecida del río es un fenómeno interesante: El río de la Colonia y el río Nef, en épocas distintas y entre los meses de Diciembre a Abril inclusive, vacian un enorme caudal de aguas en al río Baker; este aumento considerable del caudal de los ríos de La Colonia y Nef, parece que tiene su origen en al desprendimiento de las inmensas masas de nieve de sus orígenes, las qua socavadas por las lluvias y los vientos propios del verano, se precipitan licuándose y lanzando el volumen de las aguas de los ríos nombrados en el cauce del Baker. Esta crece llega sin ruido a los campos y dura más o menos 24 horas. Los mallines inundados por la crecidas no pueden utilizarse ni aún con caballares antes de que de efectúe el fenómeno, porque les animales sorprendidos por las aguas no tienen tiempo para trepar a los cerros del lado Sur u Oriente y perecen ahogados casi todos. Después de la crece estos campos pueden admitir animales.

De Agostini (1945)	Rastros recientes de inundación del río Colonia son los montones de troncos que encontramos apiñados entre los árboles de la floresta y cubiertos todavía de barro y terreno pantanoso y lleno de charcos de agua. El desbordamiento del río Colonia, que todos los veranos se repite infaliblemente desde los primeros días de enero hasta febrero, tiene en constante inquietud a los pobladores de la zona, quienes explican este fenómeno con las más extrañas hipótesis. La crecida se efectúa en 24 horas, sin que la precedan signos excepcionales ni particulares indicios, alcanzando un volumen impresionante. Una enorme masa de agua turbia y barrosa se vuelca repentinamente de la montaña y se precipita en el valle, arrastrando consigo grandes troncos de árboles arrancados de la floresta, y cubriendo totalmente el lecho del río en un ancho de 600 m. La corriente es tan impetuosa que rechaza a la del Baker y la hace retroceder por unos 15 km, elevando el nivel normal de sus aguas unos 4 m, como lo atestiguan los gajos y residuos vegetales que quedan a esa altura entre las ramas de los árboles, después de la inundación. Cuando los colonos desconocían aún el terrible poder de la creciente y, por lo tanto, descuidaban retirar el ganado a tiempo de la zona afectada, muchos fueron los animales vacunos y caballares que perecieron ahogados. Algunos esqueletos de estos animales colgaban de los árboles todavía varios meses después como macabro trofeo de la terrible inundación. Según las referencias de Vilches, que ha recorrido esos parajes en busca de sus vacunos, hay allí un lago de donde sale el río Colonia. Debemos pues seguir las inflexiones del río, caminando al pie de altos barrancos, entre guijarros casi todos de granito y diorita, desprendidos de estas terrazas fluvioglaciales por efecto de la potente erosión de las aguas durante las inundaciones. Corpulentos troncos de coihue destrozados, pero aún con sus raíces, yacen esparcidos a la orilla del río como elocuente testimonio de la potencia extraordinaria de las aguas, que, llenando a gran altura la cuenca de orilla a orilla, alcanzaron a desarraigar de la floresta aquellos árboles gigantescos. En la extremidad occidental del lago, cuyo largo calculamos en siete u ocho kilómetros, baja de la cordillera un gran glaciar que llena toda la cuenca final del valle. La costa oriental del lago, desde donde sale el Colonia, es desplayada y baja, y no hay ningún vestigio que pueda revelar desbordamiento alguno de las aguas debido a un repentino desmoronamiento producido en la margen del lago. Con todo, hay rastros positivos de un notable levantamiento del nivel del lago, señalado por un tronco gigantesco de coihue elevado unos metros sobre el nivel normal de las aguas y por otros árboles más pequeños arrastrados hacia el interior hasta unos 10 m de altura sobre la superficie ordinaria, a causa, según parece, de un rápido crecimiento del lago. No alcanzamos a ver el interior de la cordillera, pero, por la configuración del valle y del glaciar, me parece tener ya suficientes motivos para suponer que las causas de los desbordamientos de las aguas, que originan las inundaciones, deben buscarse en otro lago marginal, directamente ligado al glaciar. Se produciría el

mismo fenómeno que observamos en otros lagos andinos obstruidos por glaciares, de lo cual es típico ejemplo lo que acaece con el glaciar Moreno, del lago Argentino.

Durante la primavera, el lago marginal, obstruido por el glaciar, empieza a subir de nivel a causa del deshielo y de los torrentes glaciares que allí se descargan, logrando su mayor altura en los meses de enero y febrero, cuando llegan los intensos calores estivales. En dicho período, por la presión que ejerce sobre el hielo la masa de agua encerrada en el lago y, al mismo tiempo, por la infiltración de diversas Corrientes por entre las grietas del glaciar, que constantemente se ensanchan, se produce en el glaciar un gran corte en el que se efectúa rápidamente el vaciamiento del lago superior, descargando sus aguas en el de más abajo, el que a su vez vuelca sus aguas en el valle del río Colonia*.

** Este fenómeno es definido en glaciología con la palabra islandesa jokullhlaup, esto es, algo así como "desagüe repentino", y es de ocasional ocurrencia en los sectores englaciados de la Patagonia, el último de los cuales sucedió en la zona del glaciar Bernardo durante el invierno de 2007 (N.E.).*

Según me han asegurado los pobladores de este valle, la inundación vuelve a repetirse algunos años a fines de abril o principios de mayo, pero en forma más reducida. También en el valle del río Nef, más al norte, se produce este fenómeno de desbordamiento, aunque en menor proporción.

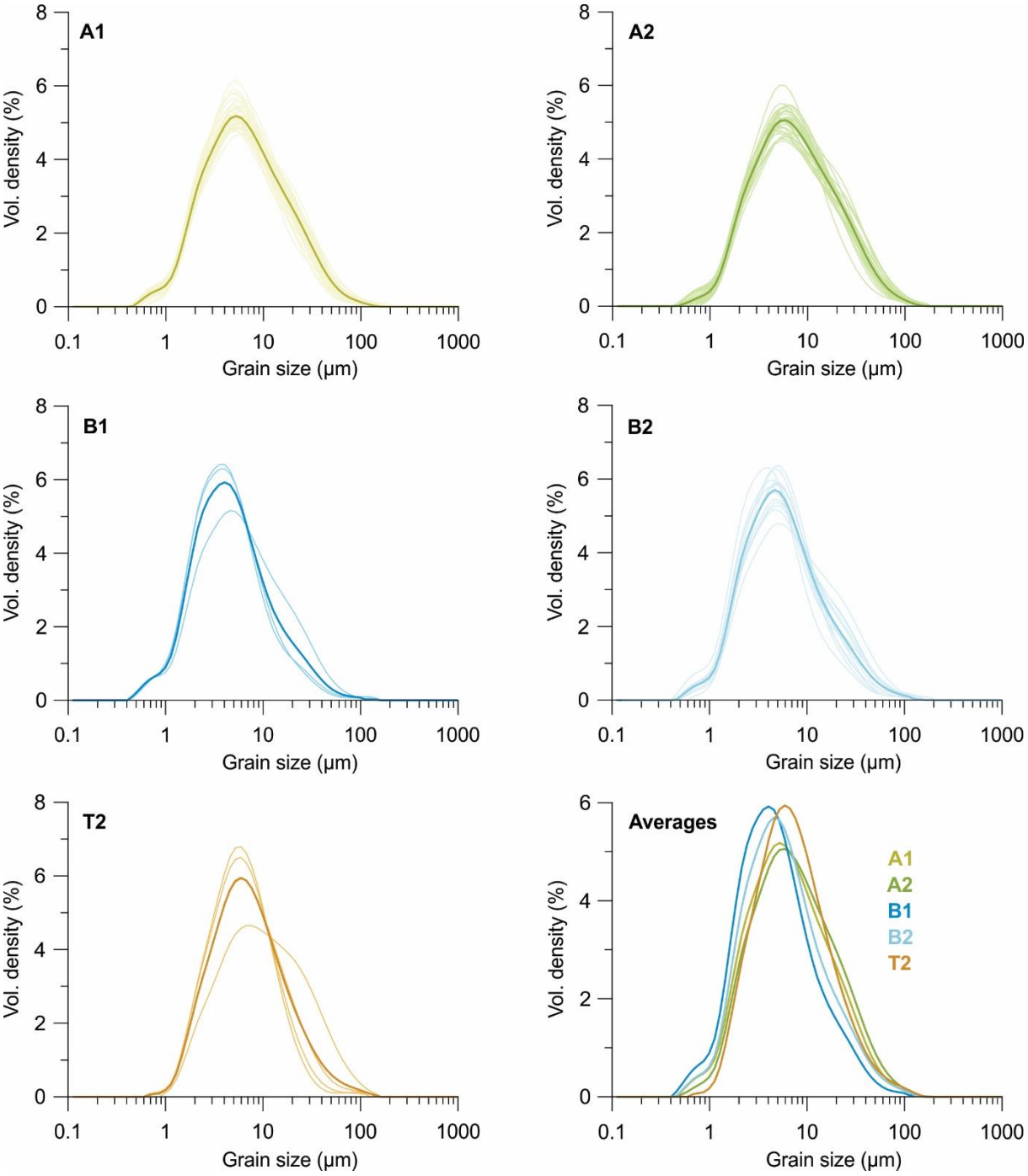

Figure S5A. Grain-size distribution of all 106 sediment samples from core FC17-08, grouped per sediment facies following Figs. 5.2 and 5.3. Facies averages are displayed as bold lines.

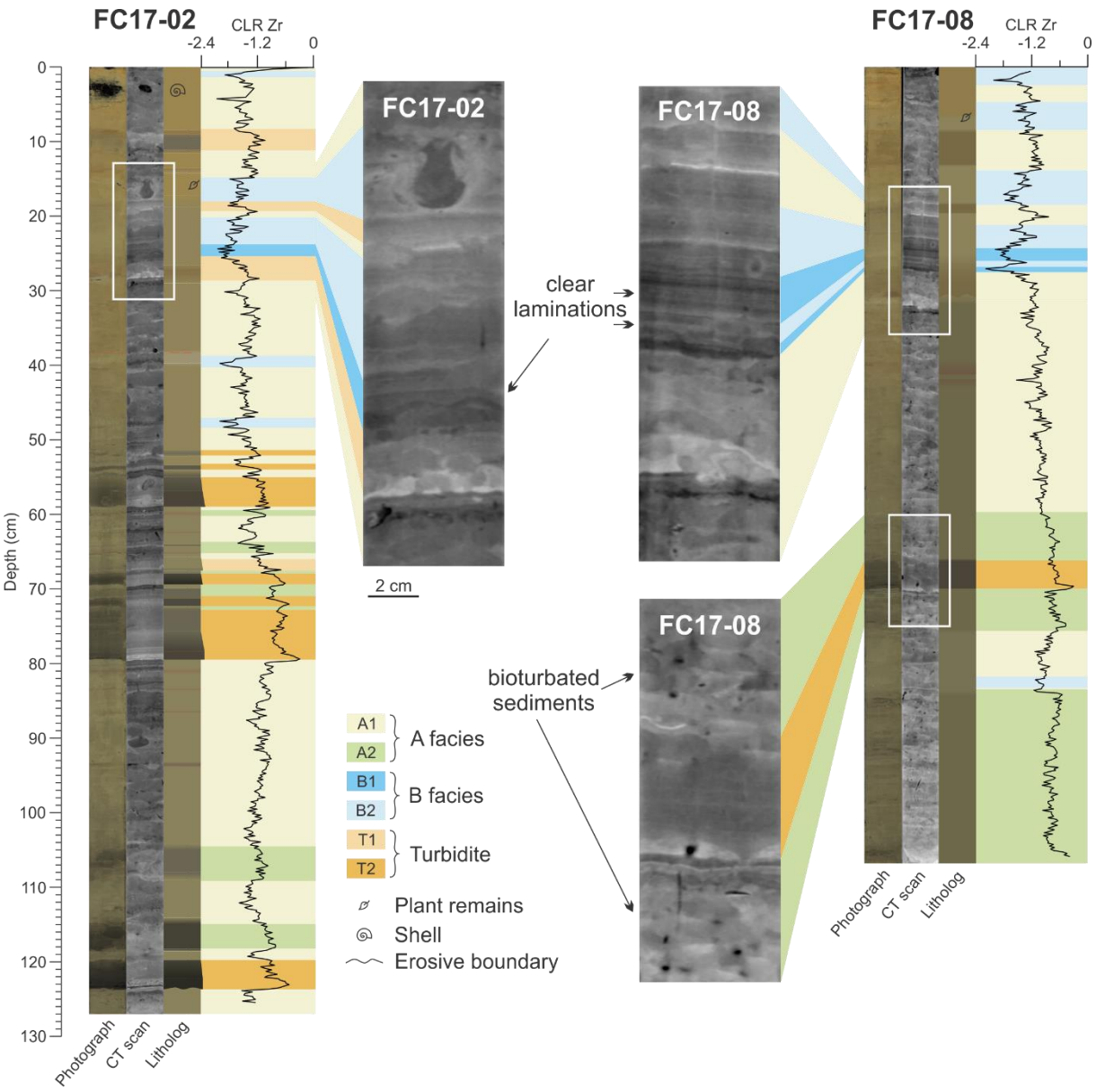

Figure S5B. Lithology of sediment cores FC17-02 and FC17-08 with enlargements of the CT scans corresponding to representative B and T deposits. Although bioturbation deforms the sediment layering throughout both cores, clear layers remain visible in the B facies, especially in the B1 facies.

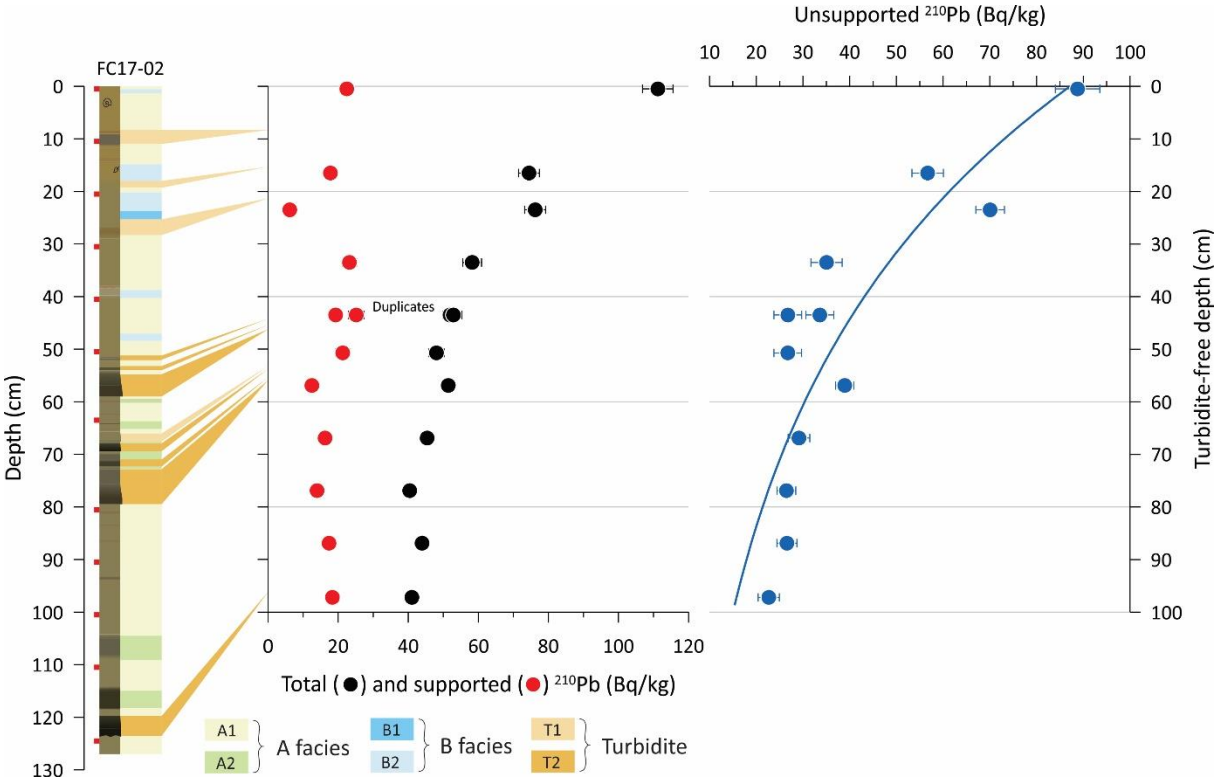

Figure S5C. ^{210}Pb chronology of sediment core FC17-02. The red squares correspond to the samples used for radionuclide analysis. Note that the final chronology was calculated based on cumulative dry mass instead of turbidite-free depth.

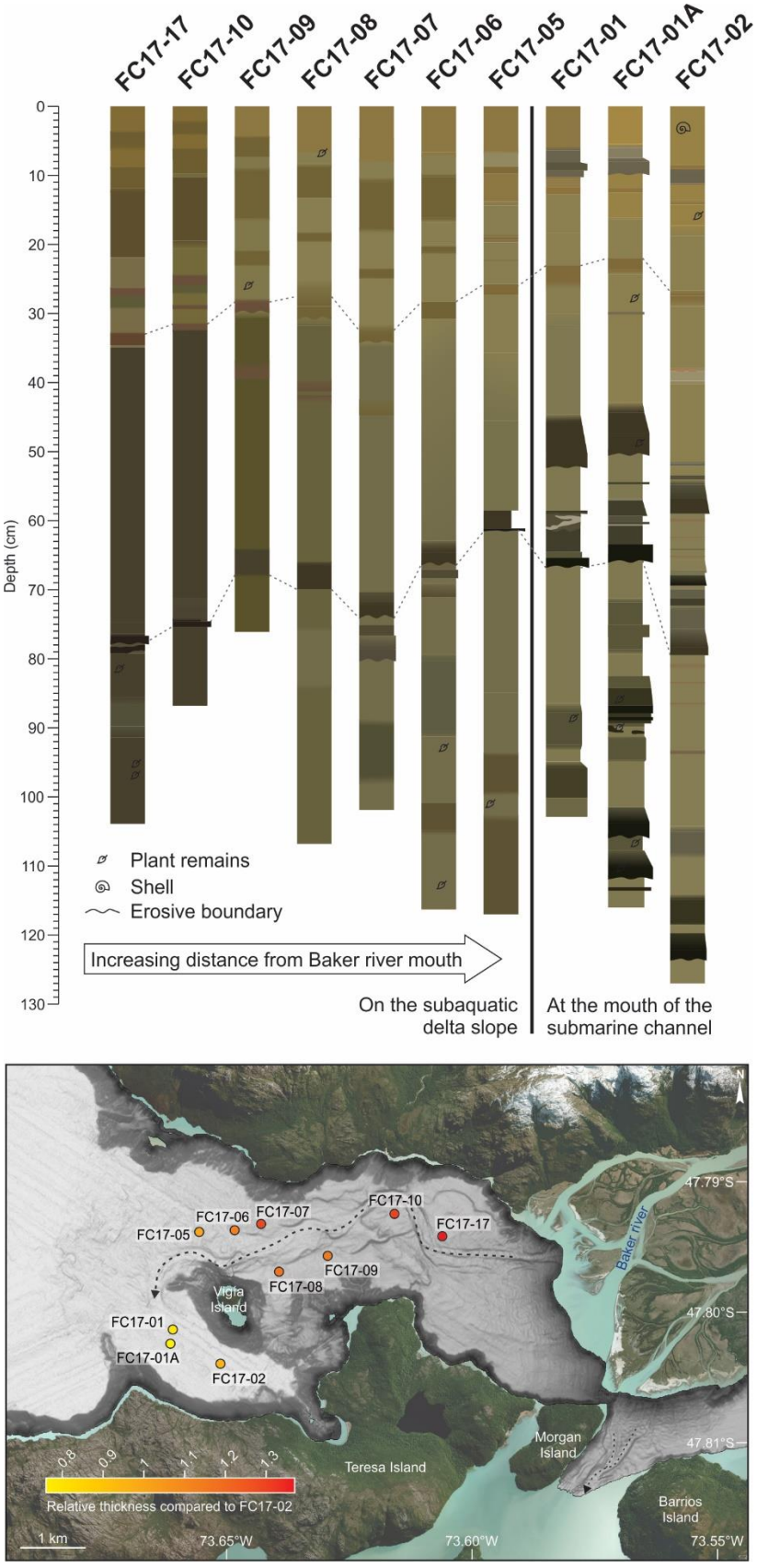

Figure S5D. Lithologs of the ten sediment cores collected at the head of Martínez Channel, with indication of the correlations used to project the age-depth model of FC17-02 (see Fig. 5.3) to the other cores. The relative thickness of the turbidite-free deposits relative to core FC17-02 is displayed on the slope map, based on the core correlations shown above.

References

Agostini, A. de (2010) Andes Patagónicos. Viajes de Exploración a la Cordillera Patagónica Austral. Tomo II. Cámara Chilena de la Construcción, Pontificia Universidad Católica de Chile y Biblioteca Nacional. Santiago de Chile.

Oportus, C. (1928) Informe sobre el problema de colonización de la zona del río Baker. Departamento de Tierras y Colonización, Ministerio de Fomento, Santiago de Chile, 120 pp.

6. Neoglacial increase in high-magnitude glacial lake outburst flood frequency, upper Baker River, Chilean Patagonia (47°S)

This chapter is based on:

Vandekerkhove, E., Bertrand, S., Mauquoy D., McWethy, D., Reid, B., Stammen, S., Saunders, K.M., and Torrejón, F. (2020) Neoglacial increase in high-magnitude glacial lake outburst flood frequency, upper Baker River, Chilean Patagonia (47°S). *Quaternary Science Reviews*, **248**, 106572.

Author contributions: EV conducted fieldwork and all laboratory analyses, interpreted the results, and wrote the manuscript. SB designed this study, obtained funding, coordinated the collaborative research activities, and wrote the manuscript with EV. DM examined the macrofossils and selected them for radiocarbon analysis. DMW processed the samples for charcoal analysis and made the charcoal counts. BR sampled rivers and measured suspended sediment concentrations. SS conducted part of the grain-size analyses for her BSc project. KMS coordinated the radionuclide measurements and interpreted the ^{210}Pb results. FT conducted field interviews and analyzed historical documents. EV and SB wrote the paper, with contributions from DM, DMW, FT, and KMS.

Abstract: Glacial Lake Outburst Floods (GLOFs) constitute a major threat in glacierized regions. Despite a recent increase in the size and number of glacial lakes worldwide, there is only limited evidence that climate change is affecting GLOF frequency. GLOFs are particularly common in the Baker River watershed (Patagonia, 47°S), where 21 GLOFs occurred between 2008 and 2017 due to the drainage of Cachet 2 Lake into the Colonia River, a tributary of the Baker River. During these GLOFs, the increased discharge from the Colonia River blocks the regular flow of the Baker River, resulting in the inundation of the Valle Grande floodplain, which is located approximately 4 km upstream of the confluence. To assess the possible relationship between GLOF frequency and climate variability, four sediment cores collected in the Valle Grande floodplain were analyzed. Their geophysical and sedimentological properties were examined, and radiocarbon-based age-depth models were constructed. All cores consist of dense, fine-grained, organic-poor material alternating with low-density organic-rich deposits. The percentage of lithogenic particles, which were most likely deposited during high-magnitude GLOFs, was used to reconstruct the flood history of the last 2.75 kyr. Results show increased flood activity between 2.57 and 2.17 cal kyr BP, and between 0.75 and 0 cal kyr BP. These two periods coincide with Neoglacial advances that are coeval with periods of lower temperature and increased precipitation. Our results suggest that GLOFs are not a new phenomenon in the region. Although rapid glacier retreat is likely responsible for high GLOF frequency in the 21st century, high-magnitude GLOFs seem to occur more frequently when glaciers are larger and thicker.

6.1. Introduction

Glacial Lake Outburst Floods (GLOFs) occur when a lake dammed by a glacier or moraine suddenly empties, resulting in the abrupt flooding of downstream environments (e.g. Benn and Evans, 2010). In glacierized regions, these events constitute a constant threat to infrastructure, livestock, and human lives. Historical data worldwide suggest that GLOFs have occurred throughout recorded history (Carrivick and Tweed, 2016). There is however only limited evidence that their frequency has changed (IPCC, 2019).

The recent increase of glacial lakes, both in size and number (e.g. Paul et al., 2007; Wang et al., 2011; Davies and Glasser, 2012; Carrivick and Quincey, 2014; Aniya, 2017; Prakash and Nagarajan, 2018; Wilson et al., 2018; Zhang et al., 2019), has led to the assumption that GLOF frequency is currently increasing, mostly due to increased glacier retreat and thinning rates (e.g. Iribarren Anacona et al., 2014; Wilson et al., 2018). However, recent studies suggest that the number of GLOFs has actually reduced since the mid-1990s in all major world regions (Carrivick and Tweed, 2016). A recent global inventory of GLOFs originating from the failure of moraine dams shows a global increase in flood frequency between 1930 and 1970, followed by a decline in recent decades, despite glacier recession (Harrison et al., 2018). The global increase in GLOF frequency around 1930 was associated with a delayed response to the warming that ended the Little Ice Age (LIA) and the recent decrease in GLOF frequency and regularity was interpreted as reflecting the climate stabilization that followed the LIA (Harrison et al., 2018). Carrivick and Tweed (2016), however, did not observe any significant trend in the number of GLOFs from moraine-dammed lakes over the last 50 years. By comparison, GLOFs from ice-dammed lakes are also known to occur during periods of glacier growth (Benn and Evans, 2010; Round et al., 2017), and their frequency globally seems to have decreased over the last 50 years (Carrivick and Tweed, 2016).

In Patagonia, GLOF frequency appears to have increased in the last three decades (Iribarren Anacona et al., 2014). They are particularly pronounced in the Baker River watershed (47–48°S), which drains most of the eastern side of the Northern Patagonian Icefield (NPI). The Colonia River, which is a tributary of the Baker River, experienced repeated GLOF events from 1881 onwards (Tanaka, 1980; Winchester and Harrison, 2000; Jacquet et al., 2017). After a 50-year long period of quiescence between the 1960s and 2008 during which no GLOFs were documented, GLOFs in the Baker River watershed restarted in April 2008, with a frequency of 1–3 per year (Jacquet et al., 2017). These GLOFs all initiated from the emptying of Cachet 2 Lake into the Colonia River (Dussaillant et al., 2010; Jacquet et al., 2017). During these events, the discharge of the Baker River roughly triples, resulting in the inundation of large floodplains.

This apparent abrupt increase in GLOF frequency in the Colonia River valley has reinvigorated discussions about the possible link between climate change and GLOF frequency. However, there is currently no conclusive answer to this question, mainly because of a lack of continuous flood records on timescales that extend beyond gauged river-flow datasets. Long-term flood records that allow for an evaluation of the drivers of flood frequency can be obtained from geological archives, such as floodplain sediments, which have proven to be valuable recorders of flood variability (e.g. Paine et al., 2002; Jones et al., 2012; Toonen et al., 2015; Lintern et al., 2016; Ishii et al., 2017; Fuller et al., 2018, 2019).

The aim of this paper is to reconstruct Baker River flood variability during the late Holocene to evaluate long-term (pre-instrumental) changes in GLOF frequency. We do so by analyzing geophysical and sedimentological data obtained on four independently-dated sediment cores collected in the Valle Grande floodplain, which is located along the upper Baker River. The results are then compared to proxy records of both glacier and climate variability to assess their potential relationships.

6.2. Setting

6.2.1. Hydrology

The Baker River (47–48°S) is located in Chilean Patagonia (Fig. 6.1a). It is the largest river in Chile in terms of mean annual discharge (~1100 m^3/sec; Dussaillant et al., 2012). The river originates from Bertrand Lake, which is directly fed by General Carrera Lake, and continues to flow southwards where

it discharges into the Martínez Channel near the town of Tortel (Fig. 6.1a). Along its approximate 190 km course, the Baker River receives meltwater from NPI outlet glaciers via (from North to South) the Nef, Colonia, and Ventisquero rivers. It is also fed by the Chacabuco, Cochrane, Del Salto, and De Los Ñadis rivers, which originate from the eastern side of the watershed. The Del Salto and De Los Ñadis rivers both receive meltwater from small mountain glaciers on the eastern side of the Baker watershed. Due to the glacial regime of the Baker River, its discharge varies seasonally from 600 m^3/s in winter to 1200 m^3/s in summer (Dussaillant et al., 2012).

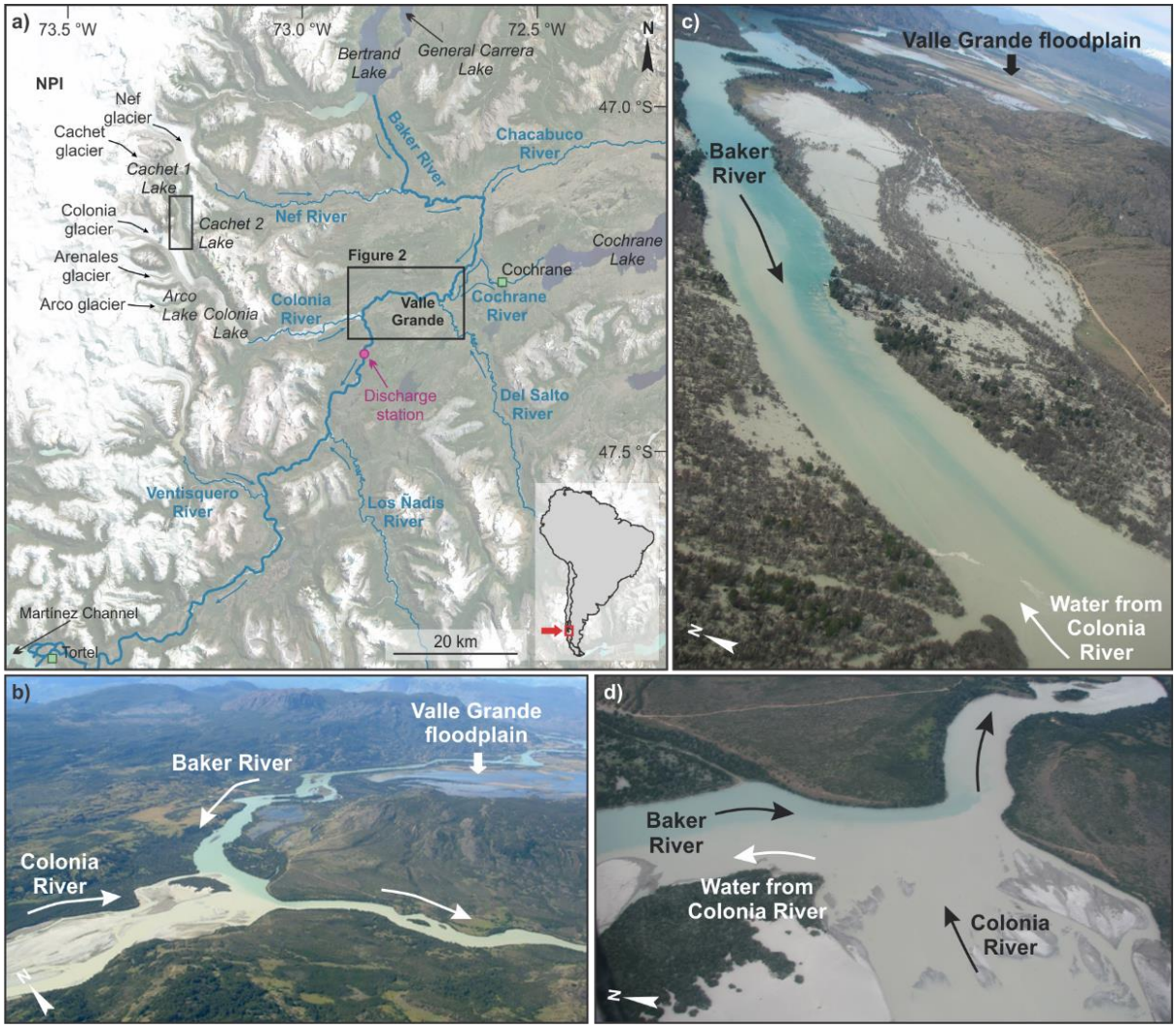

Figure 6.1. Location of the Valle Grande floodplain along the Baker River in Chilean Patagonia. **(a)** Location of the Baker River in its entire course from Bertrand Lake to Martínez Channel, with indication of the main tributaries and glaciers discussed in the text (Global Mapper World Imagery). NPI stands for Northern Patagonian Icefield. The towns of Cochrane and Tortel are indicated with green squares. **(b)** Location of Valle Grande, four km upstream of the confluence between Baker and Colonia rivers. This image was taken in February 2009, during the only known inundation of the Valle Grande floodplain due to heavy rainfall (photo credit: Horacio Parrague). **(c)** Sediment from the Colonia River flowing upstream in the Baker River towards Valle Grande during the September 2016 GLOF. This GLOF resulted in the partial inundation of the Valle Grande floodplain due to backwater flooding (photo credit: Andres Rivera). **(d)** Confluence of Colonia and Baker rivers during the December 2008 GLOF where water and sediment are flowing upstream (towards the north) in the Baker River (photo credit: Paulina Rojas). Note the lack of sediment flowing upstream during the precipitation-driven flood in (b).

6.2.2. Glaciology

The NPI, with a surface area of approximately 4000 km^2 (Davies and Glasser, 2012; Aniya, 2017), is the second largest temperate icefield. After the Last Glacial Maximum, NPI glaciers contracted and expanded several times, and different chronologies of Neoglacial advances have been postulated for the Holocene (Mercer, 1982; Aniya, 1995, 1996, 2013; Davies et al., 2020). The chronology proposed by Aniya (2013) is one of the most detailed and it includes five Neoglaciations at 5.1–4.5 cal kyr BP, 4.0–3.6 cal kyr BP, 2.8–2.0 cal kyr BP, 1.6–0.9 cal kyr BP, and during the 17^{th}–19^{th} centuries. This chronology, however, is mostly based on data from outlet glaciers of the SPI (Southern Patagonian Icefield), as studies of Holocene NPI glacier variability remain very limited. The most recent review of Patagonian glacier evolution by Davies et al. (2020) only briefly addresses Neoglacial advances but it suggests that glaciers advanced or stabilized at 6–5 cal kyr BP, 2–1 cal kyr BP, and 0.5–0.2 cal kyr BP, although Nimick et al. (2016) observed a clear advance of the Colonia Glacier at 2.9 cal kyr BP, in agreement with the formation of a large moraine by glacier Leones slightly before 2.5 cal kyr BP (Harrison et al., 2008). After the latest advance in the 17^{th}–19^{th} centuries, which is frequently associated to the LIA, all eastern NPI glaciers receded (Masiokas et al., 2009). Their total surface area loss between 1870 and 2011 has been estimated at 19.1% (Davies and Glasser, 2012). Similarly, smaller mountain glaciers located to the East of the NPI and discharging into the Del Salto and De Los Ñadis rivers, have experienced a general ice retreat during the last ~150 years (Davies and Glasser, 2012).

6.2.3. Holocene GLOFs in the upper Baker River area

Very few paleohydrological reconstructions exist along the eastern side of the NPI, and most focus on the catastrophic floods that occurred during the deglaciation (e.g. Benito and Thorndycraft, 2020). The oldest evidence of GLOF occurrence in the upper Baker River area, as identified from erosive and depositional landforms, dates back to ~12.6–11.7 kyr BP (Benito and Thorndycraft, 2020). These megaflood-type landform assemblages resulted from catastrophic floods, with volumes of around 100 km^3, at a time when the discharge of large proglacial lakes was being reorganized towards the Pacific Ocean via the Baker River (Turner et al., 2005; Glasser et al., 2016; Thorndycraft et al., 2019). During the Holocene, additional paleofloods were identified from slackwater deposits found immediately downstream of the Baker-Colonia confluence (Benito et al., 2014; Benito and Thorndycraft, 2020). The latter deposits provide evidence for at least eight floods between 7.0 and 2.5 cal kyr BP and at least three GLOFs during the last 600 years, separated by a stable period between 2.5 and 0.6 cal kyr BP. Although Lara et al. (2015) used tree rings to reconstruct Baker River streamflow during the last 250 years, their record is unfortunately insensitive to GLOFs.

The first historical evidence of GLOF occurrence in the upper Baker River area dates back to the early 1880s (Tanaka, 1980). These GLOFs originated from the Colonia River and are related to the retreat of Colonia Glacier between 1850 and 1880 (Harrison and Winchester, 2000). Due to this retreat, Arco Lake, which was at the time dammed by Colonia Glacier, released approximately 265 x 10^6 m^3 of water around 1881 (Tanaka, 1980; Winchester and Harrison, 2000, Fig. 6.1a). Afterwards, repeated GLOFs occurred in the Colonia valley from water discharged by Arco Lake. Severe flood events took place c. 1896/1897, 1914/1917, 1944 and 1963, until a drainage path eventually established between Arco and Colonia lakes in the 1960s and GLOFs ceased to occur (Winchester and Harrison, 2000; Jacquet et al., 2017).

The Colonia River experienced a new series of repeated GLOFs between April 2008 and November 2017 (Dussaillant et al., 2010; Jacquet et al., 2017). These events all resulted from the abrupt drainage of Cachet 2 Lake into the Colonia River, generally through a subglacial tunnel below the Colonia Glacier

(Fig. 6.1a; Dussaillant et al., 2010; Friesen et al., 2015). During such a GLOF event, the Baker River downstream of the confluence with the Colonia River can triple in discharge, reaching between 3000 and 3800 m^3/sec (Dussaillant et al., 2010). A total of 21 GLOFs have been recorded since April 2008 (Jacquet et al., 2017; DGA, Chile). Photographic and conversational evidence indicate that most Colonia River GLOFs result in the inundation of the Valle Grande floodplain, which is located immediately upstream of the confluence with the Colonia River (Fig. 6.1b and c and Supplementary Fig. S6A). This flooding results from the blocking of the regular Baker River water flow towards the South by the Colonia River, which in turn results in Baker River water levels rising by 4–6 m (Supplementary Table S6A; Oportus, 1928).

Historical documents suggest that the Nef River, which discharges into the Baker River upstream of Valle Grande (Fig. 6.1a), also experienced GLOFs during the last century (Supplementary Table S6A; Oportus, 1928; De Agostini, 1945). These events similarly resulted in the flooding of Valle Grande. However, the GLOFs originating from the Nef valley in the 1940s were of lower magnitude compared to those from the Colonia valley, and they only resulted in a partial inundation of the floodplain (De Agostini, 1945). The other rivers that discharge into the Baker River near Valle Grande (Chacabuco, Cochrane, and Del Salto rivers; Fig. 6.1a) have no historical records of GLOFs.

6.2.4. Valle Grande floodplain

The Valle Grande floodplain (47.30°S; 72.75°W) is located 10 km to the west of the town of Cochrane, in the upper reaches of the Baker River, approximately 4 km upstream of its confluence with the Colonia River (Figs. 6.1a and 6.2a). It has a surface area of 50 km^2 and it is the largest area of Holocene alluvial sediments along the Baker River (Ulloa et al., 2018; Benito and Thorndycraft, 2020). The sinuous Baker River meanders through the northern part of this flat area for almost 15 km and the Del Salto River crosses its eastern end before flowing into the Baker River. The floodplain, which is considerably wider south of the Baker River, contains many paleochannels and a few scroll bars (Fig. 6.2a). The paleochannels are defined by vegetated and sinuous ridges, which represent old river levees (Fig. 6.2b). Similarly, scroll bars occur as curved elevated ridges in the floodplain. The floodplain morphology is interpreted to be shaped by Holocene floods, including GLOFs from Nef and Colonia valleys (Benito and Thorndycraft, 2020). On the right bank of the Baker River, the floodplain is rather narrow and consists mainly of marshland with a few small ponds and patches of dense forest (Fig. 6.2a). On the left bank, grasslands and marshland dominate the lower elevated regions. Remaining patches of *Nothofagus* forest and scrub occur on the slightly elevated areas. Here, the floodplain is primarily used as pastureland, for which most of the original forest was cleared by burning during the first half of the 20th century (De Agostini, 1945). In addition to GLOFs, the Valle Grande floodplain can also flood during long-lasting (several days) extreme precipitation events. Such an event occurred in February 2009, during which the Baker River discharge increased to 2700 m^3/sec and the Baker river water level increased by 2.5 m downstream of the confluence with the Colonia River, in response to five consecutive days of heavy rainfall (DGA, Chile; Fig. 6.1a and b and Supplementary Fig. S6A). The February 2009 event is the only rainfall-induced flooding event reported in regional archives. By comparison, water level during the 21st century Cachet 2 GLOFs rose by an additional ~1 m (DGA, Chile).

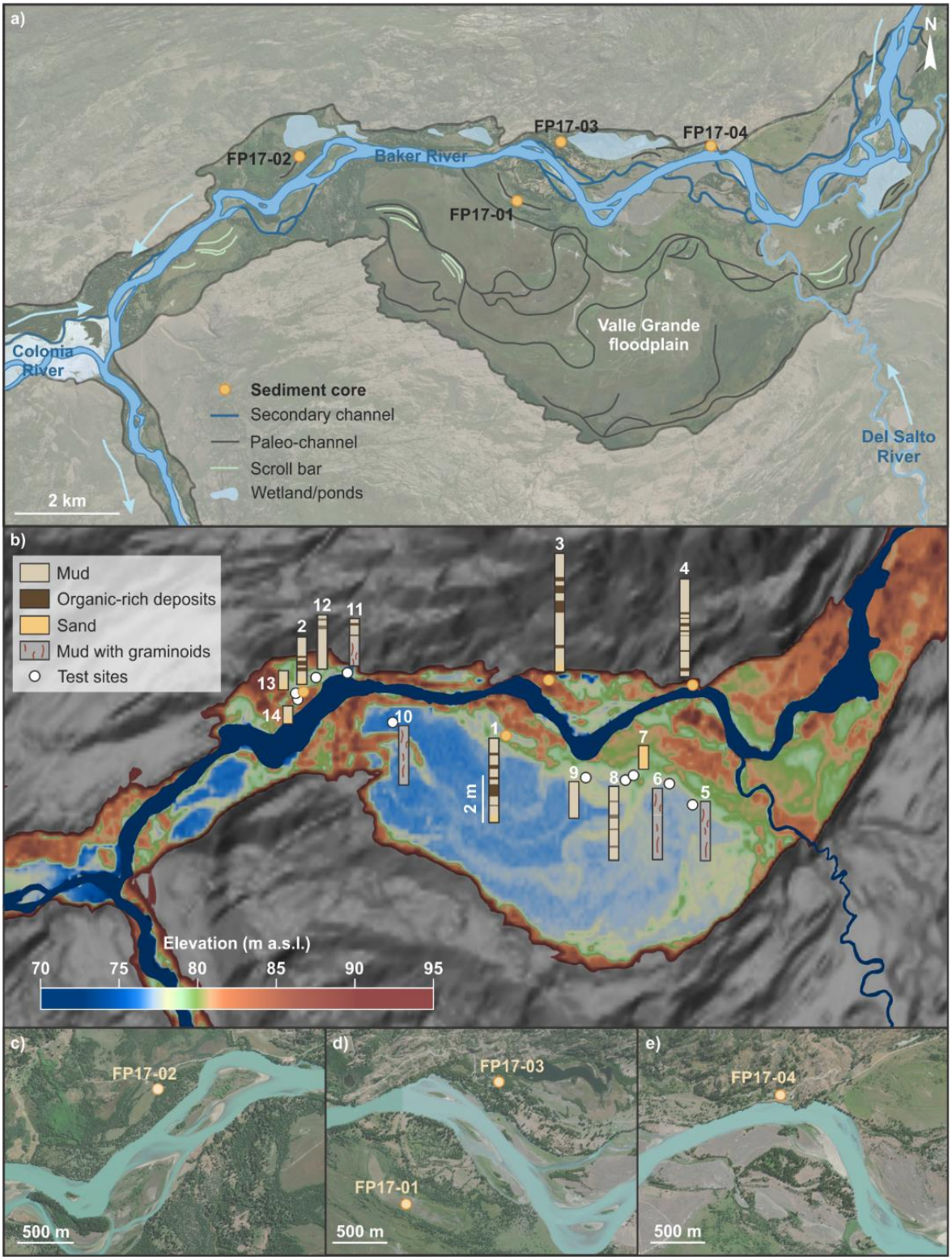

Figure 6.2. Location of the sediment cores collected in the Valle Grande floodplain. **(a)** Google Earth Imagery with the location of the four sediment cores used in this study. **(b)** TanDEMX elevation map of the Valle Grande floodplain (Wessel et al., 2018; color scale for elevations 95 m a.s.l.) is from SRTM. Simplified lithologs based on field core descriptions are displayed for the four cores (orange dots) as well as for the test locations (white dots). The absolute elevations (a.s.l.) of the collected sediment cores are 76.9 m, 80.2 m, 81.0 m, and 79.0 m for FP17-01, FP17-02, FP17-03, and FP17-04, respectively (vertical mean error <0.2 m; Wessel et al., 2018). The average Baker River elevation along the floodplain is approximately 75.0 m, with a slope of 0.01° (~2 m/10 km). The coring locations are enlarged in **(c)**, **(d)**, and **(e)**.

6.2.5. Present-day climate

Precipitation patterns in Patagonia (>40°S) display a strong longitudinal gradient driven by the blocking of humid air masses from the Pacific Ocean by the Andes. A hyperhumid climate prevails on the western side of the Andes where mean annual precipitation ranges from 5000 to 10 000 mm (Garreaud et al., 2013). There, the amount of precipitation is directly related to the strength of the Southern Westerly Wind Belt (SWWB). In eastern Patagonia, on the other hand, forced subsidence causes precipitation to decrease rapidly to less than 300 mm/yr, resulting in an arid climate (Garreaud et al., 2013). Valle Grande, which is located immediately to the east of the NPI, exhibits annual precipitation amounts of 695 mm/yr (Lenaerts et al., 2014), 934 mm/yr (WorldClim v. 2.1; Fick and Hijmans, 2017) or 933 mm/yr (CR2MET; Alvarez-Garreton, 2018) based on gridded climate data. In general, this region experiences wetter conditions in austral winter (305 mm) compared to austral summer (168 mm; WorldClim v. 2.1). The seasonal temperature difference is about 10 °C, with mean winter and summer temperatures of 4.1 °C and 14.0 °C, respectively (WorldClim v. 2.1).

6.3. Materials and methods

6.3.1. Sampling

Valle Grande was selected after an exploratory survey along the Baker River. Based on our observations, this floodplain seems to be the only one preserving a continuous flood stratigraphy. In addition, Valle Grande is located downstream of several glacial valleys. Its sediment record therefore integrates floods originating from several glacier-river systems, making it relatively independent of the evolution of any specific proglacial lake. Coring locations were selected based on their relative elevation above the Baker River, i.e., less than 6 m difference, as this corresponds to the water level rise of the Baker River during the largest historical GLOFs (Supplementary Table S6A). In summer 2016, a 25 mm diameter gouge auger was used to test 14 sites on both sides of the river, from which complete lithological descriptions were made (Fig. 6.2b). Four sites containing a complete and undisturbed stratigraphy were selected for sampling with a 52 mm diameter Russian corer in January 2017: three to the north of the river and one to the south (Fig. 6.2b–e). The sediment cores were collected in 50 cm-long sections from two different holes with a 25 cm overlap to obtain a continuous composite core at each site. All sections were stored in PVC liners and wrapped in plastic foil. The upper 50 cm was sampled using 23 cm-long aluminum boxes (4 x 4 cm) and were, as for the 50-cm long sections, collected at overlapping depth intervals and wrapped in plastic foil.

6.3.2. Sedimentological and geophysical analyses

All the Russian sediment core sections were described, imaged (linescan) and logged with a Geotek Multi-Sensor Core Logger (MSCL) at Ghent University (Belgium). Logging of gamma-ray density (^{137}Cs source) was performed at a 2 mm interval. Composite cores were made based on core descriptions and Geotek MSCL data. Afterwards, the composite cores were subsampled at a 5 mm interval, and samples were weighed, freeze-dried, and weighed again to determine their water content.

Loss-on-Ignition (LOI) was measured continuously at 5 mm resolution following Heiri et al. (2001). After freeze drying the samples, approximately 0.25 g of sediment was oven dried overnight at 105 °C and then heated at 550 °C for 4 h. The weight loss after combustion at 550 °C was used to estimate the organic content, i.e., LOI550. The inorganic content was determined by difference (100% - LOI550). Five duplicate analyses on three different samples indicated a relative error of 2.82% (1σ). The amount of

carbonate was not quantified since test measurements showed that it was negligible (LOI1000: 0.7 ± 0.5%; n = 72), in agreement with the regional lithology (Sernageomin, 2003).

Grain-size measurements were conducted on core FP17-01 at 2 cm resolution using a Malvern Mastersizer 3000 equipped with a Hydro MV dispersion module at Ghent University (Belgium). Resolution was increased to 1 cm between 0–25 cm and 44–97 cm, and to 5 mm between 26–43 cm and 98–124 cm, to capture the fine laminations described in the upper part of the core. Samples with LOI550 values >5% were first heated at 550 °C for 4 h to remove organic matter. All samples were pre-treated by adding a 30% hydrogen peroxide (H_2O_2) solution to 10 ml of de-ionized water containing the suspended sediment and set to boil until the reaction ended. Afterwards, 1 ml of HCl (10%) was added to the samples to remove carbonates. After rinsing, biogenic silica was removed by adding 1 ml of NaOH (2N). Finally, all samples were decanted before sodium hexametaphosphate was added to avoid grain flocculation. Samples were measured in triplicates during 12 s with 10% sonification.

6.3.3. Core chronologies

Radiocarbon ages, charcoal counts, and ^{210}Pb activities were obtained to establish core chronologies. Samples for radiocarbon analysis were selected in organic-rich deposits near sharp lithological boundaries (Fig. 6.3) and examined to identify macrofossils. All samples were pretreated following established protocols (Mauquoy et al., 2004). The selection of monospecific plant macrofossils for radiocarbon analysis minimized the risk of age contamination (by, e.g. plant roots). Measurements were made with an accelerator mass spectrometer at DirectAMS (USA). In addition, one bulk sediment sample from the bottom of core FP17-01 was oven dried and analyzed at NOSAMS (USA). Age-depth models were constructed independently for each core using two to six radiocarbon ages per core (Table 6.1). All ages were calibrated using the latest calibration curve for the Southern Hemisphere (SHCal13; Hogg et al., 2013). The 'proxy-ghost' function of BACON 2.3.6 was used to visualize chronological uncertainties (Blaauw and Christen, 2011). In order to refine core chronologies at the top of the cores, charcoal was counted at 1 cm resolution in the upper 140 cm and 130 cm of FP17-01 and FP17-03, respectively, at the Montana State University Paleoecology Laboratory (USA). In addition, ^{210}Pb measurements were conducted using alpha spectrometry at a 10 cm interval down to 60 and 70 cm on FP17-01 and FP17-03, respectively, at the Australian Nuclear Science and Technology Organisation (ANSTO, Australia), following methods described in Harrison et al. (2003).

6.1.1. Suspended sediment concentrations

The rivers discharging into the Baker River upstream (Nef, Chacabuco, Cochrane, Del Salto) and immediately downstream (Colonia) of Valle Grande (Fig. 6.1) were sampled for Suspended Sediment Concentration (SSC) measurement. Three sites were also sampled along the Baker River. These rivers were sampled throughout the year (n per river = 8–21) between 2008 and 2010. SSC values were obtained after manual filtration on GFF filters until saturation. Annual sediment yields were calculated by multiplying SSC by the annual volumes of water (from Dussaillant et al., 2012).

6.1. Results

6.1.1. Lithology

The sediments of all test sites, except for location 7, are dominated by mud, with frequent intercalations of organic-rich deposits (Fig. 6.2b). Sediments from the lower elevations consist mainly of mud with reddish graminoid remains, whereas locations on higher elevated areas are composed of mud

alternating with organic-rich deposits. Some of the sites display a coarse sand base, and a single location, i.e., test site 7, is fully composed of sand.

Table 6.1. Radiocarbon ages obtained on sediment cores FP17-01 to FP17-04. The ages were calibrated with Clam 2.3.4 (Blaauw, 2010), using the SHCal13 calibration curve (Hogg et al., 2013).

Core label (with location) and sample depth (cm)	Dated material	$\delta^{13}C$	^{14}C age (yrs BP ± 1σ)	2σ calibrated age range (cal yr BP)	Laboratory code
FP17-01 (47.28°S–72.77°W)					
80.0-80.5	Carex spp. leaf bases	-27.2	748 ± 26	568–682	D-AMS 028297
133.5-134.0	Carex spp. leaf bases	-30.0	1287 ± 30	1072–1267	D-AMS 031344
192.0-192.5	Carex spp. leaf bases	-28.7	1367 ± 27	1185–1297	D-AMS 028298
276.5-277.0	Carex spp. leaf bases	-28.8	2076 ± 30	1922–2084	D-AMS 028299
328.5-329.0	Bulk organic matter	-25.5	2320 ± 20	2183–2351	OS-135980
FP17-02 (47.27°S–72.82°W)					
102.0-102.5	Carex spp. leaf bases	-29.5	1050 ± 20	819–959	D-AMS 028300
142.5-143.0	Carex spp. leaf bases	-28.2	1227 ± 29	986–1181	D-AMS 028301
190.0-190.5	Carex spp. leaf bases	-26.4	1498 ± 23	1303–1374	D-AMS 028302
FP17-03 (47.27°S–72.76°W)					
83.5-84.0	Carex spp. leaf bases	-23.5	438 ± 25	334-506	D-AMS 028303
110.0-110.5	Carex spp. leaf bases	-22.9	607 ± 23	529–629	D-AMS 028304
138.5-139.0	Carex spp. leaf bases	-23.5	788 ± 26	658–724	D-AMS 028305
181.5-182.0	Carex spp. leaf bases	-16.3	1693 ± 27	1435–1692	D-AMS 028306
267.5-268.0	Carex spp. leaf bases	-28.1	2225 ± 32	2096–2313	D-AMS 031345
400.5-401.0	Carex spp. leaf bases	-29.5	2572 ± 32	2489–2747	D-AMS 031346
FP17-04 (47.27°S–72.72°W)					
191.0-191.5	Carex spp. leaf bases	-25.1	1133 ± 22	935–1057	D-AMS 028307
389.0-389.5	Carex spp. leaf bases	-32.1	2594 ± 34	2491–2755	D-AMS 031347

In the four Russian sediment cores, which are all located at higher elevations (Fig. 6.2b–e), four major facies can be identified: clastic deposits, slightly organic mud, organic-rich mud, and muddy organic matter (Fig. 6.3). The clastic deposits are composed of dense clastic material with little or no organic matter (LOI550 < 10%). Slightly organic mud and organic-rich mud represent a mixture of mud and organic matter with variable density and LOI550 values. The muddy organic matter deposits are generally thick, have LOI550 values exceeding 65%, and low density values (< 1.4 g/cc; Fig. 6.3).

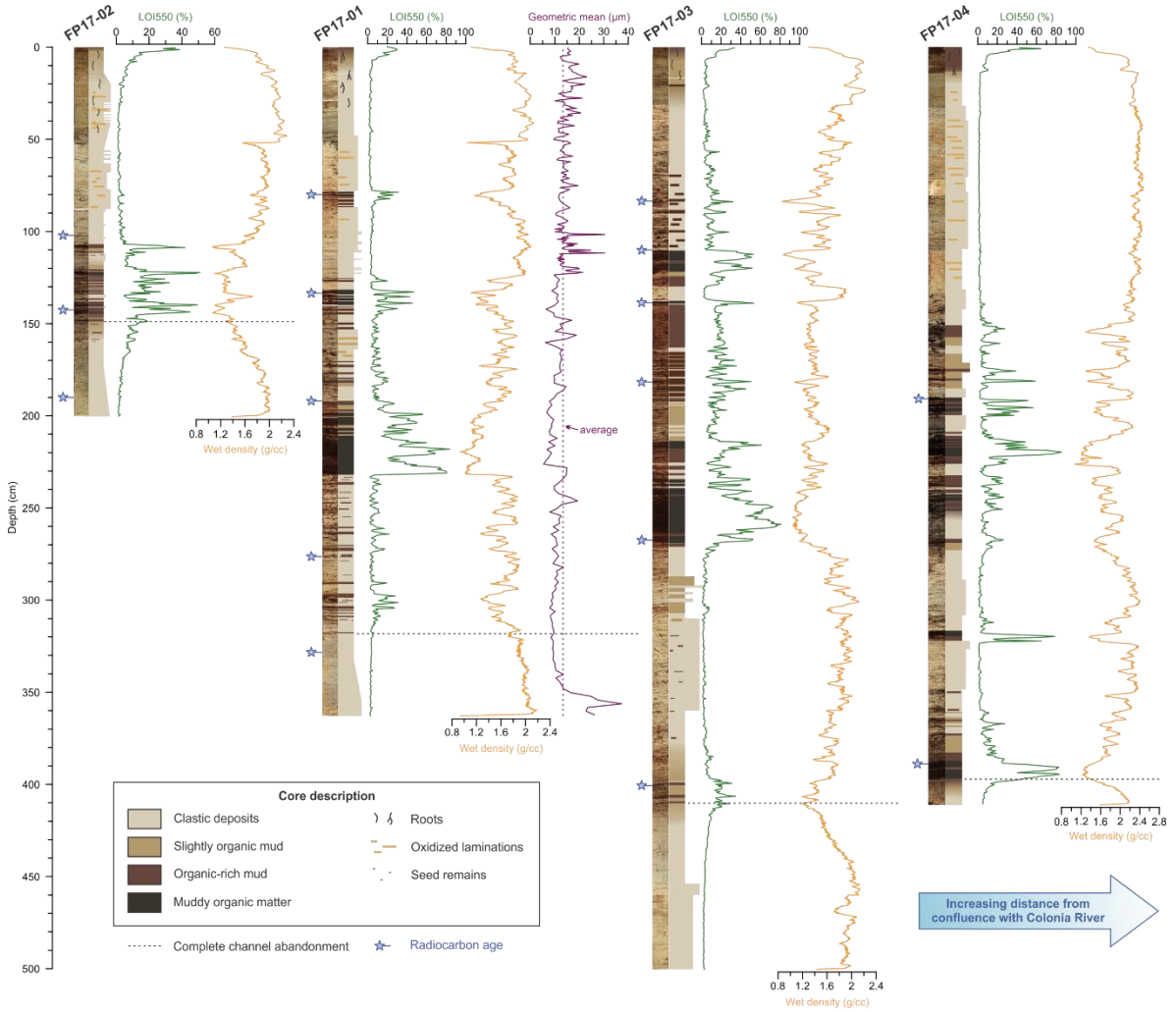

Figure 6.3. Lithology of composite sediment cores FP17-02, FP17-01, FP17-03, and FP17-04, i.e., organized with increasing distance from the confluence with the Colonia River (see Fig. 2a). Photographs are on the left, next to the lithologs. For all cores, LOI550 and wet density are displayed. For FP17-01, the geometric grain-size mean and its average value for the core (dashed purple line) are also shown. Horizontal dashed black lines represent the start of the occurrence of autochthonous sedimentation and are defined at depths of 149, 318, 411, and 397 cm for FP17-02, FP17-01, FP17-03, and FP17-04, respectively.

The upper part of all four cores is composed of clastic sediments (Fig. 6.3). The uppermost 10 to 20 cm, however, consists of modern soil, with LOI550 values increasing from bottom to top in the upper 10 cm. Root remains are visible down to a depth of 50 cm (Fig. 6.3). Discoloration by oxidation is abundant in the upper 45 cm and between 65 and 90 cm depth in FP17-02, and in the upper 130 cm in FP17-04. Three of the four cores, i.e., FP17-02, FP17-01, and FP17-03, display a fining upward trend at the bottom, from coarse sand towards silt. Grain-size measurements confirm this fining upward trend at the bottom of core FP17-01 (Fig. 6.3). These grain-size measurements also show that FP17-01 sediments mainly correspond to unimodal silt with a mean grain size of 13.4 ± 4.2 µm (1σ; Fig. S6B). In general, sediments are slightly coarser towards the top of the core. Coarser cm-thick silt layers can be found at a depth of 100 to 123 cm in FP17-01, where mean grain-size reaches up to 30 µm. Muddy organic matter deposits can be found in FP17-01 and FP17-03 between 200 and 230 cm, and 230 and 270 cm, respectively. In FP17-04, muddy organic matter deposits occur from 190–200 cm, 210–215 cm, 230–250 cm, and 380–400 cm. In FP17-02, two one-cm thick layers of muddy organic matter are found at 123 and 140 cm.

6.1.2. Age-depth models

^{210}Pb could not be used to establish core chronologies as unsupported ^{210}Pb activities could not be detected in most of the samples below the surface (Tables S6B and S6C). This suggests that the upper 10 cm of the sediment cores represent more than 150 years of sedimentation, which is supported by the relatively high organic content of these samples (Fig. 6.2), indicative of a period of slow sediment accumulation that promoted soil development. Likewise, charcoal concentrations are strongly related to organic matter content and likely represent pre-historical fire events, and thus could not be used to develop core chronologies by comparison with historical fire occurrences (Fig. S6C). The age-depth models were therefore entirely based on radiocarbon ages (Fig. 6.4). They reveal that the bottom of FP17-01, FP17-02, FP17-03, and FP17-04 reach ages of 2690 ± 251, 1465 ± 133, 3176 ± 235, and 2890 ± 225 cal yr BP, respectively (Fig. 6.4). The average sedimentation rates of the four cores are very consistent and vary between 0.13 and 0.16 cm/yr.

6.1.3. Suspended sediment concentrations

The Baker River near its source has very low SSC (1.4 ± 1.0 mg/L; Fig. 6.5, Table S6D). On its way to the Valle Grande floodplain, it picks up sediment from rivers Nef (65 ± 20 mg/L), Chacabuco (88 ± 148 mg/l), Cochrane (3.1 ± 1.3 mg/L) and Del Salto (17 ± 16 mg/L). By comparison to these rivers, SSC values in the proglacial Colonia River are significantly higher (226 ± 117 mg/L). Although SSC values during GLOFs are unknown in the Valle Grande area, extreme values of 579 mg/L and 435 mg/L were measured in rivers Chacabuco and Baker after intense precipitation, which is similar to the regular summer values measured in the Colonia River (212 – 525 mg/L). In terms of sediment yield, the Colonia River also displays the highest values, with 0.99 x 10^6 T/y, which is more than double the yield of the Baker River immediately upstream of the confluence with the Colonia River (0.45 x 10^6 T/y; Fig. 6.5).

6.2. Discussion

6.2.1. Sedimentological interpretation

The sedimentary infill of all investigated locations in the Valle Grande floodplain depends strongly on location (Fig. 6.2b). In general, the elevation of the floodplain appears to play an important role in determining the nature of the sedimentary infill. Sites at lower elevation (< 75 m a.s.l., i.e., within 1 m of the regular Baker River level) display continuous clastic infill (mud or mud with graminoids) and are therefore not suited for flood reconstruction, whereas those above 75 m a.s.l. display flood deposits (mud) intercalated within autochthonous sediments (peat or gyttja). Sites at higher elevation are less frequently flooded, which allows autochthonous sedimentation to occur. These locations could thus provide accurate archives of Baker River floods. The four Russian sediment cores are all located at elevations above 75 m a.s.l. and show such alternations of clastic material and organic-rich sediments (Fig. 6.3). As such, they register periods of high-magnitude floods but they do not reveal individual flood layers. Therefore, they allow the reconstruction of periods during which high-magnitude floods were more or less frequent, but they are not suitable to derive quantitative estimates of flood magnitude.

It should also be noted that the sensitivity of the coring sites to flooding most likely decreases through time due to sediment accretion. As sediment deposition progressively increases floodplain elevation, they will less frequently inundate with sediment-laden water (Nanson and Beach, 1977; Hooke, 1995; Saint-Laurent et al., 2010). River erosion also increases the elevation difference between the floodplain and river, resulting in a decrease in the sensitivity of the floodplain to high-magnitude floods through time.

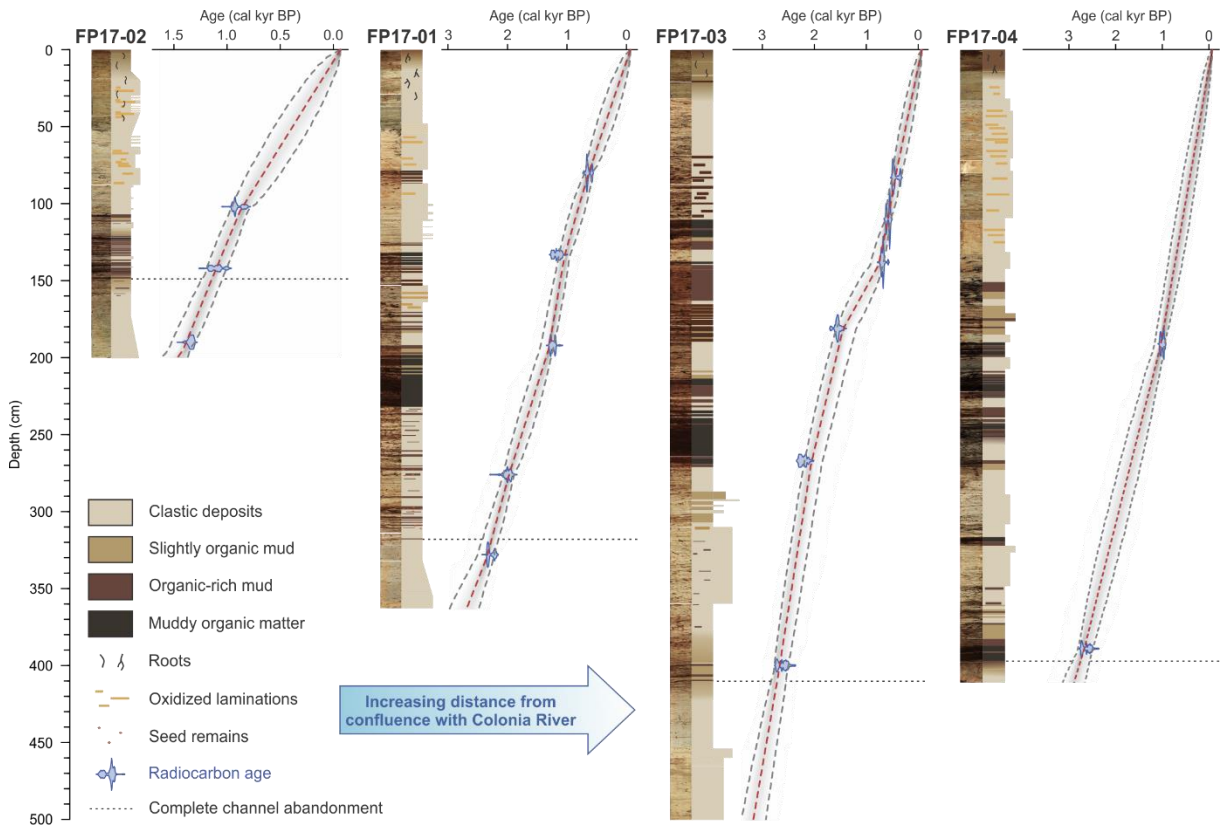

Figure 6.4. Age-depth models and corresponding error envelopes constructed with BACON 2.3.6 (Blaauw and Christen, 2011) for the four sediment cores. The cores are organized by increasing distance from the confluence with the Colonia River.

The base of cores FP17-01, FP17-02, and FP17-03 is composed of fining-upward silts and sands (Fig. 6.3), which indicates a channel abandonment process (Hooke, 1995; Toonen et al., 2012; Dieras et al., 2013). At the very bottom of the cores, coarse sand was most likely deposited during the initial abandonment of the channel, when rapid infill by coarse river bedload occurs. The overlying fining-upward deposits represent the channel being progressively cut off from the main active channel, which resulted in the deposition of a finer suspended load consisting of mud, due to the gradually decreasing flow velocities within the channel (Toonen et al., 2012). This lithological transition from coarse sand towards a finer silt fraction is absent in FP17-04 as the bottom of the channel infill was most likely not reached during coring (Fig. 6.3).

The deposits above these channel silts and sands are composed of (a) clastic alluvial material alternating with (b) organic-rich deposits containing variable amounts of autochthonous organic matter (Fig. 6.3). These alternations are interpreted as flood (clastic) deposits intercalated in-between marsh-type (organic-rich) sediments that accumulate during periods of quiescence. Such laminated channel-fill sequences represent intermittent phases of flooding from the Baker River and indicate that a paleochannel reached the stage of disconnection (Toonen et al., 2012). When clastic sediment input is reduced during periods of quiescence, organic-rich (high LOI550) material can accumulate (Fig. 6.3). On the other hand, dense, organic-poor (low LOI550) sedimentation prevails during periods of flooding. The oxidized laminations in these sediments are most likely the result of redox reactions due to fluctuations in the water table (Fig. 6.3).

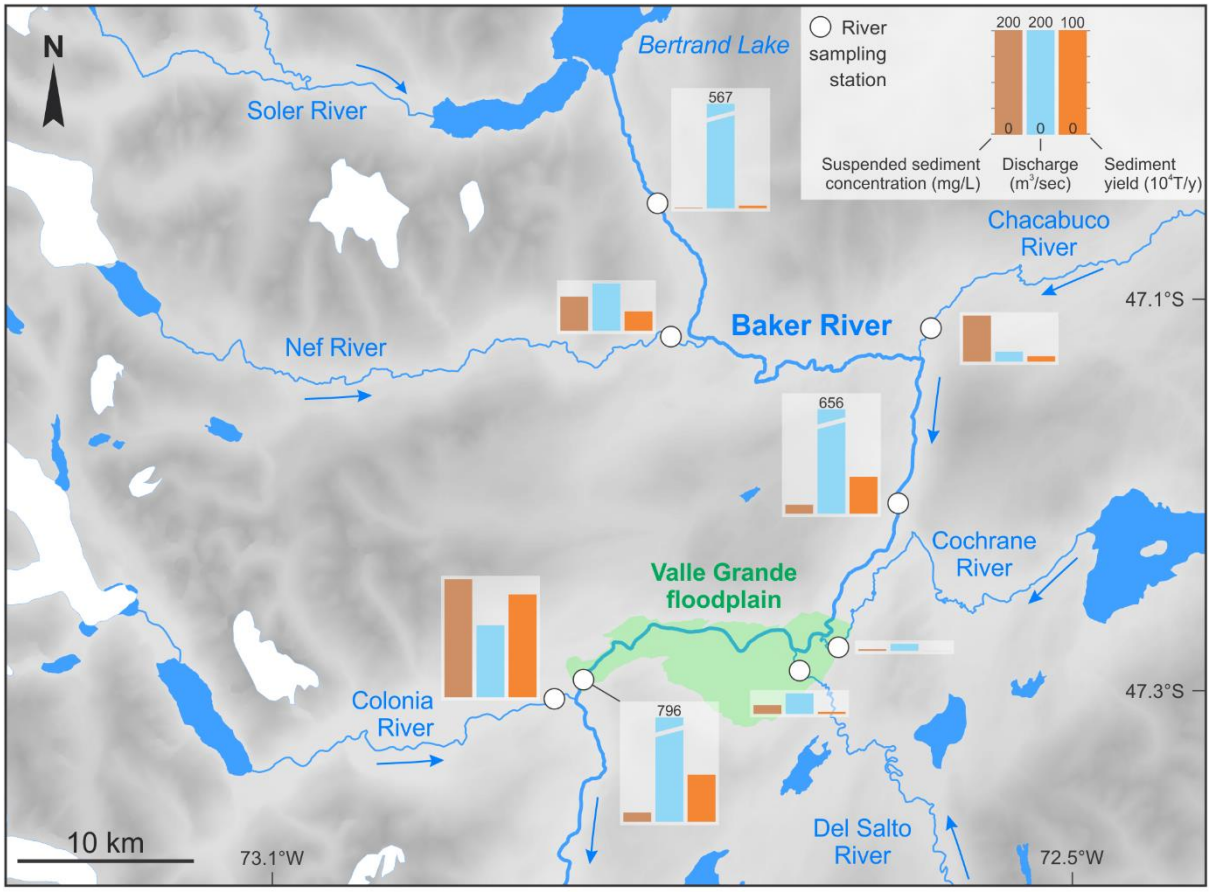

Figure 6.5. Suspended sediment concentrations (SSC), river discharge and sediment yield in the Baker River tributaries around Valle Grande and along the Baker River itself. The SSC (n per site = 8–21) and river discharge (from Dussaillant et al., 2012) values are annual averages. The values are presented in appendix (Supplementary Table S6D).

6.2.2. Flood reconstruction

Changes in sedimentology, more particularly fluctuations in the delivery of clastic material from the Baker River, are reflected by changes in LOI550 values. The input of inorganic alluvial material during flooding results in a decrease in the relative amount of organic matter, i.e., in LOI550. Consequently, the amount of inorganic material (100%–LOI550) presents a proxy for flood occurrence (e.g. Ishii et al., 2017). A flood reconstruction for each sediment core is inferred from the variations in inorganic material, which allows an evaluation of flood occurrence through time (Fig. 6a–d). For all cores, the start of the flood record is defined at the onset of the laminated channel-fill sequence, where organic-rich sedimentation starts to occur after disconnection from the Baker River is completed (Fig. 6.3). For FP17-02, FP17-01, FP17-03, and FP17-04, the onset of the flood record corresponds to 1.14 ± 0.10 cal kyr BP, 2.27 ± 0.14 cal kyr BP, 2.72 ± 0.14 cal kyr BP, and 2.75 ± 0.18 cal kyr BP, respectively (Fig. 6.4).

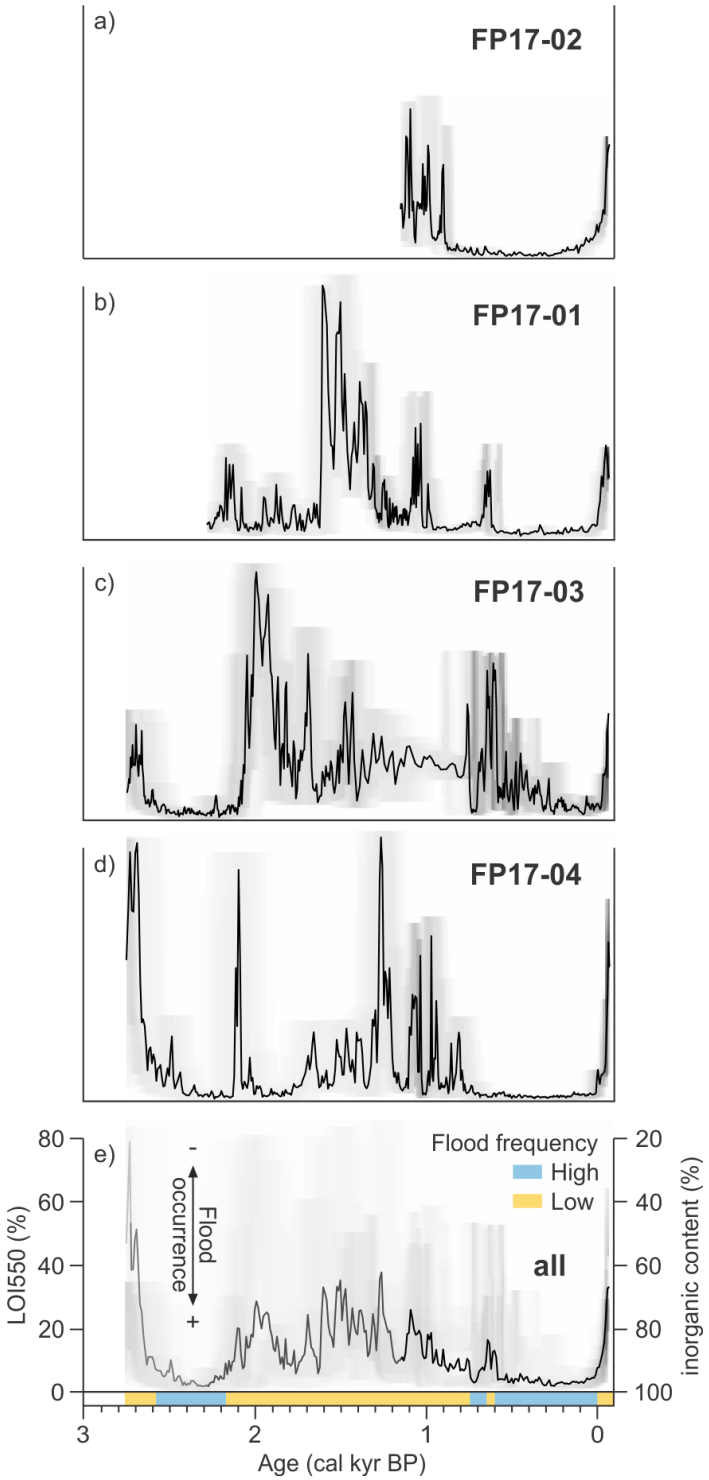

Figure 6.6. LOI550 and inorganic content (100%–LOI550) versus time for the four floodplain sediment cores **(a–d)**, plotted using the 'proxy-ghost' function of BACON 2.3.6 to visualize chronological uncertainties (Blaauw and Christen, 2011). Darker grey indicates higher probability. The lowermost graph **(e)** displays a composite curve based on the four records presented above. The grey level intensity of the solid line in the lowermost graph, represents the number of cores used to build the composite, darker corresponding to more cores.

To account for local variations in the sediment infill, including possible hiatuses, an average of the inorganic content of the four cores was established (Fig. 6.6e). The composite record, which dates back to 2.75 cal kyr BP, uses the age-depth models independently established for each core and is not based on lithological correlations. Two categories of flooding frequency can be defined in the composite

record: high flood frequency (inorganic content >90%) and low flood frequency (inorganic content <90%). The results (Fig. 6.6e) reveal that flooding occurred throughout the past 2.75 cal kyr BP. However, two phases of high flood frequency occur between 2.57 and 2.17 cal kyr BP and between 0.75 and 0 cal kyr BP. Except for isolated peaks in LOI550 in FP17-01 and FP17-03 around 0.62 cal kyr BP, these two periods of increased flooding appear in all records. Two main periods of low flood frequency are present: a first one between c. 2.75 and 2.57 cal kyr BP, and a second between c. 2.17 and 0.75 cal kyr BP. It should be noted that both FP17-01 and FP17-04 show high flood activity between 2.17 and 1.70 cal kyr BP, whereas this time window is marked by high LOI550 values, and thus low flood activity, in FP17-03. Likewise, the most recent period of high flood frequency seems to start later in FP17-03 than in the other sediment cores, suggesting a lower sensitivity of this specific site, in agreement with its particularly high elevation (6 m above the regular Baker River level). Despite apparent short increases in flooding around 1.80 and 1.15 cal kyr BP, the intermediate low flood frequency period between 2.17 and 0.75 cal kyr BP is consistent throughout all records. This period corresponds to the period identified as stable (dated at 2.5–0.6 cal kyr BP) in the stratigraphic record of Benito et al. (2014) below the confluence with the Colonia River.

6.2.3. Origin of the floods recorded in Valle Grande sediments

The input of inorganic material to the Valle Grande floodplain predominantly occurs by overbank flooding from the Baker River. The southern part of the floodplain could also be inundated by floods from the Del Salto River, but these would only be recorded in FP17-01, and possibly FP17-04 (Fig. 6.2). Historical information shows that both GLOFs and extreme precipitation floods can result in the inundation of Valle Grande. However, these two types of events may not leave the same signature in the sediment record.

Suspended sediment concentrations, and therefore the ability of the Valle Grande floodplain to record paleofloods, highly differ between GLOFs and precipitation-driven floods. Because the floodplain is located along the upper reaches of the Baker River, i.e., upstream of the confluence with most proglacial rivers (Fig. 1a), Baker River suspended sediment concentrations along the floodplain are generally very low (17 ± 17 mg/L; n = 18; Fig. 6.5). SSC at the outflow of the Colonia River, on the other hand, are much higher, i.e., 226 ± 117 mg/L (Fig. 6.5). Although SSC in other regional nonglacial rivers, such as Chacabuco, are not negligible, these rivers have a relatively low discharge year-round, resulting in low sediment yields (Fig. 6.5). Floods occurring during intense precipitation events might thus not supply sufficiently large amounts of clastic sediment to the floodplain to be registered as clear flood deposits, especially when compared to GLOFs, which are rich in suspended sediment of glacial origin. This is supported by observations made during some of the 21st century Cachet 2 GLOFs, during which SSC in the Baker River increased 8-fold downstream of the Colonia River confluence (Quiroga et al., 2011; Bastianon et al., 2012).

Historical information (Supplementary Table S6A) and recent aerial photographs (Fig. 6.1c and d) describe that the flow of the Baker River reverses during Colonia River GLOFs over a distance of up to 15 km upstream of the confluence with the Colonia River, thereby supplying glacial material from the Colonia River to the Valle Grande floodplain. In addition, GLOFs are the only events that are able to inundate the entire floodplain (De Agostini, 1945). Precipitation-driven floods only inundate the lower elevation areas (Fig. 6.1b). GLOFs also appear to occur more frequently than precipitation-driven floods in this glacierized region, as suggested by the high amount of GLOFs (21) versus precipitation-driven

floods (1) that affected Valle Grande between 2008 and 2019, and they result in consistently higher (~1 m higher) Baker River levels immediately downstream of the confluence with the Colonia River.

Most of the sediment cores from Valle Grande contain cm-thick coarse silt layers at variable depth intervals (100–123 cm in FP17- 01, 30–40 cm and 56–61 cm in FP17-02, and between 290 and 300 cm in FP17-03; Fig. 6.3). These deposits could result from higher magnitude floods, such as those originating upstream of the floodplain (e.g. from the Nef or Chacabuco rivers), as higher magnitude floods generally carry coarser particles. However, these layers could also represent meandering of the Baker River channel. Migration of the active river towards a coring site, or any change in the configuration of the floodplain that affects the connectivity between the river and a coring location (e.g. erosion of alluvial ridges that act as barriers for alluvial sediment transport), could increase the sensitivity of a site to floods. Eventually, this could cause a sudden increase in clastic input (e.g. Minderhoud et al., 2016) or the deposition of coarser sediments (e.g. Toonen et al., 2015) at one specific site. The absence of sand layers in core FP17-04 and the asynchronicity of these clastic layers in the three other cores favor this hypothesis. The influence, however, of any spatial variations in sediment deposition within the floodplain is minimized by reconstructing the flood history from the composite record, which is based on four different coring sites.

The consistently unimodal grain-size distributions throughout core FP17-01 (Supplementary Fig. S6B) suggest that the clastic sediments represent one dominant depositional process (Fig. 6.3). Although the relatively low mean grain size throughout core FP17- 01 (10–15 mm; Fig. 6.3) is compatible with a glacial origin of the sediment, it could also reflect non-glacial overbank flooding. The FP17-01 grain-size record also reveals a slight coarsening upward, which is particularly marked in the upper ~50 cm (~400 years) of the core. This suggests increased connectivity with the active river channel, although the nearest meander appears to be moving away from site FP17-01 (Fig. 6.2). Another explanation is that this increase in grain size during the last 400 years represents higher magnitude floods. This is supported by the identification of at least three GLOF deposits younger than 0.6 kyr BP in the stratigraphic record of Benito et al. (2014), which is located immediately downstream of the Colonia-Baker confluence. Since the latter site has a much higher flood sensitivity threshold (higher censoring level), this observation suggests that the upper deposits of site FP17-01 represent GLOFs of particularly high magnitude.

An important observation is that none of the sediment cores show particularly inorganic-rich deposits in the last decade (the upper 1–2 cm), although the floodplain was clearly inundated due to Colonia GLOFs several times between 2008 and 2017 (Fig. 6.1c and Supplementary Fig. S6A). Instead, the top of the records displays an apparent increase in LOI550 in the upper 10 cm (Figs. 6.3 and 6.6), suggesting that the magnitude of these GLOFs may have been too low to deposit large amounts of glacial material in the floodplain. This is supported by historical observations (Supplementary Table S6A; Oportus, 1928; De Agostini, 1945) that indicate that only the pre-1960 GLOFs, which were of higher magnitude than those of the 21st century, were able to inundate the entire floodplain. Consequently, it is likely that, at the selected, relatively elevated, coring sites, the floodplain only registers the highest magnitude GLOFs. Taken together, these observations suggest that the clastic fraction of the sediment cores collected in in the Valle Grande floodplain mostly represents high-magnitude glacial floods. The composite record (Fig. 6.6e) is therefore considered to represent the regional GLOF history, although precipitation-driven floods could also contribute to some extent to short-term changes in the sediment record, particularly at the base of the records.

6.2.4. Comparison with glacier and climate reconstructions

6.2.4.1. Relationship with glacier variability

The Baker River is predominantly fed by meltwater from outlet glaciers located along the eastern side of the NPI, superimposed on a baseflow from General Carrera Lake (Figs. 6.1a and 6.5). To examine the potential link between high-magnitude GLOF occurrence and changes in glacier mass-balance, the Valle Grande paleoflood record (Fig. 6.7a) was compared to reconstructions of Leones, Soler, Nef, Colonia, Arenales, and Arco glacier variability (Fig. 6.7b). It should be noted, however, that the available data on these glaciers is based on moraine and trimline dating and is therefore limited to reconstructions of maximum glacier advances or stabilization (Harrison and Winchester, 2000; Winchester et al., 2001; Glasser et al., 2002; Harrison et al., 2008; Nimick et al., 2016). These records are inherently discontinuous (moraine dating) and mostly cover short timescales (dendrochronology and lichenometry). Most of these records clearly show the latest advance during Neoglaciation V (Fig. 6.7b) but are too limited to reconstruct the late Holocene variations of these glaciers in detail.

The most complete glacier variability synthesis that covers the entire late Holocene is the timing of Neoglacial advances of Patagonian glaciers defined by Aniya (2013) (Fig. 6.7c). Results indicate that increased flooding coincides with Neoglacial advances III and V. Although the flood record shows a short-lived increase in flood activity c. 1.15 cal kyr BP, no high flood frequency period was registered during Neoglaciation IV. This neoglaciation, however, is not yet firmly confirmed (Aniya, 2013) and its existence is mostly based on chronological evidence from SPI glaciers, which are located c. two degrees of latitude to the south of Valle Grande. The existence of Neoglaciation IV in the NPI is only based on the analysis of two samples, including one of unknown origin, from the Soler Glacier valley (Aniya, 2013). It is therefore plausible that Neoglaciation IV only affected SPI glaciers, which would explain the discrepancy between our paleoflood record and the Aniya chronology for the 1.4–0.8 kyr time window.

An increase in high-magnitude GLOF occurrence during neoglaciations seems in contradiction with the apparent 21st century increase in GLOF frequency that is generally linked to increased glacier retreat and thinning rates (e.g. Iribarren Anacona et al., 2014; Wilson et al., 2018). It is however supported, on multidecadal timescales, by oral history and ethnographic records that clearly describe that the Colonia GLOFs before the 1960s, i.e. when Colonia glacier was larger and thicker (Harrison and Winchester, 2000), were less frequent but of higher magnitude (Supplementary Table S6A). It should also be noted that the GLOFs affecting the Valle Grande floodplain during the last century all initiated from ice-dammed lakes (Fig. 6.1a). In contrast to GLOF risks from moraine-dammed lakes, which increase during periods of glacier retreat (Benn and Evans, 2010), ice-dammed lakes generally form when drainage becomes blocked by advancing ice, leading to an increase in the risk of high-magnitude GLOF occurrence during periods of glacier growth (Round et al., 2017). In the Colonia valley for instance, the existence of the ice-dammed Cachet 2 and Arco lakes have been intermittent through time depending on the position of the Colonia Glacier (Nimick et al., 2016). A similar relation was suggested for the French Alps, where GLOFs originating from glacier-dammed lakes seem to have increased during the LIA (Vivian, 2001). GLOFs during periods of glacier advance could thus be less frequent but of higher magnitude than their modern counterparts. These results therefore suggest that the recent Cachet 2 GLOFs are relatively small compared to the high magnitude GLOFs that occurred during Neoglaciations III and V.

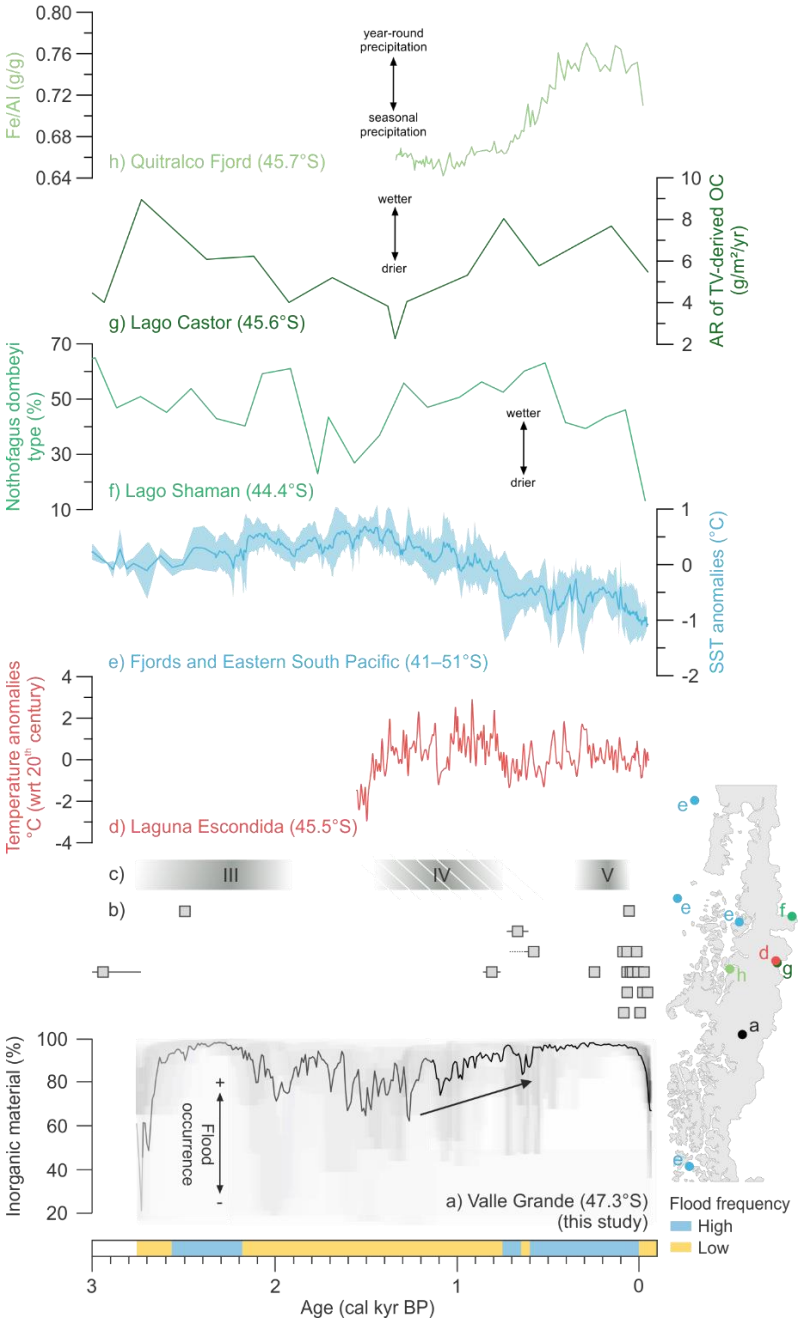

Figure 6.7. Comparison of the composite Valle Grande flood record with regional glacier, temperature, and precipitation proxy records. **(a)** The composite high-magnitude flood frequency record from Valle Grande (this study). **(b)** Glacier advances of (from top to bottom, representing North to South) Leones (Harrison et al., 2008), Soler (Glasser et al., 2002), Nef (Winchester et al., 2001; Nimick et al., 2016), Colonia (Harrison and Winchester, 2000; Nimick et al., 2016), Arenales (Harrison and Winchester, 2000), and Arco (Harrison and Winchester, 2000). **(c)** Neoglacial advances of Patagonian glaciers (Aniya, 2013). Neoglaciation IV is represented using hatching since its existence is not firmly confirmed for the NPI (Aniya, 2013). **(d)** Reconstructed annual temperature anomalies derived from biogenic silica fluxes in Laguna Escondida (45.5°S) (Elbert et al., 2013). **(e)** Sea Surface Temperature (SST) anomalies derived from records along the southern Chilean margin from 41 to 51°S: GeoB3313 (41°S; Lamy et al., 2002), MD07-3093 (44°S; Collins et al., 2019), GeoB7186 (44°S; Mohtadi et al., 2007), and MD07-3124 (51°S; Caniupán et al., 2014). **(f)** Pollen record from Lago Shaman (44.4°S; de Porras et al., 2012). **(g)** Accumulation rate of terrestrial vegetation-derived organic carbon in Lago Castor (45.6°S; Fiers et al., 2019). **(h)** Fe/Al of core PC29A from Quitralco Fjord (45.7°S) used as a proxy for precipitation seasonality (Bertrand et al., 2014). The inset map indicates the location of the different proxy records presented in the figure.

6.2.4.2. Relationship with temperature

Due to the steep longitudinal climatic gradient that occurs in Patagonia (Garreaud et al., 2013), glacier fluctuations at the western and eastern sides of the NPI tend to differ. Indeed, several studies suggest that precipitation is the primary factor driving glacier dynamics on the western side of the icefield, whereas temperature plays a more important role on the eastern side (e.g. Warren and Sugden, 1993; Hulton et al., 1994; Aniya et al., 1997; Bertrand et al., 2012). As the Baker River drains most of the eastern side of the NPI, regional glacier dynamics is believed to be primarily controlled by ablation, which is in turn driven by (summer) temperature. Multi-decadal to millennial-scale changes in temperature could therefore have indirectly affected GLOF occurrence.

Terrestrial records of temperature are rather scarce around 45–48°S in Chilean Patagonia, and most cover shorter timescales (centuries) compared to our 2.75 kyr-long GLOF record (Neukom et al., 2011; Elbert et al., 2013). On the contrary, sea surface temperature (SST) reconstructions are more abundant and often date back thousands of years. SSTs are however less representative of the regional atmospheric temperature conditions that drive changes in ablation rates.

The regional reconstruction of annual air temperature anomalies derived from biogenic silica fluxes in Laguna Escondida (Elbert et al., 2013) shows a decrease in temperature during the last 750 years, coeval with the last period of increased flood occurrence (Fig. 6.7d). Likewise, the gridded summer surface air temperature reconstructions of Neukom et al. (2011) only cover the last 1000 years, but the grid cell encompassing the Valle Grande floodplain shows a significant drop in temperature around 0.55 cal kyr BP that corresponds in timing to the shift towards increased flooding during the last 600 years.

Comparison with SST reconstructions along the southern Chilean margin (Lamy et al., 2002; Mohtadi et al., 2007; Sepúlveda et al., 2009; Caniupán et al., 2014; Collins et al., 2019) shows that, in general, increased flooding occurs during periods of lower-than average SST (Fig. 6.7e). In particular, the cooling transition between 0.90 and 0.60 cal kyr BP strongly coincides with a transition towards increased flood occurrence. Higher flood occurrence at 2.57–2.17 cal kyr BP also corresponds to lower-than-average SST values before 2.2 cal kyr BP (Fig. 6.7e). These comparisons therefore tend to show that the frequency of high-magnitude GLOFs tends to increase during colder periods, which may have been responsible for NPI glacier advances during Neoglaciations III and V.

6.2.4.3. Relationship with precipitation

As mentioned above, the influence of precipitation on flood occurrence in the Baker River basin could be two-fold. First, extreme precipitation events could induce flooding of the Baker River by direct run-off. The magnitude of these flooding events however appears much smaller than GLOFs, and their signature in our Valle Grande sediment cores is probably not as significant as high-magnitude GLOFs. Second, long-term increases in precipitation could contribute to regional glacier advances and therefore be partly responsible for the glacier advance – frequent high-magnitude GLOF relationship put forward in section 6.5.4.1.

Late Holocene flood reconstructions are almost inexistent in Chilean Patagonia and the only existing precipitation reconstructions in the Baker watershed are based on pollen records (Villa-Martínez et al., 2012; McCulloch et al., 2017). We therefore compared the Valle Grande paleoflood record to previously published precipitation proxy records to assess the relation between centennial-to-millennial variations in precipitation and high-magnitude flood occurrence. For the last 3000 years, these pollen records are dominated by *Nothofagus dombeyi*-type, indicating the persistence of humid-temperate conditions,

without any significant change. The only records that do show variations during the late Holocene are located 2–3° of latitude to the north. The pollen record of Lago Shaman (de Porras et al., 2012, Fig. 6.7f), for example, shows high-amplitude variability during the late Holocene, likely because it is located near the forest-steppe ecotone. In general, the periods of high flood occurrence at 2.57–2.17 cal kyr BP and at 0.75–0 cal kyr BP coincide with wetter conditions inferred from the pollen assemblages (Fig. 6.7f). There is, however, a mismatch during the last 500 yrs, during which floods are frequent when the Lago Shaman record indicates a transition towards drier conditions. In contrast, the Lago Castor sediment record (Fiers et al., 2019) shows increased precipitation from 2.8 to 2.2 cal kyr BP but also during the last 800 years (Fig. 6.7g). These two wet periods correspond remarkably well to periods of high flood occurrence derived from the Valle Grande sediment cores. Finally, the increase in year-round precipitation during the last 800 years is also clearly marked in the Quitralco Fjord sediment record on the western side of the NPI (Fig. 6.7h; Bertrand et al., 2014). These comparisons therefore suggest that high-magnitude GLOFs are more frequent during periods of higher year-round precipitation.

6.2.4.4. Link between GLOF occurrence and climate and glacier variability

The results presented above suggest that high-magnitude GLOFs in Valle Grande were more frequent during Neoglaciations III (2.8–2.0 cal kyr BP) and V (17^{th}–19^{th} centuries). These two periods are characterized by lower-than-average temperatures and wetter conditions, suggesting a link between climate and glacier variability, i.e. cold and wetter conditions result in a positive glacier mass balance. Although flooding caused by extreme precipitation can lead to the deposition of clastic material, the majority of the flood deposits evident in the sediment cores from Valle Grande likely represent high-magnitude GLOFs that increased in frequency during glacier advances. These results do not contradict the observation that the 21^{st} century increase in Cachet 2 GLOFs coincides with glacier retreat, but they suggest that, on longer timescales, GLOFs are of higher magnitude when glaciers are larger and thicker. This relation between larger glaciers and increase in the frequency of high-magnitude GLOFs during the late Holocene is supported by (1) historical information that indicates the presence of high-magnitude GLOFs during the first half of the 20th century; (2) the fact that larger glaciers are able to restrain larger water bodies, which in turn results in higher magnitude GLOFs when the dam fails; and (3) similar observations made on shorter timescales in the European Alps and in the Chinese Karakoram (Vivian et al., 2001; Round et al., 2017). Although the frequency of GLOFs in the Baker River watershed is currently high, the magnitude of these events appears significantly lower than those that occurred during periods of glacier advance during the late Holocene. Our results therefore suggest that the probability that a high-magnitude GLOF occurs decreases as glaciers thin and retreat.

6.3. Conclusions

The Valle Grande floodplain contains a continuous record of flood activity during the last 2.75 kyr. Our results show that elevation in the floodplain plays a major role in controlling the sediment infill. Sites at low elevation are dominated by relatively homogeneous clastic deposits and are therefore not suited for flood reconstruction. Sites at higher elevations, on the other hand, display channel-fill sequences where autochthonous organic-rich sedimentation alternates with flood deposits (clastics). These sites are the most promising in terms of flood archives. They register high-magnitude floods without being affected by minor events. Sedimentological and historical information suggest that the majority of the flood deposits recorded in Valle Grande represent high-magnitude GLOFs.

Our results indicate that high-magnitude GLOFs occurred intermittently over the last 2.75 kyr and that their frequency was particularly high between c. 2.57–2.17 cal kyr BP, and c. 0.75–0 cal kyr BP. These

two periods of high flood frequency correspond to Neoglacial advances III and V, suggesting a strong relationship between glacier advance and GLOF occurrence. Since these glacier advances seem to result from lower-than-average temperatures and wetter conditions, our results suggest a close, indirect, link between climate variability and GLOF occurrence. The recent period of increased flooding between 0.75 and 0 cal kyr BP specifically coincides with the colder and wetter conditions that resulted in the advance of Patagonian glaciers in the 15^{th}–19^{th} centuries.

Overall, our study suggests that high-magnitude GLOFs from eastern NPI glaciers occur more frequently when glaciers are larger and thicker. This relation likely reflects the ability of larger glaciers to form larger and stronger ice dams, which are in turn able to hold larger lakes. Although lake outbursts may be less frequent under these conditions, our results suggest that when they occur, they generate higher magnitude floods. These results do not contradict the apparent increase in GLOF frequency during the last decades but they suggest that, on multi-centennial timescales, GLOF are of higher magnitude when glaciers are larger. These results emphasize the need to consider different timescales when researching natural hazards, and they support the use of geological archives to complement monitoring data for proper flood hazard assessment. Based on these results, we suggest that the probability that a high-magnitude GLOF occurs decreases as glaciers thin and retreat.

Acknowledgements

We thank Eleonora Crescenzi Lanna, Loïc Piret, and Francois De Vleeschouwer for assistance in the field. Elie Verleyen and Wim Vyverman are thanked for providing the Russian corer. We are also grateful to Olaf Wuendrich for shipping samples and equipment back to Belgium. We would like to thank Horacio Parrague, Andrés Rivera, and Paulina Rojas for providing the aerial photographs shown in Fig. 6.1. Atun Zawadzki is thanked for conducting the ^{210}Pb analyses. We are grateful to Benjamin Amann, Dawei Liu and Loïc Piret for their valuable input. We thank Varyl Thorndycraft and one anonymous reviewer for providing comments that improved an earlier version of this manuscript. The research presented here was funded by the Flemish Research Foundation (FWO, Belgium; project Paleo-GLOFs G0D7916N).

References

Alvarez-Garreton, C., Mendoza, P.A., Boisier, J.P., Addor, N., Galleguillos, M., Zambrano-Bigiarini, M., Lara, A., Puelma, C., Cortes, G., Garreaud, R., McPhee, J., and Ayala, A. (2018) The CAMELS-CL dataset: catchment attributes and meteorology for large sample studies – Chile dataset. *Hydrology and Earth System Sciences*, **22**, 5817 – 5846.

Aniya, M. (1995) Holocene glacial chronology in Patagonia: Tyndall and Upsala glaciers. *Arctic Antarctic Alpine Research*, **27**, 311 – 322.

Aniya, M. (1996) Holocene variations of Ameghino Glacier, southern Patagonia. *The Holocene*, **6**, 247 – 252.

Aniya, M., Sato, H., Naruse, R., Skvarca, P., and Casassa, G. (1997) Recent glacier variations in the South Patagonian Icefield, South America. *Arctic and Alpine Research*, **29**, 1 – 12.

Aniya, M. (2013) Holocene glaciations of Hielo Patagónico (Patagonia Icefield), South America: A brief review. *Geochemical Journal*, **47**, 97 – 105.

Aniya, M. (2017) Glacier variations of Hielo Patagónico Norte, Chile, over 70 years from 1945 to 2015. *Bulletin of Glaciological Research*, **35**, 19 – 38.

Bastianon, E., Bertoldi, W., and Dussaillant, A. (2012) Glacial-lake outburst flood effects on Colonia River morphology, Chilean Patagonia. River Flow 2012, CRC Press, 573 – 579.

Benito, G., Thorndycraft, V.R. (2020). Catastrophic glacial-lake outburst flooding of the Patagonian Ice Sheet. *Earth-Science Reviews,* **200**, 102996.

Benito, G., Thorndycraft, V.R. Machado, M.J., Sancho, C., Dussaillant, A., and Meier, C.I. (2014). Magnitud y frecuencia de inundaciones Holocenas generadas por vaciamiento de lagos glaciares en el Rio Baker, Campo de Hielo, Patagonico Norte, Chile. In: Schnabel, S., Gutiérrez, Á.G. (Eds.), Sociedad Española de Geomorfología. Cáceres, Spain, pp. 24–27.

Benn, D.I., and Evans, D.J.A. (2010) Glaciers and glaciation. 2nd edition. Hodder education, London, 802 pp.

Bertrand, S., Hughen, K.A., Lamy, F., Stuut, J.-B. W., Torrejón, F., and Lange, C.B. (2012) Precipitation as the main driver of Neoglacial fluctuations of Gualas glacier, Northern Patagonian Icefield. *Climate of the Past*, **8**, 519 – 534.

Bertrand, S., Hughen, K., Sepúlveda, J., and Pantoja, S. (2014) Late Holocene covariability of the southern westerlies and sea surface temperature in northern Chilean Patagonia. *Quaternary Science Reviews*, **105**, 195 – 208.

Blaauw, M. (2010) Methods and code for 'classical' age-modelling of radiocarbon sequences. *Quaternary Geochronology*, **5**, 512 – 518.

Blaauw, M., and Christen, J.A. (2011) Flexible paleoclimate age-depth models using an autoregressive gamma process. *Bayesian Analysis*, **6**, 457 – 474.

Caniupán, M., Lamy, F., Lange, C.B., Kaiser, J., Kilian, R., Arz, H.W., León, T., Mollenhauser, G., Sandoval, S., De Pol-Holz, R., Pantoja, S., Wellner, J., and Tiedemann, R. (2014) Holocene sea-surface temperature variability in the Chilean fjord region. *Quaternary Research*, **82**, 342 – 353.

Carrivick, J.L., and Quincey, D.J. (2014) Progressive increase in number and volume of ice-marginal lakes on the western margin of the Greenland Ice Sheet. *Global and Planetary Change*, **116**, 156 – 163.

Carrivick, J.L., and Tweed, F.S. (2016) A global assessment of the societal impacts of glacier outburst floods. *Global and Planetary Change*, **144**, 1 – 16.

Collins, J.A., Lamy, F., Kaiser, J., Ruggieri, N., Henkel, S., De Pol-Holz, R., Garreaud, R., and Arz, H.W. (2019) Centennial-scale SE Pacific sea surface temperature variability over the past 2,300 years. *Paleoceanography and Paleoclimatology*, **34**, 336 – 352.

Davies, B.J., and Glasser, N.F. (2012) Accelerating shrinkage of Patagonian glaciers from the Little Ice Age (~AD 1870) to 2011. *Journal of Glaciology*, **58** (212), 1063 – 1084.

Davies, B.J., Darvill, C.M., Lovell, H., Bendle, J.M., Dowdeswell, J.A., Fabel, D., García, J.-L., Geiger, A., Glasser, N.F., Gheorghiu, D.M., Harrison, S., Hein, A.S., Kaplan, M.R., Martin, J.R.V., Mendelova, M., Palmer, A., Pelto, M., Rodés, Á., Sagredo, E.A., Smedley, R.K., Smellie, J.L., and Thorndycraft, V.R. (2020) The evolution of the Patagonian Ice Sheet from 35 ka to the present day (PATICE). *Earth-Science Reviews*, **204**, 103152.

De Agostini, A.S.S. (1945) Andes Patagónicos, Viajes de exploración a la Cordillera Patagónica Austral. Segunda edición aumentada y corregida. Buenos Aires. 436 pp.

De Porras, M.E., Maldonado, A., Abarzúa, A.M., Cáardenas, M.L., Francois, J.P., Martel-Cea, A., Stern, C.R., Méndez, C., and Reyes, O. (2012) Postglacial vegetation, fire and climate dynamics at Central Chilean Patagonia (Lake Shaman, 44°S). *Quaternary Science Reviews*, **50**, 71 – 85.

Dieras, P.L., Constantine, J.A., Hales, T.C., Piégay, H., and Riquier, J. (2013) The role of oxbow lakes in the off-channel storage of bed material along the Ain River, France. *Geomorphology*, **188**, 110 – 119.

Dussaillant, A., Benito, G., Buytaert, W., Carling, P., Meier, C., and Espinoza, F. (2010) Repeated glacial-lake outburst floods in Patagonia: an increasing hazard? *Natural hazards*, **54**, 469 – 481.

Dussaillant, A., Buytaert, W., Meier, C., and Espinoza, F. (2012) Hydrological regime of remote catchments with extreme gradients under accelerated change: the Baker basin in Patagonia. *Hydrological Sciences Journal*, **57** (8), 1530 – 1542.

Elbert, J., Wartenburger, R., von Gunten, L., Urrutia, R., Fischer, D., Fujak, M., Hamann, Y., Greber, N.D., and Grosjean, M. (2013) Late Holocene air temperature variability reconstructed from the sediments of Laguna Escondida, Patagonia, Chile (45°30'S). *Palaeogeography, Palaeoclimatology, Palaeoecology*, **369**, 482 – 492.

Fick, S.E., and Hijmans, R.J. (2017) WorldClim 2: new 1-km spatial resolution climate surfaces for global land areas. *International Journal of Climatology*, **37**, 4302 – 4315.

Fiers, G., Bertrand, S., van Daele, M., Granon, E., Reid, B., Vandoorne, W., and De Batist, M. (2019) Hydroclimate variability of northern Chilean Patagonia during the last 20 kyr inferred from the bulk organic geochemistry of Lago Castor sediments (45°S). *Quaternary Science Reviews*, **204**, 105 – 118.

Friesen, B.A., Cole, C.J., Nimick, D.A., Wilson, E.M., Fahey, M.J., McGrath, D., and Leidich, J. (2015) Using satellite images to monitor lake outburst floods—Lago Cachet Dos drainage, Chile. U.S. Geological Survey Scientific Investigations Map 3322, scale 1:15,000.

Fuller, I.C., Macklin, M.G., Toonen, W.H.J., and Holt, K.A. (2018) Storm-generated Holocene and historical floods in the Manawatu River, New Zealand. *Geomorphology*, **310**, 102 – 124.

Fuller, I.C., Macklin, M.G., Toonen, W.H.J., Turner, J., and Norton, K. (2019) A 2000 year record of palaeofloods in a volcanically-reset catchment: Whanganui River, New Zealand. *Global and Planetary Change*, 181, 102981.

Garreaud, R., Lopez, P., Minvielle, M., and Rojas, M. (2013) Large-scale control on the Patagonian climate. *Journal of Climate*, 26, 215 – 230.

Glasser, N.F., Hambrey, M.J., and Aniya, M. (2002) An advance of Soler Glacier, North Patagonian Icefield at c. AD 1222–1342. *Holocene,* 12 (1), 113 – 120.

Glasser, N.F., Jansson, K.N., Duller, G.A.T., Singarayer, J., Holloway, M., and Harrison, S. (2016) Glacial lake drainage in Patagonia (13-8 kyr) and response of the adjacent Pacific Ocean. *Scientific Reports* 6, 21064.Harrison, S., and Winchester, V. (2000) Nineteenth- and twentieth century glacier fluctuations and climate implications in the Arco and Colonia valleys, Hielo Patagónico Norte, Chile. *Arctic, Antarctic, and Alpine Research*, 32, 55 – 63.

Harrison, J., Heijnis, H., and Caprarelli, G. (2003) Historical pollution variability from abandoned mine sites, Greater Blue Mountains World Heritage Area, New South Wales, Australia. *Environmental Geology*, 43, 680 – 687.

Harrison, S., Glasser, N., Winchester, V., Haresign, E., Warren, C., Duller, G. A. T., Bailey, R., Ivy-Ochs, S., Jansson, K., and Kubik, P. (2008). Glaciar León, Chilean Patagonia: late-Holocene chronology and geomorphology. *The Holocene*, 18(4), 643 – 652.

Harrison, S., Kargel, J.S., Huggel, C., Reynolds, J., Shugar, D.H., Betts, R.A., Emmer, A., Glasser, N., Haritashya, U.K., Klimeš, J., Reinhardt, L., Schaub, Y., Wiltshire, A., Regmi, D., and Vilímek, V. (2018) Climate change and the global pattern of moraine-dammed glacial lake outburst floods. *The Cryosphere*, 12, 1195 – 1209.

Heiri, O., Lotter, A.F., and Lemcke, G. (2001) Loss on ignition as a method for estimating organic and carbonate content in sediments: reproducibility and comparability of results. *Journal of Paleolimnology*, 25, 101 – 110.

Hogg, A.G., Hua, Q., Blackwell, P.G., Niu, M., Buck, C.E., Guilderson, T.P., Heaton, T.J., Palmer, J.G., Reimer, P.J., Reimer, R.W., Turney, C.S.M., and Zimmerman, S.R.H. (2013) SHCal13 southern hemisphere calibration, 0-50,000 years cal BP. *Radiocarbon*, 55, 1889 – 1903.

Hooke, J.M. (1995) River channel adjustment to meander cutoffs on the river Bollin and river Dane, northwest England. *Geomorphology*, 14, 235 – 253.

Hulton, N., Sugden, D., Payne, A., and Clapperton, C. (1994) Glacier modeling and the climate of Patagonia during the Last Glacial Maximum. *Quaternary Research*, 42, 1 – 19.

IPCC (2019) IPCC Special Report on the Ocean and Cryosphere in a Changing Climate. Intergovernmental Panel on Climate Change, 765 pp.

Iribarren Anacona, P., Mackintosh, A., and Norton, K. P. (2014) Hazardous processes and events from glacier and permafrost areas: lessons from the Chilean and Argentinean Andes, *Earth Surf. Process. Landforms*, 40, 2 – 21.

Ishii, Y., Hori, K., and Momohara, A. (2017) Middle to late Holocene flood activity estimated from loss on ignition of peat in the Ishikari lowland, northern Japan. *Global and Planetary Change*, 153, 1 – 15.

Jacquet, J., McCoy, S.W., McGrath, D., Nimick, D.A., Fahey, M., O'kuinghttons, J., Friesen, B.A., and Leidlich, J. (2017) Hydrologic and geomorphic changes resulting from episodic glacial lake outburst floods: Rio Colonia, Patagonia, Chile. *Geophysical Research Letters*, **44**, 854 – 864.

Jones, A.F., Macklin, M.G., and Brewer, P.A. (2012) A geochemical record of flooding on the upper River Severn, UK, during the last 3750 years. *Geomorphology*, **179**, 89 – 105.

Lamy, F., Rühlemann, C., Hebbeln, D., and Wefer, G. (2002) High- and low-latitude climate control on the position of the southern Peru-Chile Current during the Holocene. *Paleoceanography*, **17**, 1 – 10.

Lara, A., Bahamondez, A., González-Reyes, A., Muñoz, A.A., Cuq, E., and Ruiz-Gómez, C. (2015) Reconstructing streamflow variation of the Baker River from tree-rings in Northern Patagonia since 1765. *Journal of Hydrology*, **529** (2), 511 – 523.

Lenaerts, J.T.M., Van Den Broeke, M.R., Van Wessem, J.M., and Jan Van Den Berg, W. (2014) Extreme precipitation and climate gradients in Patagonia revealed by high-resolution regional atmospheric climate modeling. *Journal of Climate*, **33**, 4607 – 4621.

Lintern, A., Leahy, P.J., Zawadzki, A., Gadd, P., Heijnis, H., Jacobsen, G., Connor, S., Deletic, A., and McCarthy, D.T. (2016) Sediment cores as archives of historical changes in floodplain lake hydrology. *Science of the Total Environment*, **544**, 1008 – 1019.

Masiokas, M.H., Rivera, A., Espizua, L.E., Villalba, R., Delgado, S., and Carlos Aravena, J. (2009) Glacier fluctuations in extratropical South America during the past 1000 years. *Palaeogeography, Palaeoclimatology, Palaeoecology*, **281**, 242 – 268.

Mauquoy, D., Van Geel, B., Blaauw, M., Speranza, A., and van der Plicht, J. (2004) Changes in solar activity and Holocene climatic shifts derived from 14C wiggle-match dated peat deposits. *The Holocene*, **14**, 45 – 52.

McCulloch, R.D., Figuerero Torres, M.J., Mengoni Goñalons, G.L., Barclay, R., and Mansilla, C. (2017) A Holocene record of environmental change from Río Zeballos, central Patagonia. *The Holocene*, **27**(7), 941 – 950.

Mercer, J.H. (1982) Holocene glacier variations in southern South America. *Striae*, **18**, 35 – 40.

Minderhoud, P.S.J., Cohen, K.M., Toonen, W.H.J., Erkens, G., and Hoek, W.Z. (2016) Improving age-depth models of fluvio-lacustrine deposits using sedimentary proxies for accumulation rates. *Quaternary Geochronology*, **33**, 35 – 45.

Mohtadi, M., Romero, O.E., Kaiser, J., and Hebbeln, D. (2007) Cooling of the southern high latitudes during the Medieval Period and its effect on ENSO. *Quaternary Science Reviews*, **26**, 1055 – 1066.

Nanson, G.C., and Beach, H.F. (1977) Forest succession and sedimentation on a meandering-river floodplain, northeast British Columbia, Canada. *Journal of Biogeography*, **4**, 229 – 251.

Neukom, R., Luterbacher, J., Villalba, R., Küttel, M., Frank, D., Jones, P.D., Grosjean, M., Wanner, H., Aravena, J.-C., Black, D.E., Christie, D.A., D'Arrigo, R., Lara, A., Morales, M., Soliz-Gamboa, C., Srur, A., Urrutia, R., and von Gunten, L. (2011) Multiproxy summer and winter surface air temperature field reconstructions for southern South America covering the past centuries. *Climate Dynamics*, **37**, 35 – 51.

Nimick, D.A., McGrath, D., Mahan, S.A., Friesen, B.A., and Leidich, J. (2016) Latest Pleistocene and Holocene glacial events in the Colonia valley, Northern Patagonian Icefield, southern Chile. *Journal of Quaternary Science*, 31(6), 551 – 564.

Oportus, C. (1928) Informe sobre el problema de colonización de la zona del río Baker. Departamento de Tierras y Colonización, Ministerio de Fomento, Santiago de Chile, 120 pp.

Paine, J.L., Rowan, J.S., and Werritty, A. (2002) Reconstructing historic floods using sediment from embanked flood plains: a case study of the River Tay in Scotland. The Structure, Function and Management Implications of Fluvial Sedimentary Systems (Proceedings of an international symposium at Alice Springs, Australia, September 2002). IAHS Publ. 276, 2002.

Paul, F., Kääb, A., and Haeberli, W. (2007) Recent glacier changes in the Alps observed by satellite: Consequences for future monitoring strategies. *Global and Planetary Change*, 56, 111 – 122.

Prakash, C., and Nagarajan, R. (2018) Glacial lake changes and outburst flood hazard in Chandra basin, North-Western Indian Himalaya. *Geomatics, Natural Hazards and Risk*, 9, 337 – 355.

Quiroga, E., Ortiz, P., Gerdes, D., Reid, B., Villagran, S., and Quiñones, R. (2011) Organic enrichment and structure of macrobenthic communities in the glacial Baker fjord, Northern Patagonia, Chile. *Journal of the Marine Biological Association of the United Kingdom*, 92 (1), 73 – 83.

Round, V., Leinss, S., Huss, M., Haemmig, C., and Hajnsek, I. (2017) Surge dynamics and lake outbursts of Kyagar Glacier, Karakoram. *The Cryosphere*, 11, 723 – 739.

Saint-Laurent, D., Lavoie, L., Drouin, A., St-Laurent, J., and Ghaleb, B. (2010) Floodplain sedimentation rates, soil properties and recent flood history in southern Québec. *Global and Planetary Change*, 70, 76 – 91.

Sepúlveda, J., Pantoja, S., Hughen, K.A., Bertrand, S., Figueroa, D., León, T., Drenzek, J., and Lange, C. (2009) Late Holocene sea-surface temperature and precipitation variability in northern Patagonia, Chile. *Quaternary Research*, 72, 400 – 409.

Sernageomin (2003) Mapa geologico de Chile versión digital, scale 1/1.000.000.Tanaka, K. (1980) Geographic contribution to a periglacial study of the Hielo Patagonico Norte with special reference to the glacial outburst originated from Glacier-Dammed Lago Arco, Chilean Patagonia. Centre Co Ltd, Tokyo, 97 pp.

Toonen, W.H.J., Kleinhans, M.G., and Cohen, K.M. (2012) Sedimentary architecture of abandoned channel fills. *Earth Surface Processes and Landforms*, 37, 459 – 472.

Toonen, W.H.J., Winkels, T.G., Cohen, K.M., Prins, M.A., and Middelkoop, H. (2015) Lower Rhine historical flood magnitudes of the last 450 years reproduced from grain-size measurements of flood deposits using End Member Modelling. *Catena*, 130, 69 – 81.

Thorndycraft, V.R., Bendle, J.M., Benito, G., Davies, B.J., Sancho, C., Palmer, A.P., Fabel, D., Medialdea, A., and Martin, J.R.V. (2019) Glacial lake evolution and Atlantic-Pacific drainage reversals during deglaciation of the Patagonian Ice Sheet. *Quaternary Science Reviews*, 203, 102 – 127.

Turner, K.J., Fogwill, C.J., McCulloch, R.D., and Sugden, D.E. (2005) Deglaciation of the eastern flank of the North Patagonian Icefield and associated continental-scale lake diversions. *Geografiska Annaler*, 87A, 363 – 374.

Ulloa, H., Mazzorana, B., Batalla, R.J., Jullian, C., Iribarren-Anacona, P., Barrientos, G., Reid, B., Oyarzun, C., Schaefer, M., and Iroumé, A. (2018) Morphological characterization of a highly-dynamic fluvial landscape: The River Baker (Chilean Patagonia). *Journal of South American Earth Sciences*, **86**, 1 – 14.

Villa-Martínez, R., Moreno, P.I., and Valenzuela, M.A. (2012) Deglacial and postglacial vegetation changes on the Eastern slopes of the central Patagonian Andes (47 °S). *Quaternary Science Reviews*, **32**, 86 – 99.

Vivian, R. (2001) Des Glaciers du Faucigny aux Glaciers de Mont Blanc. La Fontaine de Siloe, Montmelian.

Wang, W., Yao, T., and Yang, X. (2011) Variations of glacial lakes and glaciers in the Boshula mountain range, southeast Tibet, from the 1970s to 2009. *Annuals of Glaciology*, **52**, 9 – 17.

Warren, C.R., and Sugden, D.E. (1993) The Patagonian Icefields: a glaciological review. *Arctic and Alpine Research*, **25**, 316 – 331.

Wessel, B., Huber, M., Wohlfart, C., Marschalk, U., Kosmann, D., and Roth, A. (2018) Accuracy Assessment of the Global TanDEM-X Digital Elevation Model with GPS Data. *ISPRS Journal of Photogrammetry and Remote Sensing*, **139**, 171 – 182.

Wilson, R., Glasser, N.F., Reynolds, J.M., Harrison, S., Anacona, P.I., Schaefer, M., and Shannon, S. (2018) Glacial lakes of the Central and Patagonian Andes. *Global and Planetary Change*, **162**, 275 – 291.

Winchester, V., and Harrison, S. (2000) Dendrochronology and lichenometry: colonization, growth rate and dating of geomorphological events on the east side of the North Patagonian Icefield, Chile. *Geomorphology*, **34**, 181 – 194.

Winchester, V., Harrison, S., and Warren, C.R. (2001) Recent Retreat Glaciar Nef, Chilean Patagonia, dated by lichenometry and dendrochronology. *Arctic, Antarctic, and Alpine Research*, **33**, 266 – 273.

Zhang, G., Bolch, T., Allen, S., Linsbauer, A., Chen, W., and Wang, W. (2019) Glacial lake evolution and glacier-lake interactions in the Poiqu River basin, central Himalaya, 1964–2017. *Journal of Glaciology*, **65**, 347 – 365.

Supplementary Information

Table S6A. Historical evidence of inundation of the Valle Grande floodplain during GLOFs based on (a) interviews conducted by Fernando Torrejón from the 25th until the 31st of January 2019, and (b) written records (in Spanish).

Conversational evidence	
Interviewee	Record
(a) Luzmira Muñoz	*Doña Luzmira nació en 1951 en el sector los Ñadis a orillas del río Baker, cuando ella tenía 9 meses de edad habría ocurrido una "gran crecida del Colonia" (1951 ó 1952), de acuerdo a lo que le habría contado su mamá. Agrega, "en esa crecida se ahogó el papá de Segundo Quinto…, salió a buscar sus ovejas y entonces lo alcanzó la crecida".* *De acuerdo a su relato, cuando ella tenía 6 años (posiblemente en 1957) "se produjo una tremenda creciente del río Colonia que mató muchos animales" y a algunos colonos de la zona. Indica, "siempre había trueno cuando iba a venir la creciente... Venía una avalancha grande y después todo se recogía". Después cuando el Baker retomaba su normalidad "los árboles quedaban todos blanquitos de arenilla", refiriéndose al sedimento que cubría sus ramas y hojas.* *Finalmente relata que "todos los años habían crecidas en el Baker" y después de las crecidas, cuando salían a recolectar calafates (Berberis sp) todas las "matas de calafates estaban de color gris por la tierra", en grandes zonas ribereñas, refiriéndose muy probablemente al fino sedimento glaciar que las cubría después de cada avenida del río. Otro dato interesante entregado por Luzmira es que el sector de la "tapera de Jaque", ubicado a unos 200 ó 300 metros aguas abajo de la confluencia del Colonia en el Baker, "se inundaba completamente".*
(b) Leoncio Escobar Montecino	*A la edad de 30 años (1962), don Leoncio ya trabajaba en Valle Grande "como peón de Enrique Villalobos Ramírez, quien tenía un gran campo allí". Fue en esa época cuando presenció una "inmensa creciente" del río Colonia y Baker "entre el 1 de diciembre y el 5 de enero cuando era la creciente".* *Describe que cuando se producía la inundación "el Baker empezaba a enaltar y se sostenía, subía 10 metros, después 15 metros…, no se notaba la crecida". "En 24 horas se inundaba todo, se tapaba todo el Valle Grande…, el Baker era un sólo lago, hasta la orilla de la pasarela del Salto". (Se trataba de la antigua pasarela que estaba como a 100 metros de la actual pasarela según el mismo comentó). Agrega don Leoncio: "la creciente tenía 1000 metros de anchura cuando reventaba…, salía por arriba y debajo de los nevados…, duró como un mes todo" En este caso se refiere a la avenida del río Colonia.* *"A las 5 (AM) ya se estaba produciendo la creciente, venía un oleaje suave…, una ola tras otra, hasta que venía una grande y arrasaba con todo".*

	Don Leoncio también presenció otras inundaciones del Baker antes y después de 1962, pero éstas, según recuerda, fueron de menor magnitud a la del 62, alcanzando "sólo hasta la mitad del Valle Grande". *Refiriéndose a las crecidas del río Baker, don Leoncio entrega un importante dato, señalando que las crecidas que inundan el Valle Castillo, a continuación de Valle Grande aguas arriba, vienen directamente desde el Baker, posiblemente por avenidas del río Nef.*
(c) Cristián Arratia Vidal	*Don Cristián recuerda crecidas del Baker desde 1955 a la década de 1960, que "tapaban todo el Valle Grande hasta cerca del Valle Castillo, quedaban sólo pedacitos de cercos donde se podían ver los alambres…, lo que agarraba lo mataba todo…, los animales quedaban arriba de los ñirres".* *Menciona que "una gran creciente en los años 1962 ó 1963 inundó todo el sector del lago Vargas", su señora Rosa Vargas, presente en la entrevista, contradice las fechas indicando, con mucha seguridad, que dicha creciente "fue en 1966…".* *Aquella crecida (1966) "tapó todos los campos bajos en el sector de lago Vargas, alcanzando cerca de mi casa" (que corresponde a su actual vivienda muy cercana a la Ruta 7). "Los animales muertos iban quedando melgados por las orillas del Baker…, río abajo del corte, el río arrastraba tremendas palizadas y barro". Después de esta gran crecida del Baker don Cristián cambio su población en el campo de río Ventisquero "como 300 metros más arriba, porque en lo plano se tapa todo con el agua".* *Añade finalmente: "antes de las grandes crecidas el Baker corría más encajonado".*
(d) Arnoldo Agustín Cárdenas	*Don Arnoldo sólo menciona que entre los años 1961-1962 se produjo una "gran creciente del Colonia…, esa inundación se extendía río arriba por el Baker hasta el sector de Valle Grande…, cuando bajaba la creciente, las vacas quedaban enredadas arriba de las lengas y ñires a cinco o seis metros". Añade, "en el sector de Tortel no causó mucho daño".*

Historical documents	
Source	Record
Oportus (1928)	No puede utilizarse para colonización el hermoso mallín de unas 5 mil hectáreas situado entre le Sección La Colonia y la desembocadura del río Cochrane, en el Baker, porque la crecida de este río, que se verifica una vez en al año lo inunda completamente subiendo el agua hasta unos cuatro metros sobre el nivel premanente del río. Esta crecida del río es un fenómeno interesante: El río de la Colonia y el río Nef, en épocas distintas y entre los meses de Diciembre a Abril inclusive, vacian un enorme caudal de aguas en al río Baker; este aumento considerable del caudal de los ríos de La Colonia y Nef, parece que tiene su origen en al desprendimiento de las inmensas masas de nieve de sus orígenes, las qua socavadas por las lluvias y los vientos propios del verano, se precipitan licuándose y lanzando el volumen de las aguas de los ríos nombrados en el cauce del Baker.

	Esta crece llega sin ruido a los campos y dura más o menos 24 horas. Los mallines inundados por la crecidas no pueden utilizarse ni aún con caballares antes de que de efectúe el fenómeno, porque les animales sorprendidos por las aguas no tienen tiempo para trepar a los cerros del lado Sur u Oriente y perecen ahogados casi todos. Después de la crece estos campos pueden admitir animales.
De Agostini (1945)	Rastros recientes de inundación del río Colonia son los montones de troncos que encontramos apiñados entre los árboles de la floresta y cubiertos todavía de barro y terreno pantanoso y lleno de charcos de agua. El desbordamiento del río Colonia, que todos los veranos se repite infaliblemente desde los primeros días de enero hasta febrero, tiene en constante inquietud a los pobladores de la zona, quienes explican este fenómeno con las más extrañas hipótesis. La crecida se efectúa en 24 horas, sin que la precedan signos excepcionales ni particulares indicios, alcanzando un volumen impresionante. Una enorme masa de agua turbia y barrosa se vuelca repentinamente de la montaña y se precipita en el valle, arrastrando consigo grandes troncos de árboles arrancados de la floresta, y cubriendo totalmente el lecho del río en un ancho de 600 m. La corriente es tan impetuosa que rechaza a la del Baker y la hace retroceder por unos 15 km, elevando el nivel normal de sus aguas unos 4 m, como lo atestiguan los gajos y residuos vegetales que quedan a esa altura entre las ramas de los árboles, después de la inundación. Cuando los colonos desconocían aún el terrible poder de la creciente y, por lo tanto, descuidaban retirar el ganado a tiempo de la zona afectada, muchos fueron los animales vacunos y caballares que perecieron ahogados. Algunos esqueletos de estos animales colgaban de los árboles todavía varios meses después como macabro trofeo de la terrible inundación. Según las referencias de Vilches, que ha recorrido esos parajes en busca de sus vacunos, hay allí un lago de donde sale el río Colonia. Debemos pues seguir las inflexiones del río, caminando al pie de altos barrancos, entre guijarros casi todos de granito y diorita, desprendidos de estas terrazas fluvioglaciales por efecto de la potente erosión de las aguas durante las inundaciones. Corpulentos troncos de coihue destrozados, pero aún con sus raíces, yacen esparcidos a la orilla del río como elocuente testimonio de la potencia extraordinaria de las aguas, que, llenando a gran altura la cuenca de orilla a orilla, alcanzaron a desarraigar de la floresta aquellos árboles gigantescos. En la extremidad occidental del lago, cuyo largo calculamos en siete u ocho kilómetros, baja de la cordillera un gran glaciar que llena toda la cuenca final del valle. La costa oriental del lago, desde donde sale el Colonia, es desplayada y baja, y no hay ningún vestigio que pueda revelar desbordamiento alguno de las aguas debido a un repentino desmoronamiento producido en la margen del lago. Con todo, hay rastros positivos de un notable levantamiento del nivel del lago, señalado por un tronco gigantesco de coihue elevado unos metros sobre el nivel normal de las aguas y por otros árboles más pequeños arrastrados hacia el interior hasta unos

10 m de altura sobre la superficie ordinaria, a causa, según parece, de un rápido crecimiento del lago.

No alcanzamos a ver el interior de la cordillera, pero, por la configuración del valle y del glaciar, me parece tener ya suficientes motivos para suponer que las causas de los desbordamientos de las aguas, que originan las inundaciones, deben buscarse en otro lago marginal, directamente ligado al glaciar. Se produciría el mismo fenómeno que observamos en otros lagos andinos obstruidos por glaciares, de lo cual es típico ejemplo lo que acaece con el glaciar Moreno, del lago Argentino.

Durante la primavera, el lago marginal, obstruido por el glaciar, empieza a subir de nivel a causa del deshielo y de los torrentes glaciares que allí se descargan, logrando su mayor altura en los meses de enero y febrero, cuando llegan los intensos calores estivales. En dicho período, por la presión que ejerce sobre el hielo la masa de agua encerrada en el lago y, al mismo tiempo, por la infiltración de diversas Corrientes por entre las grietas del glaciar, que constantemente se ensanchan, se produce en el glaciar un gran corte en el que se efectúa rápidamente el vaciamiento del lago superior, descargando sus aguas en el de más abajo, el que a su vez vuelca sus aguas en el valle del río Colonia*.
** Este fenómeno es definido en glaciología con la palabra islandesa jokullhlaup, esto es, algo así como "desagüe repentino", y es de ocasional ocurrencia en los sectores englaciados de la Patagonia, el último de los cuales sucedió en la zona del glaciar Bernardo durante el invierno de 2007 (N.E.).*

Según me han asegurado los pobladores de este valle, la inundación vuelve a repetirse algunos años a fines de abril o principios de mayo, pero en forma más reducida. También en el valle del río Nef, más al norte, se produce este fenómeno de desbordamiento, aunque en menor proporción.

Table S6B. ^{210}Pb concentrations measured on core FP17-01.

Depth (cm)	Dry bulk density (g/cm^3)	Cumulative dry mass (g/cm^2)	Total ^{210}Pb (Bq/kg)	Supported ^{210}Pb (Bq/kg)	Unsupported ^{210}Pb – decay corrected to 30/06/17 (Bq/kg)
0 – 1	0.11	0.1 ± 0.1	50 ± 2	27 ± 2	24 ± 3
10 – 11	0.64	3.8 ± 0.2	1.2 ± 0.1	33 ± 3	Not detected
20 – 21	0.59	9.9 ± 0.2	38 ± 2	44 ± 4	Not detected
30 – 31	1.09	18.3 ± 0.3	37 ± 2	44 ± 4	Not detected
40 – 41	1.10	29.1 ± 0.4	37 ± 2	39 ± 3	Not detected
50 – 51	1.02	39.9 ± 0.4	40 ± 2	18 ± 2	22 ± 2
60 – 61	1.01	50.1 ± 0.4	44 ± 2	60 ± 5	Not detected

Table S6C. ^{210}Pb concentrations measured on core FP17-03.

Depth (cm)	Dry bulk density (g/cm^3)	Cumulative dry mass (g/cm^2)	Total ^{210}Pb (Bq/kg)	Supported ^{210}Pb (Bq/kg)	Unsupported ^{210}Pb – decay corrected to 30/06/17 (Bq/kg)
0 – 1	0.26	0.1 ± 0.1	102 ± 5	14 ± 1	88 ± 5
10 – 11	1.21	7.5 ± 0.4	27 ± 1	31 ± 3	Not detected
20 – 21	0.77	17.3 ± 0.4	30 ± 1	22 ± 2	8 ± 2
30 – 31	0.77	25.0 ± 0.4	17 ± 1	23 ± 2	Not detected
40 – 41	0.89	33.3 ± 0.4	34 ± 2	33 ± 2	1 ± 3
55 – 56	0.83	46.2 ± 0.4	44 ± 2	45 ± 4	Not detected
70 – 71	0.49	56.2 ± 0.4	52 ± 3	37 ± 3	14 ± 4

Table S6D. Suspended sediment concentrations (SSC) measured at eight stations on the Baker River and its tributaries (presented from North to South). Annual sediment yields were calculated by multiplying SSC by the annual volumes of water (from Dussaillant et al., 2012). See Fig. 5 for graphical representation.

River name	Latitude (°)	Longitude (°)	SSC (mg/L)	SSC 1sd (mg/L)	n	Highest SSC (mg/L)	Mean annual discharge (m^3/sec)[a]	Annual volume of water (km^3)[a]	Sediment yield (10^6 T/yr)
Baker	-47.0517	-72.8137	1.4	1.0	21	4.5	566.6	17.9	0.025
Nef	-47.1226	-72.7869	65.4	20.2	8	108.4	90.0	2.8	0.186
Chacabuco	-47.1157	-72.6061	88.1	147.7	16	578.9	18.9	0.6	0.052
Baker	-47.2053	-72.6307	17.2	17.0	18	435.4	656.1[b]	20.7	0.355
Cochrane	-47.2776	-72.6928	3.1	1.3	17	6.3	13.3	0.4	0.001
Del Salto	-47.2835	-72.7075	17.0	16.2	16	57.8	39.4	1.2	0.021
Baker	-47.2953	-72.8698	18.0	16.3	13	62.2	795.7[c]	25.1	0.452
Colonia	-47.3063	-72.8807	226.2	117.4	13	525.4	138.1	4.4	0.985

[a] From Dussaillant et al. (2012)

[b] Calculated as Q above Chacabuco + Q Chacabuco

[c] Calculated as Q below Colonia - Q Colonia

Figure S6A. Additional photographic documentation of flooding in the upper Baker River area. (a) Evidence of major GLOFs during the austral summer of 1945, which were able to uproot large trees and erode the riverbanks of the Colonia River (de Agostini, 1945). (b) Confluence of Colonia and Baker rivers during the April 2008 GLOF that resulted in the inundation of the Valle Grande floodplain (photo credit: Jonathan Leidich). (c) The extreme rainfall event in February 2009 that left parts of the Valle Grande floodplain under water (photo credit: Alexis Pezoa).

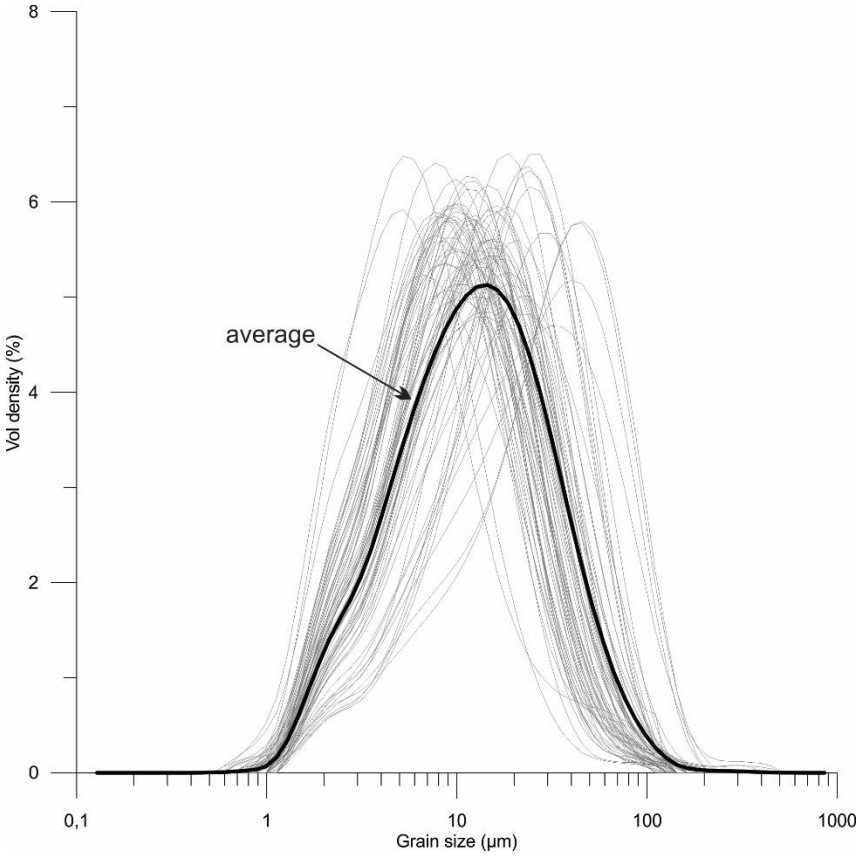

Figure S6B. Grain-size distributions of 71 samples from core FP17-01 (in grey), presenting a vertical resolution of 5 cm. The average of all samples is displayed as a black line.

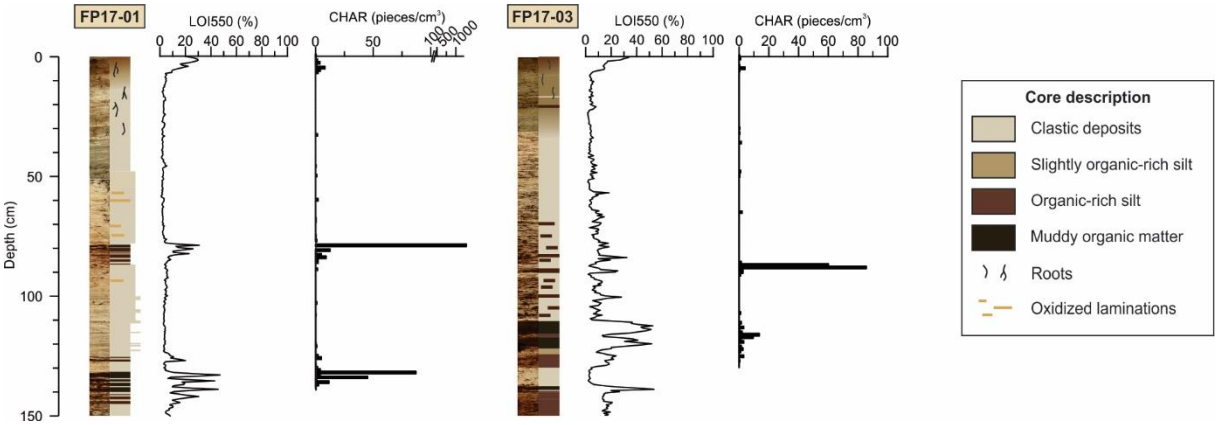

Figure S6C. Results of the charcoal analysis on cores FP17-01 and FP17-03. Photographs are on the left and lithologs are displayed on the right side. For both cores, LOI550 and the concentration of charcoal are displayed.

7. Discussion

In this chapter, the results and conclusions of the three main research chapters are supplemented with additional findings, which are then discussed together and placed in a broader context.

7.1. Geological archives of Baker River GLOFs

7.1.1. Terrestrial archives

In this thesis, sediments from the Valle Grande floodplain were successfully used to reconstruct Baker River GLOFs over the last 2.75 kyr (cf. chapter 6). Other types of terrestrial archives may however also help to reconstruct the history of Baker River GLOFs.

7.1.1.1. Other floodplains along the Baker River

Valle Grande is not the only floodplain along the course of the Baker River. Many other floodplains, including the large Vargas floodplains, can be found along Baker River (Fig. 7.1). During the 2016 and 2017 field expeditions, a total of 36 sites, of which 33 are located along the main course of the Baker River, were tested for their potential as GLOF archives. The last three locations are situated along tributaries of the Baker River, one site along the Del Salto River, and two sites along the De Los Ñadis River (Fig. 7.1). Based on our observations, few locations appear to be suited for paleoGLOF reconstruction. Although the most recent 21st century Cachet 2 GLOFs were able to increase the Baker River water level by several meters just downstream of the Baker-Colonia confluence (DGA, Chile) and that most of the sampled sites along the lower reach of the Baker River are located just a few meters above the normal Baker River water level, most sites display either continuous flood deposits (mud) or they consist of autochthonous sedimentation (peat) where flood deposits are lacking (Fig. 7.1). The only locations that display few clear flood layers, e.g. downstream the Vargas floodplain and near Cute Lake and Caleta Tortel (Fig. 7.1d), most likely registered sporadic high-magnitude GLOFs. It thus appears that most lake outbursts are not registered in the sediment record this far downstream, most likely due to a fast decline in the Baker River hydrograph during GLOFs. Cenderelli and Wohl (2001, 2003), for example, have shown that as the distance from the GLOF source increases, discharge decreases progressively.

Most flood sediments are thus deposited closer to the source valley. Indeed, several sites in the Valle Grande floodplain, which is located in the upper reach of the Baker River, present continuous flood records (Fig. 7.1b). Although the lower areas of the floodplain are dominated by homogeneous flood deposits and are not suited for flood reconstruction, relatively elevated sites display flood sequences where autochthonous organic-rich sedimentation alternates with flood deposits (clastics) (cf. chapter 6). It should be emphasized that Valle Grande is situated in a “backwater setting” during GLOFs originating from the Colonia valley. This means that the floodplain, which is located immediately upstream of the Colonia-Baker confluence, inundates because the regular Baker River water flow towards the South is blocked by inflow of Colonia River during Colonia River GLOFs (cf. chapter 6) (Fig. 7.1). Baker River water is thus pushed back and sediments might settle more easily in this relatively calm environment. During Colonia GLOFs, floodplains downstream of the Colonia-Baker confluence (Fig. 7.1) are affected by direct flooding. In case of GLOFs originating from the Nef valley direct flooding also affects the Valle Grande floodplain. These downstream locations will probably only register high-magnitude floods and might display a more heterogenous depositional pattern of GLOF sediments due to the relatively energetic conditions during flooding.

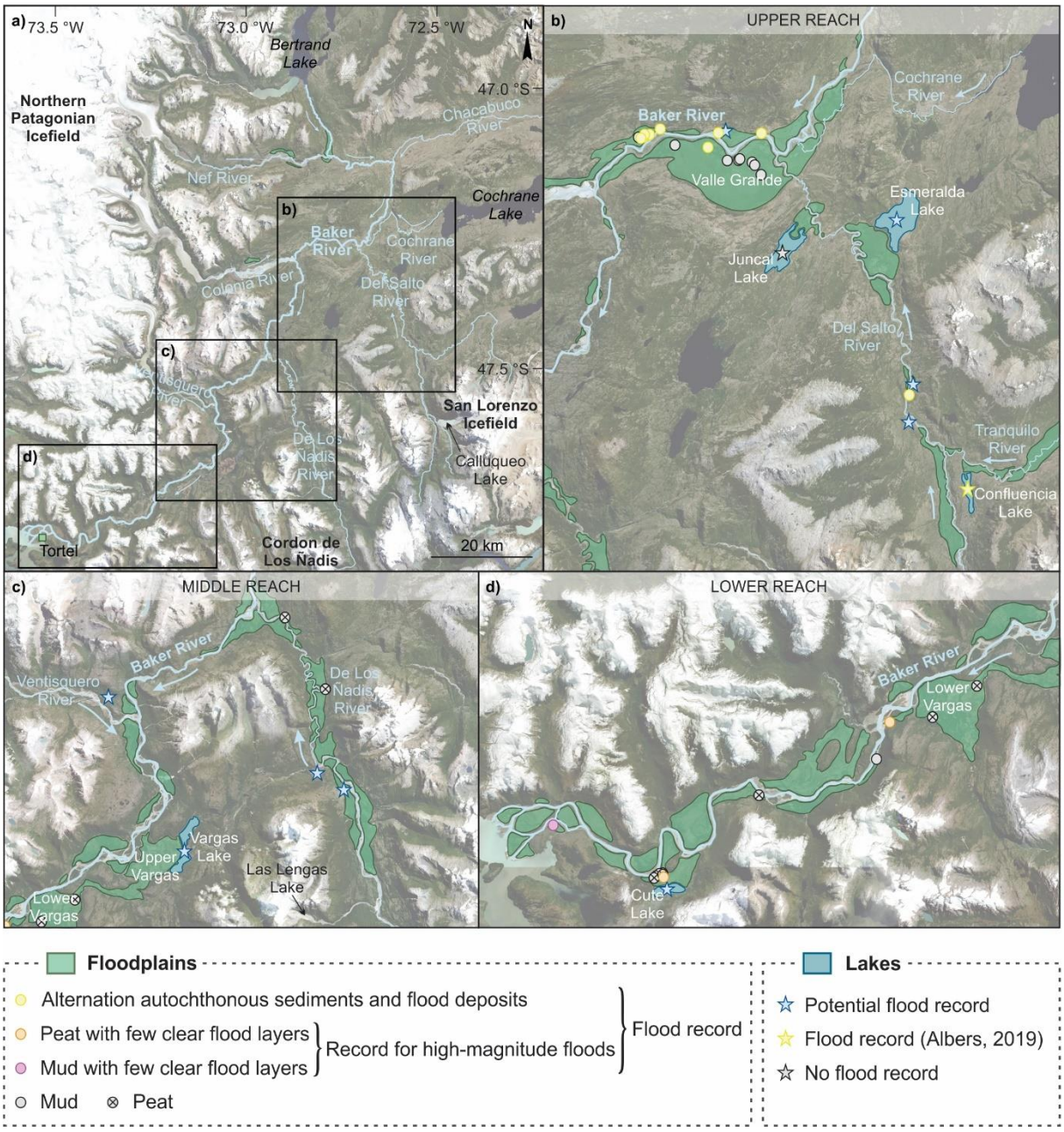

Figure 7.1. Floodplains and lakes along the Baker River and its tributaries showing potential locations to obtain GLOF records (Global Mapper World Imagery). The floodplain sites tested during the 2016 and 2017 field surveys are indicated by colored dots. Yellow stars indicate the location of sediment cores from lakes Juncal and Confluencia along the Del Salto and Tranquilo rivers, respectively (b), which were investigated by Albers (2019). Blue stars indicate lakes that were not investigated but may hold continuous flood records.

Similar observations were made in the floodplains along the tributaries of the Baker River. In the Nef valley, for example, approximately 2 km upstream the Baker-Nef confluence, 116 beds of Holocene slackwater deposits were identified (Benito and Thorndycraft, 2020), which suggests that the relatively small floodplains near the Nef-Baker confluence might hold continuous records of GLOFs originating from the Nef valley (Fig. 7.1a). In particular, the larger floodplain just upstream the Nef-Baker confluence is, similar to Valle Grande, situated in a “backwater setting”.

Another example is the sediment record from a peatbog along the Del Salto River located just 20 km downstream of the nearest San Lorenzo Glacier, i.e. Calluqueo (Fig. 7.1a–b). This sediment record was

sampled during the 2017 field expedition and was successfully used to reconstruct the mid- to late Holocene flood frequency of the Del Salto River (Rojas Aldana, 2018).

Another tributary of the Baker River further downstream, i.e. De Los Ñadis River, experienced major flooding along its entire path due to the March 1988 outburst of Las Lengas Lake (Table S7Ab–d, h, i, k). The estimated peak discharge of that GLOF (1301 m^3/s; Iribarren Anacona et al., 2014) was an order of magnitude higher than the estimated average Los Ñadis River discharge (~50 m^3/s). Despite this clear increase in discharge, GLOF deposits were absent at the investigated locations along the Los Ñadis River (Fig. 7.1c). The floodplains along the Los Ñadis River are, contrary to floodplains in a "backwater setting", only influenced by direct flooding. According to testimonies, areas that flooded were draped with white-colored mud, i.e. glacier flour, after the water withdrew (Table S7Ab, c, h, i, k). However, it is plausible that GLOF deposits are unevenly distributed along the Los Ñadis River and more concentrated in lower areas, as pointed out by one settler (Table S7Ak). Similar to Colonia GLOF deposits, the Las Lengas GLOF deposits are likely more abundant in the upper reach of the Los Ñadis River, i.e. close to the lake source.

Finally, it should be noted that the relative inaccessibility in this region forms an inevitable challenge for sampling, and many potential locations for paleoGLOF reconstruction along the middle reach of the Baker River, i.e. between the Colonia River inflow and the Vargas floodplains, could not be tested (Fig. 7.1). Despite the lack of examined locations along the middle reach of the Baker River, it appears that the potential to find GLOF deposits in floodplains is not only controlled by the elevation difference and connection with the Baker River, but it also appears to decrease relatively fast downstream of the source valley. Floodplains affected by backwater flooding during GLOFs present more promising locations compared to floodplains downstream of the confluence with the source valley. The latter most likely only register high-magnitude GLOFs and the deposition of GLOF sediments in these floodplains might be more heterogenous.

7.1.1.2. Lake sediment records

Similar to floodplains, many lakes with variable sizes, i.e. from small ponds to relatively large lakes such as lakes Esmeralda and Vargas, occur along the Baker River and its tributaries (Fig. 7.1). Some of these lakes were explored during the 2016 and 2017 field expeditions (Fig. 7.1) but many of them were not sampled due to limited accessibility.

Lake sediments from lakes Confluencia and Juncal, which are located along the Tranquilo and Del salto Rivers, respectively (Fig. 7.1b), were investigated in the framework of a master thesis project (Albers, 2019). These lakes were selected because during floods, their outflows act as a proglacial river inflow. The sediment records from these two lakes show that the lake's hydrological conditions, and particularly their connectivity with the proglacial river, influence their potential to hold a flood record. In Juncal Lake, for example, the detrital-rich background sediments appear very similar to the flood deposits as sediment-laden water from Del Salto River also regularly enters the lake during non-flood conditions (Fig. 7.1b), which makes the lake sediments unsuited for flood reconstruction. On the other hand, the sediment record from Confluencia Lake displays a clear difference between the organic-rich background sediments and the detrital-rich flood deposits, and was therefore successfully used to reconstruct the frequency of late Holocene floods from the San Lorenzo Icefield (Albers et al., 2019) (Fig. 7.1b). It should be noted, however, that this flood record does not entirely represent GLOFs, as the flood deposits are hypothesized to be related to both the emptying of proglacial lakes as well as direct increased meltwater production related to glacier retreat of the San Lorenzo Icefield (Albers et al., 2019).

In contrast to the glacial flood record from Confluencia Lake, which is not entirely the result of lake outburst floods, previous studies have successfully identified GLOF deposits in lake sediments (e.g. Xu et al., 2015; Røthe et al., 2019). In these lakes, GLOFs are recorded as event deposits that are less organic than the background sediments, but their grain-size signature is variable and appears to depend on the regional setting (cf. chapter 5).

In general, lake sediments may act as promising GLOF archives when ideal conditions are met. Potential locations for lake sediment coring in the Baker River watershed to reconstruct GLOFs are the smaller ponds in the northern part of Valle Grande or along the tributaries Del Salto and De Los Ñadis (Fig. 7.1). Cute Lake, which was mapped during the 2017 expedition, might contain a continuous GLOF record of high-magnitude GLOFs as it is directly connected to the Baker River. Yet, only the largest GLOFs might be registered as it is located far downstream (Fig. 7.1d). On the other hand, Esmeralda Lake is expected to show a similar record as Juncal Lake, where flood deposits might be difficult to distinguish from the background sediments (Fig. 7.1b).

7.1.1.3. Geomorphological assemblages

Although geomorphological assemblages were not investigated in this PhD, landforms and deposits associated with the drainage of paleolakes (e.g. raised deltas, paleoshorelines, and subaerial lacustrine sediments) that are found above the current valleys or lake floors, as well as erosional and depositional landforms downstream of paleolakes, have been shown to hold evidence for paleoGLOFs (e.g. Benito and Thorndycraft, 2020). The latter manifest in the landscape as boulder bars, eddy bars, large-scale dunes, aeolian dunes, slackwater deposits, and bedrock landforms such as potholes, waterfalls, eroded channels, etc. For example, eroded spillways on valley margins, gravel and sand bars, and antidunes found in the Baker River watershed evidence catastrophic floods that occurred at the end of the deglaciation following climate warming (~12.5 cal kyr BP) (Thorndycraft et al., 2019; Benito and Thorndycraft, 2020). Another example from the Baker River valley are the slackwater deposits, composed of sediment sequences of light greyish sand and silt deposits with parallel bedding and cross-laminations, found in back-flooded zones, such as the Baker-Nef confluence, Valle Grande, and downstream the Los Ñadis River inflow (Benito et al., 2014; Benito and Thorndycraft, 2020). These records extend way beyond the timespan of historical data, and are able to register the most catastrophic, i.e. highest-magnitude, events. However, as many of these landforms result from erosive processes, these records are often discontinuous and might not be useful to reconstruct paleoGLOFs on continuous, shorter, i.e. late Holocene, timescales.

7.1.1.4. Other terrestrial archives

Aside from geomorphological assemblages, dendrochronology and lichenometry have also successfully been used to identify and date glacial lake outbursts in the Colonia River valley (Winchester and Harrison, 2000). Although these archives can provide accurate chronologies of flood events, they often only cover post-Neoglacial times, and material is scarce. Moreover, detailed case studies are needed before these techniques can be applied as there is a wide divergence in tree colonization rates, particularly in recently deglaciated regions, due to differences in micro-environment (Warren and Sugden, 1993; Winchester and Harrison, 2000). Although these archives present accurate GLOF records, they require extensive fieldwork, are limited in time, i.e. only covering post-Neoglacial times, and are limited to GLOFs from a single lake.

7.1.1.5. How can GLOFs be distinguished from meteorological floods in terrestrial archives?

The biggest challenge in using terrestrial archives to establish GLOF histories requires being able to differentiate between deposits from lake outbursts and extreme meteorological flood events. Both GLOFs and meteorological floods, for example those induced by heavy precipitation or rain-on-snow, result in an increase of Baker River discharge and ultimately in the deposition of flood sediments.

As discussed in chapter 6, the flood deposits in Valle Grande most likely originate from high-magnitude GLOFs rather than precipitation-driven floods. GLOFs are the only events that are able to inundate the entire floodplain, whereas precipitation-driven floods only inundate the lower elevation areas in Valle Grande (Fig. 6.1b). Although the sediment contribution of glacial tributaries is significantly higher compared to non-glacial tributaries, such as Chacabuco River, which usually has a low sediment yield, suspended sediment concentrations (SSC) from these non-glacial tributaries increase significantly during extreme rainfall events (Brian Reid, pers. comm.). Flood sediments representing extreme precipitation events are however expected to be relatively coarser compared to GLOF deposits, which are entirely of glacial origin. Yet, flood deposits from the Valle Grande floodplain consistently display unimodal distributions. This suggests that these flood deposits represent one dominant depositional process, most likely related to GLOFs.

Identifying the provenance of flood deposits could help determine whether the Valle Grande flood deposits are precipitation-driven or associated with GLOFs. Liu et al. (in prep) have shown that the isotopic signature of suspended sediments from the rivers Del Salto, Colonia, and De Los Ñadis matches the isotopic composition of the bedrock lithologies in their respective watersheds, and that Sr and Nd isotopes can be used to determine the provenance of Baker River flood deposits. These isotopes are particularly promising in differentiating between the western and eastern sides of the Baker River watershed, which are underlain by clearly distinct lithologies (i.e. batholith and metamorphic complex, respectively). Therefore, the isotopic signature of sediments originating from precipitation-driven floods, which primarily affect the eastern side of the watershed, and GLOFs, which originate from NPI glaciers located in the western part of the watershed, is expected to differ significantly. Eventually, Sr and Nd isotope analysis might allow us to distinguish between GLOF deposits and sediments originating from other extreme floods in the Baker River. However, it should be noted that this method is time-consuming and expensive and can therefore not be applied in routine to a large number of flood deposits.

In contrast with the glacial nature of GLOF deposits, the signature of precipitation-driven floods is also expected to be more organic. As intense precipitation events mainly affect non-glacial tributaries in the drier eastern part of the Baker River watershed (Liu et al., in prep), erosion of riverbanks during meteorological floods entrains relatively organic-rich sediments and is expected to result in a more organic signal compared to GLOF deposits.

Finally, it may be possible to differentiate GLOF deposits from other flood sediments using sediment proxies that are specific to lakes at the origin of each GLOF. This could be expressed in, for example, diatom assemblages (i.e. presence of glacial lake diatom species) or elemental composition, which might be related to provenance. Other potential GLOF-specific properties could be determined by examining GLOF deposits of known origin. For instance, it would be interesting to explore the sediment characteristics of the 1977 Engaño GLOF (Iribarren Anacona et al., 2015) that is likely recorded in the sediments of the northern branch of General Carrera Lake.

7.1.1.6. Potential of terrestrial archives for long-term Baker River GLOF reconstructions

Generating additional long-term GLOF records would be useful to verify the relation between high-magnitude GLOFs from eastern NPI glaciers and glacier advance, which was identified from the Valle Grande flood reconstruction (cf. chapter 6). For example, the floodplains near the Baker-Nef confluence present promising locations for flood reconstructions as evidence of paleoGLOFs was found in the form of slackwater deposits (Benito and Thorndycraft, 2020) (Fig. 7.1a). Although records from this location solely present GLOFs from a single source, i.e. Nef valley, they might be less influenced by precipitation-driven floods than Valle Grande, as Nef valley is located in the upper reach of the Baker River.

7.1.2. Marine archives

Fjord sediments present promising archives of pre-historical Baker River GLOFs. In this thesis, the recent GLOFs originating from the emptying of Cachet 2 Lake were identified in the sediments of Martínez Channel as fine-grained and organic-poor deposits, intercalated in slightly coarser and more organic background sediments. This GLOF signature appears to be related to the glacial nature of the sediment input during lake outbursts (cf. chapter 5). Given the high sediment accumulation rates at the head of Martínez Channel, however, only the GLOF history of the last 40 years was recorded in our sediment cores.

7.1.2.1. Spatial distribution of GLOF deposits

The signature of GLOF deposits is relatively heterogeneous at the head of Martínez Channel. As mentioned in chapter 5, distinguishing GLOF deposits becomes less evident with increasing distance from the Baker River outflow as the background sediments become finer and less organic, i.e. become increasingly similar to GLOF deposits (Fig. 7.2).

In addition to the sediment cores presented in chapter 5, two additional cores (FC17-03 and FC17-04A; Fig. 7.2) were collected in Martínez Channel, near the southern end of Steffen Fjord. In these distal cores, which are located just ten km from the Baker River outflow, only the signature of the initial 21st century Cachet 2 GLOF appears to be visible (Fig. 7.2). To obtain an approximate chronology for sediment core FC17-03, the age-depth model of core FC17-02 was projected onto core FC17-03 using relative variations in the thickness of sediment packages that are clearly correlated. The results show that the bottom of FC17-03 corresponds to 1921 ± 16 CE. The lower part of FC17-03 thus covers the latest part of the Arco GLOF period (~1880s–1960s), which was characterized by GLOFs that were significantly larger in magnitude compared to the recent Cachet 2 GLOFs (Oportus, 1928; De Agostini, 1945; Table S7Aa, e, g). Remarkably, the Arco GLOFs do not seem to be recorded in core FC17-03 (Fig. 7.2). As these cores are located further away from the river inflow, sedimentation at these sites is also influenced by sediment input from other fjords (e.g. Steffen Fjord). Optimal coring sites for GLOF records are thus located on the delta slope, close to the river mouth, and to the east of Steffen Fjord. Given the relatively high sedimentation rate at the head of Martínez Channel, i.e. between 1.8 and 3.2 cm/yr, these fjord sediments hold high-resolution GLOF records. Yet, long sediment cores are required to establish the Baker GLOF history on longer, i.e. multi-centennial, timescales.

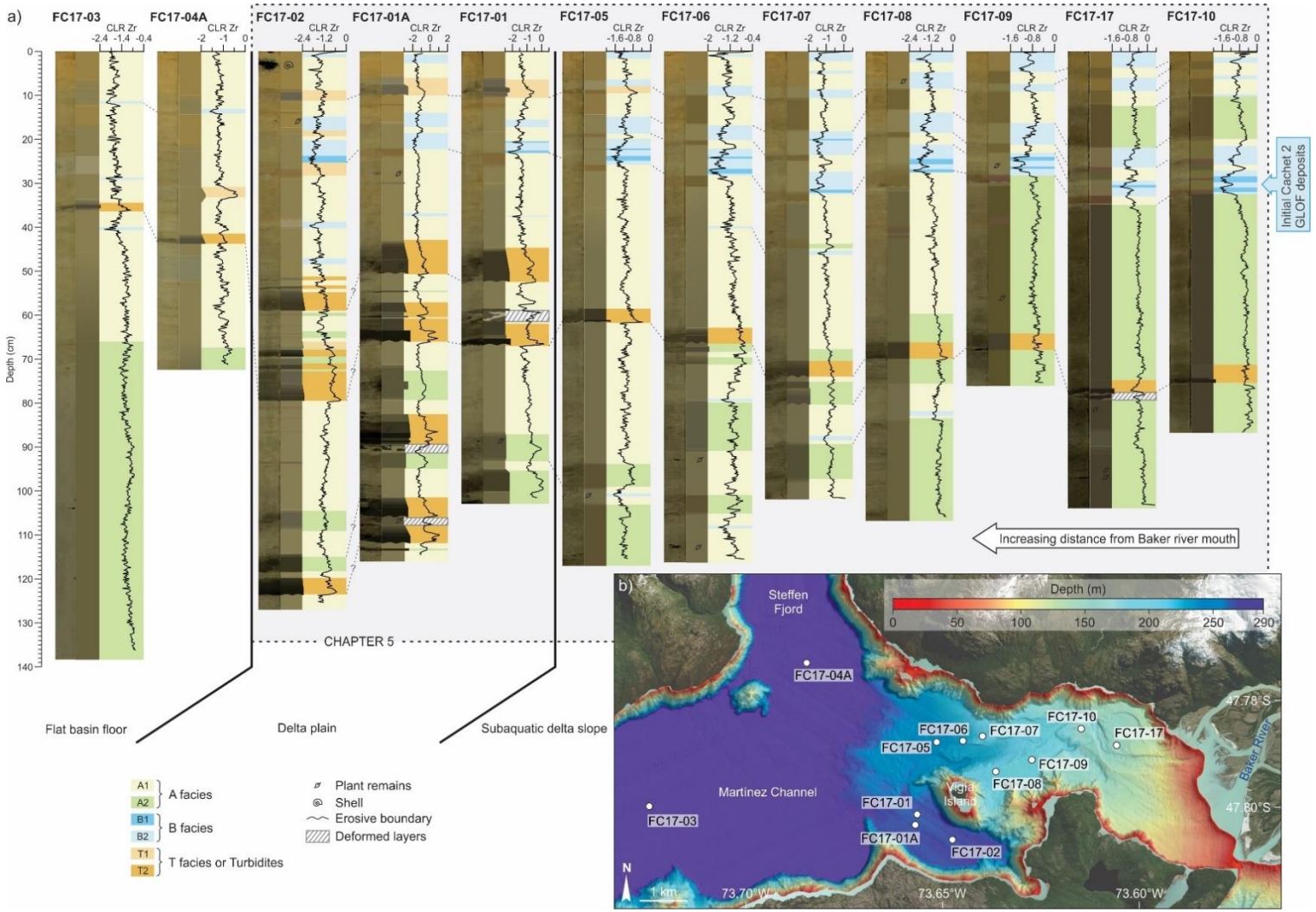

Figure 7.2. Sediment cores collected at the head of Martínez Channel. **(a)** Lithology of sediment cores collected at the head of Martínez Channel with increasing distance from the Baker River mouth to the left. Photographs are on the left and lithologs are displayed on the right. For all cores, Centered Log Ratio (CLR)-transformed Zr counts are displayed. Lithological correlations are indicated using grey dashed lines. Note that the distal cores FC17-04A and FC17-03 were not investigated in chapter 5. **(b)** Subaerial (Global Mapper World Imagery) and subaquatic topography of the Baker River delta (chapter 4), with indication of the sediment core locations (white dots).

7.1.2.2. Turbidites in fjord sediments: are they related to GLOFs?

Bathymetric imaging and sediment records indicate the frequent occurrence of turbidity currents at the head of Martínez Channel (cf. chapters 4 and 5). Turbidites are present in all fjord sediment cores but are particularly abundant in the three sediment cores located on the delta plain, i.e. in front of the main submarine channel (FC17-01, FC17-01A, and FC17-02) (Fig. 7.2). The sediment cores on the delta slope (FC17-17 to FC17-05) and on the flat basin floor (FC17-03 and FC17-04A) only display one clear turbidite between 35 and 75 cm depth. Cores FC17-04A and FC17-05 contain an additional turbidite at 33 and 10 cm depth, respectively (Fig. 7.2). Based on the color of the turbidites, they were sub-divided into two types: light (T1) and dark (T2) turbidites (cf. chapter 5). These two types reflect a difference in organic content, where T2 turbidites are enriched in organic matter. Although some of the largest recent Cachet 2 GLOFs seem to be at the origin of the T1 turbidites underlying the GLOF deposits, most GLOFs were apparently not able to trigger a turbidity current despite river SSC increasing at least one order of magnitude compared to the meltwater season (cf. chapter 4). The turbidites are most likely linked to other extreme discharge events, such as heavy rainfall or rain-on-snow events (cf. chapter 5).

A detailed comparison between the timing of precipitation-driven floods and the occurrence of turbidites in core FC17-02, which is located on the delta plain in front of the main submarine channel (Fig. 7.2), shows that there are, in general, significantly more floods than turbidites (Fig. 7.3). Some correlation is visible between the timing of T2 turbidites and the most extreme floods. For example, the thick T2 turbidite that is present in all sediment cores between 35 and 80 cm depth (73–80 cm in core FC17-02; Fig. 7.3), and that was dated 1994 ± 5 CE (Fig. 7.2), is most likely associated with the August 1992 rain-on-snow event (cf. chapter 5). This is supported by Liu et al. (in prep), who showed that this T2 turbidite originated from the eastern side of the Baker River watershed, i.e. the part of the watershed that is more prone to erosion during intense precipitation because of its relatively dry nature (Liu et al., in prep), thus suggesting a meteorological trigger for this turbidite. It cannot be excluded that large magnitude GLOFs in the past could also have triggered turbidity currents at the head of Martínez Channel. Large GLOFs originating from lakes located closer to the Baker River delta, with possibly higher suspended sediment concentrations, for example, may have been able to generate turbidity currents.

Although an individual sediment layer-to-event association is not feasible, as shown for the GLOFs from Cachet 2 Lake in chapter 5, the simultaneous occurrence of T2 turbidites and extreme floods, and the T2 turbidites' coarse and organic-rich nature (cf. chapter 5) suggest that the turbidites within our sediment cores are triggered by extreme discharge events induced by heavy precipitation. Their nature is similar to that of the background sediment in cores located in the upper slope region, i.e. FC17-17 and FC17-10 (Fig. 7.2), which means that these turbidites can also result from delta slope failures, possibly triggered by extreme discharge events such as extreme rainfall or rain-on-snow events, to maintain maximum slope stability (Syvitski and Shaw, 1995). To determine the exact triggering mechanism(s) of the turbidites, detailed monitoring at the head of Martínez Channel using, for example, turbidity sensors at various depths and an acoustic doppler current profiler at the fjord bottom in front of the main submarine channel, is necessary. Repeated suspended sediment sampling and bathymetric surveys, as conducted at the Squamish Delta in British Columbia, Canada (e.g. Clare et al., 2016; Hizzett et al., 2018; Hage et al., 2019), could also help to examine how these turbidites are formed.

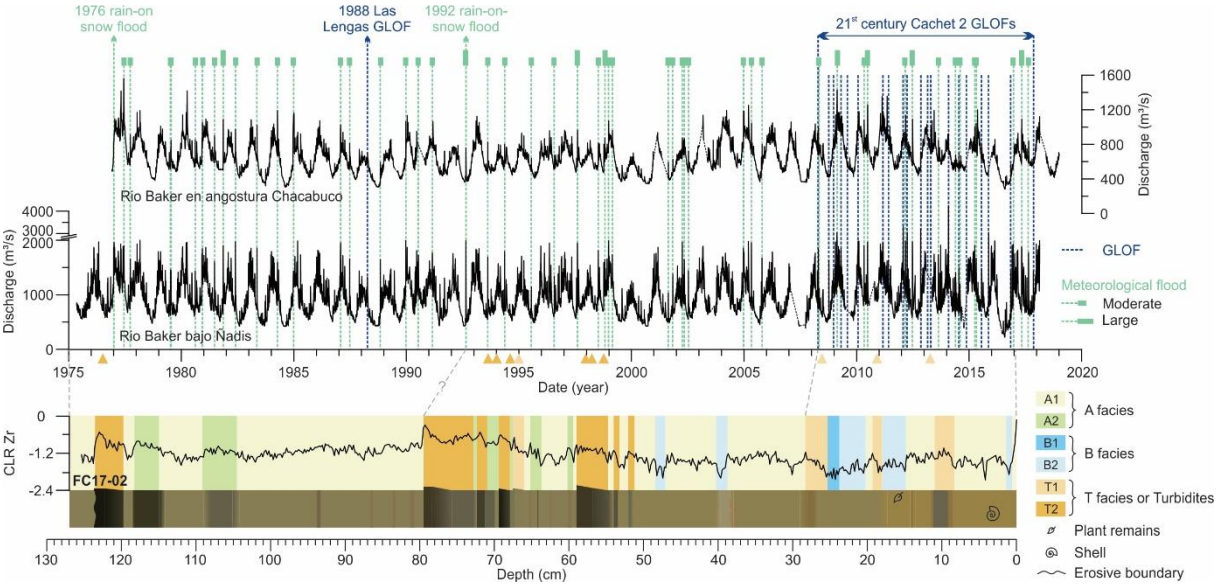

Figure 7.3. Baker River discharge data compared to core FC17-02. The upper and lower graphs display the Baker River discharge data derived from DGA stations Rio Baker en angostura Chacabuco and Rio Baker bajo Ñadis, respectively (see Fig. 3.8 for the exact location). Precipitation-driven floods were identified based on discharge data of the two stations and precipitation data (Alvarez-Garreton et al., 2018). Floods before 1979 were determined using discharge data only. A distinction was made between moderate and large floods, where moderate floods imply that discharge doubles compared to baseline values, and large floods are characterized by a threefold increase in discharge. According to the age model (chapter 5), the bottom of sediment core FC17-02 corresponds to 1975 ± 9 CE, and correlations are indicated using grey dashed lines.

7.1.2.3. Unique context of the Baker River and implications for other fjord environments

As shown in chapter 5, the Martínez-Channel-Baker River system is particularly well-suited for paleoGLOF reconstructions. This primarily results from a clear contrast between the fjord background sediments, which are relatively organic as a significant portion of the watershed is vegetated, and the purely glacial nature of GLOF deposits (cf. chapter 5). For paleoGLOF reconstructions, this implies that identifying GLOF deposits in fjords that are directly and/or solely fed by the proglacial river of interest, i.e. where background sediments are similar in nature to lake outburst deposits, would be challenging. This is the case in Steffen Fjord, for example, which is situated immediately south of the NPI and is mainly fed by meltwater from Steffen Glacier via the relatively short proglacial Huemules River (cf. chapter 4). Contrary to the organic nature of the background sediments at the head of Martínez Channel, the background sediments in Steffen Fjord have TOC values that resemble those of GLOF deposits at the head of Martínez Channel (0.27 ± 0.07 %; cf. chapter 4). This complicates the identification of GLOF deposits, which may only be discernible by their slightly coarser signature (Piret et al., 2021). However, it should be noted that other proxies may be able to distinguish GLOF deposits in fjord sediments. Analysis of phosphorous concentrations, organic carbon stable isotopes ($\delta^{13}C$), and diatoms did not prove to be successful at the head of Martínez Channel. Nevertheless, these proxies might work elsewhere.

In addition, the difference between GLOF deposits and background sediments might have varied in the past due to changes in glacier cover, formation of proglacial lakes, vegetation density, precipitation, and temperature. For example, the GLOF signal is expected to be less distinct when background sediments are finer and less organic, due to, e.g., increased glacier cover and lower vegetation density. On the contrary, less meltwater input, higher vegetation density, higher temperatures, and/or increased

precipitation result in coarser background sediments, which enhances the contrast between GLOF deposits and background sediments. The ability to identify GLOF deposits in fjord sediments is thus always relative to the composition of the background sedimentation.

Finally, the potential to register GLOFs in fjord sediments also depends on the baseflow of the river. The Baker River has a high mean annual discharge of ~1100 m^3/s (Dussaillant et al., 2012). Although the river is subjected to GLOFs from several valleys, making it independent from the evolution of any specific proglacial lake, this also implies that smaller GLOFs are diluted relatively easily, both in terms of water volume and SSC. Consequently, smaller GLOFs might not be visible in the sediment record. Although the recent Cachet 2 Lake outbursts, which released an estimated 101 to 251 x 10^6 m^3 of water, were large enough to be registered in the fjord sediments (Fig. 7.2), the March 1988 Las Lengas GLOF appears to be absent from the Baker River discharge data and from the fjord sediment records, as its volume (4.36 x 10^6 m^3) and overall meltwater and sediment contribution to the Baker River, were much lower (cf. chapter 5 and Liu et al., in prep). In case of a large river such as Baker, the signal of smaller outbursts could be insignificant in Martínez Channel sediments, and only high-magnitude GLOFs are clearly registered in the fjord's sediments. For lake outbursts with a small flood volume, terrestrial archives closer to the source might be better suited for flood reconstructions. This, however, also implies that smaller rivers with a low baseflow yield a more distinctive GLOF signal and low-magnitude GLOFs in such rivers could be registered in the marine sediment record. In other words, aside from the watershed's properties (slope, parent material, etc.) and geomorphology (e.g. lateral erosion), the signature of GLOF deposits in fjord sediments is highly influenced by the ratio between the water volume released by the GLOF and the river's baseflow.

7.1.3. Comparison between terrestrial and marine archives

In general, GLOF sediments in both terrestrial and marine archives have an organic-poor signature. Lake outbursts trigger extreme floods that release large amounts of meltwater, glacial sediment, and debris (Benn and Evans, 2010). Still, their hydrographs attenuate relatively fast downstream (Cenderelli and Wohl, 2001, 2003), and the largest contribution of suspended sediment during GLOFs is therefore derived from erosion of lake-bed and alluvial deposits in the upper watershed rather than riverbank erosion further downstream (Bastianon et al., 2012). Hence, GLOF deposits in terrestrial (cf. chapter 6, e.g. Benito et al., 2014), lacustrine (e.g. Xu et al., 2015; Røthe et al., 2019), and marine archives (cf. chapter 5) are less organic compared to the background sediments, reflecting the glacial nature of the source material.

The grain-size signal of GLOF deposits in terrestrial archives appears to be a function of magnitude and/or distance from the drained lake. For example, slackwater deposits associated with Baker megafloods in the upper reach of the watershed, i.e. close to the source valley, consist of light greyish, i.e. less organic, sediments of variable grain size (silt to sands) (Benito et al., 2014). GLOF sediments found in the Valle Grande floodplain are overall fine-grained, still, the coarser layers in the record might represent larger magnitude GLOFs (cf. chapter 6). On the other hand, most of the suspended load is transported downstream and deposited in fjord sediments, where the fine-grained GLOF signature is a function of sediment availability, i.e. the amount of glacial sediments that is released during GLOFs (cf. chapter 5).

Both floodplains and marine environments are dynamic settings due to their relatively fast geomorphic evolution. Floodplains act as natural traps for GLOF sediments when river water levels increase during

flooding, and they have the potential to hold continuous long-term GLOF records. Because of rapid changes of the meandering river system, an extensive field survey with test sampling prior to coring is crucial to identify the most promising locations in floodplains. Such a survey permits the identification of sediment features and the visualization of spatial variations within the floodplain. Ideal coring locations are found in paleochannels and, as adopted in Valle Grande, sediment records from multiple locations should be combined to exclude local signals (e.g. shifting of the main river channel, changes in local channel activity, elevation, etc.), and to account for local variations in the sediment infill (e.g. Ishii et al., 2017; Fuller et al., 2018; cf. chapter 6). In fjords, a paleoGLOF record can be established using a similar multi-core and multi-proxy approach, as applied to the fjord sediments at the head of Martínez Channel (cf. chapter 5). In addition, bathymetric imaging and a seismic survey could help to identify submarine channels and buried erosional surfaces, respectively. By comparison, lakes have a higher preservation potential than fjords and are expected to hold more continuous records.

Dating sediments collected in floodplains is rather easy using radiocarbon analysis as organic matter is relatively abundant in the background sediments. Dating fjord and lake sediments mostly fed by glacial rivers, on the other hand, is challenging. For example, despite being able to successfully construct a core chronology based on radionuclide analysis for relatively young sediments (< 150 yrs) (cf. chapter 5), the age error is relatively high to allow for individual sediment layer-to-event association. Dating older sediments also requires a different chronological technique, such as radiocarbon analysis. Yet, the lack of sufficient in-situ organic material might pose an issue.

The differentiation between GLOFs and other extreme discharge events is relatively clear in the fjords sediments at the head of Martínez Channel (cf. chapter 5). As mentioned in section 7.1.2.3, this might not be the case for all (proglacial) marine archives. The origin of flood deposits in other terrestrial archives, such as floodplains and lakes, might be less straightforward to identify. Aside from GLOFs, increased meltwater input or precipitation-driven floods should also be considered as potential causes for flood deposits.

Finally, the temporal resolution of flood reconstructions significantly varies between archives. Fjord sediments constitute high-resolution GLOF archives due to their relatively high sedimentation rate and are useful to generate multi-centennial GLOF records. In general, sediments accumulate relatively slowly in floodplains, which are therefore better suited to observe long-term, i.e. multi-millennial, changes in GLOF frequency.

7.2. Historical and instrumental records of Baker GLOF history

Aside from geological archives, the Baker River flood history can also be established using instrumental records, as well as testimonies, i.e. written and spoken evidence, and iconographic documents from explorers and early settlers. They provide independent records, with a precision that cannot be matched by geological archives. In a remote region such as the Baker River watershed or other parts of Patagonia, where instrumental data are often scarce, field interviews, and written and iconographic documents can provide complementary and detailed information on flood events.

Some historical information was used in chapter 5, but that chapter only made use of testimonies covering the last 50 years as this time-window corresponds to the maximum period of time covered by the examined fjord sediment cores. However, written and conversational evidence dating back to as early as the 1880s and 1940, respectively, was examined for this thesis (Fig. 7.4).

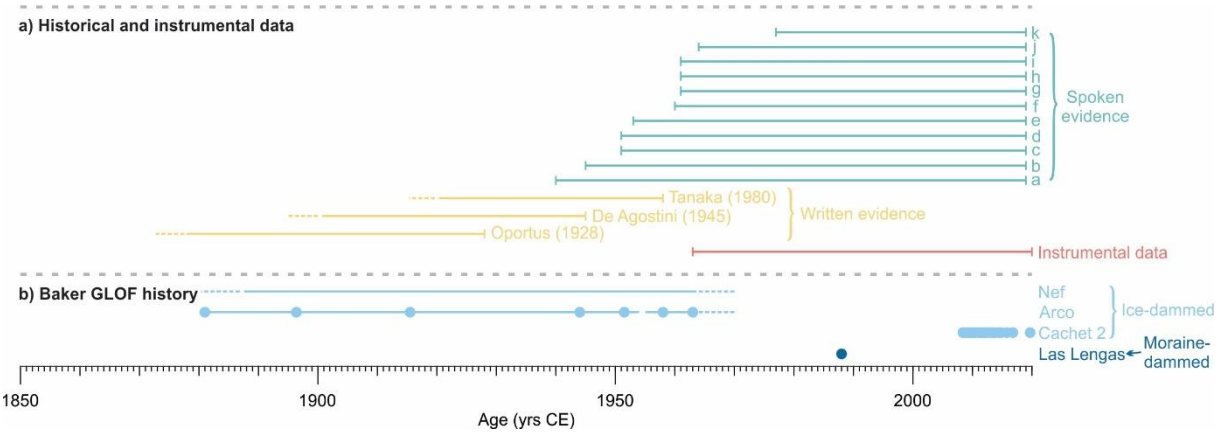

Figure 7.4. Historical, i.e. spoken and written, evidence and instrumental data of the Baker River GLOF history from the ice-dammed lakes Nef, Arco, and Cachet 2, and the moraine-dammed Las Lengas Lake. **(a)** The length of each horizontal line represents the duration of the record. The historical records on Baker River GLOFs are presented in Supplementary Information Table S7A. Conversational evidence was obtained from local inhabitants in the early settlements along the Baker River and its tributaries; (a) Leoncio Escobar Montecino, (b) Misael Maldonado, (c) Luzmira Muñoz, (d) Ramón Ángel Caucamán Tabares, (e) Cristián Arratia Vidal, (f) René Vargas Sandoval, (g) Arnaldo Agostín Cárdenas, (h) Marisol Pizarro Ganga, (i) Nilda Pizarro Ganga, (j) José Becerra Vidal, and (k) Orfelina Casanova Muñoz. Written evidence comprises Tanaka (1980), Oportus (1928) and De Agostini (1945). Instrumental data is derived from DGA (Chile). **(b)** Horizontal lines represent periods with known GLOF occurrence. Confirmed years with GLOF occurrence are highlighted with a dot. Note that the 1977 and 2000 GLOFs from lakes Engaño (Iribarren Anacona et al., 2015) and Calafate (Harrison et al., 2006) are not included as they occurred upstream of General Carrera Lake and were therefore filtered and buffered before reaching Baker River.

The oldest historical evidence on GLOFs in the Baker River watershed are the written records from explorers Carlos Oportus (Oportus, 1928), Alberto M. De Agostini (De Agostini, 1945), and from the Chilean-Japanese expedition lead by Tanaka (Tanaka, 1980) (Fig. 7.4). They mention GLOFs that occurred around 80 years before the first instrumental records, which only started in 1963 (DGA, Chile). Such written and iconographic documents from explorers provide detailed information on flood events from a more objective perspective compared to testimonies from local inhabitants since these explorers traveled through most of the Baker region. For example, Tanaka (1980) was the first and only one to report on GLOFs from the Arco valley before the first detailed study by Winchester and Harrison (2000). Both Tanaka (1980) and De Agostini (1945) documented the destructive power of the Colonia GLOFs during the first half of the 20th century.

In addition to written sources, field interviews of early settlers provide valuable information on the timing and characteristics of historical GLOFs. However, spoken records from inhabitants require careful interpretation because of their subjectiveness and potential mistakes during the transmission of information. In addition, the events need to be corroborated by multiple testimonies before these spoken records are integrated and used as reliable information. Although they are not as continuous as geological GLOF archives, they do provide independent GLOF records that can complement geological information. For example, at least five settlers describe the annual occurrence of GLOFs originating from the Colonia valley between 1881 and the 1960s (Table S7Aa, c, e–g). This frequent GLOF occurrence is in agreement with geological evidence of repeated flooding, as derived from at least 38 sand and coarser sediments lining the Arco valley walls and moraine flanks (Winchester and Harrison, 2000). Another example is the Las Lengas GLOF, a flood event that was previously dated between 1987 and

1998 using LANDSAT images (Iribarren Anacona et al., 2014). Testimonies were used to precisely pinpoint the timing of this GLOF to March 1988 (Table S7Ab–d, h, i, k). Despite this event being highly destructive along the Los Ñadis River, it cannot be observed on instrumental records due to Baker River's high baseflow (cf. chapter 5). Finally, conversational evidence was also used to reveal previously unidentified floods. For example, two interviewees refer to a major Baker River flood in 1977 (Table S7Af, j, f; Fig. 7.4), resulting from extreme rainfall in December 1976 (cf. chapter 5). As such, older type B deposits in the fjord sediment cores could tentatively be linked to this intense rain-on-snow event (cf. chapter 5). Without historical archives, this event might have remained unidentified.

Historical archives are also able to reveal specific flood conditions and the impact of the events on the local population. For example, conversational records describe the Colonia floods in great detail since many settlers attempted to establish cattle farms in the Valle Grande floodplain. Local inhabitants recall that during the flood events between 1881 and the 1960s, large waves of water and debris rushed down the Colonia valley and inundated the valley over its entire width. Due to the increased Colonia River discharge, water from the Baker River was pushed back 15 km upstream of the confluence with Colonia River (Oportus, 1928; Table S7Aa, e, g). Within 24 hours, water levels in Baker River increased by at least 4 m and resulted in the complete inundation of Valle Grande floodplain for several days, reaching the confluence of Del Salto River (Tanaka, 1980; De Agostini, 1945). As such, these GLOFs were significantly larger in magnitude compared to the most recent 21st century GLOFs from Cachet 2 Lake, which were only able to partially inundate Valle Grande (cf. chapter 6). According to several testimonies, the largest Colonia floods took place at the beginning of the 1950s, more specifically in 1951/1952, and in 1962/1963 (Table S7Aa, c, e–g). The written and spoken records also show that the 20th century Colonia GLOFs were most destructive close to the source. They point out that these GLOFs caused major damage to infrastructure and frequently resulted in the loss of human lives and livestock (Table S7Ac, e, g, j), whereas downstream, the floods were less destructive and caused little damage (Table S7Ag). In addition to the GLOFs originating from the Colonia valley, historical documents as well as conversational records point out that the Nef River also experienced GLOFs in the first half of the 20th century, although the Nef GLOFs had a lower magnitude compared to the concurrent GLOFs from Colonia valley (Oportus, 1928; De Agostini, 1945; Table S7Aa; Fig. 7.4).

Aside from providing crucial information on GLOFs in the Baker River watershed, conversational records also highlight an interesting fact about the Baker River. Three witnesses recall that the Baker River was more confined in the first half of the 20th century, and that its width increased significantly from the mid-20th century onwards, occupying more and more farmlands along the river (Table S7Ac, e, f). This observation likely represents an increase in meltwater input and sediment contribution due to glacier recession. In addition, an increase in glacial sediment input over the past century might also explain why sediments are, in general, becoming finer and less organic towards the top of the fjord sediment cores at the head of Martínez Channel (Fig. 7.2). On the contrary, instrumental records show no significant change in Baker River discharge in the past 45 years (DGA, Chile), possibly because meltwater input is counterbalanced by decreasing precipitation (Garreaud et al., 2013).

Instrumental records consist of Baker River discharge and SSC data, which were measured from 1963 onwards, and between 1976 and 2003, respectively, in the framework of the HidroAysén project for hydroelectric dam building purposes (HidroAysén, 2010). These instrumental records can give an estimate on flood magnitude and can be useful to pinpoint specific dates of events. For example, instrumental records were used to define the exact timing of the "early 1977" flood that two witnesses

refer to (Table S7Af, j; Fig. 7.4), to the 28th–30th of December 1976 (DGA, Chile). A limitation of instrumental data is that the source of GLOFs cannot be fully traced without careful monitoring of the tributaries. In contrast, historical records can provide information about the GLOF source. As an example, testimonies from local inhabitants allowed to link the Colonia GLOFs of the first half of the 20th century to Arco Lake, which was at the time blocked by Colonia Glacier, rather than from Colonia Lake itself (De Agostini, 1945; Tanaka, 1980).

Historical archives and instrumental data thus present a powerful and complementary source of information to accurately interpret historical flood conditions and calibrate sediment records. The resolution and timescale of historical archives in the Baker River watershed are intermediate between the low-resolution, multi-millennial flood record of Valle Grande, and the daily resolution of instrumental data which only cover the last decades. In combination with geological archives, such as the high-resolution fjord sediments, they allow reconstructing the Baker GLOF history during the last ~140 years (Fig. 7.4b). This period is particularly interesting since it is defined by a general glacier recession following the last Neoglacial advance during the 17th–19th centuries (Aniya, 2013). The value of historical records to document GLOFs has also been demonstrated in other parts of the world, such as continental Europe and Iceland, where records can cover the past five centuries (Carrivick and Tweed, 2016).

7.3. GLOF occurrence and climate variability

The results of this thesis suggest a close, but indirect, link between GLOF occurrence from ice-dammed lakes in the upper Baker River watershed and climate change. High-magnitude GLOFs from eastern NPI glaciers appear to occur more frequently when glaciers are larger and thicker, at times when climate is cooler and wetter (cf. chapter 6). During Neoglacial maxima, larger glaciers are able to form larger and stronger ice dams, which are in turn able to hold larger lakes (Fig. 7.5). Lake outbursts may be less frequent under such climate conditions, however, when they occur, they generate higher magnitude floods. On the contrary, during periods of minimum glacier extent, ice and glacial lake volumes are low. Consequently, ice dams break more frequently, but they produce lower magnitude GLOFs, which is currently the case with the recent Cachet 2 GLOFs (Fig. 7.5).

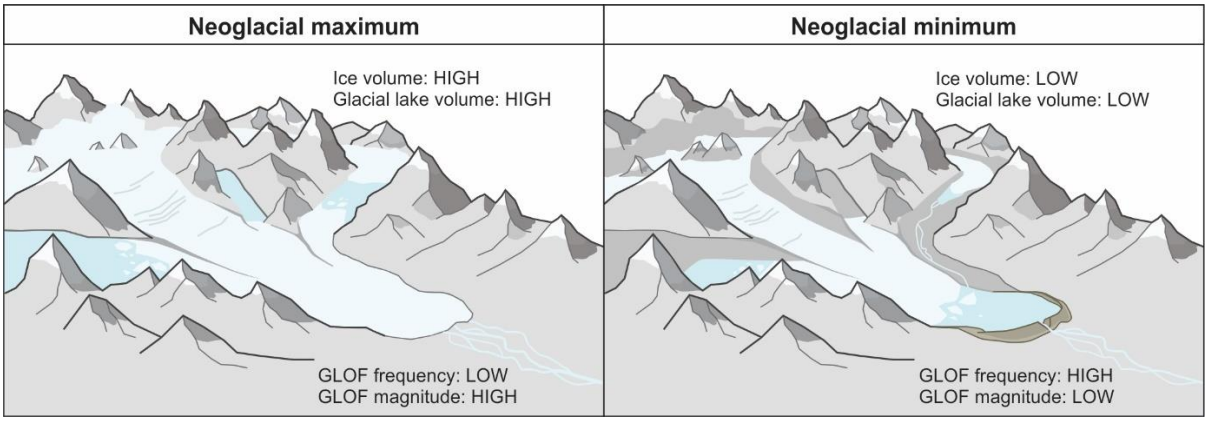

Figure 7.5. Conceptual figure illustrating how GLOF frequency and magnitude change with ice and lake volume. During Neoglacial maxima, ice volume and glacial lake volume are high and high-magnitude GLOFs are predominant. On the other hand, ice volume and glacial lake volume are low during Neoglacial minima, resulting in frequent low-magnitude GLOFs.

The findings of this thesis, which show that high-magnitude GLOFs from ice-dammed lakes are more frequent during Neoglacials compared to periods in between Neoglacials, are in agreement with other studies that hypothesize an increased GLOF risk from ice-dammed lakes at times of glacier advance (Vivian et al., 2001; Benn and Evans, 2010; Round et al., 2017; Bazai et al., 2021). The most straightforward explanation is that larger glaciers can hold larger glacial lakes (cf. chapter 6). Moreover, as ice margins extend further downstream during Neoglacial maxima, more side valleys can be obstructed and in turn form ice-dammed lakes. Compared to moraine-dammed lakes, ice-dammed lakes often have multiple filling and draining cycles because of rapid glacier dynamics. Ice creep rapidly closes off drainage paths after the lake empties and repeated GLOFs can occur from the same lake. It could also be argued that large-scale glacier dynamics of ice recession and growth nested within Neoglacial maxima can result in multiple GLOF cycles from a single valley.

In contrast to GLOFs from ice-dammed lakes, how GLOFs from moraine-dammed lakes are related to climate change throughout the Quaternary remains unclear. GLOFs from moraine-dammed lakes may be increasing with glacier recession since they are related to the formation of moraine-dammed glacial lakes (e.g. Clague and Evans, 2000; Harrison et al., 2018). The current hypothetical link between climate change and GLOF occurrence is that the current increase in proglacial lake size and number as glaciers thin and retreat, will result in an increase in GLOF risk from moraine-dammed lakes (Fig. 7.5) (e.g. Harrison et al., 2018). However, the worldwide compilation of Harrison et al. (2018) shows that GLOF frequency from moraine dam failures currently declines, despite progressing glacier recession. The reasoning behind this current decline remains unclear and requires more investigation.

Interestingly, GLOFs from Arco and Cachet 2 lakes seem to have occurred at a similar frequency. Yet, it appears that the time period during which GLOFs originated from Arco Lake (i.e. 1881–1960s) was much longer in comparison with the current sequence of Cachet 2 GLOFs, which appears to be ending (2008–present) (Fig. 7.4). Arco Lake repeatedly drained over a period of approximately 85 years before a permanent drainage path was established, whereas the Cachet 2 GLOFs seem to come to an end after occurring during about a decade (Fig. 7.6). The most recent Cachet 2 GLOF occurred in November 2020, after a three-year long period without GLOFs. However, it appears that the time it takes for the ice dam to form is increasing with time. Once formed, the ice dam is also failing much faster than at the beginning of the sequence ~ten years ago, as observed by the decreasing trend in peak discharge during GLOFs since 2015 (Figs. 7.6 and S7A). The lake thus empties before it reaches large volumes, creating only relatively low magnitude GLOFs. The latter implies that the strength of the ice dam is decreasing and GLOFs from Cachet 2 Lake might cease in the near future. For now, it appears that Arco Lake experienced more filling and drainage cycles, suggesting that the Colonia ice dam remained more stable during the longer Arco GLOF period. The short time period during which the Cachet 2 GLOFs occurred compared to the Arco GLOF period might thus reflect the accelerated retreat and thinning of Colonia Glacier during the last decades.

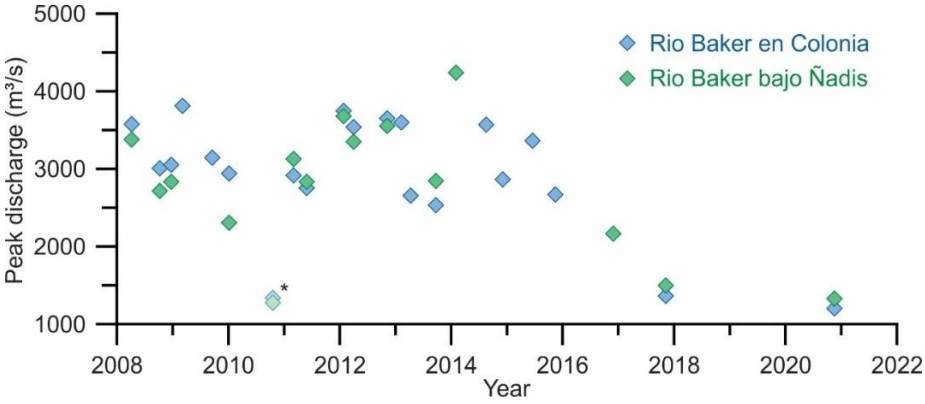

Figure 7.6. Peak discharges measured along the Baker River at DGA stations Rio Baker en Colonia (blue) and Rio Baker bajo Ñadis (green) (see Fig. 3.8 for location) during the 21st century Cachet 2 Lake outbursts. *Note that the October 2010 GLOF is not clearly visible in the discharge data (Fig. S7A), however, this event was previously identified by Jacquet et al. (2017).

References

Albers, S. (2019) Lake sediment records of late Holocene proglacial floods from the San Lorenzo Icefield (Patagonia). Master dissertation, Ghent University, Belgium, 60 pp.

Albers, S., Araneda, A., and Bertrand, S. (2019) Lake sediment records of late Holocene proglacial floods from the San Lorenzo Icefield (Patagonia). In: Jongerendag – Journée des jeunes, Abstracts of communications presented at the 'Master Day' meeting, Gent. *Geologica Belgica*, **23**(1–2), p. 88.

Alvarez-Garreton, C., Mendoza, P.A., Boisier, J.P., Addor, N., Galleguillos, M., Zambrano-Bigiarini, M., Lara, A., Puelma, C., Cortes, G., Garreaud, R., McPhee, J., and Ayala, A. (2018) The CAMELS-CL dataset: catchment attributes and meteorology for large sample studies – Chile dataset. *Hydrology and Earth System Sciences*, **22**, 5817 – 5846.

Aniya, M. (2013) Holocene glaciations of Hielo Patagónico (Patagonia Icefield), South America: A brief review. *Geochemical Journal*, **47**, 97 – 105.

Bastianon, E., Bertoldi, W., and Dussaillant, A. (2012) Glacial-lake outburst flood effects on Colonia River morphology, Chilean Patagonia. River Flow 2012, CRC Press, 573 – 579.

Bazai, N.A., Cui, P., Carling, P.A., Wang, H., Hassan, J., Liu, D., Zhang, G., and Jin, W. (2021) Increasing glacial lake outburst flood hazard in response to surge glaciers in the Karakoram. *Earth-Science Reviews*, **212**, 103432.

Benito, G., Thorndycraft, V.R. Machado, M.J., Sancho, C., Dussaillant, A., and Meier, C.I. (2014). Magnitud y frecuencia de inundaciones Holocenas generadas por vaciamiento de lagos glaciares en el Rio Baker, Campo de Hielo, Patagonico Norte, Chile. In: Schnabel, S., Gutiérrez, Á.G. (Eds.), Sociedad Española de Geomorfología. Cáceres, Spain, pp. 24–27

Benito, G., and Thorndycraft, V.R. (2020). Catastrophic glacial-lake outburst flooding of the Patagonian Ice Sheet. *Earth-Science Reviews,* **200**, 102996.

Benn, D.I., and Evans, D.J.A. (2010) Glacial lakes and outburst floods. *In: Glaciers and glaciation*. vol. 2 Hodder education, London, pp. 86 – 96.

Carrivick, J.L., and Tweed, F.S. (2013) Proglacial lakes: character, behavior and geological importance. *Quaternary Science Reviews*, **78**, 34 – 52.

Carrivick, J.L., and Tweed, F.S. (2016) A global assessment of the societal impacts of glacier outburst floods. *Global and Planetary Change*, **144**, 1 – 16.

Clague, J.J., and Evans, S.G. (2000) A review of catastrophic drainage of moraine-dammed lakes in British Columbia. *Quaternary Science Reviews*, **19**, 1763 – 1783.

Clare, M.A., Hughes Clarke, J.E., Talling, P.J., Cartigny, M.J.B., and Pratomo, D.G. (2016) Preconditioning and triggering of offshore slope failures and turbidity currents revealed by most detailed monitoring yet at a fjord-head delta. *Earth and Planetary Science Letters*, **450**, 208 – 220.

Cenderelli, D.A., and Wohl, E.E. (2001) Peak discharge estimates of glacial lake outburst floods and 'normal' climatic floods in the Mount Everest region, Nepal. *Geomorphology*, **40**, 57 – 90.

Cenderelli, D.A., and Wohl, E.E. (2003) Flow hydraulics and geomorphic effects of glacial lake outburst floods in the Mount Everest region, Nepal. *Earth Surface Processes and Landforms*, **28**, 385 – 407.

De Agostini, A.S.S. (1945) Andes Patagónicos, Viajes de exploración a la Cordillera Patagónica Austral. Segunda edición aumentada y corregida. Buenos Aires. 436 pp.

Dussaillant, A., Buytaert, W., Meier, C., and Espinoza, F. (2012) Hydrological regime of remote catchments with extreme gradients under accelerated change: the Baker basin in Patagonia. *Hydrological Sciences Journal*, **57**, 1530 – 1542.

Fuller, I.C., Macklin, M.G., Toonen, W.H.J., and Holt, K.A. (2018) Storm-generated Holocene and historical floods in the Manawatu River, New Zealand. *Geomorphology*, **310**, 102 – 124.

Garreaud, R., Lopez, P., Minvielle, M., and Rojas, M. (2013) Large-scale control on the Patagonian climate. *Journal of Climate*, **26**, 215 – 230.

Hage, S., Cartigny, M.J.B., Sumner, E.J., Clare, M.A., Hughes Clarke, J.E., Talling, P.J., Lintern, D.G., Simmons, S.M., Silva Jacinto, R., Vellinga, A.J., Allin, J.R., Azpiroz-Zabala, M., Gales, J.A., Hizzett, J.L., Hunt, J.E., Mozzato, A., Parsons, D.R., Pope, E.L., Stacey, C.D., Symons, W.O., Vardy, M.E., and Watts, C. (2019) Direct monitoring reveals initiation of turbidity currents from extremely dilute river plumes. *Geophysical Research Letters*, **46**, 11310 – 11320.

Harrison, S., Glasser, N., Winchester, V., Haresign, E., Warren, C., and Jansson, K. (2006) A glacial lake outburst flood associated with recent mountain glacier retreat, Patagonian Andes. *The Holocene*, **16**, 611 – 620.

Harrison, S., Kargel, J.S., Huggel, C., Reynolds, J., Shugar, D.H., Betts, R.A., Emmer, A., Glasser, N., Haritashya, U.K., Klimeš, J., Reinhardt, L., Schaub, Y., Wilshire, A., Regmi, D., and Vilímek, V. (2018) Climate change and the global pattern of moraine-dammed glacial lake outburst floods. *The Cryosphere*, **12**, 1195 – 1209.

HidroAysén (2010) Centrales hidroeléctricas de Aysén S.A. – HidroAysén. Caracterización del régimen sedimentológico y efectos de la construcción de centrales del PHA. Anexo 2D, apéndice 4, parte 2. 687 pp.

Hizzett, J.L., Hughes Clarke, J.E., Sumner, E.J., Cartigny, M.J.B., Talling, P.J., and Clare, M.A. (2018) Which triggers produce the most erosive, frequent, and longest runout turbidity currents on deltas? *Geophysical Research Letters*, **45** (2), 855 – 863.

Jacquet, J., McCoy, S.W., McGrath, D., Nimick, D.A., Fahey, M., O'kuinghttons, J., Friesen, B.A., and Leidlich, J. (2017) Hydrologic and geomorphic changes resulting from episodic glacial lake outburst floods: Rio Colonia, Patagonia, Chile. *Geophyscial Research Letters*, **44**, 854 – 864.

Iribarren Anacona, P., Norton, K.P., and Mackintosh, A. (2014) Moraine-dammed lake failures in Patagonia and assessment of outburst susceptibility in the Baker Basin. *Natural Hazards and Earth System Sciences*, **14**, 3243 – 3259.

Iribarren Anacona, P., Mackintosh, A., and Norton, K (2015) Reconstruction of a glacial lake outburst flood (GLOF) in the Engaño Valley, Chilean Patagonia: Lessons for GLOF risk management. *Science of the Total Environment*, **527-528**, 1 – 11.

Ishii, Y., Hori, K., and Momohara, A. (2017) Middle to late Holocene flood activity estimated from loss on ignition of peat in the Ishikari lowland, northern Japan. *Global and Planetary Change*, **153**, 1 – 15.

Liu, D., Bertrand, S., Vandekerkhove, E., and Renson, V. (in prep) Provenance of historical flood deposits preserved in fjord sediments (Baker River, Patagonia): A combined Sr-Nd isotopic perspective. *Journal of Geophysical Research: Earth Surface*

Oportus, C. (1928) Informe sobre el problema de colonización de la zona del río Baker. Departamento de Tierras y Colonización, Ministerio de Fomento, Santiago de Chile, 120 pp.

Piret, L., Bertrand, S., Hawkings, J., Kylander, M., Torrejón, F., Amann, B., and Wadham, J. (2021) High-resolution fjord sediment record of a retreating glacier with growing intermediate proglacial lake (Steffen Fjord, Chile). *Earth Surface Processes and Landforms*, **46**, 239 – 251.

Rojas Aldana, A. (2018) Evolution of San Lorenzo proglacial floods (Patagonia) during the late Holocene: Are they related to glacier variability? Master dissertation, Ghent University, Belgium, 34 pp.

Røthe, T.O., Bakke, J., and Støren, E.W.N. (2019) Glacier outburst floods reconstructed from lake sediments and their implications for Holocene variations of the plateau glacier Folgefonna in western Norway. *Boreas*, **48**, 616 – 634.

Round, V., Leinss, S., Huss, M., Haemmig, C., and Hajnsek, I. (2017) Surge dynamics and lake outbursts of Kyagar Glacier, Karakoram. *The Cryosphere*, **11**, 723 – 739.

Syvitski, J.P.M., and Shaw, J. (1995) Sedimentology and geomorphology of fjords. *In: Perillo, G.M.E. (Ed.)* Geomorphology and Sedimentology of Estuaries. Amsterdam, Elsevier, pp. 113 – 178.

Tanaka, K. (1980) Geographic contribution to a periglacial study of the Hielo Patagonico Norte with special reference to the glacial outburst originated from Glacier-Dammed Lago Arco, Chilean Patagonia. Centre Co Ltd, Tokyo, 97 pp.

Thorndycraft, V.R., Bendle, J.M., Benito, G., Davies, B.J., Sancho, C., Palmer, A.P., Fabel, D., Medialdea, A., and Martin, J.R.V. (2019) Glacial lake evolution and Atlantic-Pacific drainage reversals during deglaciation of the Patagonian Ice Sheet. *Quaternary Science Reviews*, **203**, 102 – 127.

Vivian, R. (2001) Des Glaciers du Faucigny aux Glaciers de Mont Blanc. La Fontaine de Siloe, Montmelian.

Warren, C.R., and Sugden, D.E. (1993) The Patagonian Icefields: a glaciological review. *Arctic and Alpine Research*, **25**, 316 – 331.

Winchester, V., and Harrison, S. (2000) Dendrochronology and lichenometry: colonization, growth rate and dating of geomorphological events on the east side of the North Patagonian Icefield, Chile. *Geomorphology*, **34**, 181 – 194.

Xu, M., Bogen, J., Wang, Z., Bønsnes, T.E., and Gytri, S. (2015) Pro-glacial lake sedimentation from jökulhaups (GLOF), Blåmannsisen, northern Norway. *Earth Surface Processes and Landforms*, **40**, 654 – 665.

Table S7A. Historical evidence of Baker River GLOFs. (a) Interviews conducted by Fernando Torrejón from the 25th until the 31st of January 2019, and (b) written records (in Spanish).

Conversational evidence	
Interviewee, Date, Location	Record
(a) Leoncio Escobar Montecino, 25/01/2019, Cochrane	Don Leoncio nació en río Oro en 1932. Su padre Leonor Escobar provenía de Rancagua y se estableció en río Oro posiblemente en 1902 (antes que se determinara la línea divisoria de límites entre Chile y Argentina). Su madre era originaria de la localidad de Quilleco (Región del Bibío). En esos tiempos sólo habían tres familias colonizadoras en río Oro señala don Leoncio: "*la de Juan Pizarro, Pedro Muñoz Jara y Leonor Escobar*". Cuando fueron expulsados de río Oro por la gendarmería argentina, la familia de don Leoncio se estableció en el sector del "*lago Juncal, en diciembre de 1940*" (entonces él tenía 8 años). Según su relato, en 1940, en el actual sector donde se encuentra el pueblo de Cochrane, "*había como cinco casas no más, todo estaba lleno de vacunos*". En 1948 trabajaba como peón en la estancia Baker, en el valle Chacabuco, En 1960, a los 28 años, acompañó la expedición japonesa que hizo estudios en el lago Colonia y alrededores, junto a "*René Comesaña y Cuyul…, el del bote*". A la edad de 30 años (1962), don Leoncio ya trabajaba en Valle Grande "*como peón de Enrique Villalobos Ramírez, quien tenía un gran campo allí*". Fue en esa época cuando presenció una "*inmensa creciente" del río Colonia y Baker entre el 1 de diciembre y el 5 de enero cuando era la creciente*". Describe que cuando se producía la inundación "*el Baker empezaba a enaltar y se sostenía, subía 10 metros, después 15 metros…, no se notaba la crecida*". "*En 24 horas se inundaba todo, se tapaba todo el Valle Grande…, el Baker era un sólo lago, hasta la orilla de la pasarela del Salto*". (Se trataba de la antigua pasarela que estaba como a 100 metros de la actual pasarela según el mismo comentó). Agrega don Leoncio: "*la creciente tenía 1000 metros de anchura cuando reventaba…, salía por arriba y debajo de los nevados…, duró como un mes todo*" En este caso se refiere a la avenida del río Colonia. Siguiendo las instrucciones recibidas, cuando empezó la inundación, don Leoncio le dio aviso a su patrón y les ensilló dos caballos para ir a "*verla desde unos motecitos*". "*A las 5 (AM) ya se estaba produciendo la creciente, venía un oleaje suave…, una ola tras otra, hasta que venía una grande y arrasaba con todo*". "*El patrón casi fue alcanzado por la crecida, estaban tomando fotografías, debieron salir al galope del lugar…*". Recuerda además que con la creciente de 1962 "*venían nubes de moscos que*

	entraban por la boca, molestaban en la cara, los caballos tenían manchones de moscos encima del cuero, era una plaga de moscos terrible…, duraba uno o dos meses". "*A las 5 (AM) ya se estaba produciendo la creciente, venía un oleaje suave…, una ola tras otra, hasta que venía una grande y arrasaba con todo*". Don Leoncio también presenció otras inundaciones del Baker antes y después de 1962, pero éstas, según recuerda, fueron de menor magnitud a la del 62, alcanzando "*sólo hasta la mitad del Valle Grande*". Refiriéndose a las crecidas del río Baker, don Leoncio entrega un importante dato, señalando que las crecidas que inundan el Valle Castillo, a continuación de Valle Grande aguas arriba, vienen directamente desde el Baker, posiblemente por avenidas del río Nef.
(b) Misael Maldonado, 26/01/2019, Cochrane	Don Misael nació en 1945, su papá llegó en 1932 al sector de San Lorenzo, desde Puerto Montt, estableciéndose en la confluencia de los ríos el Salto y Tranquilo. En referencia a la crecida del río Los Ñadis comenta que: "*habría sido entre los días 6-8 de marzo…, entre 1985-1987*", pero su esposa, presente también en la conversación señala que "*fue después…",* sin precisar el año, tomando como referencia la fecha de nacimiento de uno de sus hijos. Cuenta don Misael: "*fue una crecida rápida…, duró desde las 5 hasta las 11 de la noche, dejó todo lleno de barro…, traía grandes palos y lengas*" (*Nothofagus pumilio*). En el sector Los Canelos, curso medio del río Los Ñadis, donde se ubica su campo, la altura de la crecida alcanzó aproximadamente "*los 4 metros…, me llevó unos terneros, tapó valles con arena*". Comenta que "*entre octubre y noviembre el Ñadis siempre iba crecido, para pasar a caballo había que esperar 1 ó 2 días a que bajara, pero nunca había crecido tanto el río*". Don Misael también hace algunas alusiones a las "*crecientes del Colonia*", pero sin aportar datos de mayor relevancia, diciendo eso si que "*el Colonia se le atravesaba al Baker, haciendo que la creciente llegaba hasta el Valle Castillo*".
(c) Luzmira Muñoz, 25/01/2019, Los Ñadis region, Cochrane	Doña Luzmira nació en 1951 en el sector los Ñadis a orillas del río Baker, cuando ella tenía 9 meses de edad habría ocurrido una "*gran crecida del Colonia*" (1951 ó 1952), de acuerdo a lo que le habría contado su mamá. Agrega, "*en esa crecida se ahogó el papá de Segundo Quinto…, salió a buscar sus ovejas y entonces lo alcanzó la crecida*". De acuerdo a su relato, cuando ella tenía 6 años (posiblemente en 1957) "*se produjo una tremenda creciente del río Colonia que mató muchos animales*" y a algunos colonos de la zona. Indica, "*siempre había trueno cuando iba a venir la creciente... Venía una avalancha grande y después*

	todo se recogía". Después cuando el Baker retomaba su normalidad "*los árboles quedaban todos blanquitos de arenilla*", refiriéndose al sedimento que cubría sus ramas y hojas. Finalmente relata que "*todos los años habían crecidas en el Baker*" y después de las crecidas, cuando salían a recolectar calafates (Berberis sp) todas las "*matas de calafates estaban de color gris por la tierra*", en grandes zonas ribereñas, refiriéndose muy probablemente al fino sedimento glaciar que las cubría después de cada avenida del río. Otro dato interesante entregado por Luzmira es que el sector de la "*tapera de Jaque*", ubicado a unos 200 ó 300 metros aguas abajo de la confluencia del Colonia en el Baker, "*se inundaba completamente*". Doña Luzmira llama a la gran crecida del río Los Ñadis "*el reventón del Ñadis…*" y aunque no recuerda bien la fecha exacta dice que ocurrió en el verano, entre los años 1988-1990. Añade que aquella "*crecida duró como 3 horas... Se perdieron yeguarizos y otros animales que quedaban enganchados arriba de los ñirres*" (se refiere a la especie arbórea Nothofagus antárctica). "*Quedó una gran palizada y mucho barro en las riberas del río cuando bajó la creciente*". Recuerda además que la crecida dañó las dos pasarelas del río Ñadis "una la dobló y otra la cortó". Don Arturo Arriagada, esposo de Luzmira, presente en la entrevista, agrega que su antigua casa, hoy desaparecida, que se ubicaba al costado de la actual Ruta 7, en un lugar aún reconocible, "*quedó rodeada de agua y palos…, yo iba poniendo cañas para ver como subía el nivel de la creciente*". La hermana de don Arturo, que también vivía en las cercanías "*amaneció en una balsa con el agua hasta las rodillas*". Señala finalmente que "*el Ñadis crecía todos los años…, pero nunca se había visto una tan grande*". *"… don Pablo Pizarro Ganga, antiguo poblador del sector (hoy fallecido), quien le contó de la gran crecida del Ñadis entre 1988 y 1990, había ocurrido por causa del "reventón del arroyo Las Lengas" (afluente del Ñadis) ubicado frente al campo de ese poblador, que hizo que "el río Ñadis alcanzara dos metros de altura…, en partes menos en partes más*". Tanto en el lecho del río Los Ñadis como en sus riberas se pueden observar esparcidos antiguos restos de troncos de árboles, muchos de los cuales, según don Ramón, corresponderían a aquellos "*arrastrados por la creciente del Ñadis*".
(d) Ramón Ángel Caucamán Tabares, 26/01/2019, Los Ñadis sector, Cochrane	Nacido el 4-II-1951 en Cochrane, ocupó el sector alto de la cuenca del río Los Ñadis alrededor de 1999. En este caso se trata de un informante cuyo relato es de segunda mano o de oídas, pues fue don Pablo Pizarro Ganga, antiguo poblador del sector (hoy fallecido), quien le contó de la gran crecida del Ñadis entre 1988 y 1990, había ocurrido por causa del "*reventón del arroyo Las Lengas*" (afluente del Ñadis) ubicado frente al campo de ese poblador, que hizo que "*el río Ñadis alcanzara dos metros de altura…, en partes menos en partes más*". Tanto en el lecho del río Los Ñadis como en

	sus riberas se pueden observar esparcidos antiguos restos de troncos de árboles, muchos de los cuales, según don Ramón, corresponderían a aquellos "*arrastrados por la creciente del Ñadis*".
(e) Cristián Arratia Vidal, 31/01/2019, Vargas Lake sector, Tortel	Don Cristián nació en 1939 en Vilcún (Región de la Araucanía), llegó a trabajar a un campo en el sector Balsa Baker en 1953, a la edad de 14 años. (1953), donde también trabajaba su padre. En 1959 se estableció junto a su familia paterna en el sector río Ventisquero (Ventisquero Chico), ribera oeste del Baker, río abajo del Corte San Carlos. Don Cristián recuerda crecidas del Baker desde 1955 a la década de 1960, que "*tapaban todo el Valle Grande hasta cerca del Valle Castillo, quedaban sólo pedacitos de cercos donde se podían ver los alambres…, lo que agarraba lo mataba todo…, los animales quedaban arriba de los ñirres*". Menciona que "*una gran creciente en los años 1962 ó 1963 inundó todo el sector del lago Vargas*", su señora Rosa Vargas, presente en la entrevista, contradice las fechas indicando, con mucha seguridad, que dicha creciente "*fue en 1966…".* En aquel entonces don Cristián se encontraba en su campo del río Ventisquero señalando que: "*el agua se metió adentro de la casa, estaba con mi mamá en el fogón [cocina]…, deben haber sido las 9 de la noche, pues aún no me acostaba, cuando fue el golpe de agua grande…, una caja con una gallina con pollos flotaba en el fogón…, abrí la puerta y se me entró toda el agua.... Con el agua más arriba de la cintura salí a buscar mis animales que estaban en el bajo…, los saqué. Desde el corte San Carlos hacia abajo la creciente tapó todo*". Aquella crecida (1966) "*tapó todos los campos bajos en el sector de lago Vargas, alcanzando cerca de mi casa*" (que corresponde a su actual vivienda muy cercana a la Ruta 7). "*Los animales muertos iban quedando melgados por las orillas del Baker…, río abajo del corte, el río arrastraba tremendas palizadas y barro*". Después de esta gran crecida del Baker don Cristián cambio su población en el campo de río Ventisquero "*como 300 metros más arriba, porque en lo plano se tapa todo con el agua*". Don Cristian también menciona una gran creciente del río Baker en el año 2005, atribuida al vaciamiento repentino del lago Cachet, narrando que en el sector de la confluencia del los ríos Vargas y Baker "*donde está el muelle, el río iba tapadito de palos…, espeso de palos…, el agua llena de barro, no se podía andar ni en bote…, después han venido crecientes pero más chicas*". Añade finalmente: "*antes de las grandes crecidas el Baker corría más encajonado*". Don Cristián también recordó la gran crecida del río Los Ñadis, al preguntarle si esta habría ocurrido en 1988, respondió: "*por ahí tuvo que ser…, deje mis caballos y aperos en un puesto en Ñadis bajo, las riendas y espuelas las colgué en un árbol…, cuando vino la crecida en la noche el puestero alcanzó a soltar mis caballos…, cuando regresé sólo*

	recuperé las riendas y las espuelas…, las monturas y lo demás se perdió todo; a los días. *después aparecieron los caballos*". "*Esa creciente fue tan fuerte que dio vuelta la pasarela de donde la señora Rosa Quinto*", refiriéndose a la pasarela que se encontraba en el sector Ñadis bajo, que aún existe.
(f) René Vargas Sandoval, 31/01/2019, Caleta Tortel	Don René nació el 4-V-1960 en el sector de Lago Vargas, conversando sobre las grandes inundaciones causadas por el río Baker indica: "*en 1977 se produjo la última creciente grande del Baker, a la casa de mi mamá le llegó el agua…, se le inundó toda la huerta y parte del campo*". El campo de doña Julia Sandoval, su madre, se ubica a orillas del Baker en el sector del mismo lago Vargas. Continua señalando don René: "*el Baker antes tenía menos cauce, ahora es más ancho, el Baker…, cuanto campo se ha comido*". Se refiere, con mucha probabilidad, a que antiguamente la caja del río era más angosta.
(g) Arnoldo Agustín Cárdenas, 25/01/2019, Caleta Tortel	Nacido el 25-XII-1950, en la localidad de Perito Moreno, Argentina, el año 1961 se vino al Baker y en 1972 se radicó definitivamente en Caleta Tortel. Don Arnoldo sólo menciona que entre los años 1961-1962 se produjo una "*gran creciente del Colonia…, esa inundación se extendía río arriba por el Baker hasta el sector de Valle Grande…, cuando bajaba la creciente, las vacas quedaban enredadas arriba de las lengas y ñires a cinco o seis metros*". Añade, "*en el sector de Tortel no causó mucho daño*".
(h) Marisol Pizarro Ganga, 26/01/2019, sector bajo Ñadis, Cochrane	Su familia llegó al sector los Ñadis en 1940, doña Marisol nació el 29-VI-1961. Según recuerda la crecida del río "*habría sido entre 1990-1992*". Entonces "*el lago se desforonó [sic] en el fundo El Triste*", nombre del campo de su hermano Pablo (ya fallecido) que estaba en la ribera norte del río Los Ñadis, frente al estero Las Lengas. Llamaremos también lago Las Lengas al relativamente pequeño lago proglaciar que menciona doña Marisol y que se vació repentinamente sobre el estero del mismo nombre, generándose el evento que llevó al desbordamiento catastrófico del río Los Ñadis. Marisol continua relatando: "*tiró mucha arena…, donde vivía Pablo, tapó todo de arena…, la crecida llegó a casi dos metros de su casa*". "*El lago tenía un cerrito en el centro, que ya no estaba después que se vació. La crecida del Ñadis salió con todo…, se vino con lengas, arrasó con los potreros, animales, cercos…, desaparecieron varias casas en Ñadis bajo, en esa parte la crecida habría alcanzado los 7 metros en lo plano…, depositó barro en los campos que duró como tres años. El potrero de mi mamá desapareció todo…, perdió todos los chivos…, los yeguarizos quedaron encajados en los árboles*".
(i) Nilda Pizarro Ganga, 27/01/2019, Cochrane	Doña Nilda, hermana mayor de Marysol Pizarro, no recuerda bien el año en que se produjo la catastrófica avenida del río Ñadis señalando: "*puede haber sido el año 1988 ó el 89…, el arroyo Las Lengas se desbordó en el río*

	Ñadis…, en Los Canelos lo limpió todo, a los árboles les sacó la corteza". Los Canelos es el sector donde se encuentra el campo de don Misael Maldonado. En el campo de su mamá, sector bajo Ñadis, cuenta que el río "*comenzó a crecer rápido, viejito del puesto salió con el agua al cuello…, el potrero donde estaba el puesto se lo llevó todo, se llevó los chivos de la mamá…, quedó tapado con barro y greda gris, pero en la primavera salió pasto. Después de la crecida doma Nilda dice que "el río bajó super-rápido, en casi dos horas…, las yeguas quedaron arriba de los ñirres, desde el puente nuevo [Ruta 7] hasta la pasarela [Ñadis bajo], se veían los animales colgando de los ñirres y mucha palería*".
(j) José Becerra Vidal, 25/01/2019, Caleta Tortel	Nacido en río Bravo el 29-II-1964, hijo de Roberto Becerra Valdés quien llegó a Tortel desde Toltén (Región de la Araucanía), entre los años 1947-1948, y Juana Vidal Trenco, pobladora de Cochrane. Don José recuerda una gran crecida del Baker ocurrida "*el 7 de enero 1977…, es la más grande que he visto*". Cuenta que, "*el Baker venía de lado a lado, tapo todo, playas, barrancas…, sólo se veía la parte de arriba del monte*"; se refiere a que solo quedaban visibles las copas de los árboles del bosque ribereño. El sector las Brisas (Tortel), "*estaba todo tapado de agua*". Cuenta don José que la inundación bajó paulatinamente durante una semana hasta que el río alcanzó nuevamente su nivel normal. Recuerda muy bien dicha crecida del Baker pues en ella se ahogaron su cuñado y sobrinos que venían en una balsa, comenta "*yo con mi papá veníamos en otra balsa y nos salvamos…".* La crecida "*arrasaba con todo en Tortel, chalanas y botes…, si uno tenía maderas y animales se lo llevaba todo; días después, cuando salía a buscar leña en bote, encontraba animales flotando, todos hinchados*" en el fiordo Baker.
(k) Orfelina Casanova Muñoz, 29/01/2019, Vargas Lake sector, Tortel	Hija de don Bautista Casanova Fuentes y doña Irma Zulema Muñoz Gajardo, doña Orfelina nació en 1959 en el sector de Laguna Larga. En 1977, junto a su marido Pablo Pizarro Ganga, se radicó en el fundo El Triste, sector Ñadis medio, frente al estero Las Lengas. Doña Orfelina fue testigo presencial de la inusual crecida del río Ñadis, ocurrida "*los primeros días de marzo de 1988…, mi hija Sofía tenía 3 años*". Según nos relata, de acuerdo a lo que le contaba su esposo Pablo, al lago (Las Lengas) le caían témpanos del ventisquero "*que estaba allí encima…*"; en la actualidad, el aludido ventisquero o glaciar se encontraría más alejado del lago. "*Ese verano fue bastante caluroso y seco, el río [Los Ñadis] venía bajo; como a las 10 de la mañana empezó a crecer un poquito y en las orillas se juntaron muchas hojitas y una espuma blanca…, Pablo me dijo que rara la crecida del río*".

	Orfelina cuenta que fue a buscar cebollas a la huerta que tenía en el bajo cerca del río, mientras tanto la crecida del estero Las Lengas, que desembocaba en la ribera sur del río Los Ñadis, frente a su campo "*estaba formando una represa de palos*". Cerca de las 11 de la mañana aquella represa acumuló tanta agua que "*reventó, se empezó a venir toda esa cuestión…, se vino de un golpe*". Un poco antes Pablo había ido al "*potrero del bajo a sacar unos chivos…, entonces reventó ese inmenso montón de palos y el golpe de agua los tiró para afuera*" (se refiere a Pablo y sus animales). La violenta crecida del estero Las Lengas, según el relato de Orfelina, "*volvió para atrás el Ñadis, unos mil metros más o menos…, todo lo que estaba emplayado [sic] quedó tapado de agua*". La crecida llegó a metros de su casa, mientras sacaban las cosas más importantes y las llevaban al cerro donde se refugió Pablo Orfelina y sus 3 hijas. La altura a la que llegó el agua en su campo habría alcanzado entre los "*10 ó 15 metros*" según nos cuenta, "*a un coigüe grande del bajo le llegó el agua hasta la copa…, quedó blanquito*", (sería por (sedimento acarreado por la crecida); "*la anchura del río se desparramó*". "*El ruido que produjo todo eso fue impresionante*". A las cuatro de la tarde el Ñadis tenía el caudal previo a la gran crecida dice Orfelina, "*el río iba bajito, bajito…*". *En las riberas del "Ñadis quedó un puro barrial hasta mismo abajo, quedó pura arena, era de color plomo como yeso…, después se secaba y era un polvillo. Las lengas quedaron blanquitas*". La crecida que arrastró todo este sedimento glaciar descortezó los árboles ribereños "*les sacó toda la cáscara*". Río abajo se rellenaron muchos bajos en ambas riberas del Ñadis: "*se formaron potreros planitos donde creció mucho pasto…, como en Los Canelos donde Misael Maldonado*". Allí la mayor intensidad de la crecida se manifestó alrededor de los 5 de la tarde, cuenta doña Orfelina, mientras que en el curso inferior del Ñadis "*la crecida pasó como a las 11 de la noche*" arrasando con animales y casas cuyos pobladores debieron refugiarse en pequeños cerros donde "*se amanecieron…, como la familia de Rosa Quinto*". En las riberas del curso inferior del Ñadis quedaron "*animales colgados de los árboles, yeguarizos colgados de las patas*". Con posterioridad al evento, unos cuantos día después de ocurrido el evento el esposo de doña Orfelina fue a explorar la zona llegando al lago del que nacía el estero Las Lengas, comentándole que éste habría quedado vacío, según sus palabras, Pablo de dijo: "*el lago quedó seco*".

Written documents	
Source	Record
Oportus (1928)	No puede utilizarse para colonización el hermoso mallín de unas 5 mil hectáreas situado entre le Sección La Colonia y la desembocadura del río

	Cochrane, en el Baker, porque la crecida de este río, que se verifica una vez en al año lo inunda completamente subiendo el agua hasta unos cuatro metros sobre el nivel premanente del río. Esta crecida del río es un fenómeno interesante: El río de la Colonia y el río Nef, en épocas distintas y entre los meses de Diciembre a Abril inclusive, vacian un enorme caudal de aguas en al río Baker; este aumento considerable del caudal de los ríos de La Colonia y Nef, parece que tiene su origen en al desprendimiento de las inmensas masas de nieve de sus orígenes, las qua socavadas por las lluvias y los vientos propios del verano, se precipitan licuándose y lanzando el volumen de las aguas de los ríos nombrados en el cauce del Baker. Esta crece llega sin ruido a los campos y dura más o menos 24 horas. Los mallines inundados por la crecidas no pueden utilizarse ni aún con caballares antes de que de efectúe el fenómeno, porque les animales sorprendidos por las aguas no tienen tiempo para trepar a los cerros del lado Sur u Oriente y perecen ahogados casi todos. Después de la crece estos campos pueden admitir animales.
De Agostini (1945)	Rastros recientes de inundación del río Colonia son los montones de troncos que encontramos apiñados entre los árboles de la floresta y cubiertos todavía de barro y terreno pantanoso y lleno de charcos de agua. El desbordamiento del río Colonia, que todos los veranos se repite infaliblemente desde los primeros días de enero hasta febrero, tiene en constante inquietud a los pobladores de la zona, quienes explican este fenómeno con las más extrañas hipótesis. La crecida se efectúa en 24 horas, sin que la precedan signos excepcionales ni particulares indicios, alcanzando un volumen impresionante. Una enorme masa de agua turbia y barrosa se vuelca repentinamente de la montaña y se precipita en el valle, arrastrando consigo grandes troncos de árboles arrancados de la floresta, y cubriendo totalmente el lecho del río en un ancho de 600 m. La corriente es tan impetuosa que rechaza a la del Baker y la hace retroceder por unos 15 km, elevando el nivel normal de sus aguas unos 4 m, como lo atestiguan los gajos y residuos vegetales que quedan a esa altura entre las ramas de los árboles, después de la inundación. Cuando los colonos desconocían aún el terrible poder de la creciente y, por lo tanto, descuidaban retirar el ganado a tiempo de la zona afectada, muchos fueron los animales vacunos y caballares que perecieron ahogados. Algunos esqueletos de estos animales colgaban de los árboles todavía varios meses después como macabro trofeo de la terrible inundación. Según las referencias de Vilches, que ha recorrido esos parajes en busca de sus vacunos, hay allí un lago de donde sale el río Colonia. Debemos pues seguir las inflexiones del río, caminando al pie de altos barrancos, entre guijarros casi todos de granito y diorita, desprendidos de estas terrazas fluvioglaciales por efecto de la potente erosión de las aguas durante las inundaciones. Corpulentos troncos de coihue destrozados, pero

aún con sus raíces, yacen esparcidos a la orilla del río como elocuente testimonio de la potencia extraordinaria de las aguas, que, llenando a gran altura la cuenca de orilla a orilla, alcanzaron a desarraigar de la floresta aquellos árboles gigantescos.

En la extremidad occidental del lago, cuyo largo calculamos en siete u ocho kilómetros, baja de la cordillera un gran glaciar que llena toda la cuenca final del valle. La costa oriental del lago, desde donde sale el Colonia, es desplayada y baja, y no hay ningún vestigio que pueda revelar desbordamiento alguno de las aguas debido a un repentino desmoronamiento producido en la margen del lago. Con todo, hay rastros positivos de un notable levantamiento del nivel del lago, señalado por un tronco gigantesco de coihue elevado unos metros sobre el nivel normal de las aguas y por otros árboles más pequeños arrastrados hacia el interior hasta unos 10 m de altura sobre la superficie ordinaria, a causa, según parece, de un rápido crecimiento del lago.

No alcanzamos a ver el interior de la cordillera, pero, por la configuración del valle y del glaciar, me parece tener ya suficientes motivos para suponer que las causas de los desbordamientos de las aguas, que originan las inundaciones, deben buscarse en otro lago marginal, directamente ligado al glaciar. Se produciría el mismo fenómeno que observamos en otros lagos andinos obstruidos por glaciares, de lo cual es típico ejemplo lo que acaece con el glaciar Moreno, del lago Argentino.

Durante la primavera, el lago marginal, obstruido por el glaciar, empieza a subir de nivel a causa del deshielo y de los torrentes glaciares que allí se descargan, logrando su mayor altura en los meses de enero y febrero, cuando llegan los intensos calores estivales. En dicho período, por la presión que ejerce sobre el hielo la masa de agua encerrada en el lago y, al mismo tiempo, por la infiltración de diversas Corrientes por entre las grietas del glaciar, que constantemente se ensanchan, se produce en el glaciar un gran corte en el que se efectúa rápidamente el vaciamiento del lago superior, descargando sus aguas en el de más abajo, el que a su vez vuelca sus aguas en el valle del río Colonia*.

** Este fenómeno es definido en glaciología con la palabra islandesa jokullhlaup, esto es, algo así como "desagüe repentino", y es de ocasional ocurrencia en los sectores englaciados de la Patagonia, el último de los cuales sucedió en la zona del glaciar Bernardo durante el invierno de 2007 (N.E.).*

Según me han asegurado los pobladores de este valle, la inundación vuelve a repetirse algunos años a fines de abril o principios de mayo, pero en forma más reducida. También en el valle del río Nef, más al norte, se produce este fenómeno de desbordamiento, aunque en menor proporción.

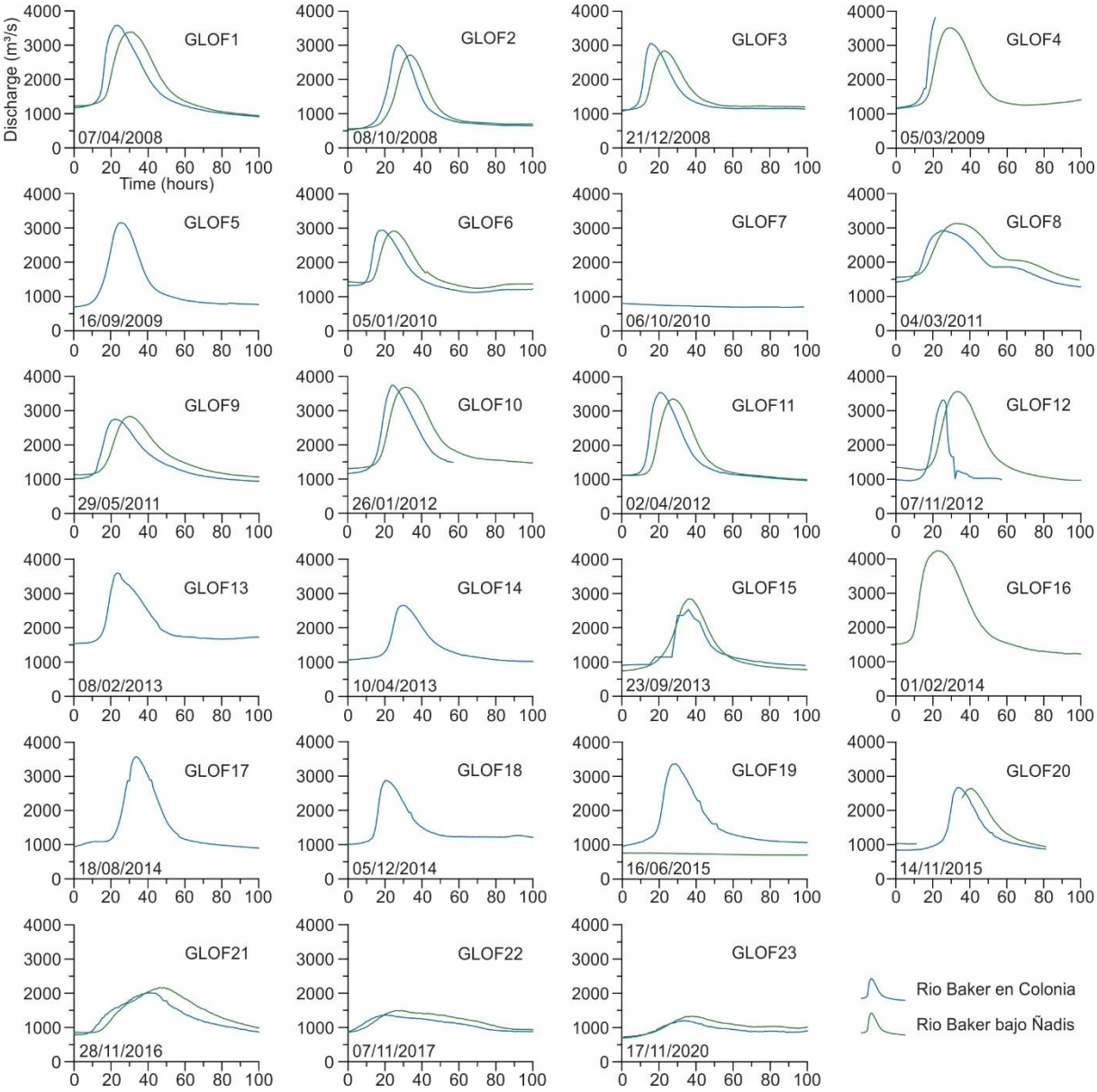

Figure S7A. Hydrographs of GLOFs from Cachet 2 Lake measured along the Baker River at DGA stations Rio Baker en Colonia (blue) and Rio Baker bajo Ñadis (green) (see Fig. 3.8 for location). GLOF peak discharges are decreasing and becoming less defined since 2015. Note that GLOF7 is not visible on the hydrograph, however this event was previously identified by Jacquet et al. (2017).

8. Conclusions and outlook

8.1. Conclusions

In this section, the research questions that were identified in the introduction of this thesis are answered.

1. How are Baker River GLOFs recorded in fjord sediments?

High-resolution bathymetric imaging shows that the subaquatic delta at the head of Martínez Channel is deeply incised by sinuous channels. The presence of sediment waves and coarser sediment within these channels reflects recent sediment transport by turbidity currents (chapter 4). This is confirmed by the abundant turbidites in fjord sediment cores on the delta plain in front of the main submarine channel (chapter 5). Although the turbidity currents are likely triggered by extreme discharge events at the Baker River outflow (chapter 4), most GLOFs were not able to create turbidity currents. Instead, the turbidites at the head of Martínez Channel are most likely associated with heavy rainfall or rain-on-snow events. Our results show that the 21st century GLOFs that originated from the emptying of Cachet 2 Lake are registered in the sediments of Martínez Channel as fine-grained and organic-poor deposits, intercalated in slightly coarser and more organic background sediments. The composition of the GLOF deposits reflects the release and transport in suspension of high amounts of glacial flour during GLOFs.

Although the occurrence of Baker River GLOFs during the 21st century is recorded in the sediments of Martínez Channel, our results show that not all GLOFs are registered as individual layers. Indeed, 21 GLOFs from Cachet 2 Lake occurred between 2008 and 2017, but only three to six layers are visible in the cores. In case of high GLOF frequency, i.e. GLOFs occurring less than ~one year apart, it is not possible to distinguish each individual event as the GLOF deposits are not separated by enough background sediments. Our results also show that the deposits with the clearest GLOF signature represent the first events of this sequence, which suggests that sediment availability plays a more important role than flood magnitude in controlling GLOF deposit properties. In other words, GLOF magnitude cannot be reconstructed using fjord sediments.

Although fjord sediments may not always register GLOF frequency and magnitude, this thesis highlighted the potential of fjord sediment archives to provide long-term, i.e. multi-centennial, GLOF records at high temporal resolution. Given the unique context of the Baker River system, i.e. a significant portion of the watershed is vegetated resulting in a clear lithological contrast between GLOF deposits and background sediments, our results may only be applicable to fjord sediments deposited in similar climate and environmental settings. Fjord sediments may only be usable as GLOF archives in temperate regions, where the nature of the GLOF and background deposits are clearly distinct.

2. How are Baker River GLOFs recorded in terrestrial and historical archives?

The floodplains along the Baker River constitute another reliable archive of past GLOF occurrence. Based on our observations from 36 floodplain sites along the Baker River and its tributaries, we showed that the potential to register GLOFs is not only controlled by the elevation above and connection with the river, but also by the distance from the source valley (chapter 7). Locations downstream of the confluence of the source valley with the Baker River, which are affected by direct flooding, most likely only record the highest magnitude GLOFs. At these locations, GLOF sediments might not be deposited homogenously across the floodplains. The most promising floodplain along Baker River is Valle Grande,

which is located upstream of the confluence with the Colonia River, and is affected by backwater flooding during GLOFs originating from the Colonia valley. In Valle Grande, GLOF sediments are distinguished by their lower organic content compared to the background sediments, due the high input of glacial sediments released during GLOFs. Some of these organic-poor deposits may however also represent precipitation-driven floods.

A last group of archives that has proven to be useful to interpret and calibrate geological records of GLOF occurrence is historical archives. They comprise written and spoken records from explorers and early settlers in the Baker River watershed. Although they require careful interpretation due to their subjectiveness and potential mistakes during the transmission of information, these archives provide independent GLOF records that complement geological archives and they contain detailed information on flood conditions and on their societal impact. In the Baker River region, they revealed previously unidentified events, and were used to locate the source of specific GLOFs.

In both marine and terrestrial archives, Baker River GLOFs are registered as organic-poor deposits, reflecting the release, transport, and deposition of large amounts of material of glacial origin during GLOFs. Marine archives, in which the organic-poor and finer signature of GLOF sediments contrasts with the background sediments, can be used to reconstruct Baker River GLOF occurrence at high temporal resolution. Although the fine-grained signature of GLOF deposits in fjord sediments is somewhat counterintuitive, as extreme discharge events are generally recorded as coarse-grained deposits due to the extreme hydraulic conditions, our results show that they clearly reflect the glacial nature of the sediment released during GLOFs. They represent glacial sediment settling from the buoyant plume, and ultimately draping the fjord bottom relatively independently of the bathymetry. Floodplain archives, on the other hand, do not display a temporal resolution that is as high as fjord sediments due to their slow accumulation rate, but they are better suited to generate continuous, multi-millennial, GLOF records and eventually, to observe long-term changes in GLOF frequency. The origin of flood deposits in floodplain archives, however, might be more challenging to determine. Complementary to these two geological archives are the historical sources of GLOF evidence, whose temporal resolution and quality of information are intermediate between geological archives and instrumental data.

3. Is there a relationship between GLOF frequency and climate variability during the late Holocene?

The flood record obtained from the Valle Grande floodplain presents a continuous 2.75 kyr record of flood activity (chapter 6). Sedimentological and historical information suggest that the flood deposits primarily represent high-magnitude GLOFs. Results from this thesis indicate that high-magnitude GLOFs occurred intermittently in the upper Baker River over the past 2.75 kyr, and that their frequency was particularly high between c. 2.57–2.17 cal kyr BP, and c. 0.75–0 cal kyr BP. Comparison with proxy records of glacier variability shows that periods of increased high-magnitude GLOF occurrence are coeval with Neoglaciations III and V. As these glacier advances seem to result from lower-than-average temperatures and wetter conditions, a strong, but indirect, relationship is suggested between climate variability and GLOF occurrence. We hypothesize that, on multi-millennial timescales, high-magnitude GLOFs from eastern NPI glaciers occur more frequently when glaciers are larger and thicker, as such glaciers are able to form larger and stronger ice dams, which in turn hold larger lakes.

Therefore, our results suggest that the probability that high-magnitude GLOFs from ice-dammed lakes occur decreases as glaciers thin and retreat. Although isolated cases of new lakes formed behind large glaciers could still produce large GLOFs locally, the likelihood of large lake drainage and therefore high-

magnitude GLOF occurrence decreases. Conversely, GLOF risk from moraine-dammed lakes may increase during glacier recession because of the rapid growth of glacial lakes and formation of new lakes.

In summary, the main research highlights of this thesis are:

- Multibeam mapping of the fjord-head delta of Chile's largest river revealed deep active channel-levee systems;
- In fjord sediments, GLOFs are registered as fine-grained organic-poor layers, and not as turbidites, reflecting the large amount of glacial sediments released during GLOFs;
- The 2.75 kyr flood record generated from Valle Grande floodplain sediments suggests that high-magnitude GLOFs were more frequent during Neoglaciations III and V, in response to colder and wetter climate conditions, which implies a close, indirect, link between climate change and GLOF occurrence;
- High-magnitude GLOF frequency decreases as glaciers thin and retreat.

8.2. Outlook

This thesis improved our understanding of the relationships between GLOF occurrence and climate change. However, this research also generated several new questions that could receive further attention.

In this study, GLOFs were reconstructed using fjord and floodplain sediment archives. Because of the high accumulation rates at the head of Martínez Channel, the investigated fjord sediment cores only cover the last ~40 years. To establish a continuous, multi-centennial, high-resolution record of pre-historical Baker River GLOFs using fjord sediments, multiple long sediment cores should be collected at the head of Martínez Channel. Optimal coring locations are located on the delta slope, relatively far away from any submarine channel influence, but close enough to the river mouth (for example near core locations FC17-08 and FC17-09) to ensure a good contrast between GLOF deposits and background sediments. Prior to collecting long sediment cores, a seismic survey should be conducted at the head of Martínez Channel to detect paleo-erosional surfaces resulting from channel migration. Acquiring longer sediment cores would not only allow to reconstruct Baker River GLOFs on longer timescales, but it would also allow us to investigate the signature of the GLOFs from other NPI glacier-lake systems, i.e. Nef Lake and the higher-magnitude GLOFs from Arco Lake that occurred between the 1880s and 1960s. Finally, it should be noted that finding in-situ organic material to establish chronologies for such long records might be challenging.

The results of this thesis show the particularly high potential of marine sediments to reconstruct GLOF occurrence. The Baker River system is particularly well-suited to generate GLOF records since a significant part of its watershed is vegetated, resulting in a clear contrast between the background sediments, which are relatively organic, and the GLOF deposits, which have a purely glacial nature. Examining GLOF deposits in other GLOF-prone fjord regions would be useful to investigate the influence of the watershed's properties, such as vegetation density, river baseflow, meltwater/precipitation ratio, etc, or the influence of intermediate lakes, on the signature of GLOFs in fjord sediments. Based on our results, we anticipate that marine archives might only record GLOFs efficiently in temperate regions such as parts of Canada, New Zealand, and South America. Marine archives in glacierized regions at higher latitudes, such as Greenland, Alaska, and Scandinavia, will most likely not be useful to reconstruct GLOFs as the background sediments are as organic-poor as the GLOF deposits. Likewise, deposits from

GLOFs in tidewater glacier fjords, or those affecting watersheds with short proglacial rivers, even at low latitudes, are expected to be difficult to distinguish from fjord sediments. A comparative study of how historical GLOFs are recorded in fjord sediments is however needed to confirm these assumptions.

This thesis hypothesized that the flood deposits encountered in the Valle Grande floodplain predominantly originated from high-magnitude glacial floods. However, precipitation-driven floods could also contribute to some extent to short-term changes in the sediment record. Determining the provenance of the flood deposits would allow us to verify whether the flood deposits indeed represent GLOFs, as the regional GLOFs mostly originate from NPI glaciers. The latter could be done using Sr and Nd isotopes since Liu et al. (2020) have shown that these two isotopes allow differentiating the bedrock lithologies in the western and eastern part of the Baker River watershed. An alternative approach would be to investigate the floodplains of Nef valley, which are expected to be less influenced by meterological floods. This way, the established GLOF record can be compared with the Valle Grande flood record, and the apparent relationship between the occurrence of high-magnitude GLOFs from eastern NPI glaciers during Neoglacials can be tested. However, the Nef record would be limited to GLOFs originating from a single source valley, whereas the Valle Grande record integrates GLOFs from several valleys, thus making it relatively independent of the evolution of individual glacier-river systems due to morphological differences.

One of the archives that has not been investigated in details in this thesis are lake sediments. Several lakes were explored but many of them were too inaccessible for sampling. As for the marine and floodplain archives analyzed in this thesis, the results obtained on lakes Confluencia and Juncal show that glacial flood deposits can be differentiated from the organic-rich background sediments when ideal hydrological conditions are met (Albers, 2019). However, as for floodplain sediments, distinguishing between meteorological flood deposits and GLOF deposits is not straightforward. The main lake of interest to develop a Baker River GLOF reconstruction is Cute Lake, which is located along the Baker River, a few kilometers upstream of Martínez Channel. Due to its location in the lower reach of the Baker River, and direct connection with the river, it might only register the higher magnitude GLOFs. Yet, as it is located downstream of all glacier valleys, it has the potential to integrate all GLOF sources from the lower Baker River watershed. In the upper Baker River watershed, ideal locations to investigate the signature of GLOFs in lake sediments, and eventually to construct GLOF records, are Plomo Lake and the northern branch of General Carrera Lake, where the flood deposits from the 1989 outburst of Laguna del Cerro Largo and from the 1977 Engaño GLOF, respectively, can be used as a reference. Particularly in the northern branch of General Carrera Lake, deposits from GLOFs and precipitation-driven floods are expected to differ significantly, i.e. floods induced by extreme precipitation most likely result in organic-rich deposits, compared to the organic-poor signal of GLOF sediments.

The findings of this thesis also indicate that there is a close, but indirect, link between climate change and GLOF occurrence. High-magnitude GLOFs from eastern NPI glaciers occur more frequently during Neoglacials, at times when climate is cooler and wetter. Although the link between high-magnitude GLOF occurrence and larger and thicker glaciers may be valid worldwide, the relationships between climate and GLOF occurrence may differ in regions where glaciers respond differently to climate. In New Zealand, for example, high-magnitude GLOF occurrence is also expected to be linked to a cooler and wetter climate since New Zealand's climate and glacier variations are similarly controlled by the position and strength of the SWWB (e.g. Putnam et al., 2010; Kaplan et al., 2010). This hypothesis should however be tested by generating GLOF reconstructions in New Zealand.

In addition, we suggested a link between climate and the occurrence of high-magnitude GLOFs from ice-dammed lakes. By comparison, little is known about the influence of climate change on the evolution of GLOFs from moraine-dammed lakes. Future studies in GLOF-prone regions worldwide should thus investigate if GLOFs from moraine-dammed and ice-dammed lakes respond differently to climate change. Doing so will require generating additional records of GLOFs from ice-dammed lakes.

Finally, a better knowledge of the relations between climate change and GLOF occurrence is crucial to determine the probability of large flood occurrence and to improve flood hazard assessments (e.g. Merz et al., 2014; St. George et al., 2020). Current flood strategies and prevention are mostly based on instrumental and historical records. Due to their short duration, the latter may, however, miss the rare extreme events. Long-term flood records should be generated in other GLOF-prone regions, where they can be of great importance to plan infrastructure development projects such as hydroelectric dams, especially since electricity demand is increasing as economies grow (e.g. Himalayas). They would also reduce the vulnerability of communities to floods, via, for example integrating flood risk assessments and spatial planning. In addition, pressure sensors should be routinely installed in hazardous lakes to detect abrupt drainages and function as warning systems to prevent casualties and limit damages. Finally, the formation and growth of glacial lakes in most of the world's glacierized regions and the increasing water demand offer an opportunity to reduce GLOF risk as well as to respond to the increasing freshwater supply demand by artificially controlling lake drainage.

References

Albers, S. (2019) Lake sediment records of late Holocene proglacial floods from the San Lorenzo Icefield (Patagonia). Master dissertation, Ghent University, Belgium, 60 pp.

Kaplan, M.R., Schaefer, J.M., Denton, G.H., Barrell, D.J.A., Chinn, T.J.H., Putnam, A.E., Andersen, B.G., Finkel, R.C., Schwartz, R., and Doughty, A.M. (2010) Glacier retreat in New Zealand during the Younger Dryas stadial. *Nature*, 467, 194 – 197.

Liu, D., Bertrand, S., Villaseñor, T., Van Dijck, T., Fagel, N., and Mattielli, N. (2020) Provenance of northwestern Patagonian river sediments (44–48°S): A critical evaluation of mineralogical, geochemical and isotopic tracers. *Sedimentary* Geology, 408, 105744.

Merz, B., Aerts, J., Nielsen-Arnbjerg, K., Baldi, M., Becker, A., Bichet, A., Blöschl, G., Bouwer, L.M., Brauer, A., Cioffi, F., Delgado, J.M., Gocht, M., Guzzetti, F., Harrigan, S., Hirschenboeck, K., Kilsby, C., Kron, W., Kwon, H.-H., Lall, U., Merz, R., Nissen, K., Salvatti, P., Swierczynski, T., Ulbrich, U., Viglione, A., Ward, P.J., Weiler, M., Wilhelm, B., and Nied, M. (2014) Floods and climate: emerging perspectives for flood risk assessment and management. *Natural Hazards and Earth System Sciences*, 2, 1559 – 1612.

Putnam, A.E., Denton, G.H., Schaefer, J.M., Barrell, D.J., Andersen, B.G., Finkel, R.C., Schwartz, R., Doughty, A.M., Kaplan, M.R. and Schlüchter, C. (2010) Glacier advance in southern middle-latitudes during the Antarctic Cold Reversal. *Nature Geoscience*, 3, 700 – 704.

St. George, S., Hefner, A.M., and Avila, J. (2020) Paleofloods stage a comeback. *Nature Geoscience*